Open Research Online

The Open University's repository of research publications
and other research outputs

A combined PSK/ASK transmission system for commercial telephony via satellite

Thesis

How to cite:

Colby, Roger J (1984). A combined PSK/ASK transmission system for commercial telephony via satellite. PhD thesis The Open University.

For guidance on citations see FAQs.

© 1983 The Author

https://creativecommons.org/licenses/by-nc-nd/4.0/

Version: Version of Record

Link(s) to article on publisher's website:
http://dx.doi.org/doi:10.21954/ou.ro.0000f927

Copyright and Moral Rights for the articles on this site are retained by the individual authors and/or other copyright owners. For more information on Open Research Online's data policy on reuse of materials please consult the policies page.

oro.open.ac.uk

DX 72566/87

UNRESTRICTED

A COMBINED PSK/ASK TRANSMISSION SYSTEM FOR COMMERCIAL TELEPHONY VIA SATELLITE

A DISSERTATION SUBMITTED TO THE

OPEN UNIVERSITY

for the degree of

DOCTOR OF PHILOSOPHY

by

ROGER J. COLBY B.Sc(Hons)

Date of Submission: January 1983
Date of Award: 19.12.84

JANUARY, 1983

ProQuest Number: 27777180

All rights reserved

INFORMATION TO ALL USERS
The quality of this reproduction is dependent on the quality of the copy submitted.

In the unlikely event that the author did not send a complete manuscript
and there are missing pages, these will be noted. Also, if material had to be removed,
a note will indicate the deletion.

ProQuest 27777180

Published by ProQuest LLC (2020). Copyright of the Dissertation is held by the Author.

All Rights Reserved.
This work is protected against unauthorized copying under Title 17, United States Code
Microform Edition © ProQuest LLC.

ProQuest LLC
789 East Eisenhower Parkway
P.O. Box 1346
Ann Arbor, MI 48106 - 1346

A COMBINED PSK/ASK TRANSMISSION SYSTEM FOR COMMERCIAL TELEPHONY VIA SATELLITE

ABSTRACT

This study addresses three modulation schemes capable of increasing the voice channel capacity of the INTELSAT TDMA/DSI System operating with INTELSAT V spacecraft. In particular, a combination digital Amplitude-Shift Keying/Phase-Shifting Keying (APK) technique is evaluated with respect to signal design, thermal noise performance, bandwidths limitations, co-channel interference, adjacent channel interference, TWT distortion and modem complexity in an INTELSAT TDMA system environment. In a linear channel some APK signal designs are known to require significantly less average SNR than PSK to achieve the same probability of symbol error. However, when operated through a satellite channel containing at least one TWT, the reduction in average power required to accommodate amplitude variations causes APK performance to fall below that of PSK for the same alphabet size. Signal predistortion and/or TWT linearization can eliminate the effect of TWT distortion and restore the performance advantage, although the overall performance of APK is still inferior to PSK. However, in a heavily interference limited environment, such as INTELSAT V, the lower average power requirements caused an APK system to perform better, in some cases considerably better, than the corresponding PSK case.

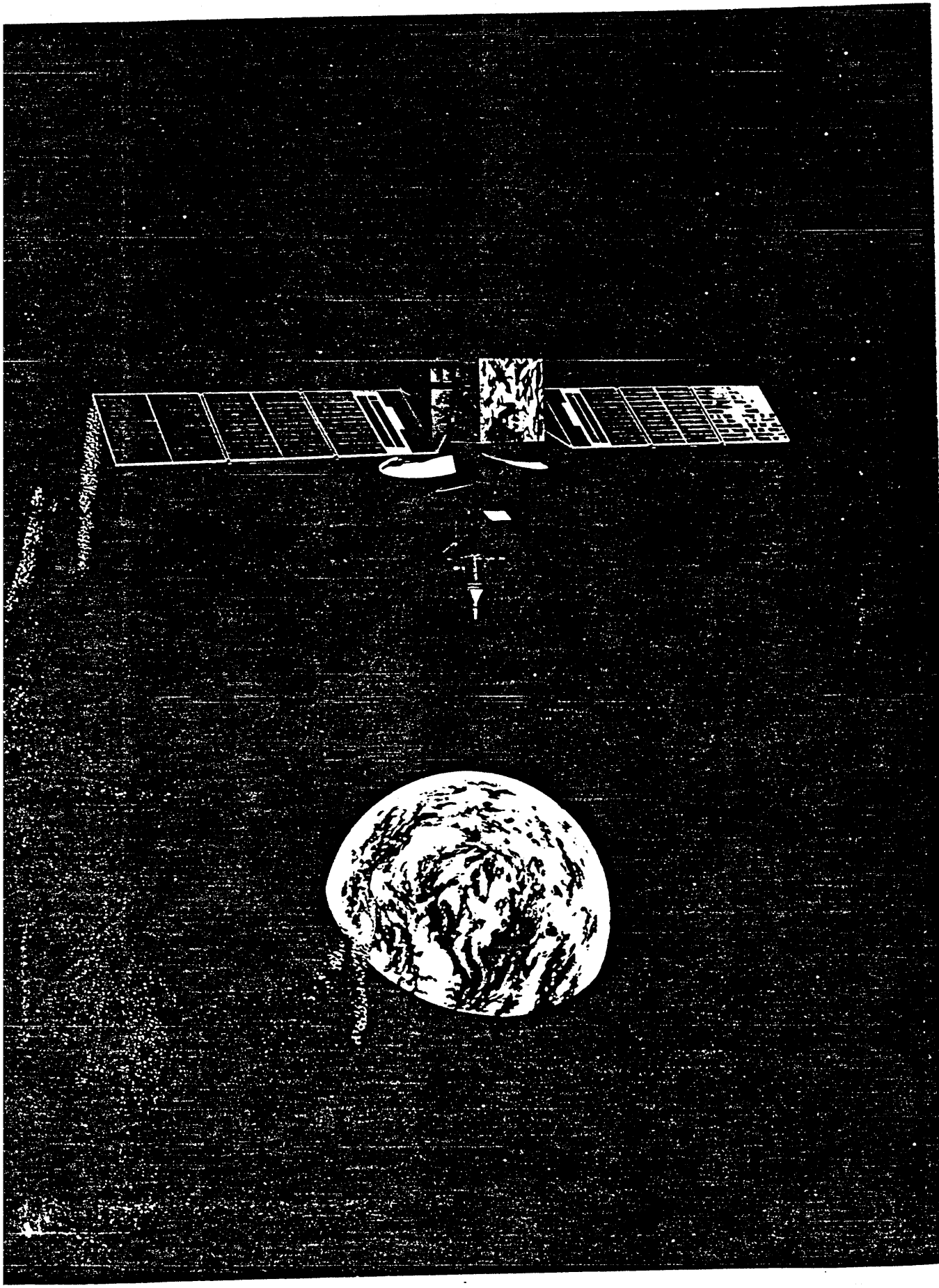

INTELSAT V

Modem implementation considerations include how the signal set can be generated, the type and method of predistortion compensation, the detection method and the equipment required for the reconstruction of phase and amplitude references. The evaluation techniques of APK described include mathematical models, computer simulations (including the development of a unified error performance expression) and logical extrapolation from the QPSK case. Finally, a simple 8 level APK hardware modem was constructed and evaluated. It is concluded that an APK system may be of advantage as a retrofit in the INTELSAT TDMA system operating at 6/4 GHz, but be of significant advantage at 14/11 Ghz where the higher signal/noise ratios can yield an increase in capacity of up to 50 percent.

ACKNOWLEDGEMENTS

This project has been pursued for a little over a decade and in this period many people have influenced the author and/or the project through discussions, practical help and advice, and by example. Of these many people, a few stand out as having exceptional influence.

The study reported in this thesis is based on a piecewise examination of the multitude of effects present in a non-linear satellite channel. The techniques enabling the analysis of these effects in a logical and sequential manner (for the QPSK case) were developed by L. Ludquist, R. A. Harris and R. A. Gough during the time the author was seconded to ESA/ESTEC. Much credit must be given to this team for laying the ground work for future studies such as that conducted by the author. In this thesis, the analytical techniques for the 8-phase PSK, APK-A and APK-B cases are supported by an extrapolation of the results from a comprehensive program of practical tests conducted, using the ECS breadboard model. The quality and accuracy of these tests results were principally due to the efforts of Mr. D. W. Prouse of BTI. To validate the extrapolation exercise, computer simulations were devised and many hours of coding,

processing and plotting were needed. Mr. S. Baker (COMSAT Labs) and Mr. A. Lee (INTELSAT) were of invaluable assistance and gave of much of their free time to meet the author's tight time scales. Likewise, the review and criticism of the mathematical annex was under taken by Mr. R. Bedford who dealt patiently with the panics often displayed by the author.

However, no matter how good the technical material or writing, the overall quality of the product is strongly influenced by the quality of the word processing. In this regard, the author considers himself very fortunate in being able to leave this function entirely to Mrs. A. Tillette, who gave hundred of hours of her own time to produce this document. Mrs. Tillette's accuracy, attention to detail and cheerful professionalism, considerably helped in meeting seemingly impossible deadlines.

At the outset and until 1981, the author benefited from the skill and experience of Mr. A. K. Jefferies of BTI, who functioned as external supervisor and contributed much of the very early advice and guidance. From 1981, the duties of external tutor fell to Dr. S. J. Campanella of COMSAT Labs. Dr. Campanella has many talents not the least of which is the ability to

combine technical excellence with considerable good humor under pressure; which has proved to be immensely valuable to the author.

During the life of this project, the author has worked in England, Holland and now the United States. This could have easily placed insurmountable difficulties in the path of the project's completion. However, throughout the last eleven years, the Open University's appointed internal supervisor Dr. J. Monk has provided an essential thread of continuity. The final quality of this study is due in no small measure to his persistence, technical guidance and attention to detail and is gratefully appreciated by the author.

Finally, the author must record his gratitude to his wife Rosalind for continuous and unwaivering support, for hours of proof-reading and the fortitude to bear all those lost week-ends; and to his children Andrew and Simon, who didn't understand why Daddy was locked in that room with all that paper - but left him alone anyway.

To Rosalind, Andrew and Simon

..... "A slow sort of country!" said the Queen. "Now, here, you see, it takes all the running you can do, to keep in the same place. If you want to get somewhere else, you must run at least twice as fast as that!".

Lewis Carroll

TABLE OF CONTENTS

FIGURE LIST

FIGURE LIST

FIGURE LIST

FIGURE LIST

FIGURE LIST

FIGURE LIST

FIGURE LIST

FIGURE LIST

GLOSSARY

(LIST OF ABBREVIATIONS)

Abbreviation		Definition
ACI	-	Adjacent Channel Interference
AOR	-	Atlantic Ocean Region
AFC	-	Automatic Frequency Control
AGC	-	Automatic Gain Control
AM	-	Amplitude Modulation
AWGN	-	Additive White Gaussian Noise
BER	-	Bit Error Rate
BG	-	Board of Governors (INTELSAT)
BTI	-	British Telecom International
CCI	-	Co-Channel Interference
CDC	-	Control and Delay Channel
C/N	-	Carrier-to-Noise Ratio
CW	-	Continuous Wave
DC	-	Direct Current
DSI	-	Digital Speech Interpolation
DNI	-	Digital Non-Interpolated Unit
CCITT	-	Consultive Committee for International Telephone and Telegraph
E_b/N_o	-	Energy per bit to Noise Ratio
e.i.r.p.	-	Effective Isotropic Radiated Power

GLOSSARY

(LIST OF ABBREVIATIONS)

Abbreviation		Definition
ECS	-	European Communications Satellite
ESC	-	Engineering Service Circuit
FEC	-	Forward Error Correction
FDMA	-	Frequency Division Multiple Access
FM	-	Frequency Modulation
FM/FDMA	-	Frequency Modulation/Frequency Division Multiple Access
G/T	-	Ratio of Antenna Gain to Receiver Noise Temperature Used to Calculate Carrier-to-Noise Ratio
HPA	-	High Power Amplifier
HSE	-	Host Station Equipment
IF	-	Intermediate Frequency
IMUX	-	Input Multiplexing Filter
INTELSAT	-	International Telecommunications Satellite Organization
I/O	-	Input/Output
IOC	-	INTELSAT Operations Center
IOCTF	-	IOC TDMA Facility
IOR	-	Indian Ocean Region

GLOSSARY

(LIST OF ABBREVIATIONS)

Abbreviation		Definition
ISI	-	Inter Symbol Interference
ISIM	-	Inter Symbol Interference Modulation
LNA	-	Low Noise Amplifier
MP	-	Master Primary
MP-1	-	Major Path - 1
MP-2	-	Major Path - 2
MPR	-	Master Primary Reference Station
MPRT	-	Master Primary Reference Terminal
NED	-	Noise Equivalent Degradation
OTS	-	Orbital Test Satellite
OMUX	-	Output Multiplexing Filter
PR	-	Primary Reference Station
PBR	-	Primary Reference Burst
PLU	-	Phase Lock Unit
PM	-	Phase Modulation
POR	-	Pacific Ocean Region
PRBS	-	Pseudo Random Binary Sequence
PRI	-	Primary Path Satellite
PRT	-	Primary Reference Terminal
PSK	-	Phase Shift Keying

GLOSSARY

(LIST OF ABBREVIATIONS)

Abbreviation		Definition
QPSK	-	Quadanary Phase Shift Keying
RB1	-	Reference Burst 1
RB2	-	Reference Burst 2
RF	-	Radio Frequency
RT	-	Reference Terminal
RTE	-	Reference Terminal Equipment
SC	-	Service Channel
SCMPI	-	Silent Channel Multipath Interference
SCPC	-	Single Channel Per Carrier
SHF	-	Super High Frequency
SNR	-	Signal to Noise Ratio
SOF	-	Start of TDMA Frame
SOTMF	-	Start of Transmit Multiframe
SPE	-	Signal Processing Equipment (of RTE)
SRB	-	Secondary Reference Burst
SSOG	-	Satellite System Operations Guide
T_m	-	Multiframe Period or Duration
TDMA	-	Time Division Multiple Access
TRMS	-	TDMA Reference and Monitoring Station
TRT	-	Timing Reference Transponder

GLOSSARY

(LIST OF ABBREVIATIONS)

Abbreviation		Definition
TSM	-	TDMA System Monitor
TTY	-	Telegraphic Teletype
TWT	-	Travelling Wave Tube
TWTA	-	Travelling Wave Tube Amplifier
ULPC	-	Up Link Power Control
UW	-	Unique Word
VOW	-	Voice Order Wire
XPD	-	Cross Polar Discrimination

A COMBINED PSK/ASK TRANSMISSION SYSTEM FOR COMMERCIAL TELEPHONY VIA SATELLITE

SECTION 1

INTRODUCTION

1.1 Historical Background

Since the foundation of the International Telecommunications Satellite Consortium (INTELSAT), the telephone channels circuit capacity of successive families of satellites has risen progressively from 240 to more than 12,000 one way telephone channels. The present generation satellites, INTELSAT V's, have capacities of the order of 12,000-15,000 voice channels and will mark a further stage in satellite development by inaugurating a limited amount of digital transmission using time division multiple access (TDMA) techniques. Up to the time of writing, the present satellite system was almost exclusively based on frequency modulation (FM) and frequency division multiple access (FDMA), whereas the first digital transmissions will use 4-level phase shift keying (QPSK). However, the demand for satellite circuits

and the limited radio frequency bandwidth available for such services, suggests that more efficient use of the available bandwidth would be desirable.

As traffic demands increase, the demand on the transmission capacity of satellites increases and bandwidth efficiency of the signal modulation method becomes as important as detection efficiency. Thus, the poor bandwidth efficiency of the commonly employed biphase and quadriphase PSK modulation may be viewed as a significant limitation on communication satellite capacity. One way to increase the data capacity for a given bandwidth allocation is to increase the symbol alphabet size, for example, by the use of 8-phase PSK.

However, 8-phase PSK requires a significantly better carrier to noise power ratio than QPSK for the same error rate. It will be shown that this extra power requirement may not be available in the INTELSAT V satellite. It is, therefore, useful to explore alternatives.

M-ary modulation techniques combining both phase and amplitude keying (PSK/ASK) have been proposed by several authors [1,2,3]. They have suggested various signal set designs (called amplitude/phase keying (APK))

and have shown these to require less peak or average power than M-ary PSK to achieve the same symbol error probability (for $M \geq 8$) when both have the same alphabet size (spectral occupancy). These preliminary analyses, however, assumed an ideal, distortion-free (and in some cases low speed) channel which is a poor approximation to a transponder operating under bandwidth, power and interference constraints.

1.2 Organization of Study

This study, after reviewing the INTELSAT satellite system, performs a comprehensive analysis of two PSK/ASK (APK) systems to determine the symbol error performance for a realistic satellite transponder channel with heavy spectral filtering, TWT non-linearities and severe interference (the practical case). Practical aspects of modem implementation and reference recovery, are also included to provide a more complete picture of APK operation. The modulation system is compared with 8-phase PSK by using theoretical calculations, computer simulations and extrapolated results obtained from a QPSK simulator under realistic conditions.

The study is broken down into eight well defined areas:

1. Introduction
2. Commercial Satellite System
3. Modulation Selection and Thermal Noise Performance
4. Linear Channel Analysis
5. Non-Linear Channel Analysis
6. Operation in the higher frequency bands (11/14 GHz)
7. Modem Considerations
8. Conclusions

Section 2 provides a more detailed historical background to the project by showing that the capacity of commercial satellites has steadily been increased from only a few telephone channels 20 years ago to more than 12,000 telephone and 2 TV channels at the time of writing. Originally, the capacity of successive satellites had been increased by increasing transmitted power. In the later satellites, spacial and polarization frequency reuse techniques provided significant capacity increases. However, the latest satellites employ so much frequency reuse that the satellite link becomes interference limited. Further frequency reuse therefore,

will not yield significant capacity increases. In consequence, the need to further increase capacity under these conditions leads to the notion that a more bandwidth efficient modulation method is required. To provide the basis for the theoretical performance of the candidate replacement modulation methods, a link budget for an INTELSAT V series spacecraft is developed showing that the selected method must operate with a total carrier to noise and interference (C/(N+I)) power ratio of about 15 dB.

In Section 3, the theoretical BER vs C/N performance of various 8 level techniques is examined, together with 4-phase PSK. Before being able to compute the bit error rate (BER) performance of the APK candidates, it was necessary to optimize the amplitude ratios of the inner and outer signal sets (ring ratios) by using simple graphical techniques and a unified error rate expression developed by the author. The results show that 8-phase PSK performs better than two simple forms of amplitude/phase (APK) hybrid modulation, when the analysis is performed solely on the basis of BER vs peak signal to noise ratio. Accordingly, if there were no other considerations, (i.e., if the satellite channel were truly linear and only corrupted by Gaussian noise) 8-phase PSK would be chosen. However, this is not the case. In particular, since the channel performance is dominated by

interference from other nominally identical channel possessing the same frequency and since the average power of APK modulation schemes is less than the corresponding PSK case, the overall performance in a heavily interference limited environment will favor the APK schemes. For this reason, the theoretical BER vs C/N performance characteristics was used to estimate the performance of 8-phase PSK and the two candidate APK schemes in a linear (and later in the more practical non-linear) satellite system experiencing band limitation, co-channel and adjacent channel interference and modem imperfections.

In Section 4, the mechanisms are identified which prevent the theoretically obtainable performance being obtained in a practical satellite system employing linear power amplifiers. To do this, a satellite end-to-end channel (link) is examined to identify those elements which influence channel performance. These elements are then combined into a simple transmission model and the performance degradation effects are grouped into imperfect modulation and demodulation, channel filtering effects and co-channel, adjacent channel and multipath interference effects. Using a computer simulation of a satellite channel and performance measurements obtained from the ESA/ESTEC OTS hardware satellite model, it is possible to

conclude that adjacent channel and multipath interference in the linear channel is negligible and may be ignored, but the other effects in a homogeneous, interference limited linear channel, give (for the same error rate) the APK-B system an advantage of almost 1 dB S/N over 8-phase PSK which in turn is 3.4 dB better that the Type-A system.

Section 5 shows that the linear channel, although much easier to analyze, is a poor approximation to the real case where the satellite TWTA will be operated close to saturation. Accordingly, the techniques developed for the linear case were applied to the non-linear channel to obtain reliable estimates of the three candidates' performance in a practical satellite system by including the mechanisms which arise (or are affected by) non-linear operation of the earth station or satellite TWTA's. When this was done it became apparent that design rules based on the Nyquist criteria cannot be directly applied in this case and non-conformance with the Nyquist criterion means that freedom from ISI at the sampling instant can no longer be obtained. Furthermore, by the use of computer generated signal space diagrams, the interaction between the non-linearity and any subsequent filtering was shown to further increase the ISI signal power causing the interfering signal to vectorally add and thus act as a power elevating "pedestal" for the noise effectively

decreasing the noise power required to cause a given error rate. A balance point was expected where the improvement in down-link C/N no longer dominates the increased distortion caused by the increased signal power demanded from the TWTA. Accordingly, the performance of the three 8-symbol candidates was evaluated as a function of TWTA back-off and the analysis showed that the PSK modulation method was more tolerant of the distortion than the APK systems and in consequence was able to use more power on the down-link to improve the receiver C/N.

The relatively large back-off required for the APK signal sets was shown upon examination of the non-linear characteristics of the TWTA's to be due to the power transfer non-linearity compressing the APK ring ratios and a precompensation (expansion) technique was used to obviate the TWTA compression effect. The use of this precompensation is shown to fully restore the best attainable linear channel performance of the APK modulation methods and so the effect of the am/pm conversion was considered next. The calculations showed that all three methods gave unsatisfactory performance and indicated that some form of compensation would be necessary. A simple linear phase equalizer of 3°/dB was tried and the combination of predistortion and phase

equalization restored the optimum BER performance of the three candidates to 10^{-6}, 10^{-8} and 10^{-9} for APK-A, APK-B and 8-phase PSK, respectively.

Since INTELSAT V is known to be an interference limited spacecraft, considerable emphasis was placed on the effect of Co-channel Interference. Using results obtained by the author on a QPSK satellite simulator, estimates were made of the performance degradation at the anticipated interference C/I levels of 22 dB in the up-link and down-link and it was noted that in this case the APK systems perform better than the 8-phase PSK case due to the lower average power of the APK signal sets which was considered to be a major advantage in an interference limited environment.

To complete the study, Adjacent channel and Multipath interference effects were assessed under the spectrum spreading conditions associated with non-linear operation of the TWTA's and the various resulting performance degradations were incorporated in a 6/4 GHz link budget to give the predicted link budgets for the three candidates. The result shows that the APK-B system (at expected BER of 10^{-5}) out-performs 8-phase PSK and APK-A at 3×10^{-3} and 10^{-2}, respectively. It is concluded that although the single channel performance of

8-phase PSK is superior to APK, the lower average power requirement of APK-B leads to an overall improvement in the error rate of almost two orders of magnitude over the 8-phase PSK case at 6/4 GHz in a heavily interference limited environment.

The superior performance of the APK-B method under co-channel interference conditions led to an investigation [reported in Section 6] of the performance of the three candidates in a 14/11 GHz environment where deep fades and associated depolarization are common occurrences.The results show that all three candidate methods will operate satisfactorily in the 14/11 GHz environment, while increasing the transmission capacity of the link by 50% relative to the QPSK system. The link budgets show that the available clear weather C/N is greatly in excess of that needed for a threshold error rate of 10^{-4}. Specifically, 8-phase PSK, APK-A and APK-B show C/N margins of 6 dB, 8 dB and 10 dB, respectively when multipath is not considered. These margins provide protection against precipitation induced fades and the higher margins associated with APK-B would result in the satellite system being useable for a greater fraction of the year (APK-B would be useable for 99.99% of the year (1 hour outage), while 8-phase PSK would be useable 99.94% of the year (about a 5 hour outage)). For

the high cost INTELSAT circuits, these differences are significant and further indicate the robustness of the APK-B system in a heavily interference limited environment.

In Section 7, various practical modem effects are considered. The link budget estimates used throughout this study are based on extending various QPSK results to the 8-phase PSK, APK-A and APK-B cases. Since these results were obtained using QPSK modems, it was considered important to compare the methods that may be employed in the candidate modulation methods' modems to identify differences in attainable modem performance. To this end, basic modem designs were examined and at an early stage, the importance of the reference recovery circuits was recognized. Accordingly, some considerable time was spent on examining the elements within these cicuits, particularly the carrier and clock recovery loops. The assessment of these recovery loops was completed by investigating the techniques available to establish an amplitude reference for the APK systems. Finally, attention was directed towards the construction of an APK modem. This was designed to be an overlay to an existing QPSK modem and although limited by available budget and manpower, this overlay technique was verified, but much could be refined in a commercial development.

The conclusions in Section 8 show that the need to expand the traffic carrying capacity of the INTELSAT system leads to the desire to improve the bandwidth efficiency by the use of higher order alphabets than the current 4-level QPSK system. A cursory examination showed that 16-ary systems could not be made to operate in the INTELSAT V environment because the required carrier-to-noise ratio cannot be supported by this satellite. Attention was thus directed to 8-ary signal sets and several promising candidates were identified and evaluated. On the basis of the first examination, the number of candidates was narrowed to three: 8-phase PSK and two types of amplitude-phase shift keying (APK-A and APK-B). The objective of this study was to evaluate the performance of the candidates in a realistic environment.

The results show that one APK method appears to offer superior performance over 8-phase PSK, and will meet baseband signal to noise ratios required for normal commercial telephone traffic. The study was limited by budget and manpower and should now be repeated without these restrictions. If the results are verified, the capacity of an INTELSAT V satellite channel could be increased by about 50%, thus reducing the connection cost. Furthermore, APK is shown to be a simple technique promising low mechanization costs. The possibility also

exists that the technique could be applied as an overlay or adjunct to the existing QPSK/TDMA equipment further reducing the cost of implementation. The hardware equipment constructed during this study was based on this technique.

It is concluded that although the basic single channel thermal noise performance of APK-B is inferior to 8-phase PSK, its lower average power requirements yield significant performance advantages in a heavily interference limited environment, especially 14/11 GHz. For this reason, it is considered appropriate that an 8 level APK-B system be further investigated for use as a retrofit of the INTELSAT V TDMA networks in order to increase the available traffic carrying capacity by 50%.

SECTION 2

THE COMMERCIAL SATELLITE SYSTEM

2.1 Historical Background

International satellite communication was first seriously contemplated as a commercial feasibility in the 1950's, a decade after the scientist and science-fiction author Arthur C. Clarke[4] had postulated the possibility. In 1957, the USSR launched Sputnik, the world's first artificial satellite (Figure 2.1). The first communication satellite, "SCORE", was launched by the USA in December 1958. This satellite was built with relatively simple off-the-shelf VHF equipment and lasted for 12 days before its batteries were exhausted. Early trials with active satellites, such as Courier (1960), continued to exhibit problems due to premature power supply and electronic device failures which led to the fear that active satellites would not be economically or even physically viable.

Later, experiments conducted by the American Telephone and Telegraph Company (ATT) and the National Aeronautics and Space Administration (NASA) were based on "passive-reflector" satellites[5] (Figure 2.2). These

large metallized-plastic balloons, such as Echo I (1960), had circular orbits of 1600 km and were reasonably reliable, lasting a few years before re-entering the earth's atmosphere. However, all passive satellite links suffer from very large path losses in the order of 300 dB. This required the use of 10 kW transmitters with very high gain antenna, which even so resulted in only a few telephone channels. Furthermore, the orbits were too low for effective long distance communications due to line of sight limitations arising from the curvature of the earth. Attention was thus returned to active satellites.

In 1962, the communications satellite TELSTAR I, was successfully place in a low altitude orbit (Figure 2.3). The orbit of this satellite was such that it moved fairly rapidly relative to the earth, with the result that its periods of visibility to a transmitting or receiving station was limited to about 30 minutes. Nevertheless, experimental transatlantic television pictures were successfully received in the United Kingdom, France and the United States.

Following these successes, TELSTAR II and the Relay[6] series of satellites were all low altitude spacecraft asynchronous with the earth's surface. However,

in 1963 SYNCOM I was launched (Figure 2.4). Like its asynchronous predecessors, SYNCOM had a limited power output and was essentially experimental, but a sufficiently powerful rocket was used to place it in a circular orbit, coplanar with the equator, and of such an altitude (35,790 km) that its orbital period equalled that of the earth. Thus it maintained a "fixed" position relative to all points on the earth's surface, and so provided continuous coverage of about one third of the Globe and obviated the need for elaborate tracking facilities at each earth terminal.

Following this successful demonstration of a geostationary satellite, it was decided that the world's first commercial communication satellite, "Early Bird", would occupy a similar orbit over the Atlantic Ocean. Early Bird, later renamed INTELSAT I, was launched in 1965, with a capacity of either 240 telephone circuits or one medium quality television channel. INTELSAT I consisted of two amplifying repeaters - or transponders - one normally handling west-to-east traffic and the other east-to-west. Because each transponder was designed with an amplitude limiting characteristic, this satellite was capable of access by only a single FM transmission per transponder.

The first satellite with a multiple access facility was INTELSAT II, also geostationary, which was originally designed to provide support communications for the NASA APOLLO project.

During 1967, INTELSAT II's were placed in orbit to cover the Atlantic and Pacific Ocean zones, and in December 1968, the first satellite designed to form part of a Global communications network was launched. This was INTELSAT III, which had the capacity of about 1200 telephone channels plus one medium quality television channel. Despite launch vehicle and spacecraft failures, INTELSAT III's operated in all three ocean regions simultaneously, thus providing world coverage with the exception of the polar regions. This satellite was designed with a mechanically despun antenna such that the antenna continuously pointed towards earth while the main satellite body spun about its axis to achieve orbital stability. The satellite carried two transponders each of 250 MHz bandwidth which allowed multiple access by between 10 to 20 earth stations.

By this time, it was recognized that a small number of wide bandwidth transponders was not an efficient method of providing multiple access for a large number of earth stations. Accordingly, the next generation of

satellites, INTELSAT IV (Figure 2.5), was designed to have 12 transponders of 36 MHz bandwidth which gave a capacity of about 4000 voice circuits together with 2 television channels. The antenna on this satellite were also despun, but in addition to the conventional "global" coverage antenna, two steerable narrow beam parabolic antenna were provided to focus the transmit microwave beams on the high density traffic routes to improve the attainable signal-to-noise ratio and hence increase the traffic carrying capacity. The first of the INTELSAT IV series of spacecraft became operational in March 1971 over the Atlantic Ocean and this was followed by a further six satellites. The use of the higher gain (smaller coverage area) antenna increases the signal to noise ratio for a given input power relative to the wider global coverage beams and and the INTELSAT IV spacecraft were the first to be limited in capacity by the available bandwidth rather than the satellite transmit power[7,8].

The large number of relatively small bandwidth transponders proved to be a successful arrangement and the next generation of spacecraft, INTELSAT IV-A, were designed to be an improved version of its predecessor. The INTELSAT IV-A carries 20 transponders of 36 MHz bandwidth giving a capacity of 6000 voice circuits together with two TV channels. The satellite uses a

sophisticated combination of feed-horns and parabolic antenna which allows a particular transponder to operate in either a global, spot or hemi-beam mode [hemi-beams and especially the narrower spot beams, allow selective illumination of the east or west coverage area, which in turn allows the same frequencies to be used in both the east and west]. The first INTELSAT IV-A became operational on 13 July 1975 and until recently, those satellites provided the INTELSAT global coverage.

Wideband digital transmission is likely to make its operational debut on the INTELSAT V series spacecraft and the modulation methods described in this Report are orientated towards the INTELSAT V (and follow-on satellites) transmission requirements. The INTELSAT V satellite incorporates many technical innovations such as the use of non-spinning three axis stabilization, steerable solar arrays and the use of orthogonal polarizations which enable the same frequency bands to be used twice in the same beam by invoking using polarization discrimination. Seven INTELSAT V's are planned and each has a capacity of about 12,000 voice circuits and two TV channels. The transmission characteristics of an INTELSAT V network will be discussed in detail in the next sub-section.

2.2 Satellite Link Parameters for an INTELSAT V System

The INTELSAT V spacecraft is an active repeater communications satellite intended for use in a geosynchronous equatorial orbit (Figure 2.6). INTELSAT V, which is designed for a life of seven years, is a body (three axis) stabilized spacecraft with solar cell "paddle" arrays which are steered in order to track the sun. This represents a significant departure from previous INTELSAT spacecraft which were all spin stabilized with solar arrays covering the cylindrical body. It is expected that sufficient fuel will be carried to enable the spacecraft to be kept within $\pm 0.1°$ of its assigned longitudinal position and within $\pm 0.1°$ of the equatorial plane.

The INTELSAT V communications subsystem operates in two frequency band pairs:

a) The 6/4 GHz band (5,925 to 6,425 MHz up-link and 3,700 to 4,200 MHz down-link), and

b) The 14/11 GHz band (14,000 to 14,500 MHz up-link together with 10,950 to 11,200 and 11,450 to 11,700 MHz down-link).

The spacecraft utilizes these bands in seven distinct coverage areas, five at 6/4 GHz and two at 14/11 GHz (Figure 2.7). Reuse of the frequency bands between coverage areas is accomplished by means of spatial isolation. Reuse of the frequency bands within a coverage area is accomplished by means of polarization discrimination. Table 2.1 summarizes the coverages and the associated polarizations, while Figures 2.8 and 2.9 show the hemi and global coverage areas and Figure 2.10 shows the coverage areas for each of the three ocean regions, which together provide global coverage. These coverage zones are defined by various performance characteristics which must be met at a specified set of earth station locations (e.g., signal to noise and signal to interference ratios). The specifications require that, once in orbit, each spacecraft must be able to interconnect the various antenna via ground command thus interconnecting the various coverage areas of a particular ocean region. The two spot beam antenna, which operate at 14/11 GHz, illuminate only a small coverage area of the earth's surface. These spot beams are steerable under ground control over a limited portion of the earth's disk to interconnect particular areas.

Band	Coverage	Polarization	
		Up-Link	Down-Link
6/4 GHz	Earth	Left-Hand Circular	Right-Hand Circular
	West Hemispheric	Left-Hand Circular	Right-Hand Circular
	East Hemispheric	Left-Hand Circular	Right-Hand Circular
	Zone 1	Right-Hand Circular	Left-Hand Circular
	Zone 2	Right-Hand Circular	Left-Hand Circular
14/11 GHz	East Spot	Linear	Linear
	West Spot	Linear	Linear

* The polarization of the east spot coverage shall be orthogonal to that of the west spot coverage.

TABLE 2.1 INTELSAT V COVERAGE BEAMS

The interconnection of receive and transmit coverage areas necessary to establish the desired signal paths are accomplished by connecting the antenna corresponding to the appropriate areas to the input and output of the various channels within the spacecraft. Figure 2.11 shows a simplified arrangement where two receive spot beams can be connected to several channels of different bandwidths, which in turn, can be connected to several transmit antenna. These connections are established by ground control and the available range of connections is designed to allow considerable flexibility in the traffic handling capabilities of the spacecraft. Each interconnection can be realized independently for each channel, although a channel can interconnect only one receive coverage area to one transmit coverage area. Figure 2.12 shows the transponder plan for INTELSAT V, in particular the manner by which the 12 transmission channels can be connected to the various coverage areas. [From this figure, it will be noted that many of the channels extend over more than one transmission channel number. Under these circumstances, the channel is identified by a multiple channel number, e.g., channel (1,2) or (7,12). In the case of channel (7,8), the dotted line in the channelization plan indicates that on the up-link the channelization consists of two independent

channels, 7 and 8; but on the down-link, these channels are combined to form a single channel (7,8)]. The much simplified block diagram of the INTELSAT V communication subsystem is shown in Figure 2.13. Reading left to right, it will be seen that the receive 6 GHz signals are routed to low-noise amplifiers and down converted to the 4 GHz band. The down converted signals are then filtered in the channelizing banks and routed to the interconnection switches. The selected signals are then translated to the appropriate transmit frequency and following power amplification, are combined with other channels and routed to the selected transmit antenna.

A satellite communication system is characterized by a number of general features, viz:

1) Frequency bands employed.
2) The manner by which the bands are apportioned into a number of contiguous channels.
3) The performance of the low noise receiver amplifier (LNA).
4) The available trasmit power for each channel.
5) The gain of the antenna.
6) The leakage between antennas operating in the same frequency bands.

The effects are summarized in Figure 2.14 which shows a channel linking two earth stations via a satellite. Starting at the transmitter, it is normal to perform a series of gain/loss calculations with the ultimate aim of determining the signal-to-noise ratio in the demodulator of the receiving earth station. The calculations are termed "Link Budgets". A simple link budget is shown in Figure 2.14.

2.3 Typical Link Budget for Digital Transmission through INTELSAT V

At the time of writing, digital transmission (using TDMA/PSK) will probably begin by using channel (3,4) and the hemi-beams in the East and West Atlantic regions. Consideration of the proposed symbol rate (60-Mbaud or 120 Mbit/s) and the channel spacing (80 MHz) suggests that the care must be taken to prevent mutual interference between signals in adjacent channels. At the same time, a mixture of economic, technological, and propagation effects combine with the requirement of coverage areas and traffic requirements to limit the signal-to-noise available at the receiver and possibly to impose non-linear operation on the earth station transmitters and the satellite TWTA's (traveling wave tube amplifiers). The requirement for good separation between

the adjacent channels and non-linear amplifier operation tend to conflict with one another, but fortunately an acceptable balance can be achieved.

Frequency reuse by polarization discrimination and geographical (spacial) separation leads to cross-polar (co-channel) interference stemming from imperfect antenna alignment, polarization purity, signal leakage within the spacecraft, and atmospheric depolarization. At 6/4 GHz and especially 14/11 GHz, atmospheric attenuation and depolarization can be significant, and a suitable allowance must be made in the link budget. The atmospheric effects are time varying phenonema which can be described in statistical terms. The performance requirements are therefore expressed in terms of percentages of time for which certain performance standards must be met. The transmission design must aim to achieve a performance in accordance with the requirement-stations and seek to obtain the most economic overall system configuration.

[Atmospheric propagation variations cause changes in attenuation, noise temperature, non-linear distortion, and co-channel (cross-polar) and adjacent channel interference. These changes may occur at the same time, or independently, as the different up-links are affected,

but a full analysis is considered outside the scope of this study. Provided that certain constraints are satisfied, a balance can be achieved between the different performance requirements and consequently this study uses, for the most part, only the "clear weather" transmission analysis, with the effects of propagation variations only being discussed in qualitative terms.]

2.4 Clear Weather Transmission Analysis [6/4 GHz, Hemi-Beams, Channel (3,4)]

Although many of the stages contained in the following analysis are general ones, the clear weather analysis will be based on the existing proposal of QPSK modulation through INTELSAT V channel (3,4) using hemi-beams at 6/4 GHz. It will thus be necessary during the study of the new modulation scheme to rework the analysis to reflect the different properties of the new modulation method.

Figure 2.14 showed a simplified block diagram of the satellite transmission link, highlighting the principal features of interest for transmission analysis. Close packing of the channels and non-linear amplification give rise to adjacent channel interference and adjacent channel multipath distortion. This must be controlled, at

least in part, by filtering in the earth station and the satellite repeater. At this stage in the transmission system design, it must be assumed that the satellite characteristics are fixed, at least for the foreseeable future. Therefore, only the ground station characteristics can be adjusted to produce the correct trades between the various distortions and interferers. However, the various filters give rise to performance imperfections and, in conjunction with the earth station and satellite amplifiers, to various non-linear effects. These factors need to be balanced in the transmission design with the need for adequate signal-to-noise ratio, and an allowance must be made for cross-polar interference effects.

A detailed analysis of the performance of an APK system operating in the INTELSAT V environment is made in Sections 4 and 5. As a starting point for the subsequent analysis and comparison of 8-phase PSK and the new modulation method, sufficient information now exists to calculate a clear weather link budget for a standard INTELSAT earth station. The salient parameters of such an earth station are as follows:

Antenna

- 30 meters diameter
- steerable in azimuth and elevation
- tracks geostationary satellites to within 0.02°
- G/T* typically 40.7 at an elevation of 28.2°
- e.i.r.p. typically 86 dBW**

Using this data, together with the satellite characteristics discussed in Section 2.3, and making allowance (unsubstantiated at the moment) for interference and practical implementation effects, allows a tentative clear weather link budget to be formulated. This is shown in Table 2.2.

From this link budget, it can be seen that the estimated carrier-to-noise ratio (C/N) will be of the order of 20 dB, but that after an allowance has been made for the interference effects, the effective C/N ratio will be of the order of 15 dB.

* G/T: Ratio of antenna gain to receiver noise temperature used to calculate carrier-to-noise ratio.

** e.i.r.p.: effective isotropic radiated power.

In order to compare this carrier-to-noise ratio with the performance in terms of bit-error-rate (BER) as required by CCITT, it is necessary to generate equations which relate C/N performance to BER. It is also necessary to assess the impact on the system of interferers in order to justify the assumptions made in arriving at the tentative link budget. To complete the picture, it is necessary to assess the impact of this system on other systems in the adjacent and cross-polar channels.

2.5 Summary

This section provides historical background to the project. It has been shown that the capacity of commercial satellites has steadily been increased from only a few telephone channels 20 years ago to more than 12,000 telephone and 2 TV channels at the time of writing. Originally, the capacity of successive satellites had been increased by increasing transmitted power. In the later satellites, spacial and polarization frequency reuse techniques provided significant capacity increases. However, the latest satellites employ so much frequency reuse that the satellite link becomes interference limited. Further frequency reuse therefore,

will not yield significant capacity increases. In consequence, the need to further increase capacity under these conditions leads to the notion that a more appropriate modulation method is required. This is the subject of the next section. However, to provide the basis for the theoretical performance of candidate replacement modulation methods in the next section, this section concluded by explaining the concept of a link budget and showing the link budget of an INTELSAT V series spacecraft. The results show that the selected method must operate with a total carrier to noise and interference (C/(N+I)) power ratio of about 15 dB.

TABLE 2.2

Clear-Sky 6/4 GHz Link Budget
UK to USA East-Hemi to West-Hemi

No Terrestrial or Inter-network Interference Included
Atlantic Satellite Longitude: 335.5°E
Single Carrier

Up-Beam	6 GHz	UK
Down-Beam	4 GHz	USA
Occupied Bandwidth	72 MHz	

Line #	Up-Link (noise only)	Units	Parameters	Remarks
1	Saturation Flux Density	(dBW/m^2)	-72.0	Nominal high-gain specs
2	G/T of Satellite	(dB/K)	-11.6	Min. G/T specs
3	C/N at Saturation	(dB)	30.0	Elevation: 25.2°
4	Input-Backoff	(dB)	4.0	6.175 GHz
5	C/N	(dB)	26.0	Path Loss: 200.3 dB
	Down-Link (noise only)			
6	Saturation e.i.r.p.	(dBW)	29.0	Min. specified e.i.r.p.
7	Earth-Station G/T	(dB/K)	40.7	Elevation: 28.2°
8	Pathloss	(dB)	196.3	3.95 GHz
9	C/N at Saturation	(dB)	24.2	
10	Output Backoff	(dB)	0.8	From Figure 5.8
11	C/N	(dB)	23.4	
	Up-Link (noise + interference)			
12	C/N	(dB)	26.0	From Line 5 (noise only)
13	C/I Clear Sky	(dB)	21.5	
14	C/N + C/I = Net C/(N+I)	(dB)	20.18	Combine Lines 12 & 13
	Down-Link (noise + interference)			
15	C/N	(dB)	23.4	From Line 11 (noise only)
16	C/I Clear Sky	(dB)	21.5	
17	Adjacent Channel Interference Loss Estimate	(dB)	1.0	HPA input backoff: 10 dB
18	C/N + C/I = Net C/(N+I)	(dB)	18.33	Combine Lines 15, 16, 17
	Combined Up-Link & Down-Link			
19	Overall C/(N+I)	(dB)	16.15	Combine Lines 14 & 18
20	Miscellaneous Loss	(dB)	1.0	Modem performance variation; antenna tracking error, etc.
21	Total Available C/(N+I)	(dB)	15.15	

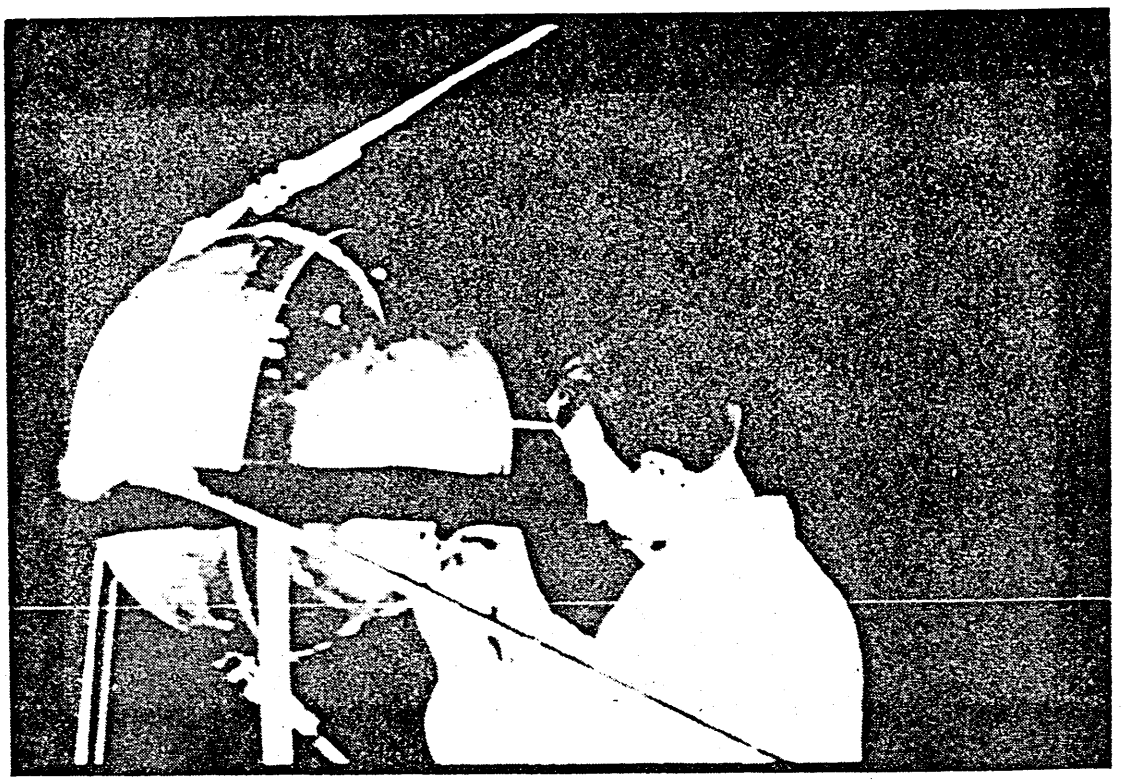

FIG 2.1 SAUTNIK: The world's first artificial satellite

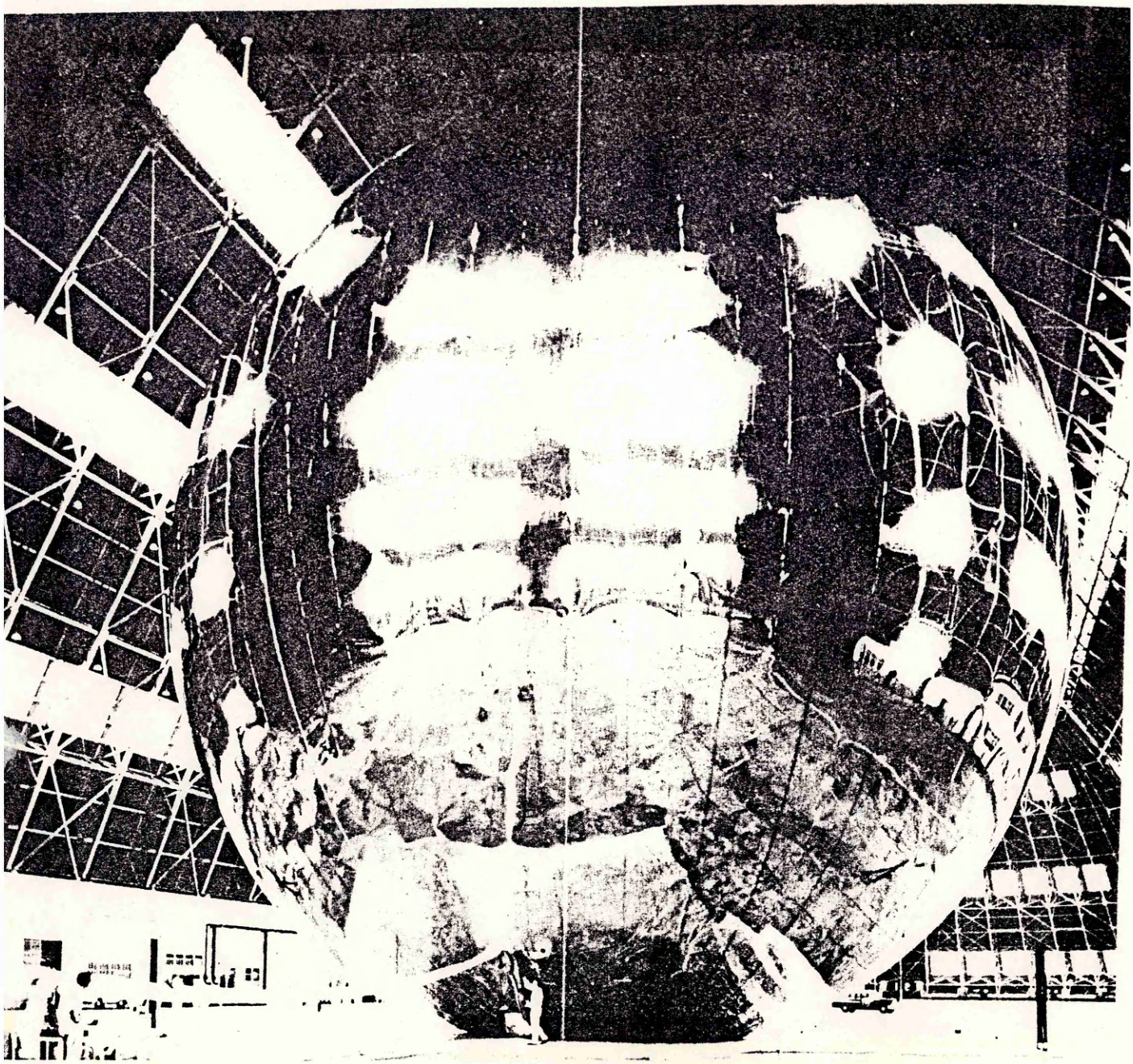

FIG 2.2 ECHO I

INTELSAT II

INTELSAT I (EARLY BIRD)

INTELSAT IV

TELSTAR

INTELSAT III

FIG 2.3 TELSTAR and five Generations of Intelsat satellites

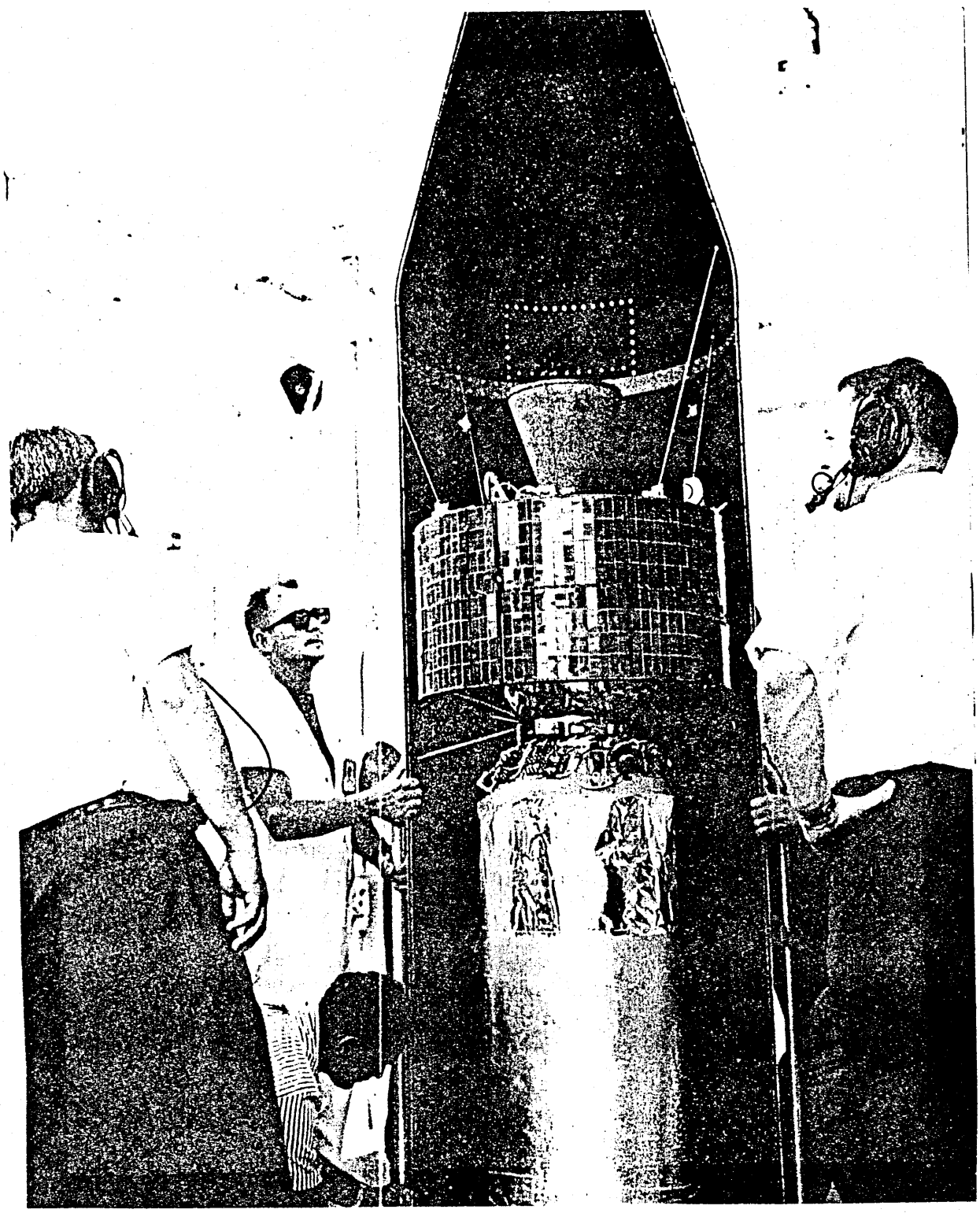

SYNCOM

FIG 2.4

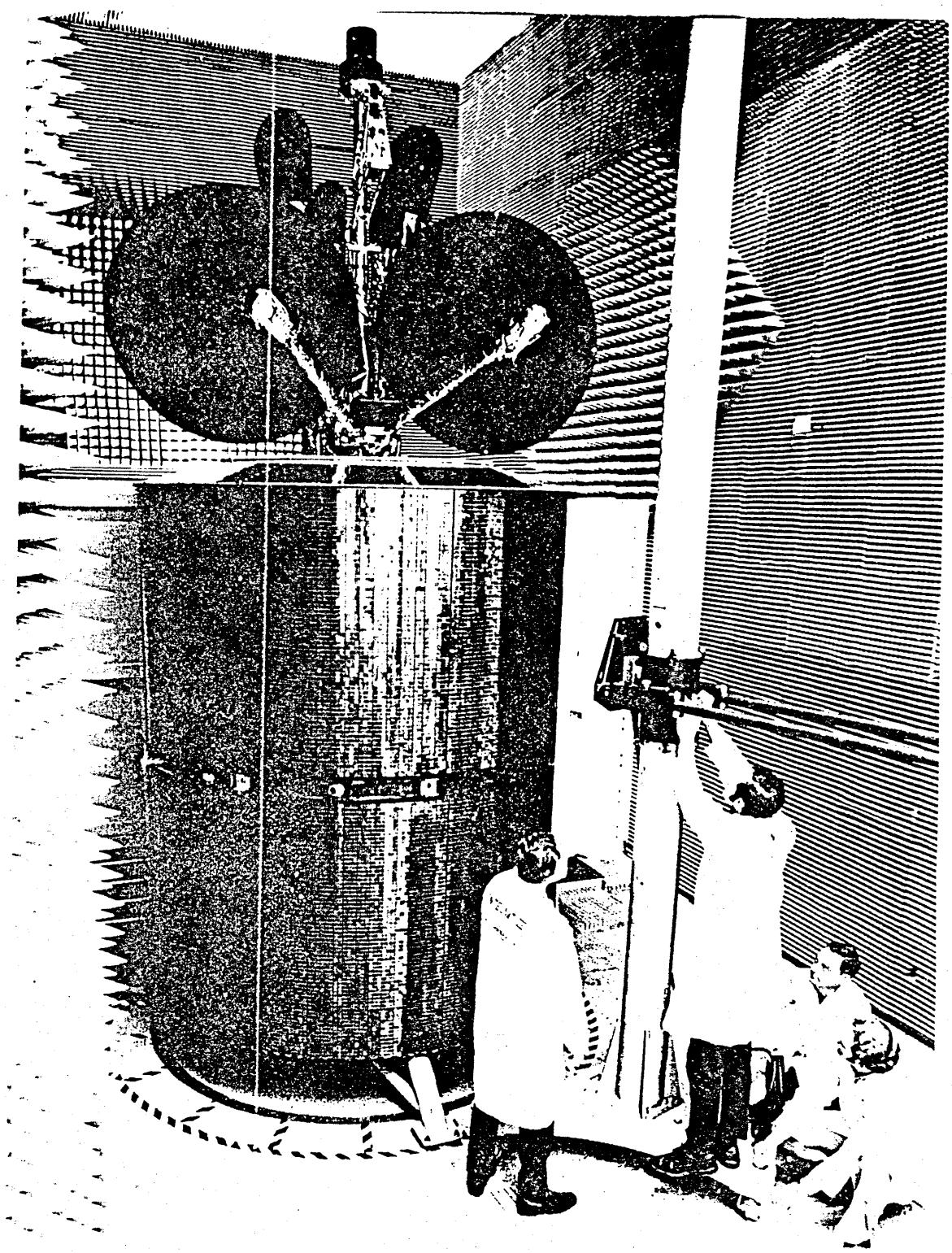

FIG 2.5 INTELSAT IV

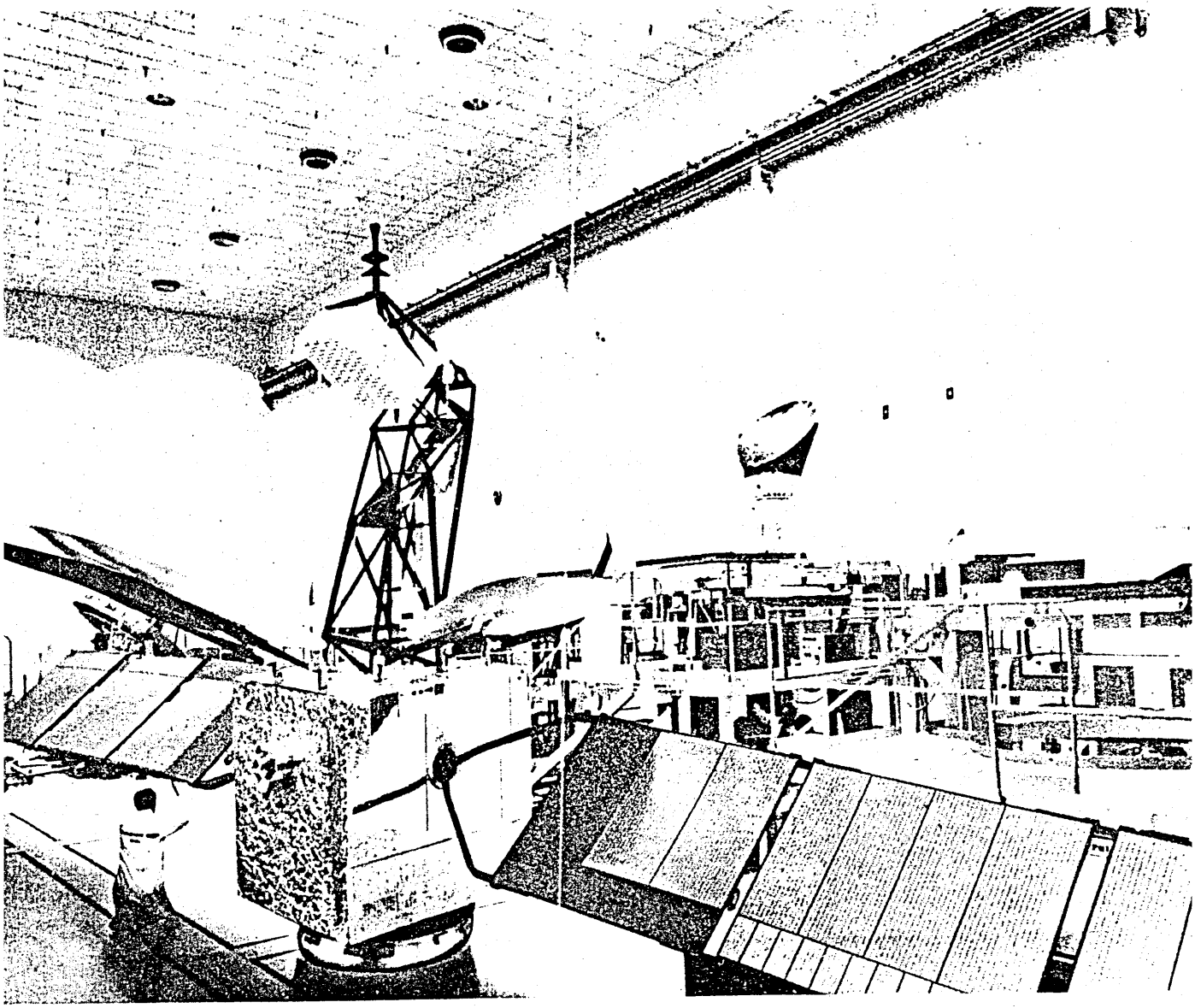

FIG 2.6 INTELSAT V

From / To	West Spot	East Spot	West Hemi	East Hemi	Zone 1	Zone 2	Global
West Spot	(1–2) (5–6) (7–12)	(1–2) (5–6) (7–12)	(1–2) (5–6)	(1–2) (5–6)	(7–8)	(7–8)	
East Spot	(1–2) (5–6) (7–12)	(1–2) (5–6) (7–12)	(1–2) (5–6)	(1–2) (5–6)	(7–8)	(7–8)	
West Hemi	(1–2) (5–6)	(1–2) (5–6)	(1–2) (3–4) (5–6) (7) (8) (9)	(1–2) (3–4) (5–6) (7) (8) (9)	(3–4) (5–6)	(3–4) (5–6)	
East Hemi	(1–2) (5–6)	(1–2) (5–6)	(1–2) (3–4) (5–6) (7) (8) (9)	(1–2) (3–4) (5–6) (7) (8) (9)	(3–4) (5–6)	(3–4) (5–6)	
Zone 1	(7–8)	(7–8)	(3–4) (5–6)	(3–4) (5–6)	(1–2) (3–4) (5–6) (7–8)	(1–2) (3–4) (5–6) (7–8)	
Zone 2	(7–8)	(7–8)	(3–4) (5–6)	(3–4) (5–6)	(1–2) (3–4) (5–6) (7–8)	(1–2) (3–4) (5–6) (7–8)	
Global							(7–8) (9) (10) (11) (12)

FIGURE 2.7 INTELSAT V BEAM INTERCONNECT CAPABILITIES

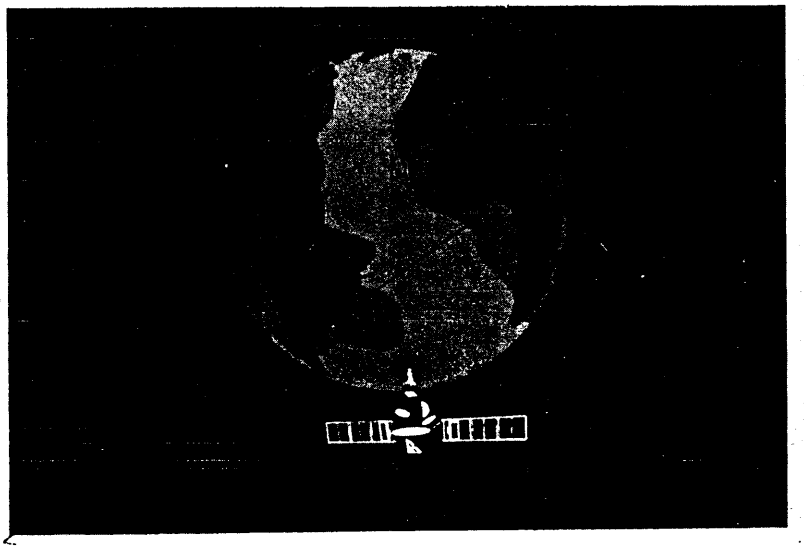

FIGURE 2.8 INTELSAT V SPOT, HEMI AND GLOBAL BEAMS (TEMP PHOTO)

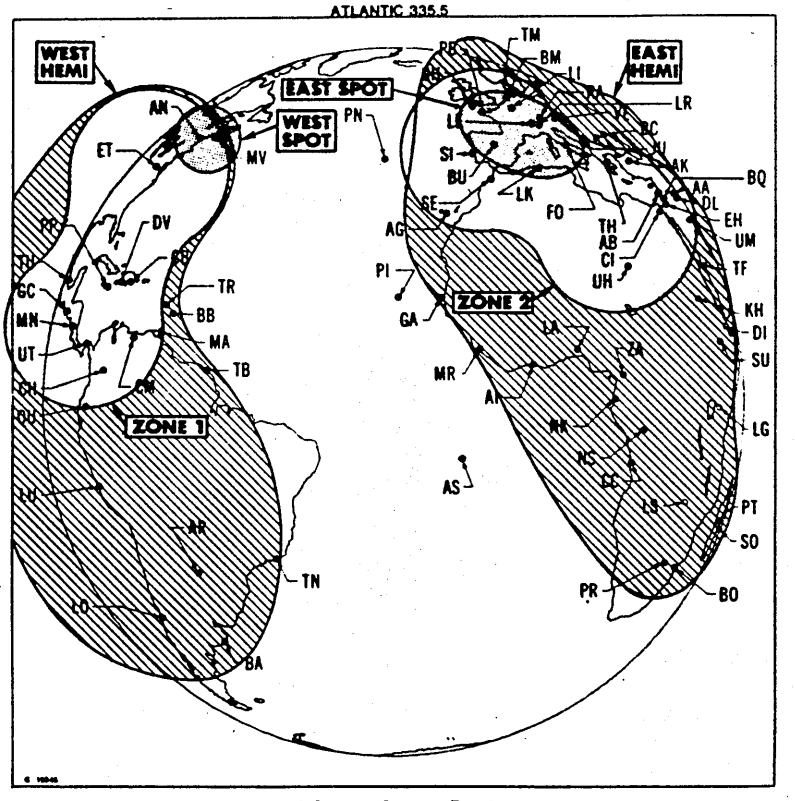

a. *Atlantic Ocean Region*

FIGURE 2.9 INTELSAT V ATLANTIC OCEAN REGION ANTENNA COVERAGE

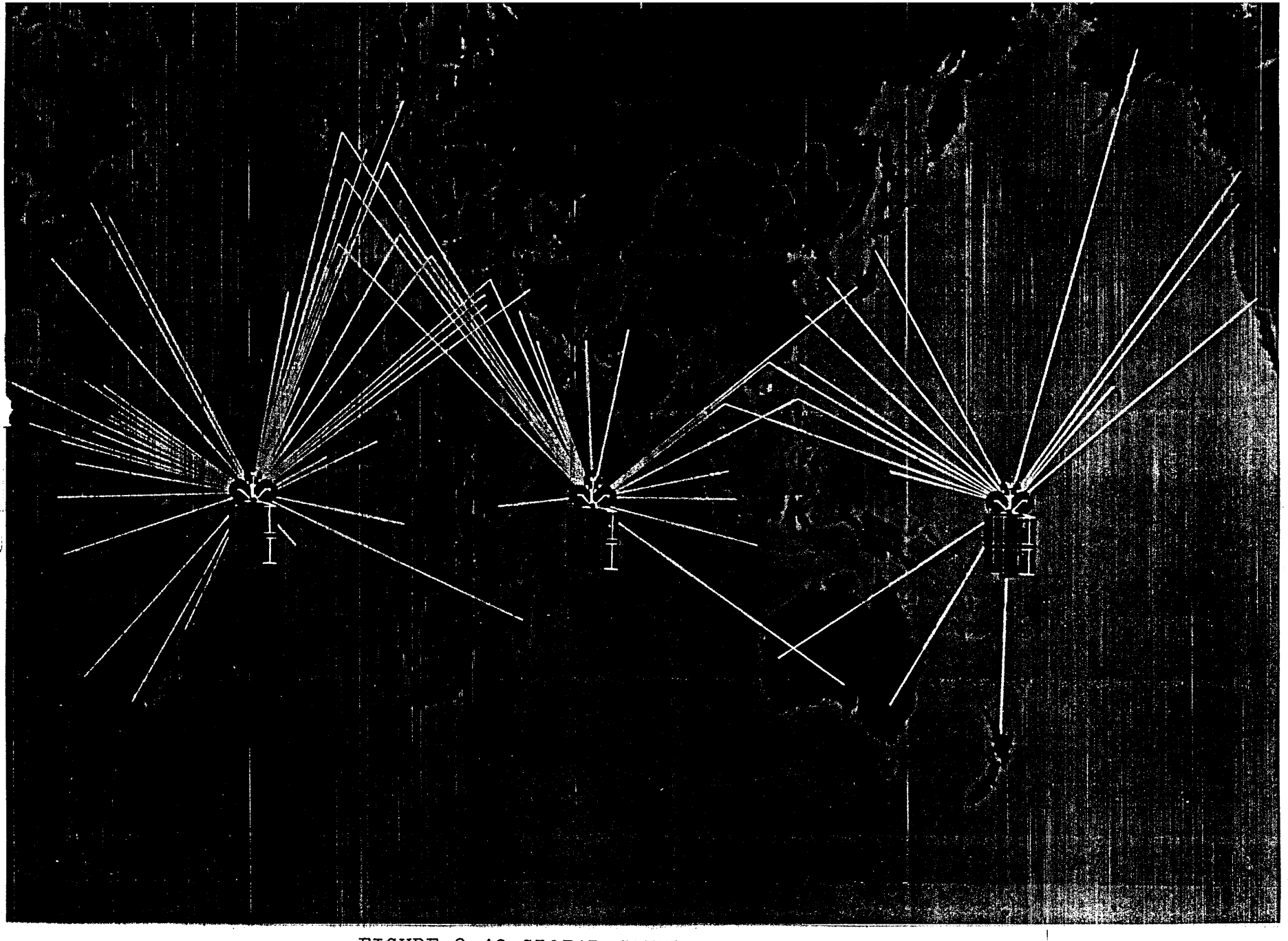

FIGURE 2.10 GLOBAL COVERAGE SATELLITE POSITIONS

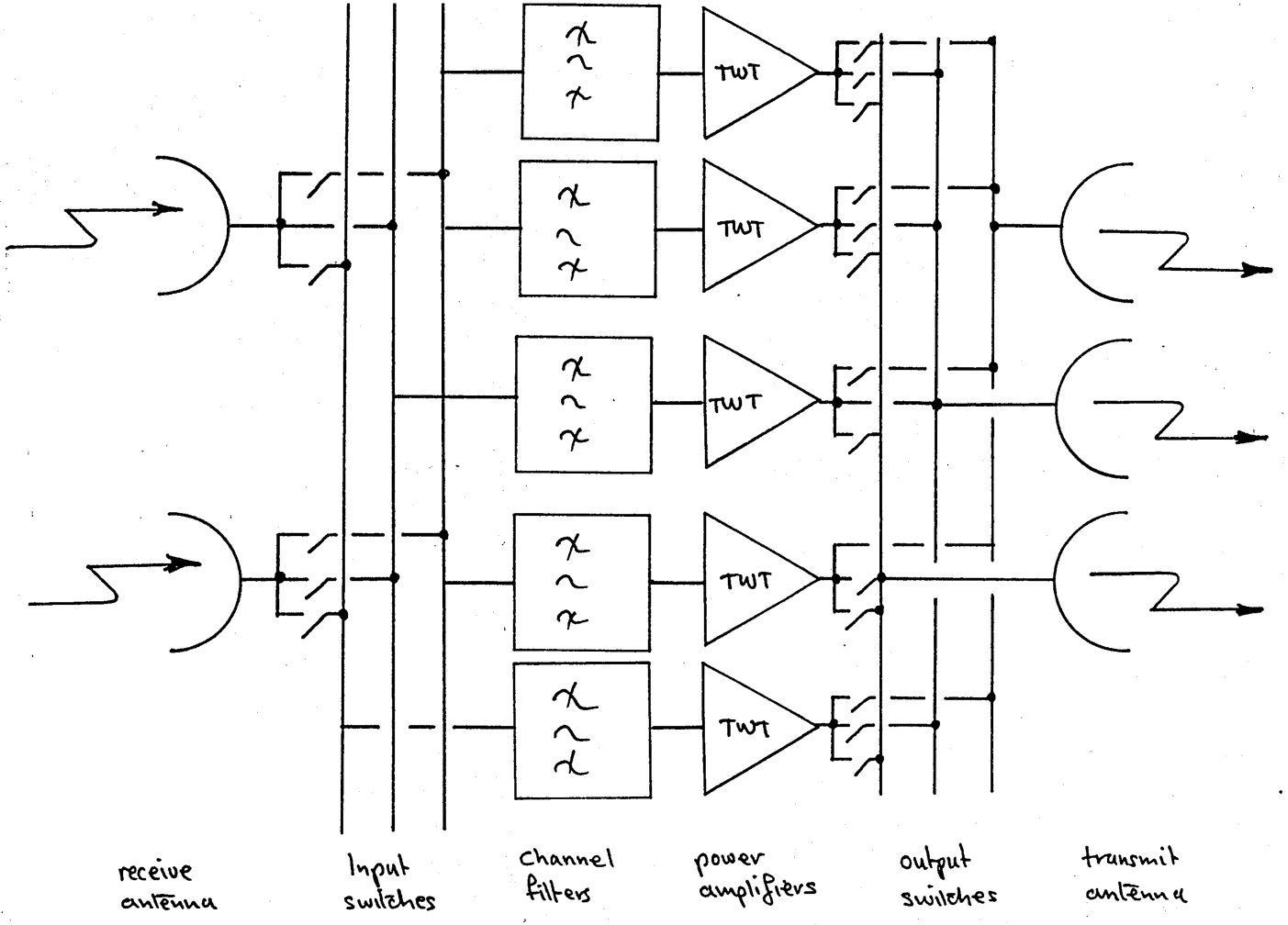

FIGURE 2.11 SIMPLIFIED SATELLITE CHANNEL SWITCHING ARRANGEMENT

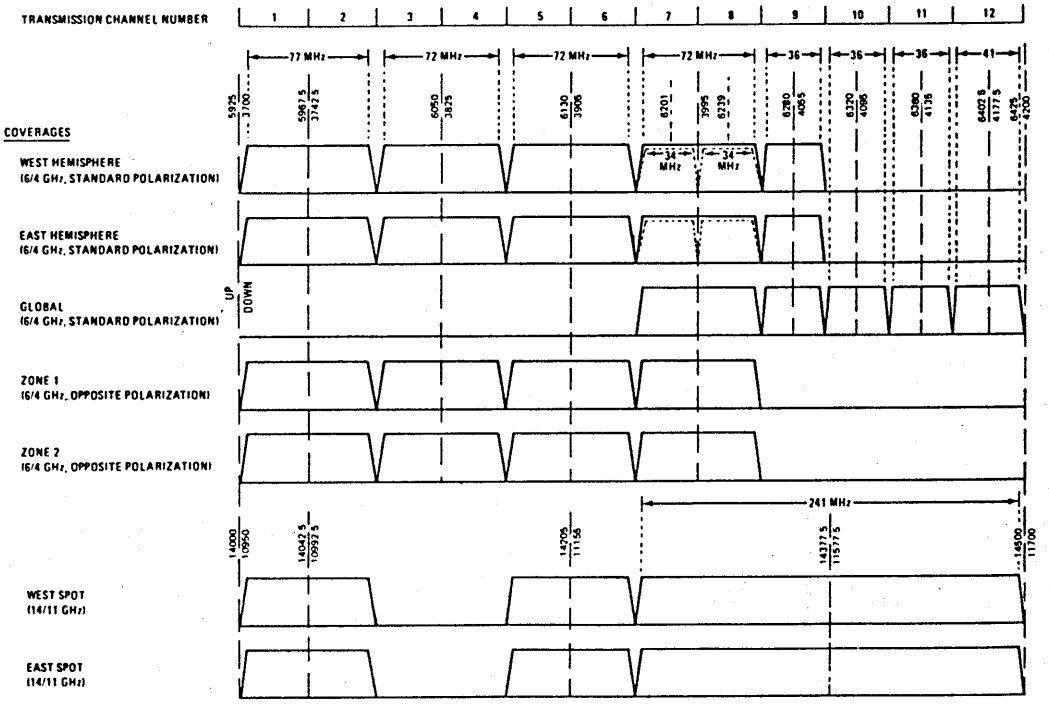

FIGURE 2.12 INTELSAT V TRANSPONDER PLAN

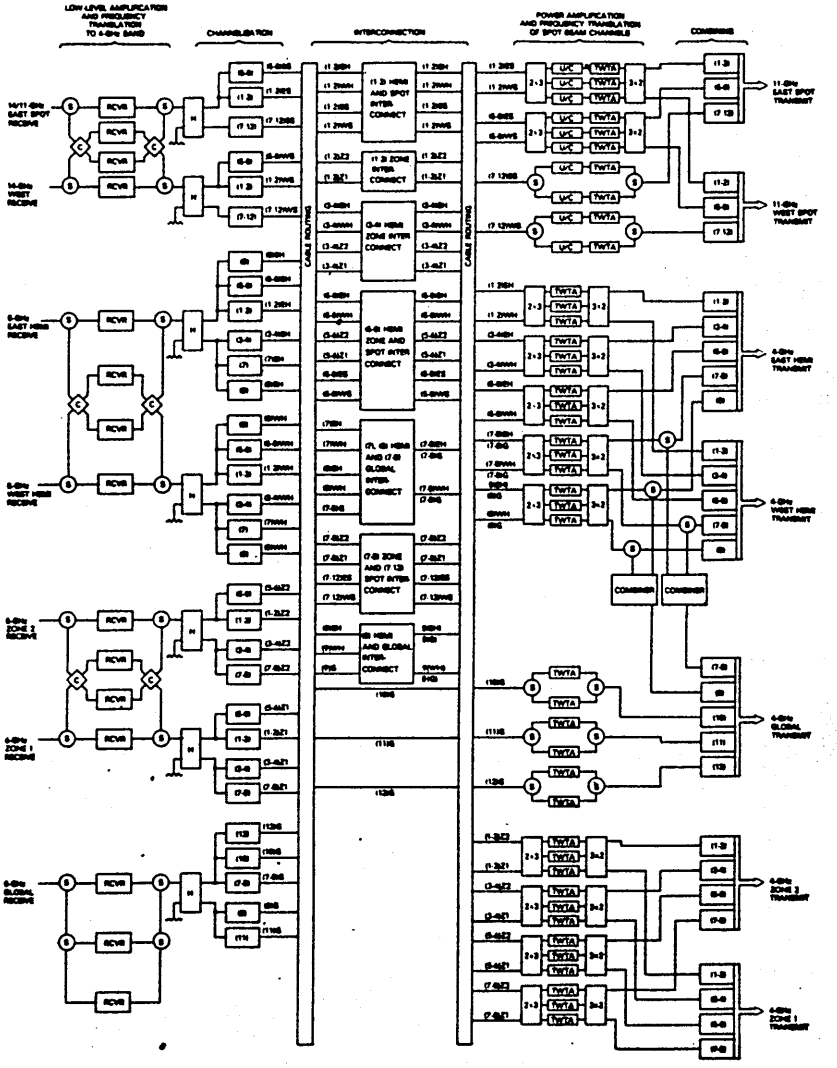

FIGURE 2.13 INTELSAT V COMMUNICATION SUBSYSTEM

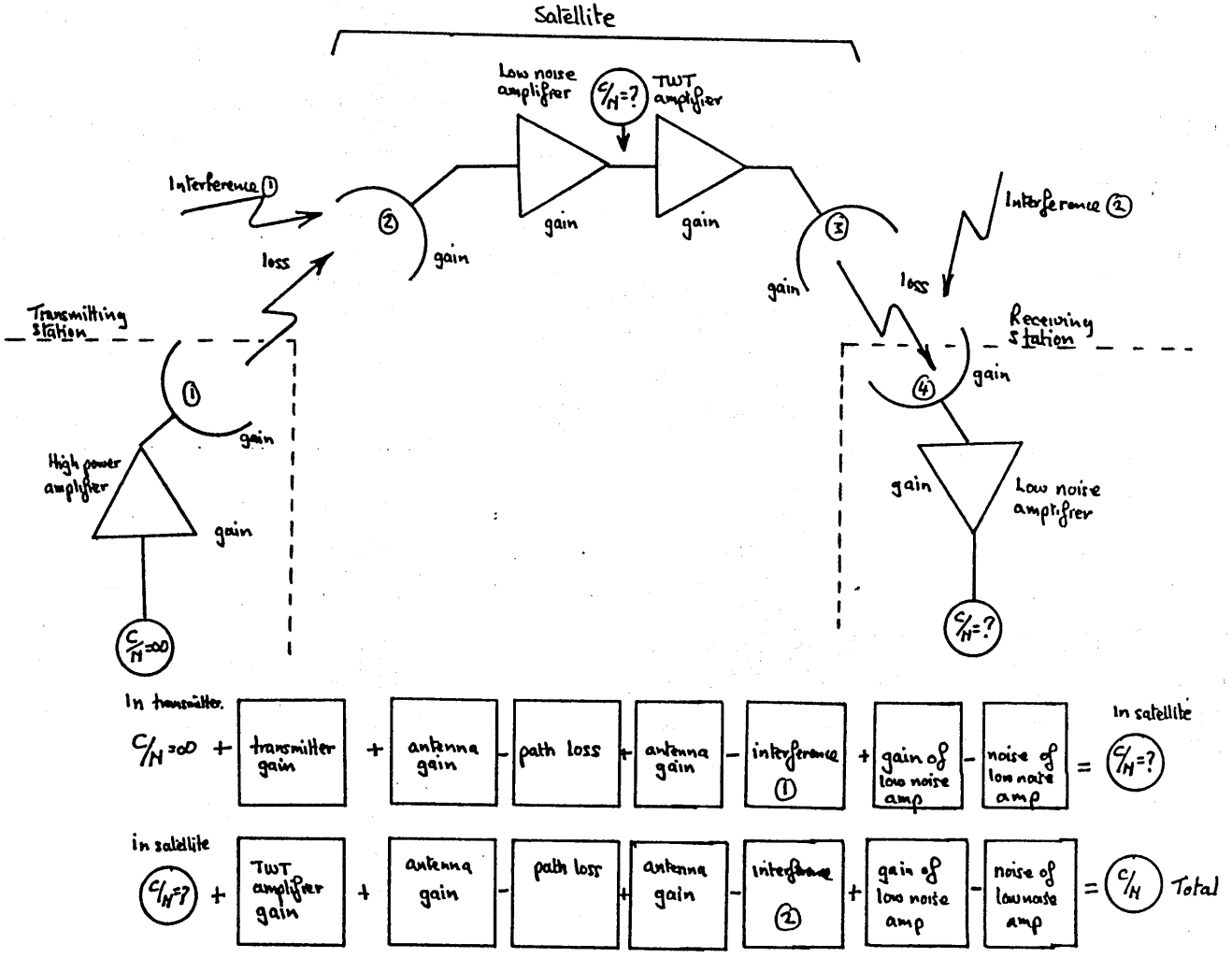

FIGURE 2.14 SIMPLE SATELLITE AND LINK BUDGET

SECTION 3

MODULATION SELECTION AND THERMAL NOISE PERFORMANCE

3.1 Introduction

Over the comparatively short history of commercial voice communications via satellite, a change of emphasis has occurred from power efficiency to bandwidth efficiency. This change has two causes: Firstly, technology has, to a large extent, alleviated the power limitation problem. Secondly, the remarkable increase in traffic has resulted in demands for satellite capacity which currently can only be satisfied by allocating bandwidth to that service. As was discussed in Section 2, INTELSAT has attempted to effectively increase the available bandwidth by reusing the same frequency bands by combinations of polarization discrimination and the use of spacially separated beams. These techniques are called frequency reuse. Each time the frequency is reused, interference is caused to all other users of those frequencies in the satellite. This is due to imperfect isolation between the beams containing reused bands. The isolation between beams is currently limited by antenna technology and the resulting interference sets the upper limit to the attainable channel performance. In general,

signal power cannot be used to overcome this interference since any improvement in one beam would be at the expense of all other beams using that frequency band. Thus, the satellite system is said to be interference and bandwidth limited not power limited. This can be seen from the link budget in Section 2 where the thermal noise power can be seen to be 4 dB less than the interference power level.

One area still open to further refinement is the modulation method. As other avenues become exhausted, attention becomes increasingly focused on the bandwidth efficiency of the signal modulation method.

To this purpose, much research has been devoted to the analysis of the performance of combined amplitude and phase modulation (APK) systems [9,10,11], which have been shown to require less average signal-to-noise ratio than PSK or ASK alone when the alphabet size is equal to or greater than 8 and a distortionless channel is perturbed only by additive Gaussian noise.

However, when digital data are to be transmitted over a satellite channel, a realistic analysis of the performance of a candidate modulation technique must consider the peculiar characteristics of such a channel.

The purpose of this Section is to select and evaluate the thermal noise performance of candidate APK signal sets suitable for increasing the channel capacity of the overall INTELSAT TDMA/DSI system. This performance is displayed in terms of bit-error-rate (BER) probability versus Carrier-To-Noise Ratio (C/N).

In order to exhibit a distinct advantage over the existing QPSK transmission system, the selected digital modulation method should exhibit tolerance to thermal noise, bandwidth constraints, interference and satellite link distortion (the tolerance to bandwidth constraints should lead to greater bandwidth efficiency). For practical reasons, the selected system must be compatible with the existing QPSK/TDMA system (Reference 41) and should also be simple to implement, test and align.

In this section, candidate modulation methods are discussed and selected methods are further analyzed in terms of transmission performance. However, in this section, only the effect of band-limited Gaussian noise is considered. The other forms of transmission impairments will be described and considered later in Sections dealing with Linear Channel, Non-Linear Channel and modulator/demodulator considerations. For each candidate system, the approach used is to specify the system in the (vector)

message space, define the particular decision boundaries to be used, and to derive expressions for the probability of the received signal plus noise being outside of these boundaries. Finally, the expressions are combined in order to determine the resulting BER as a function of signal-to-noise ratio for an ideal demodulation system employing the defined decision bounds.

In particular, the requirement to examine 8-phase PSK together with several types of APK has led to the development of a specific method of analysis chosen because of its general applicability to all classes of phase and amplitude digital modulation schemes, which employ straight line decision bound.

As shown in the Annex 1, this method provides a uniform analysis tool for both PSK and APK schemes, and where the signal constellation and decision bound geometry permits, one derivation can satisfy widely different modulation schemes.

3.2 Signal Characterization

The analysis views the candidate methods in a vector space. In order to reduce the analytical work to manageable proportions, pre-screening of the identified

candidates is worthwhile. For this purpose, drawings of the candidate methods (also in vector space) are used. These are called signal space diagrams. Signal space diagrams will be shown to be a powerful tool in the understanding of the degradation mechanisms in the satellite link and will be developed from the very simple types used in candidate signal set evaluations to more complex types which derive from the interaction of filters and non-linearities.

In this subsection, signal space diagrams are shown for a variety of candidate modulation methods ("signal sets"). For the more promising methods, expressions are presented that mathematically represent the signal sets and to derive their theoretical error rate versus additive thermal noise performance. For the chosen method(s), a computer simulation was used to verify the mathematical analysis. Firstly, PSK is described, and as indicated earlier, subjected to the same mathematical analysis as the other candidates ("other" candidates because 8-phase and 16-phase PSK systems must be considered as a candidate M-ary modulation method).

3.2.1 Phase Shift Keying (PSK)

The term PSK, or (in 4 level systems) QPSK, defines only the most fundamental characteristics of the modulation scheme, i.e., that information is transmitted by the possible phase states of the carrier. (It will be seen later that the manner by which the carrier changes states has a strong influence on the transmission performance, particularly in a non-linear channel).

In a digital PSK system, digital data are transmitted by the transmission of a carrier of constant amplitude (V_{pk}), constant angular frequency (w_c), but having different relative phases chosen from an alphabet of discrete and well defined steps. The signal space diagram for a QPSK system is shown in Figure 3-1. Such an alphabet or set of message signals, s(t), may be described by the general function:

$$s(t) = V_{pk} \cos [w_c t + \phi(i)]$$

where i indicates the selected signal from the alphabet set.

For equal steps in phase, this message signal can also be represented by:

$$s(t) = \sqrt{\frac{2E}{T_0}} \cos\left[\omega_c t + \frac{2\pi i}{m}\right]$$

where:

E = energy content of the message signal s(t) for one symbol,

T_o = duration of the symbol,

m = number of symbols in the symbol set.

In essence, the function of the demodulator is to determine which relative phase has been transmitted and to accomplish this in the presence of additive Gaussian noise and interference. In practice, the received signal is sampled at the system symbol clock rate at a point midway in the duration of the symbol. The decision as to which phase has been transmitted is taken at the sampling instant. (Sampling is employed because the intersymbol interference associated with the transmission of digital signals through a bandwidth limitation is at a minimum at the midway point in the symbol duration as will be seen later in Section 4).

Coherent detection is accomplished by generating an accurately phase sychronized reference signal in the demodulator, with which the incoming PSK signal is compared. In practical demodulators, methods are available to ensure an essentially noise and jitter free reference signal to an acceptable accuracy.

The performance of any digital system is partly characterized by the probability of transmission noise causing an incorrect decision or error. In a PSK system, digital information is conveyed by the phases of a carrier signal varying (relative to some local reference) in a quantized manner in sympathy with the modulating (baseband) signal. At the receiver, a decision is made as to which phase has been transmitted by comparison with the local reference phase. An error occurs when noise accompanying the wanted signal causes the receiver to incorrectly interpret the received signal. Figure 3.1 shows a generalized PSK system having four degrees of freedom. In this four phase system, an error will occur if a noise component has an amplitude/phase characteristic sufficient to produce a resultant (wanted carrier plus noise plus interference) signal which will fall across the decision bound. Note that each signal constellation point has only two straight line bounds associated with its x-y plane. Note also that the figure shows the "signal space

diagram" which traces the trajectory of all possible changes in phase states. [This type of figure is to be used extensively in the analysis of the non-linear channel].

3.2.1.1 PSK Error Rate Characteristic As A Function Of Noise

The CCITT sets performance requirements for digital transmission systems in the form of bit error rates (BER). In consequence, a system analysis starts by considering the BER performance for various signal to noise ratios.

The detailed error rate/noise analysis is contained in Annex 1, and the results are well established [12,13]. In this section the stages in the method will be highlighted and the results quoted. The approach used is to specify a PSK + additive Gaussian noise system in the message (vector space), in order to determine the resulting BER as a function of signal-to-noise ratio for an ideal demodulation system.

Examination of Figure 3.1 shows that the straight line decision bounds for M-ary PSK will always be in the form of a "pie" around the constellation point. Thus,

only two decision bounds require consideration. Furthermore, since the geometry is symmetrical and identical for all signal vectors, only one derivation is required. The derivation results are as follows:

QPSK $$P_e = \text{erfc} \frac{1}{\sqrt{2}} \sqrt{C/N}$$

8-phase PSK $$P_e = \text{erfc} \left[\frac{\tan \pi/8 \quad \sqrt{C/N}}{\sqrt{1 + [\tan \pi/8]^2}} \right]$$

where P_e is the probability of error.

This is shown plotted in Figure 3.2 in the form of BER versus C/N for the 4-phase and 8-phase cases. These standard results show three well defined regions, asymptotic to the horizontal axis, asymptotic to the vertical axis and a transition region. At poor signal/noise ratios (worse than 3 dB), the error rate performance tends towards a limiting condition of 50% error rate, whereas at very good signal to noise ratios (better than 25 dB), the error rate tends to a limiting condition of no errors (BER = ∞). The region displayed in Figure 3.2 is the transition region, which because of the practical significance of the carrier to noise power ratios and corresponding error rates, is the region of greatest usefullness to the system designer.

These curves, however, still show some of the tendencies of the extreme (limiting) cases, such that the improvement in BER for a given C/N increase is greater at higher C/N ratios than for the lower ratios.

BER versus C/N curves form a basic tool in system analysis and will be used extensively (together with their varients) in the subsequent sections in order to assess the performance of the digital channel.

3.2.2 Amplitude Phase Keying (APK)

The purpose of this section is to identify, describe and quantify octonary APK signal sets which appear to have performance and/or implementation advantages in the INTELSAT TDMA environment. Designs minimizing peak power are of interest because in the TDMA system, only one carrier is present in the satellite transponder's TWT at a time enabling the TWT to be operated at or near maximum power output (saturation), hence, the system is peak power limited.

The optimum APK signal set will be initially defined as one that minimizes the average probability of symbol error in thermal noise under ideal conditions. It

should not be concluded that a universal optimum has been discovered. An optimum is critically dependent on its environment.

Modulation techniques combining amplitude and phase keying have been proposed by several authors[14,15,16]. These authors have suggested various signal set designs which are shown to require less peak or average power than the equivalent PSK system to achieve the same error rate. Many, if not all, of these preliminary analysis assumed an ideal, distortion-free channel which is an extremely poor approximation to a satellite link. Additionally, an additional practical constraint is necessary, this being that the selected method should be entirely compatible with the existing INTELSAT QPSK/TDMA system. In this section, only the thermal noise performance will be assessed. However, some concessions for subsequent system constraints are necessary to simplify future work, specifically the need to address error rate versus peak C/N conditions.

3.2.2.1 Selection of Candidate Signal Sets - A Discussion

Much research has been devoted to the performance of combined amplitude/phase modulation systems. It has been well established that these systems perform better

than PSK for alphabet sizes of 8 and higher. From the available solutions, an 'optimum' must be selected and "fitted" to the INTELSAT TDMA system. Thus, it seems appropriate to briefly review the previous work.

The principal theoretical work was performed by B. Dunbridge[17] as he extended the work of Weber[15] and Balakrishnan[18] to asymmetric signal design. He disproved an earlier claim of Lucky and Hancock[2], that equal spacing of the signals about the unit circle was optimum for small carrier-to-noise ratios (CNR).

Lucky and Hancock have investigated the problem of optimum APK signal design using a "building block" approach for the calculation of the error probabilities for certain signal-plane decision regions. The resulting approximation for total symbol error probability was then differentiated with respect to the signal amplitudes and phases to determine optimum design.

Lucky and Hancock give specific designs for both high and low CNR. The computational complexity associated with the differentiation of a large number of complex variables subject to the specified constraints makes it difficult to extend their results to higher alphabets. Also, as mentioned above, their approximations for the

error probability do not lead to the correct results for low SNR. Results obtained in a comprehensive study performed by TRW under INTELSAT sponsorship[19], showed Lucky and Hancock's results for high CNR are also incorrect for M = 8 and 16.

Some theoretical guidance for very large signal sets is available from Shannon[19] and Blachman[20] in their consideration of the signal statistics of optimum analog AM and PM systems at high CNR. Shannon has shown that under an average power constraint, the channel capacity is maximized with a signal that is uniformly distributed in phase and Rayleigh distributed in amplitude. However, in the case of interest (peak power constraint) the capacity is maximized by a signal uniformly distributed in phase with an amplitude probability density which increases linearly with amplitude up to the peak amplitude constraint.

The approach employed in Reference 18 has been extended by the author to use these available theoretical results as guidelines in an empirical search for good designs which are compatible with INTELSAT TDMA system. Reasonable designs are then chosen as candidates to be evaluated for link performance.

In this study only octonary candidate designs will be considered, primarily due to the need to increase the INTELSAT TDMA system's channel capacity without modifying the symbol rate (all currently identified higher alphabet designs (including 16-phase PSK) require a carrier-to-noise ratio greater than the INTELSAT V channel can provide). Most of these designs fall into four categories: those with the signal vectors arranged on concentric circles and those with triangular, rectangular or hexagonal grid arrangements. The circular and the rectangular sets are attractive because of their implementation convenience. The triangular sets yield high performance because over an infinite plane, triangular packing is very efficient.

In the following discussion and figures, the signal designs have been scaled such that, for all but the circular sets, the nearest neighbor distance is unity. For the circular sets, the signals on each ring are (initially) separated by unity distance but the inter-ring distance is not unity.

3.2.2.2 Octonary Signal Sets

For octonary signal sets, five candidate configurations have been identified. These are shown in

Figure 3.3. In this and the following figures, minimum distance neighbors are connected and the scale is such that this minimum distance is unity.

The first design is a 3 x 3 grid minus the center point and belongs to the rectangular-decision-region category. This set is included due to its ease of generation and demodulation. The second and third candidates are a (1,7) circular set and a triangular design. The circular set appears, from principles set forth in the discussion, to be capable of good performance under peak and average power conditions, whereas the triangular set should perform well under average power conditions (more uniform amplitude distribution). The fourth is a double circle with four signals per circle, denoted as (4,4) design. This candidate is included because of its similarity to QPSK system (practical constraints). The fifth candidate is a variation of the fourth candidate where the outer circle is rotated 45° resulting in the signals lying on eight lines separated by 45°. This candidate should perform better under peak power conditions than the fourth candidate (inner ring closer to outer ring). However, it cannot be as easily generated from QPSK as the fourth set.

Two additional designs were investigated in Reference 18 but considered to be unsuitable as candidates. The hexagonal design, due to its 6-ary nature, cannot be formed into a reasonable 8-ary set. The (3,5) circular design is clearly inferior to the (4,4) design in terms of intercircle versus intracircle distances (poor peak power) and is not directly compatible with QPSK.

3.2.2.3 Selection of Signal Sets

To select a Signal Set for the final analytical process, the strengths and weaknesses of a particular candidate must be matched to the requirement of the system. In particular, since the TWTA's employed in the satellite are limited in peak power, preference (although not exclusively) should be given to those sets which are inherently better in terms of peak power, i.e., linear phase distribution and linearly increasing amplitude distribution. Compatibility with the INTELSAT QPSK/TDMA system is also a prime selection criteria.

Reference 19 compares (among many others) the performance of the first four candidates identified above. It concludes that the 1,7 design is optimum for peak power

while the other three candidates perform worse than 8 phase PSK. To the author, it is clear that the 1,7 design should perform better, it is not clear that the other methods should necessarily be inferior to PSK. Closer examination of the signal sets analysis in reference 15 shows that the inter-ring distances and mutual phase shifts were not varied with a view to improving the performance. A primary motivation of performing the current study arrives from compatibility of the new modulation method in the INTELSAT system with that already employed (i.e., QPSK). The 1,7 system rectangular and the triangular system do not have the advantage of the similarity with QPSK, however the 4,4 circular designs do. These designs can be viewed as two QPSK modulation systems accessing the same channel, the two being discriminated by different power levels. This is recognized even at this stage as being capable of affecting considerable implementation advantages. Furthermore, preliminary study showed that 4,4 circular design could be made to perform better than 8 phase PSK if the inter-ring distance was optimized. For these reasons, it was decided to study the two circular designs further (henceforth, referred to as Type A (4,4 circular) and Type B (4,4 offset circular).

3.2.2.4 APK Error Rate Characteristics As A Function of Noise

In this section, two octonary systems are examined, having been chosen for compatibility with the INTELSAT TDMA system and ease of implementation of the receivers. A description of the two modulation schemes is given, together with a discussion of the decision bounds which may be used. These models are then used to produce expressions for the error probability of both schemes in the presence of additive Gaussian noise. A detailed description of the method is contained in Annex 1.

3.2.2.4.1 Type A

The first PM-AM modulation scheme (Type A) uses two amplitude levels and 4 phase positions.

In Figure 3.4, the position of the signal points is presented, together with the optimum decision regions for the case of an additive white Gaussian noise channel (continuous line). (Optimum decision placement is assumed to be such that the error performance of all signal points are equal).

3.2.2.4.2 Type B

The second PM-AM modulation scheme (Type B) is an example of two in-quadrature 4-level PAM signals.

The signal space diagram is presented in Figure 3.5 together with the optimum decision regions.

3.2.2.5 Evaluation of Error Probability

Before embarking on a mathematical evaluation of the bit error probability as a function of carrier to noise ratio, it is necessary to review the placement of decision bounds. Initially, this review will use graphical methods.

Because of the amplitude factor in both schemes, the first natural consideration is a circular bound permitting straight envelope detection. However a cursory inspection of this regime reveals a number of disadvantages:

i) Type A and Type B performance becomes identical because for a given maximum amplitude the minimum noise amplitude to cause an error becomes identical.

ii) Because the circular bound is not centred on the tip of a signal vector, the available error-free space around the point is not maximized, i.e., the space around a signal vector tip is not distributed in such a way as to allow the maximum amplitude of noise while maintaining an error free performance.

To overcome these shortcomings, a more suitable bound is the line describing the locus of points equidistant from neighbouring points, which, for Type A would be of the from $y = a-x$ in the x, y signal space. A choice of such bounds exists for Type B schemes:

a) A line joining the origin to the bisection of the minimum distance between the two signal vector tips.

b) The locus of equidistant points. This will always have a positive slope but will only intersect the origin when the inner signal amplitude equals the outer signal amplitude, i.e., 8-phase PSK case.

Figure 3.6 shows the upper right hand quadrant of a Type A APK system, together with the lower right quadrant of a 8-phase PSK system for comparison purposes. For the APK set, the outer signal points are represented by x_o and y_o, each having 10 arbitrary amplitude units. The inner signal points are represented by x_1 and y_1, (whose distance from the origin will be varied in order to seek an optimum level). There are two decision bounds. The first is a straight line from the origin at 45° to the lines joining the two signal points to the origin. The second is a circular amplitude decision with its center on the origin, and a radius such as to place the bound between the x_1 and x_o signal points. In the 8-phase case, only one boundary is used at the 45° point. Considering firstly y_1, the lowest noise power which will cause an error is given by r_1 (to the x_1/y_1 decision bound) and r_2 (y_1/y_o decision bound). For the x_1 case, the distance to the x_1/x_o decision bound will be assumed to be also equal to r_2 and the distance to the x_1/y_1 decision is equal to r_1. The table in Figure 3.6 shows the manner by which r_1 and r_2 vary over the range $0 \leq y_1 \leq 10$. These are shown plotted in the insert graph. Also shown on this insert is peak power (= 100 arbitrary units, and average power computed as $(x_0^2 + x_1^2)/2$. For the 8-phase PSK

case, only r_1 is relevant and this is shown at 3.83 arbitrary units. Also for 8-phase PSK, peak power = average power = 100 arbitrary units.

The curves for r_1 and r_2 show an intersect at $x_1 = 4.2$. To a first order approximation, when $r_1 = r_2$, the error probabilities of x_1 and x_o are equal which produces the lowest overall combined error rate. Note that $r_1 = r_2 = 2.9$, which is less than the 8-phase PSK case at 3.83. This suggests inferior performance to 8-phase PSK. However, the Type A APK system uses significantly less average power ($\sim$2 dB).

3.2.2.6 Evaluation of the Error Probability for the Type B

A graphical approach is also taken initially for the Type B system (Figure 3.7). Again, in this case the upper right quadrant shows part of the APK system, while the lower right hand quadrant shows the 8-phase PSK. In the Type B system, x_o and y_o are of 10 arbitrary units magnitude and are orthogonal, while y_1 is at 45°. The y_1/y_o decision bound is the normal to the mid point between y_o and y_1. The x_1/y_1 decision bound is the line joining the origin and x_o. From this diagram, r_2 is seen to be the minimum noise power necessary to cross the y_1/y_o decision bound, while r_1 is the

corresponding x_1/y_1 noise component. The table shows how r_1 and r_2 vary over the range $0 \leq x_1 \leq 10$. The insert graph shows these results plotted. Note that the condition $r_1 = r_2$ occurs at $y_1 = 5$. This may be assumed to be the lowest error rate. Under these conditions, $r_1 = r_2 = 3.7$. However, 8-phase PSK has $r_2 = 3.83$ and again the performance seems inferior. Also plotted in Figure 3.7 is the average and peak power requirements showing again that APK requires significantly less average power.

Figure 3.8 shows the Type B system again, but this time with the simplified decision regions corresponding to the first proposal in Section 3.2.2.5. Using the same technique, an error bound is established as a circle with the center at the origin and with a radius equal to a point midway between y_o and y_1. As before, r_1 is the minimum distance to the x_1 and y_1 lines. However, the minimum for the y_1/y_o decision region is no longer r_2 but r_3 for y_1 and r_4 for y_o, since these are the minimum distances to the decision bound. Over the range $0 \leq x_1 \leq 10$, the results are shown in the insert graph. Note that, a simple average of r_3 and r_4 (r_5) intercepts r_1 at $y_1 = 4.2$ given an r distance of 2.9; exactly the same as the Type A system.

It is apparent that the performance of the Type B system can be degraded to the performance of the Type A system by the use of these greatly simplified boundary conditions.

3.2.2.7 Results and Comparisons of Two Methods

In this section, the algebraic results will be used in order to compare the candidate APK systems and to compare both modulation schemes with an octonary CPSK system.

The first problem to be analyzed is the optimum partitioning of the signal power between the amplitude levels, i.e., the choice of the signal level ring ratios.

3.2.2.8 Performance of Type A Schemes

It is apparent that decreasing the inner signal amplitude to a low value will decrease the errors associated with the outer signal at the expense of the inner signal. Conversely, there will be some amplitude at which the errors associated with both signals will increase proportionately due to the equal proximity to the decision bound. The analysis contained in Annex 1 supports this hypothesis, and shows that BER is minimumn for k = 0.42 (Figure 3.9) in the following expression:

$$BER = \frac{1}{2}\left\{erfc\frac{1}{\sqrt{2}}\sqrt{\frac{C}{N}} + \frac{1}{2}erfc\frac{(1-k)}{2}\sqrt{\frac{C}{N}} + erfc\frac{K}{\sqrt{2}}\sqrt{\frac{C}{N}} + \frac{1}{2}erfc\frac{(1-k)}{2}\sqrt{\frac{C}{N}}\right\}$$

where $\left\{erfc\frac{1}{\sqrt{2}}\sqrt{\frac{C}{N}} + \frac{1}{2}erfc\frac{1-K}{2}\sqrt{\frac{C}{N}}\right\}$ is the

error probability associated with outer signal,

and $\left\{erfc\frac{K}{\sqrt{2}}\sqrt{\frac{C}{N}} + \frac{1}{2}erfc\frac{(1-K)}{2}\sqrt{\frac{C}{N}}\right\}$ is the

error probability associated with the inner signal,

and $k = \dfrac{\text{inner signal amplitude } (A_i)}{\text{outer signal amplitude } (A_o)}$ (ring ratio)

and $C = \dfrac{A_o^2}{2}$

These results are shown in Figure 3.10.

3.2.2.9 Performance of Type B Schemes

Both decision bounds discussed above have been analyzed (Annex 1), and it is shown that the method employing true locus of the equidistant points is

optimum. The functions involved show that this bound exhibits a minimum overall error probability when the amplitude ratio is approximately 0.54. This arises from the following interaction. At a ratio of unity, performance and decision bounds are identical to 8-phase PSK. As the inner signal amplitude decreases, the straight line distance to the next signal point decreases until a minimum is reached at 0.707. Further decreases in the amplitude will now increase the separation resulting in decreased error probability associated with the locus bound. However, the inner signal is now approaching the quadrature bounds of the x-y axes and thus error probabilities begin to increase once again. The mimimum is pronounced and for all practical C/N ratios, is given by k = $\frac{0.54}{\sqrt{2}}$ in the following expression:

$$BER = \frac{1}{2}\left\{ erfc\sqrt{\frac{C}{N}}\,\frac{1-K}{K}\,\frac{1}{\sqrt{1+\left(\frac{1-K}{K}\right)^2}}\,\frac{\sqrt{(1-K)^2+K^2}}{2\cos\left[\tan^{-1}\frac{K}{1-K}\right]} + erfc\sqrt{\frac{C}{N}}\,\frac{\sqrt{(1-K)^2+K}}{\sqrt{1+(1-2K)^2}}\,\frac{|1-2K|}{2\cos\left[\tan^{-1}\frac{1}{|1-2K|}\right]} + erfc\,K\sqrt{\frac{C}{N}}\right\}$$

Substitution of k = $\frac{1}{\sqrt{2}}$ will yield 8-phase PSK BER.

These results are also shown in Figure 3.10.

3.3 Summary

Traditionally, INTELSAT has sought to increase the traffic capacity of satellites by increases in transmitted power level and by reuse of the allocated bandwidth by spacial and polarization separation techniques. This combination is becoming incapable of satisfying the ever increasing capacity demands because the resulting severe co-channel interference is leading to a situation of diminishing returns. Accordingly, attention is directed to alternative forms of modulation which can increase traffic carrying capacity without requiring increases in transmitted power. (i.e., more power efficient methods). In this section, the theoretical BER vs C/N performance of various 8 level techniques has been examined, together with 4-phase PSK. Before being able to compute the bit error rate (BER) performance of the APK candidates, it was necessary to optimize the amplitude ratios of the inner and outer signal sets (ring ratios). This was accomplished using simple graphical techniques and using a unified error rate expression developed by the author and shown in Annex 1. The results show that 8-phase PSK performs better than two simple forms of amplitude/phase (APK) hybrid modulation, when the analysis is performed solely on the basis of BER

vs peak signal to noise ratio. Specifically, at a BER of 10^{-6}, 8-phase PSK requires 0.5 dB less C/N than APK-B, with an optimum ring ratio of 0.54 and 2.4 dB less than APK-A, with a ring ratio of 0.42. Accordingly, if there were no other considerations, (i.e., if the satellite channel were truly linear and only corrupted by Gaussian noise) 8-phase PSK would be chosen. However, this is not the case. In particular, since the channel performance shown in the link budget in Table 2.2 is dominated by mutual interferers and since the <u>average</u> power of APK modulation schemes is less than the corresponding PSK case, the overall performance in a practical system may produce a different optimum choice.

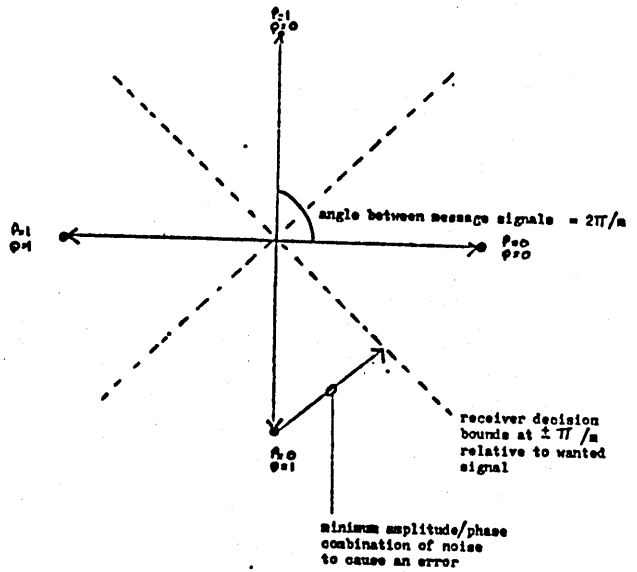

where i = constituent member of the code alphabet of the size m

A generalised M(ary) PSK system

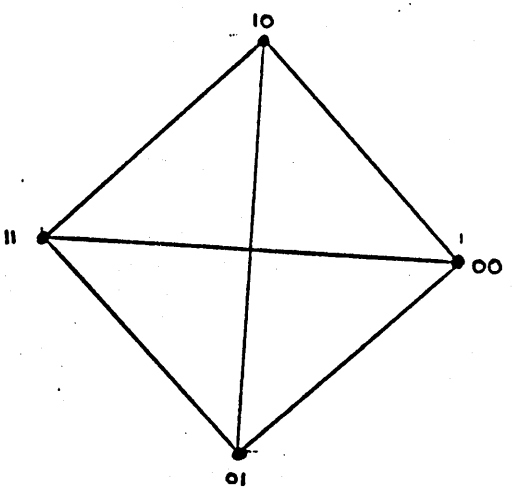

SIGNAL SPACE DIAGRAM

FIGURE 3.1 FOUR PHASE P.S.K.

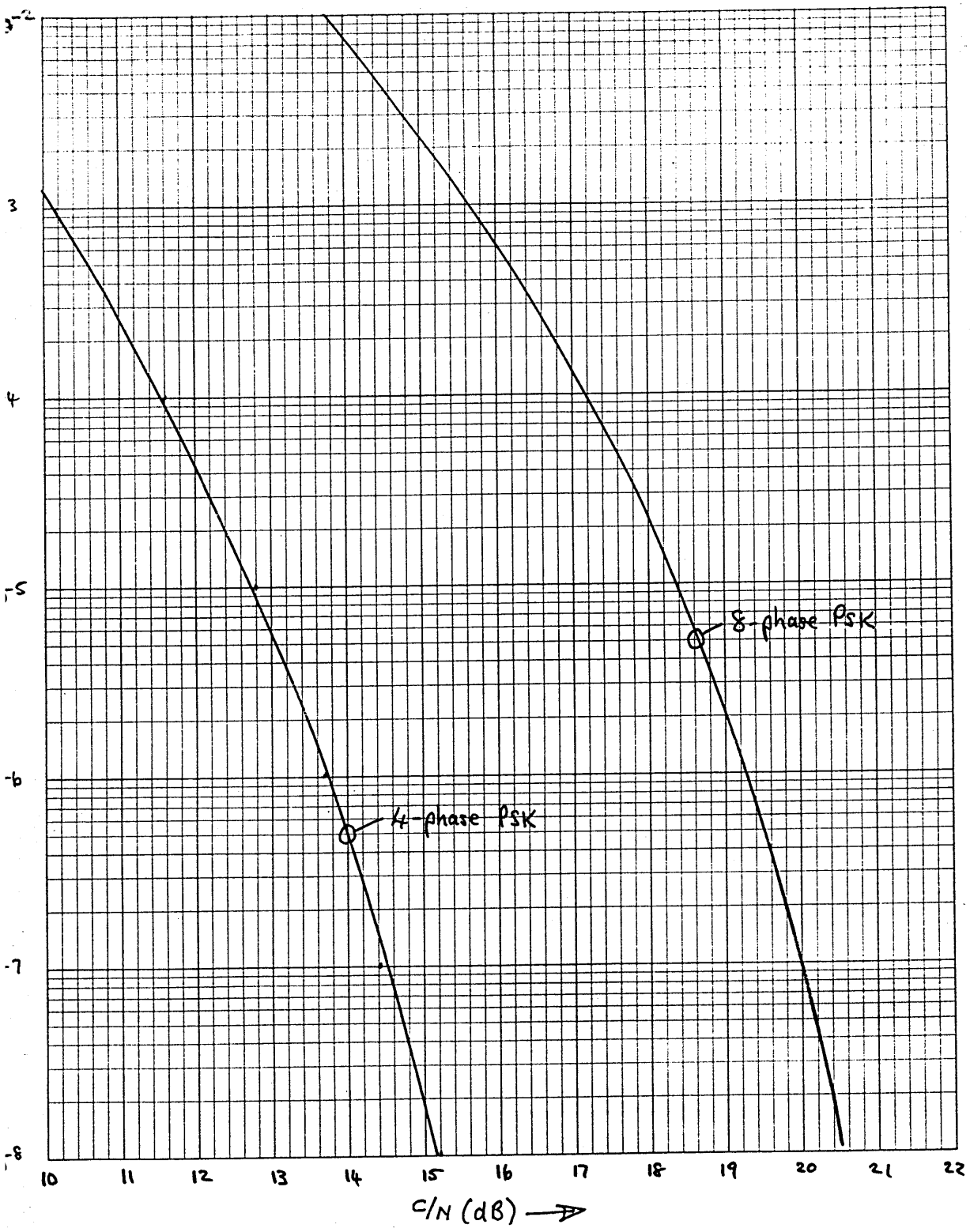

FIGURE 3.2 BER VS C/N FOR
4- PHASE 8-PHASE

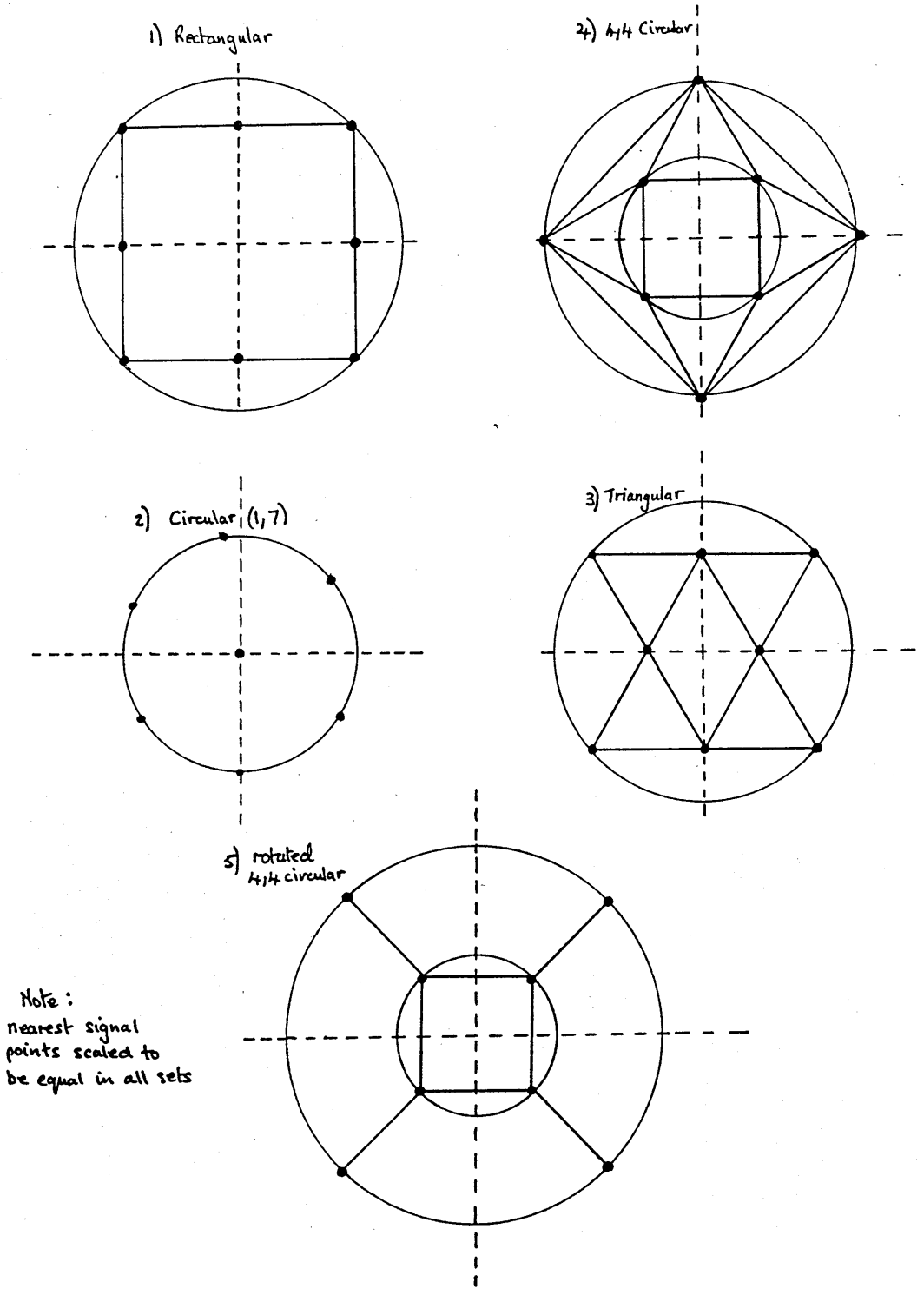

FIGURE 3.3 OCTONARY SIGNAL SETS

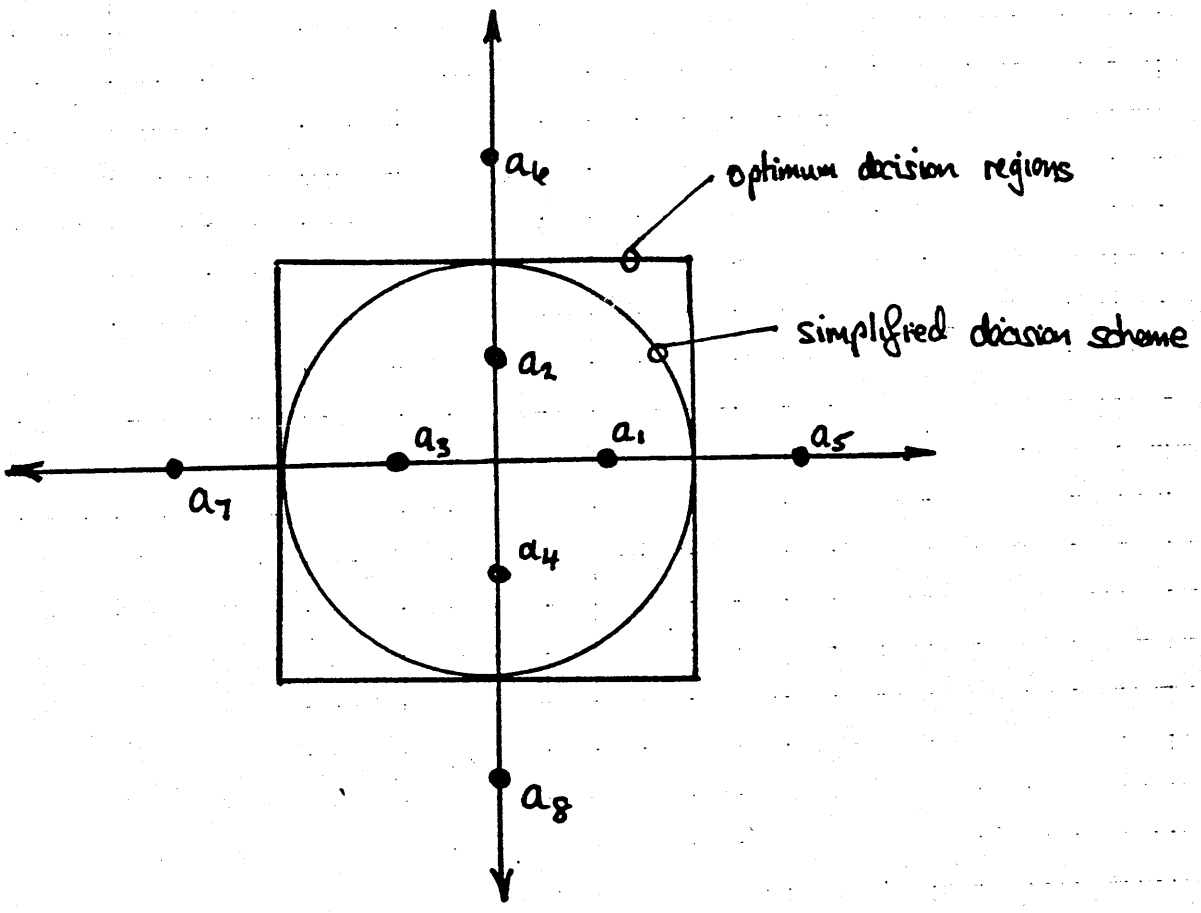

FIGURE 3.4 TYPE A APK SIGNAL
SPACE DIAGRAM

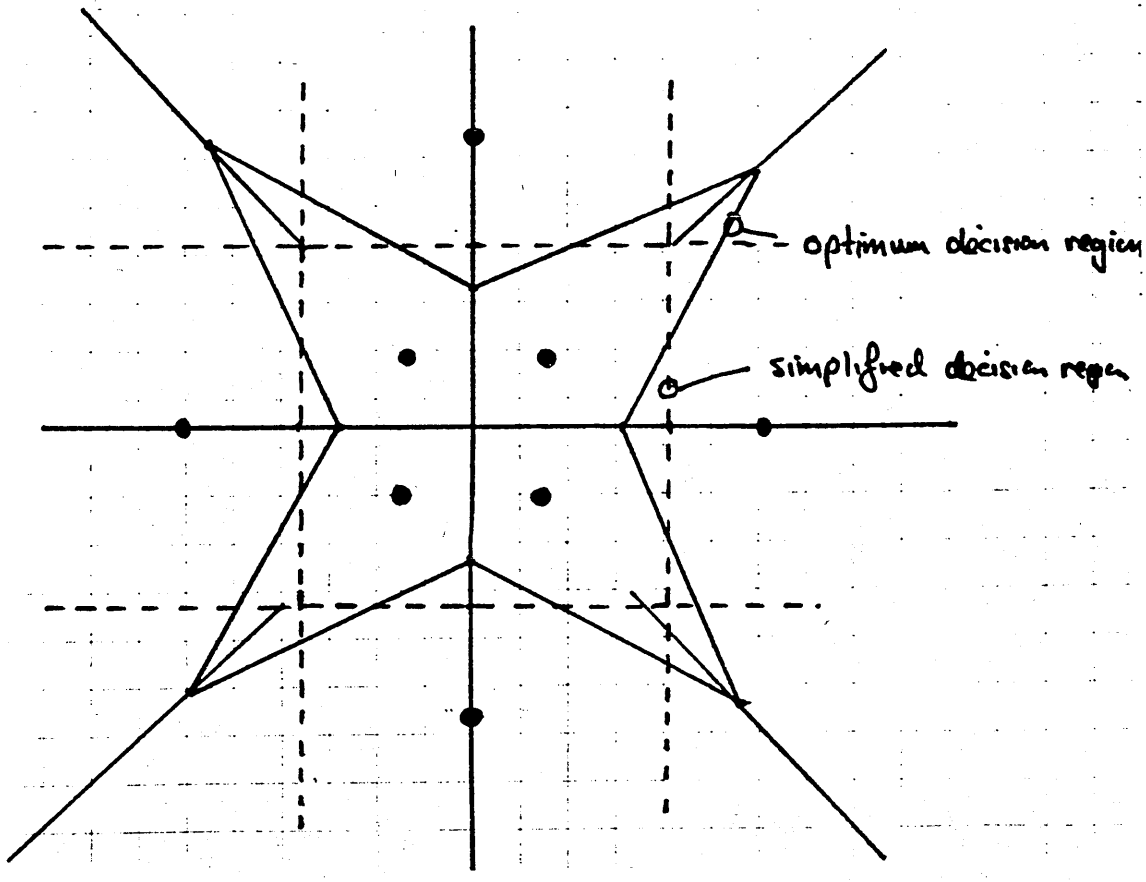

FIGURE 3.5 TYPE-B APK SIGNAL
SPACE DIAGRAM

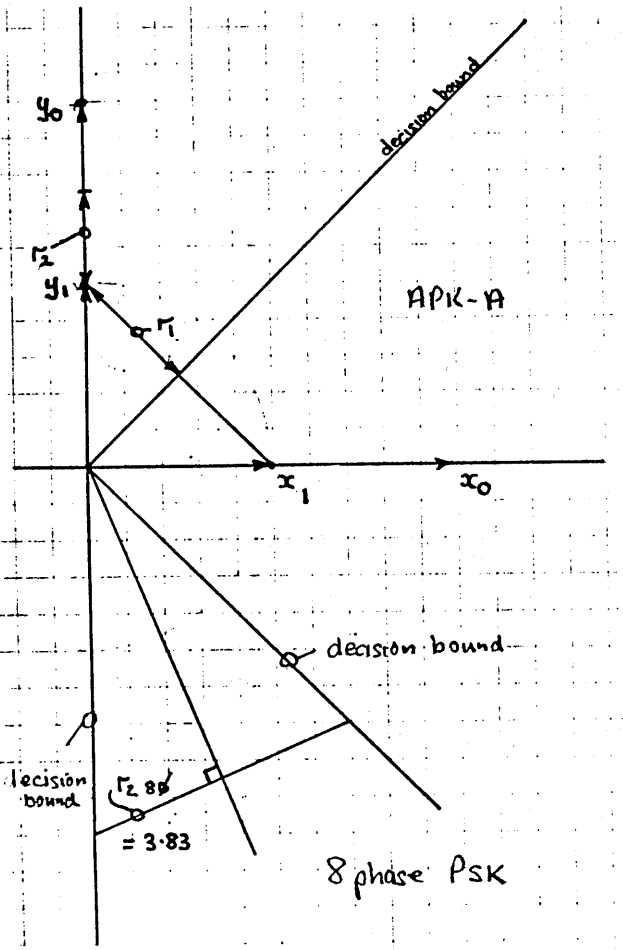

y_1	r_1	$2r_2$	r_2	P
1	0·707	9	4·5	50·5
2	1·414	8	4	52
3	2·12	7	3·5	54·5
4	2·83	6	3	58
5	3·53	5	2·5	62·5
6	4·24	4	2	68
7	4·95	3	1·5	74·5
8	5·66	2	1	82
9	6·36	1	0·5	90·5
10	7·07	0	0	100

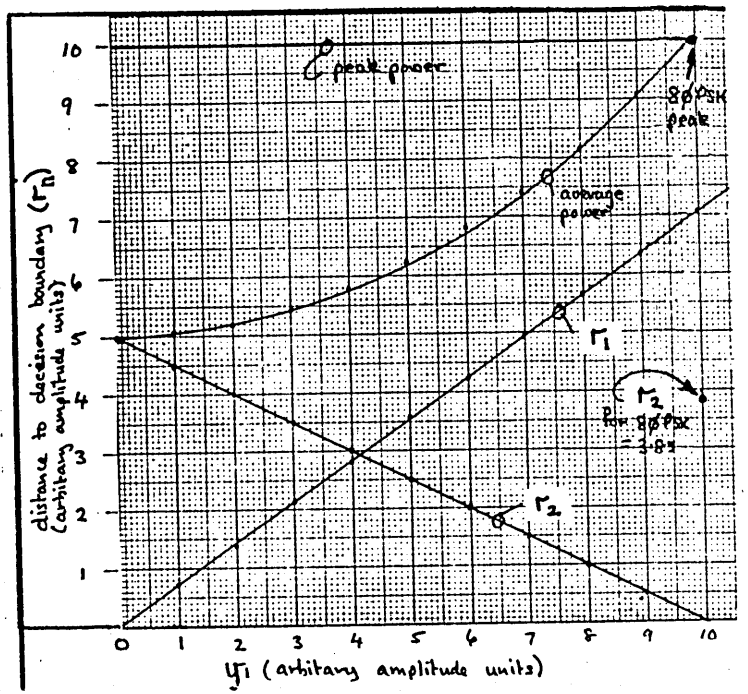

FIGURE 3.6 TYPE-A APK SYSTEM VARIATIONS IN DECISION BOUND PLACEMENT

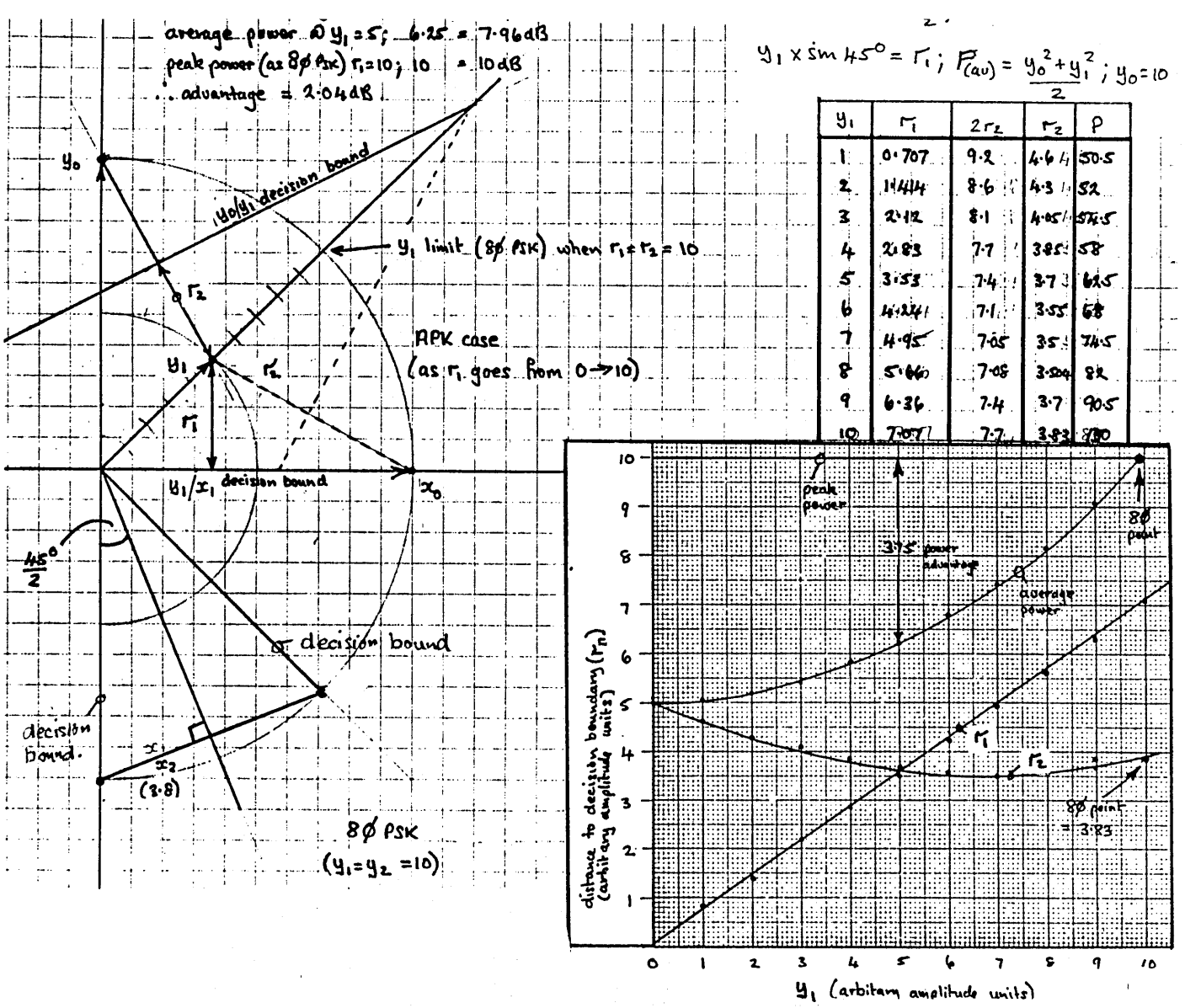

y_1	r_1	$2r_2$	r_2	P
1	0·707	9·2	4·64	50·5
2	1·414	8·6	4·3	52
3	2·12	8·1	4·05	54·5
4	2·83	7·7	3·85	58
5	3·53	7·4	3·7	61·5
6	4·242	7·1	3·55	68
7	4·95	7·05	3·5	74·5
8	5·660	7·05	3·524	82
9	6·36	7·4	3·7	90·5
10	7·07	7·7	3·83	100

FIGURE 3.7 TYPE-B APK SYSTEM
VARIATIONS IN DECISION
BOUND PLACEMENT

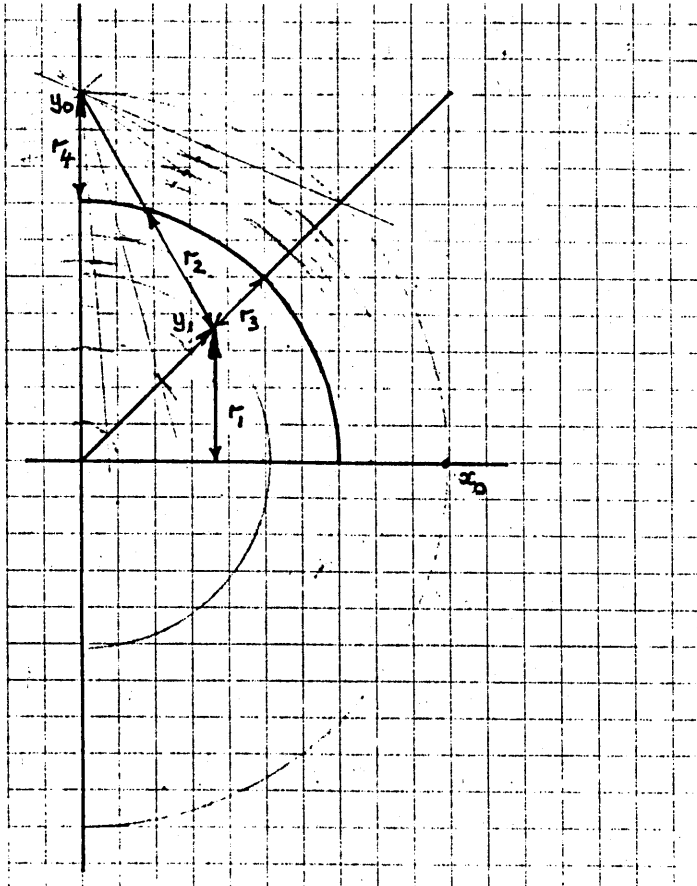

instead of r_1 and r_2 (=3.5 when optimum) we have r_3 (=2.1) and r_4 (=2.9) when r_1 is set to optimum on other basis (ie $r_1 = r_2$) ($y_1 = 5$)

- Question: what value of y_1 is optimum for the circular decision bound? (define r_5 as $(r_3+r_4)/2$)

y_1	r_1	r_2	r_3	r_4	r_5
0	0	3.0	5	5	5
1	0.707	4.6	4.4	4.6	4.5
2	1.414	4.3			
3	2.12	4.05	3.1	3.9	3.5
4	2.83	3.95			
5	3.53	3.7	2.1	2.9	2.5
6	4.24	3.55			
7	4.95	3.5	0.9	2.1	1.5
8	5.66	3.504	0.3	1.7	1.0
9	6.36	3.7	-0.2	1.2	0.5
10	7.07	3.83	-0.8	0.8	0

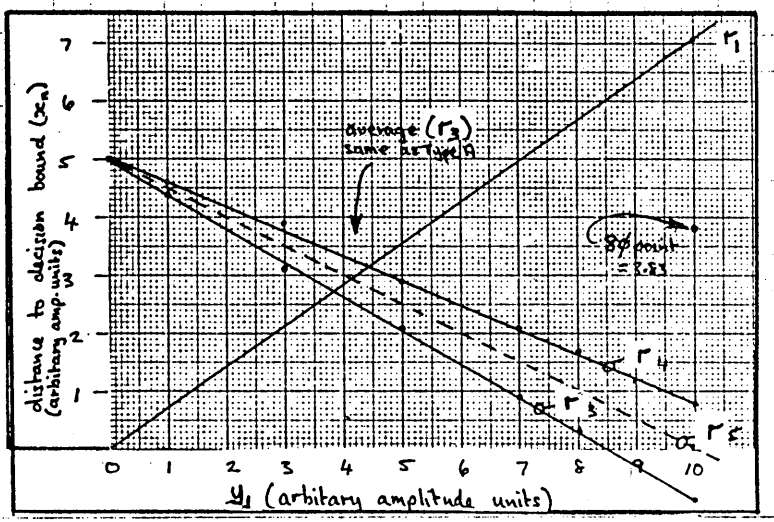

FIGURE 3.8 TYPE-B APK SYSTEM
SIMPLIFIED DECISION BOUND

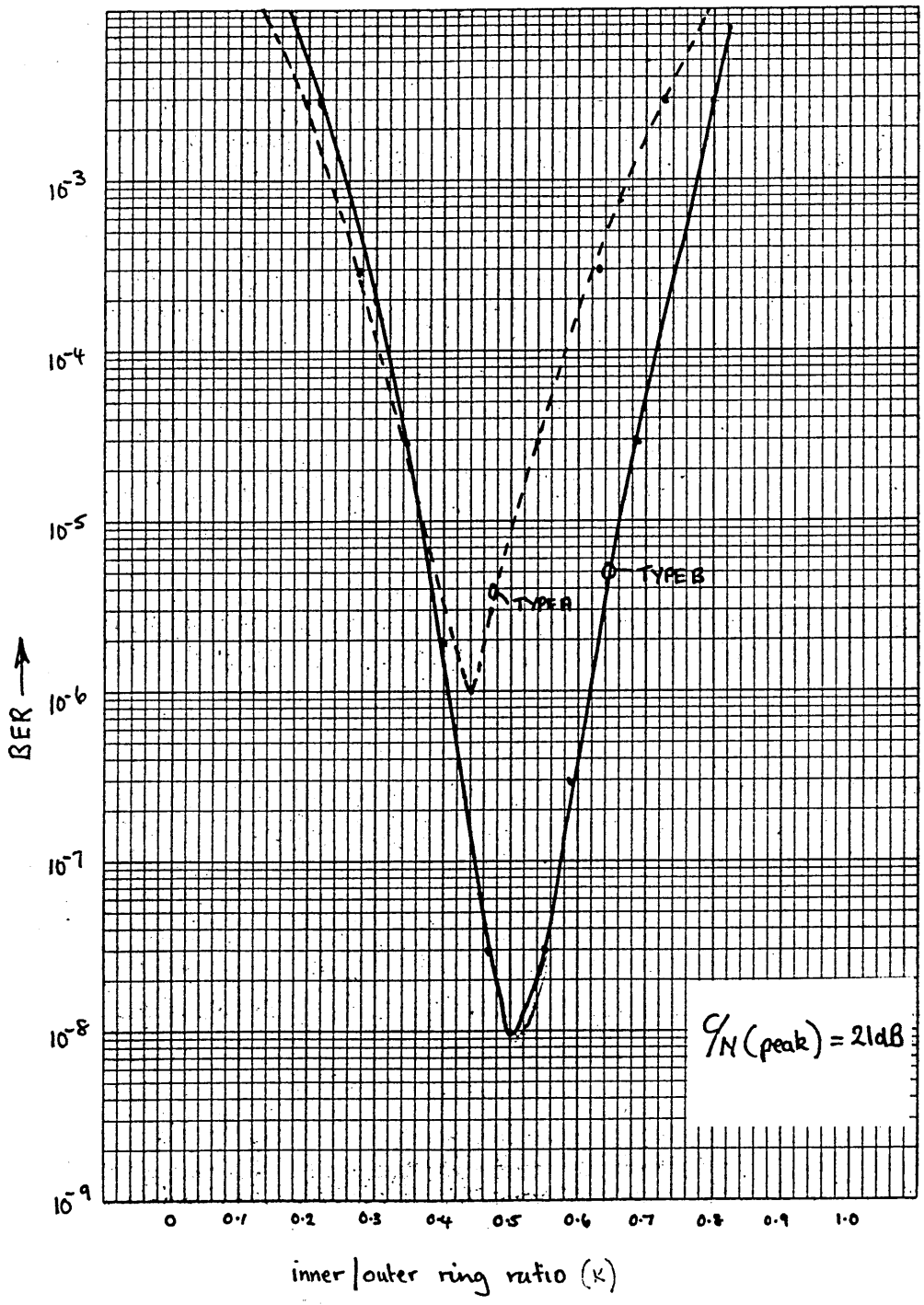

FIGURE 3.9 COMPARISON OF TYPE-A AND TYPE-B APK SYSTEM. BER vs k

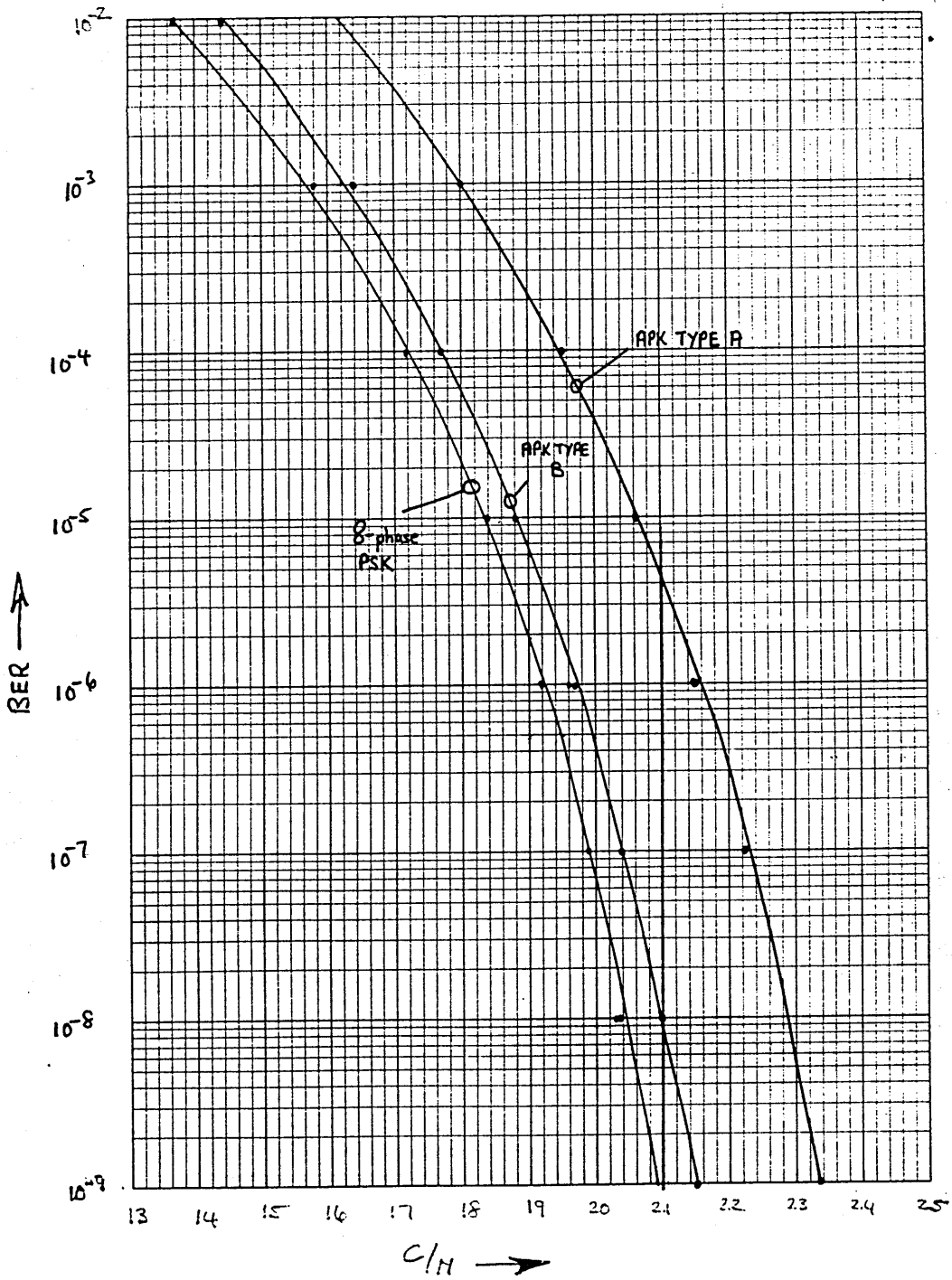

FIGURE 3.10 BER vs C/N FOR APK-A APK-B AND 8-PHASE PSK

SECTION 4

LINEAR CHANNEL ANALYSIS

4.1 INTRODUCTION

Traveling wave tube amplifiers (TWTA's) are employed as power amplifiers in the earth station and satellite transmitters. These amplifiers possess very pronounced non-linear power transfer characteristics and a thorough analysis of the satellite communications system must include these non-linear effects. However, many of the fundamental modulation, demodulation, bandwidth restrictions and interference effects are difficult to analyze in a non-linear environment. For this reason, this study will start by considering the earth station and satellite as linear amplifiers together constituting a linear channel.

This section describes the mechanisms which result in imperfect performance in 8-phase and APK systems operating in a linear channel. The approach used is to generate empirical design tools which can be used in isolation and together in order, ultimately, to optimize a digital satellite system. The tools are based on an extention of the extensive QPSK techniques, many developed

by the author for European and INTELSAT satellite systems. Where the analogy between the QPSK model and the 8-phase/APK systems becomes doubtful or breaks down, purpose designed computer simulations are used to assess the system performance. Throughout the analysis, 8-phase PSK is used as the performance reference.

The section starts by describing the whole communication system and aspects of the INTELSAT V satellite, the INTELSAT TDMA system and an earth station. From this description, a transmission model for the system is established which will be used in the remaining sections.

Using this model, in-band distortion and out-of-band emission effects are considered in order to establish the criteria by which the characteristics of the channel shaping filters are selected. Next co-channel interference effects are considered, including the sources of CCI and the effect of the resulting degradation. Finally, adjacent channel interference effects, adjacent channel multipath effects, and overall link performance optimization will be considered.

Optimization of a digital satellite system is concerned with the variation of various transmission

parameters in order to seek the best overall performance of the system. The aim is to optimize the whole transmission path of the satellite. In this thesis, the various topics are examined in isolation and a generalized optima for each is identified. When all the topics have been addressed, the interactions and cumulative effects are assessed, rather than attempting to calculate an overall optimum directly. The relative importance of the various phenomena become clear and are highlighted, so any changes in the optimized system, that should later prove to be necessary, can be directed to the most rewarding area.

4.2 System Description

In this sub-section, the overall INTELSAT TDMA/DSI system will be described with a view to identifying the elements in the transmission path which influence the attainable performance. This will be accomplished by first reiterating the satellite characteristics and then describing the earth station equipment. From these descriptions, the transmission path elements contributing to the link performance will be identified and discussed. Finally, this information is used to construct a suitable transmission model, which

will enable the link performance of the three candidate modulation methods to be accurately determined.

The INTELSAT TDMA/DSI System comprises a satellite, four "reference" earth stations and a number of traffic earth station terminals (Figure 4.1). The reference and traffic stations transmit to the satellite in short sequential bursts organized in a fixed repetative 2 ms period called a Frame, which occupies the entire transponder's bandwidth for the duration of each burst.

4.2.1 The INTELSAT V Satellite

TDMA operation will be inaugurated in the INTELSAT system using the INTELSAT V spacecraft, an active repeater communications satellite intended for use in a geosynchronous equatorial orbit. As explained earlier, this satellite can operate on two frequency band pairs:

a) The 6/4 GHz band (5,925 to 6,425 MHz up-link and 3,700 to 4,200 MHz down-link), and

b) The 14/11 GHz band (14,000 to 14,500 MHz up-link together with 10,950 to 11,200 and 11,450 to 11,700 MHz down-link).

For the present, only the 6/4 GHz band will be considered. (The performance analysis is similar in both bands, but the higher frequency bands suffer considerable excess path attenuation during heavy precipitation. The effects of this will be considered later.)

Figure 4.2 shows a much simplified diagram of the satellite and its frequency bands. Each frequency band is further subdivided (channelized) into a number of 80 MHz nominal bandwidth contiguous channels. Each channel has an associated input and output band pass multiplexing filter and a traveling wave tube power amplifier (TWTA). In each band, two sets of channels are provided on each of two polarizations.

Two sets of channels sharing the same polarization and frequency dictate the use of two antennae having sharply delineated and unique earth coverage beam patterns (spacial separation). In these ways, the frequency band is used four times and each channel is uniquely identified by the combination of frequency, polarization and antennae beam (coverage area). As will be seen later, Frequency Reuse gives rise to interference caused by imperfect antenna alignment and polarization purity and by atmospheric depolarization. This interference is a major limitation to the attainable

performance of the satellite system. Consideration of the symbol rate (60 Mbaud) and the channel spacing (about 80 MHz) makes it clear that care must be taken to prevent mutual interference between signals in adjacent channels. At the same time a mixture of economic, technological and propagation effects combine with coverage and traffic requirements to limit the carrier-to-noise ratio available at the receiver and to demand non-linear operation of the earth station transmitters and the satellite TWTA's. The requirements for good separation between the different signals in adjacent channels and non-linear amplifier operation tend to conflict with each other and as will be seen later in Section 5, it is necessary to construct an acceptable balance. Throughout this section, however, only linear amplifier characteristics are assumed.

4.2.2 Earth Station Configuration

From a link performance perspective, the reference stations and the traffic stations can be considered to be identically equipped. Figure 4.3 shows a typical earth station configuration. In general, the earth station can be considered to be equipped with a number of transmission chains which correspond to channels within the satellite. Two groups of chains are employed, one group for each polarization. Each chain comprises a

modulator connected to a frequency converter (up converter) at a convenient intermediate frequency (IF). The center frequency of the output of the up converter corresponds to the center frequency of the appropriate channel within the satellite. In the case of INTELSAT V, this could be in the 6 GHz or 14 GHz super high frequency (SHF) band. The SHF output is then fed to a power amplifier before being combined with other chains' outputs and the other polarization's group of chains. Finally, the ensemble is transmitted to the satellite. TWTA's or wideband Klystrons are commonly employed as power amplifiers and the special effects associated with non-linear operation of these devices will be considered in Section 5. In this section they will be considered linear and fully transparent to the signal.

The receive side also employs two groups of chains, one group for each polarization. The channels received from the satellite in the 4 or 11 GHz bands are first passed through a low noise amplifier (LNA). One LNA is provided for each polarization. The SHF output of the LNA's then passes through channelizing filters with a center frequency and bandwidth which matches the corresponding channels at the output of the satellite. For each chain, an SHF to IF frequency converter (down converter) is employed which feeds a demodulator to recover the baseband signal.

4.2.3 Transmission Chain Elements Contributing To Link Performance

From consideration of this generalized earth station configuration, and the previous satellite configuration, it is possible to identify the elements of interest from a link performance perspective. This is shown in Figure 4.4. As will be discussed later, an 8-phase PSK or an APK modulator operating with square wave signalling (the general case), produces a spectrum of the form $(\sin x)^2/x^2$. Clearly in an environment of close channel spacing, this signal must be essentially limited to the boundaries of the appropriate channel. This gives rise to the need for a channel shaping filter which is normally incorporated within, or immediately external to, the modulator. (It will be seen that the selection of the filter is one of the more critical choices to be made in the system design.) In general, the up converters do not contribute measurable signal degradation and can, in consequence, be ignored. In this linear channel analysis, the effects of the transmitter TWTA's will also be ignored. When the various chains are combined, the close channel spacing may give rise to a "linear" adjacent channel problem caused by the spectral overlap of the various channelizing filters. Similarly, when the two polarizations are combined prior to transmission,

imperfect antenna alignment and polarization purity together with atmospheric depolarization gives rise to significant levels of in-band (co-channel) interference.

INTELSAT V is equipped with two identical sets of antenna, each set covering approximately one half of the visible earth's surface. This area of coverage is called a zone.

When the signals from the earth stations in one zone are received by the satellite, they are first subject to polarization separation to separate the two sets of channels. This will tend to increase the Co-channel interference level because of imperfect antenna alignment and polarization purity of the two zones' satellite receive antenna. The signal from the wanted set of channels and the unwanted (Co-channel interference) signal are next both subjected to broad band amplification after which they are passed to demultiplexing (channelizing) filters. Linear adjacent channel interference will be caused by the spectral overlap within these channelization filters. Next, the signals from each channel in the set are subjected to power amplification by a dedicated TWTA. Finally, the outputs of all the set's TWTA's are combined which, as before, gives rise to mutual adjacent channel interference. Next, the other set of channels (for the

other polarization) are combined to form the ensemble, which results in a further increase in Co-channel interference from this operation and also from leakage from the ensemble in the other zone's antenna.

Still further co-channel interference will arise, within the ensemble, from the atmospheric depolarization prior to arrival at the earth station antenna, and from the imperfect alignment and polarization purity of this antenna. The LNA is a linear device and does not contribute to the overall link degradation other than to dominate the overall carrier-to-noise ratio. The channelizing filters introduce linear adjacent channel interference due to spectral overlap of the filter band edges giving imperfect isolation between contiguous channels. Finally, in the transmission chain an SHF to IF down converter and a demodulator are used. The down converter will introduce no measurable degradation.

The demodulator, however, is one of the most critical elements within the entire transmission system. Figure 4.5 shows simple block diagrams of representative 8-phase PSK and APK demodulators. The demodulator contains a receive channel shaping filter, which is designed to essentially maximize the signal to noise ratio within the demodulation process. To perform the APK demodulation, the incoming signal may be compared with

in-phase, quadrature and amplitude reference carrier signals resulting in three analogue data streams which are then sampled at the symbol rate in order to reconstitute the transmitted P, Q and R data streams. In principle, for 8-phase PSK only phase comparison is necessary. All the elements within the demodulator can (and do) contribute to the overall demodulator (and hence link) performance. The channel shaping filter must be chosen with considerable care in order that an acceptable compromise may be reached between (for example) in-band distortion and adjacent channel rejection. The reference carrier and symbol clock signals are obtained by processsing the incoming signal. The reference carrier may be obtained by raising the APK-A or 4-phase PSK waveform to the power of 4 (or 8 in a APK-B or 8-phase PSK system). This removes the modulation and this signal is then applied to a narrow band filter, the output frequency of which is divided by four (eight) to form a stable reference. The clock reference is commonly constructed by envelope detection and subsequent filtering of the IF. The amplitude reference necessary for APK may be obtained by a peak detector following a mean sensing AGC and a fixed ratio level comparator. Errors in constructing these references directly affect the accuracy with which the demodulation process may be accomplished. These mechanisms will be dealt with in detail in a later section.

4.2.4 Transmission Model

Certain elements of the generalized transmission model contribute little to the overall link performance. A simpler model would therefore be adequate.

In this section, the critical elements of the link are identified and a simpler transmission model formed (Figure 4.6). The modulator of the "wanted" path drives a channel shaping filter, an up-converter and a power amplifier. The center frequency of this channel is f_2, the contiguous adjacent channels are at f_1 and f_3. Following adjacent channel combination, the source of the Co-channel interference (the other polarization's channels having identical frequencies f_1', f_2' and f_3') is also combined. These are shown as a single source of co-channel interference from the earth station. This composite band of channels arrives at the satellite together with other sources of interference from identically equipped stations. After polarization separation, the wanted channel f_2 is filtered, power amplified and filtered again. The adjacent channels f_1 and f_2 are treated similarly and then all three are combined [first with themselves and then with the other polarization f_1', f_2' and f_3']. This composite band of channels is then applied to the earth station input

together with sources of interference from other stations. In the earth station, f_2 is selected by a filter, down converted channel filtered and applied to the demodulator to extract the wanted stream. Note that the other polarization channels f_1', f_2' and f_3', and the adjacent channels f_1 and f_3 are not shown within the earth station. This is because these chains do not contribute to the performance of the wanted channel after the input to the earth station.

4.3. Modulation and Demodulation Effects That Modify Theoretical Obtainable Performance

The Theoretical Obtainable Performance derived in Section 3 cannot be achieved in practice due to performance imperfections arising from limitations due to practical channelizing. Although generally referred to as APK modulation, the severe bandwidth restriction imposed by the close channel spacing means that the modulation method is more accurately described as double-sideband quadrature binary-amplitude suppressed carrier modulation.

This section on the manner by which a linear digital satellite systems may be optimized, will be solely concerned with digital (APK and 8-phase PSK) satellite channels such as may be employed in the INTELSAT TDMA

system using INTELSAT V. All effects associated with a full satellite system (e.g., adjacent, multipath and co-channel interference) will be considered.

4.3.1 In-Band Distortion and Channel Filtering Considerations

This sub-section is intended to provide a tutorial background to the subject. The theoretical aspects of channel filtering are well covered by standard works and the treatment here will be purely descriptive.

The APK and 8-phase PSK spectrum follows a $(\sin^2 x)/x^2$ power density distribution[20] and it is very much wider than the channel under consideration. Spectra are shown in Figure 4.7 derived from computer simulations of the wideband APK and 8-phase PSK signals. The spectra are almost identical. The spectral distribution is identical, but the absolute power level is different. In the 8-phase PSK case, each signal point has the same power (= peak power). In the APK case, the average power is reduced by the lower amplitude inner signal level ring (up to about 2 dB). This has important implications for interference considerations as we shall see in later sections. Clearly, in a channelized environment, bandwidth restriction must be made in order

that reasonably efficient use may be made of the available bandwidth of the transmission medium. Additionally, in the practical system, the signal will arrive at the receiver accompanied by a significant amount of noise and interference. The function of the channel filters is to minimize the error rate for the signal set operation in a noisy environment while at the same time satisfying a specification for out-of-band emission. This is achieved by tailoring the filter response to pass the wanted signal spectrum, but sharply reject other signals outside this area. The problems of out-of-band emissions will be addressed at a later stage, and for now it is sufficient to bear in mind that there is a requirement for minimizing interference to channels located in the frequency spectrum adjacent to the channel under consideration.

In the linear channel, there are two main criteria which are used to arrive at optimum channel filtering. These are:

a) That there should be no intersymbol interference at the decision instant in the receiver.

b) That the receive filter should match the incoming signal spectrum.

The requirement for zero intersymbol interference (ISI) can be met by the use of Nyquist's first criterion[21] which requires that the real-valued transmittance function of an ideal filter be modified to provide skew symmetry about the cut-off frequency. This results in a receiver spectrum which has a skew-symmetrical amplitude roll-off characteristic centered at half the symbol rate (Nyquist rate). Figure 4.8 shows the pulse response of a family of so-called cosine roll-off filters which satisfy this skew criteria. The effect of the Nyquist filtering is to give acceptable bandwidth limitation without causing ISI at the sampling instant. Figure 4.9 shows a sketch of several continuous pulses which have been filtered so as to give zero ISI at the sampling instant. Figure 4.9 also shows a photograph of a set of pulses in a typical demodulator.

The requirement for matched receive filters will be achieved when the transfer function of the receive filter is the complex conjugate of the receive signal spectrum.[22] Since the channel is linear, this implies that both the transmit and receive filters should have the skew-symmetric form of power roll-off centered on the Nyquist rate and that the filters must be of a linear phase form. At this stage, we are not concerned with any other forms of bandwidth restriction or interference from

other sources, and so we can conclude that for the linear channel a very sharp or very gentle roll-off filter would, in principle, give identical performances[23].

The Nyquist arguments are concerned with ideal signals, in particular the aforegoing is based on impulse signalling. Practical modulators would probably use non-return-to-zero (NRZ) square wave input signals which, unlike an impulse signal do not have a uniform "white" amplitude spectral distribution but are rather of a $(\sin^2 x)/x^2$ form, as shown earlier. It is thus usual to correct for this by applying a compensating filter of $x^2/(\sin^2 x)$ form to the transmitter[23]. The effect of this is to restore ideal signalling conditions over the band of interest. This is shown in Figure 4.10.

In some QPSK systems, for reasons of economy in procurement, identical filters may be employed at the transmitter and receiver such that each filter receives the square root of the compensating $x^2/\sin^2 x$ characteristic. It is reasonable to extend this to APK and 8-phase PSK. QPSK studies indicate that there are no performance disadvantages in doing this[24].

In the performance comparisons presented here, the transmitter channel shaping filter is assumed to have

a cosine roll-off response raised to the power of a constant (x). This allows a wide range of filter characteristics to be considered by varying the roll-off factor and the transmitter power law "x". Figure 4.11 shows the amplitude response of a family of cosine roll-off filters. Figures 4.12, 4.13 and 4.14 show an elementary wideband linear channel (i.e., having no transmit and receive channel shaping filters) showing the signal space diagrams of both candidate APK and 8-phase PSK methods, respectively. The signal space diagrams used throughout this study have been obtained from a comprehensive QPSK channel simulation model (CHAMP) produced by COMSAT, modified by the author to give 8-phase PSK and APK results[25]. In a wide band linear channel, the APK signal space diagrams consist of eight points arranged as four points lying on each of two circles of constant amplitude joined by straight lines corresponding to transitions of the baseband signal. The differences between the two candidates is seen to be rotation of the outer circle relative to the inner. For 8-phase PSK, the classic octagonal is seen with straight lines joining all the signal points. When cosine roll-off filters are employed to meet the requirements of close channel spacing, the effects shown in Figure 4.15 result. By way of example, an 8-phase PSK linear system is chosen using 40% cosine roll-off channel filtering. As can be seen,

the degree of overshoot of the trajectories between the signal points has been introduced by the filters. This corresponds to an increase in the amplitude modulation (am) component of the signal. In order to keep the performance analysis manageable, it is generally assumed that the receiver filter complements that in the transmitter to produce a full cosine roll-off response centered around the clock frequency. If the transmitter and receiver filters were connected back to back, the received signal would conform to Nyquist's First Criterion and there would be no intersymbol interference (ISI) at the optimum sampling point. This is shown in the figures. Note that the sampled scatter diagram shows considerable dispersion when observed after only one square root Nyquist filter. However, when observed after the two filters are connected back to back (full Nyquist), the dispersion is almost zero and the signal trajectories are very much more orderly. The degree of scatter is due to intersymbol interference since no noise was included in the channel. It can readily be seen that the average error rates will be greater when a dispersion exists since it lowers the average energy of the noise component required to make an error. Further, if the shaping were divided equally between transmitter and receiver (x=0.5) the receiver filter would be 'matched' to the transmitted signal and the optimum signal detection would be

obtained. This holds true for any cosine roll-off factor. Figures 4.16 and 4.17 show the modified-CHAMP computer generated signal space diagrams for 100%, 50%, 40%, 30% and 0% cosine roll-off cases for APK Types A and B, respectively. It will be noted that the degree of overshoot between the signal points greatly increases as the roll-off is decreased. In the linear channel, this is of no consequence, but it will be seen that this effect has very serious implications for the non-linear channel.

Any departure from these basic conditions, such as additional filtering, non-linear amplification, or non-root-Nyquist transmit filtering, automatically means that the Nyquist receiver filter is sub-optimal. It has, however, the advantage of analytical simplicity, and receiver optimisation exercises reported later show that it gives a good guide to the best performance that can be obtained. Away from the optimum, the performance can be improved by trading distortion against noise bandwidth and interference rejection.

4.4 Co-Channel Interference Effects

4.4.1 Sources of Co-Channel Interference (CCI) and Associated Effects

Even in the absence of atmospheric depolarization some cross-polar interference will be produced by imperfect antenna cross-polar discrimination characteristics, by misalignment of transmit and receive antennas on both the uplink and the downlink, by signal leakage between spacially separated antenna and by interference from terrestrial sources (See Figure 4.18). A given interfering signal will combine with the wanted signal at the satellite receive antenna. The interfering signal will combine again with the wanted signal after being amplified in separate linear repeater chains. [It should be remembered that the repeater chains are most often operated non-linearily, as will be seen in Section 5] Furthermore, it is believed that the relative phase-shifts between cross-polar repeater chains will vary slowly and that there exists a possibility of substantial coherent recombination of uplink and downlink co-channel interference. This could produce an interference level as much as 3 dB worse than that indicated by simple power addition of the two separate interference sources[26].

Severe attenuation is mainly caused by rain. Climatic conditions and the geographic separation of earth stations in the INTELSAT TDMA system, ensure that rain rates which are sufficient to cause significant attenuation occur independently at the different earth-station locations. They also occur relatively infrequently and so it is possible to consider that only one earth station is affected at a time.

When an earth station suffering a precipitation induced fade transmits a TDMA burst to the satellite, the burst suffers more attenuation than the other bursts arriving from all other locations. This can give rise to burst-to-burst level variations at the receiver, to an increase in the relative levels of co-channel interference signals, and to a decrease in the uplink carrier-to-noise ratio. By reducing the input level to the satellite linear amplifier, it will also cause a reduction in satellite output power and hence in the carrier-to-noise ratio on the downlink.

The INTELSAT system uses a higher frequency band on the uplink than on the downlink and since a given rain rate causes more attenuation at higher frequencies it is important to control the uplink effects carefully. The

enhancement of the uplink interference and noise levels can be countered either by ensuring that the clear-weather levels are low, or by using Up-Link Power Control (ULPC) to keep the wanted signal level constant. This latter approach complicates the system and requires several dB of "spare" transmitter power. It also has the side-effects of increasing co-channel interference from a cross-polar transmitter which is suffering simultaneous attenuation and depolarization, together with several other unattractive effects. In order to keep the up-link noise sufficiently low in clear weather, the transmiter would then need to be operated close to saturation, leaving little spare power for ULPC. In principle, such an arrangement would allow a moderate degree of ULPC to be used, but whether this would be an advantage is not completely clear. ULPC is considered in more detail later.

The signals arriving at the affected earth station will all be attenuated to the same extent during a rain event, and so their relative levels will not be altered.

4.4.2 Co-Channel Interference Degradation Effects

Co-channel Interference (CCI), as its name implies, is associated with interference from a channel possessing the same (or similar) frequency and usually a similar bandwidth. In attempting to quantify the effects of such interference, the various sources of interference can be placed in two main classifications: uplink and downlink.

The overall objective is to use the generalized transmission model to derive the results necessary to allow design rules to be produced to predict the degradation resulting from various CCI power levels and numbers of CCI signals in the practical satellite system. In addition, it is necessary to assess the sensitivity of the system to CCI under different channel filtering conditions in order to decide if the general in-band results derived earlier need to be modified when CCI effects are considered.

Figure 4.19 shows the transmission model configured for CCI investigations. The method of measuring the bit error rate (BER) degradation proceeds by establishing the reference performance of the channel in the presence of various levels of added down-link noise,

but in the absence of other forms of disturbance. These BER vs C/N reference curves are obtained for various cosine roll-off factors. To evaluate the degradation due to interferences, known levels of interference are injected in the system at points chosen to simulate the real interference sources. A wholly digital environment will be considered and the interferers are thus PSK and/or APK modulated.

4.4.3 Co-Channel Interference Results

In the linear channel, the effect of co-channel interference can be simply assessed. This is particularly so when many separate sources of interference combine in the link. In the INTELSAT V link, four, five or six separate interference sources may be present, corresponding to the other satellite beams and terrestrial sources of interference. A number of independent interference sources can be modeled accurately by thermal noise of the same power level[27]. Figures 4.20, 4.21 and 4.22 show bit-error-rate (BER) curves versus carrier-to-noise C/N for various carrier power to interference power (C/I) ratios (30, 25, 20, 17 and 15 dB) for APK type A, type B and 8-phase PSK, respectively. The results are based on experiments by the author using the

ESA/ESTEC OTS satellite model reported in Reference 30. These curves are difficult to use for link budget work since link budgets are formed from the addition of thermal noise powers. However, at a given error rate, the degradation caused by an interference can be represented by an equivalent thermal noise increase which will achieve the same error rate performance. The additional thermal noise is called the Noise Equivalent Degradation (NED). It is thus usual to replot the C/I results in the form of excess noise equivalent degradation versus C/I ratios. This converts the effect of the interferer to an equivalent noise power. This equivalent power is only valid at a particular C/N ratio and so the results are obtained at the appropriate clear weather C/N (in this case 21 dB) (Table 4.1). This is shown in Figure 4.23 for the three candidate modulation schemes. The INTELSAT V link budget (Section 2) predicted a C/I ratio of 21.5 dB on the up-link and down-link. For the linear channel, this will result in a C/I at the demodulator of 18.5 dB. From Figure 4.23, this results in a noise equivalent degradation of 3.85, 3.25 and 4.4 dB for APK Type A, B and 8-phase PSK, respectively. However, it is important to note that these results are obtained on the basis of a homogenous environment. For example, in a wholly APK environment where the interference sources are also APK

C/N dB	C/N lin	C/I = 15dB	C/I = 17dB	C/I = 20dB	C/I = 25dB	C/I = 30
13	19.95	10.9	11.2	12.2	12.7	12.9
14	25.12	11.46	11.9	13.03	13.7	13.9
15	31.62	12.0	12.5	13.8	14.5	14.9
16	39.8	12.5	13.0	14.8	15.3	
17	50.1	12.9	13.4	15.2	16.4	
18	63.09	13.2	13.9	15.9	17.2	
19	79.43	13.5	14.2	16.5	18.02	
20	100	13.8	14.5	17	18.8	19.6
21	125.9	14.0	14.8	17.5	19.54	20.5
22	158.49	14.2	15.0	17.9	20.2	21.4
23	199.52	14.4	15.2	18.23	20.9	22.2
24		14.5	15.4	18.6	21.5	23

TYPE B APK (decrate = 2.0 dB)

C/N		C/I=15 (50.1)	C/I=17 (79.4)	C/I=20 (158.5)	C/I=25 (501)	C/I=30 (1584.9)
13	19.95	11.5	12.0	12.5	12.8	12.9
14	25.12	12.2	12.8	13.4	13.8	13.9
15	31.62	12.8	13.5	14.2	14.7	14.9
16	39.8	13.5	14.2	15.0	15.7	15.9
17	50.1	14.0	14.9	15.8	16.6	16.8
18	63.09	14.5	15.5	16.5	17.5	17.8
19	79.43	14.9	15.9	17.2	18.4	18.8
20	100	15.2	16.5	17.9	19.2	19.7
21	125.9	15.5	16.9	18.5	20.0	20.6
22	158.49	15.8	17.3	18.9	20.8	21.5
23	199.52	16.0	17.5	19.7 ~~22.9~~	21.5	22.5
24	251.18	16.2	17.8	19.9	22.2	23.4

TYPE A APK (decrate = 1.0 dB)

C/N		C/I = 15 (39.8)	C/I = 17 (63.9)	C/I = 20 (125.9)	C/I = 25 (398)	C/I = 30 (1259)
13	19.95	11.2	11.8	12.8	12.7	12.8
14	25.12	11.8	12.5	13.2	13.7	13.7
15	31.62	12.5	13.2	14.0	14.7	14.7
16	39.8	12.9	13.9	14.8	15.6	15.6
17	50.1	13.5	14.5	15.5	16.5	16.5
18	63.09	13.9	15.0	16.2	17.4	17.4
19	79.43	14.3	15.46	16.9	18.2	18.2
20	100	14.5	15.9	17.5	19.0	19.0
21	125.9	14.8	16.2	17.9	19.8	19.8
22	158.49	15.03	16.5	18.5	20.5	20.5
23	199.52	15.2	16.8	18.9	21.2	21.2
24	251.18	15.4	17.0	19.2	21.9	21.9

TABLES 4.1 FOR FIGURES 4.20, 4.21 and 4.22:

NOISE EQUIVALENT CCI

signals, the C/I ratios given by the link budget are de-rated to accommodate the lower average power of APK signals. For a Type B system, this results in a reduction of 2.04 dB and 1.03 dB for a Type A system. The 8-phase PSK reference case with a 18.5 dB C/I ratio indicates a wholly constant envelope (e.g., PSK) environment.

The linear performance of both APK methods was shown in Section 3 to be inferior to PSK. However, the APK systems have been shown to perform better than PSK in a homogenous interference environment. Specifically, INTELSAT V is an interference limited satellite and it should be noted that the lower average power for the APK case results may produce an improvement in overall degradation over the 8-phase PSK case. Therefore, on the one hand, APK performs better than PSK in an interference limited environment, but the reverse is true for the simple thermal noise case. In order to investigate the composite effect, Figure 4.24 shows the performance of the three candidates at C/I = 20 dB, in which the Type B APK method is showing a 1 dB improvement over 8-phase PSK. This effect will be considered further in the non-linear analysis.

4.5 Adjacent Channel Interference

Adjacent Channel Interference (ACI), as the name implies, is caused by a spillover of power from the adjacent channel(s) in the frequency spectrum. This spillover of power is caused by the use of imperfect multiplexing filters and their interaction with the spectral shaping introduced by the transmit and receive channel shaping filters. The interaction of these filters and the tradeoff between practical complexity (and in the case of the satellite, the attendant weight and cost penalties) together with the resulting degradation from the in-band and adjacent channel effects is complex and not readily amenable to mathematical evaluation. Additionally, because of the interaction of the multiplexing filters and the proximity of the adjacent channels, a small proportion of the wanted signal can fall into the adjacent channels and then recombine with the wanted signal giving rise to a particularly damaging type of interference known as multipath. Because of the complex nature of interfering effects associated with the presence of adjacent channels, comprehensive series tests and simulations have been conducted by the author and reported in Reference 35.

4.5.1 The Generation of ACI

The generalized transmission model in Figure 4.6 can be used to assess the effect of ACI. APK and 8-phase PSK signals are generated and suitably arranged in the frequency band in order to load the three channels. The three channels are located side by side in the frequency spectrum such that channel 2 is the wanted channel. By choosing channel 2 as the wanted channel, the effects of channel 1 into 2, 3 into 2, and 1 + 3 into 2 can be studied.

Figure 4.25 shows the idealized channel spectral shape and multiplexing arrangements, and under these arrangements no ACI can occur. However, when the real situation is substituted, the interaction of the out-of-band characteristics of channel shaping filters and multiplexing filters shows that some of the energy from the adjacent transmission can fall into the wanted channel, thereby causing interference. This is also shown in Figure 4.25.

4.5.2 Method of Determining ACI Degradations

Figure 4.6 showed that the transmission model has three contiguous transponders. Clearly, if the center transponder (channel 2) is chosen as the wanted channel, then it is possible to conduct adjacent channel interference tests using 1 into 2, 3 into 2 and 1 + 3 into 2. It should be noted that in the single ACI case, the unused transponder is switched off.

4.5.3 Adjacent Channel Interference Results

In Section 5, it will be shown that ACI is to a large extent dominated by the non-linear spectral regrowth effects. Nevertheless, there exists a linear component of ACI caused, as has been explained, by overlap of the band-edge of the channelizing filters. Figure 4.26 show a wideband 60 MS/s 8-phase PSK signal at the output of the modulator. Also shown in this figure are two 40% cosine roll-off channel filters arranged at the INTELSAT V channel spacing of 80 MHz. Note that the skirts of the two filters overlap such that energy from one channel will enter the other. The overlap is shown in isolation to the right of the two filters. At this stage, it can be seen

that the signal is more than 30 dB below the wanted signal and leads to the general conclusion that linear channel ACI with 40% cosine roll-off filters and 80 MHz channel spacing may be ignored, since the ACI contribution will be negligible in comparison with noise powers less than 20 dB below the wanted signal.

4.6 Summary

In this section, the mechanisms are examined which prevent the theoretically obtainable performance described in Section 3 from being obtained in a practical satellite system employing linear power amplifiers. Firstly, a satellite end-to-end channel (link) is examined to identify those elements which influence channel performance. These elements are then combined into a simple transmission model and the performance degradation effects are grouped into imperfect modulation and demodulation, channel filtering effects and co-channel, adjacent channel and multipath interference effects. Using a custom modified satellite channel computer simulator and hardware measurements performance using the ESA/ESTEC OTS satellite model, it is possible to conclude that adjacent channel and multipath interference in the linear channel is negligible and may be ignored.

Using the expected C/I ratios of 18.5 dB and the clear weather C/N ratio of 21.5 dB obtained from the link budget (Table 2.2), 8-phase PSK gives an error rate of 6.2×10^{-5}, while the Type-A APK system gives 1.2×10^{-3} and the Type-B system 2.1×10^{-5}. Thus, on the basis of linear channel performance in a homogeneous interference limited environment, the APK-B system offers an advantage of almost 1 dB over 8-phase PSK which in turn is 3.4 dB better that the Type-A system.

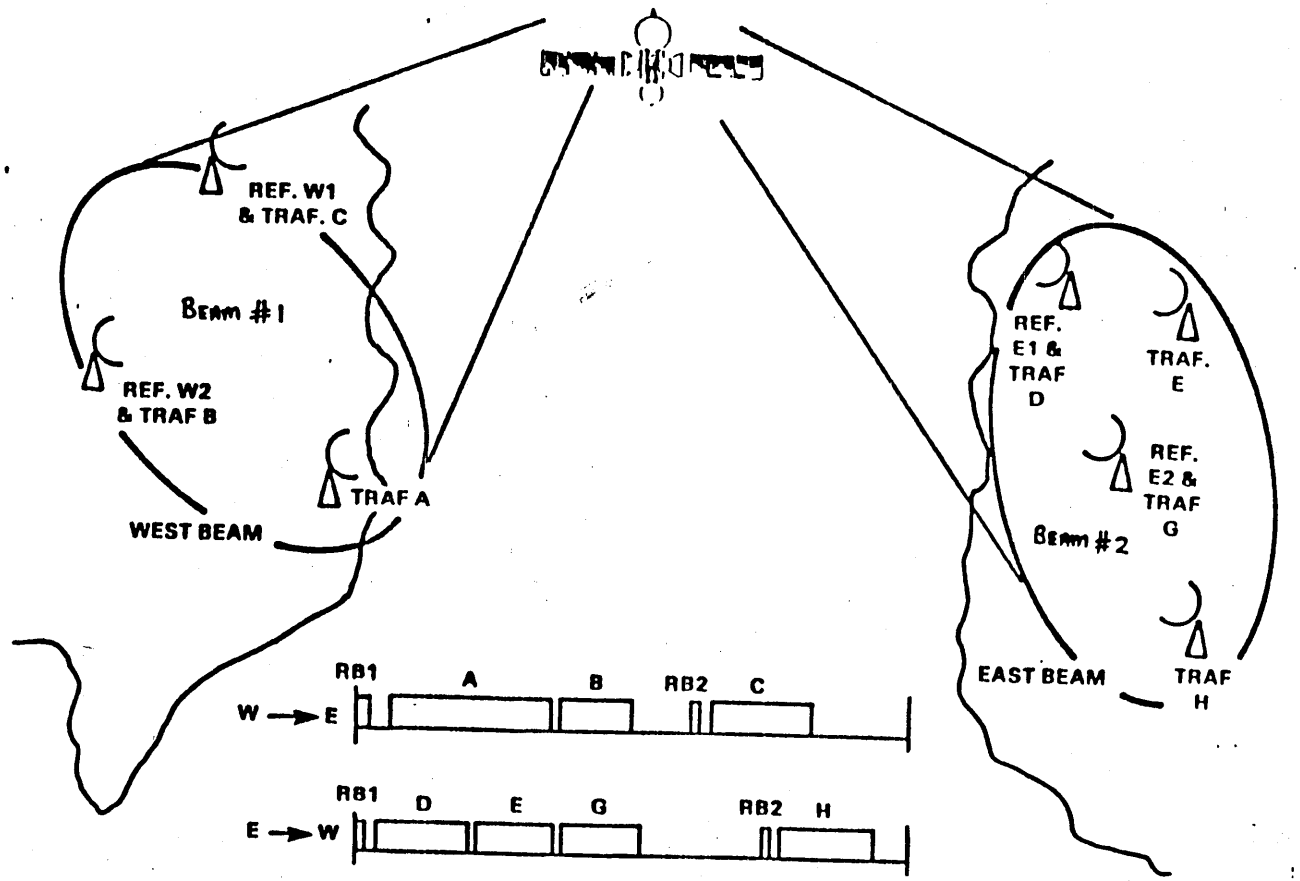

FIGURE 4.1 THE INTELSAT TDMA/DSI SYSTEM

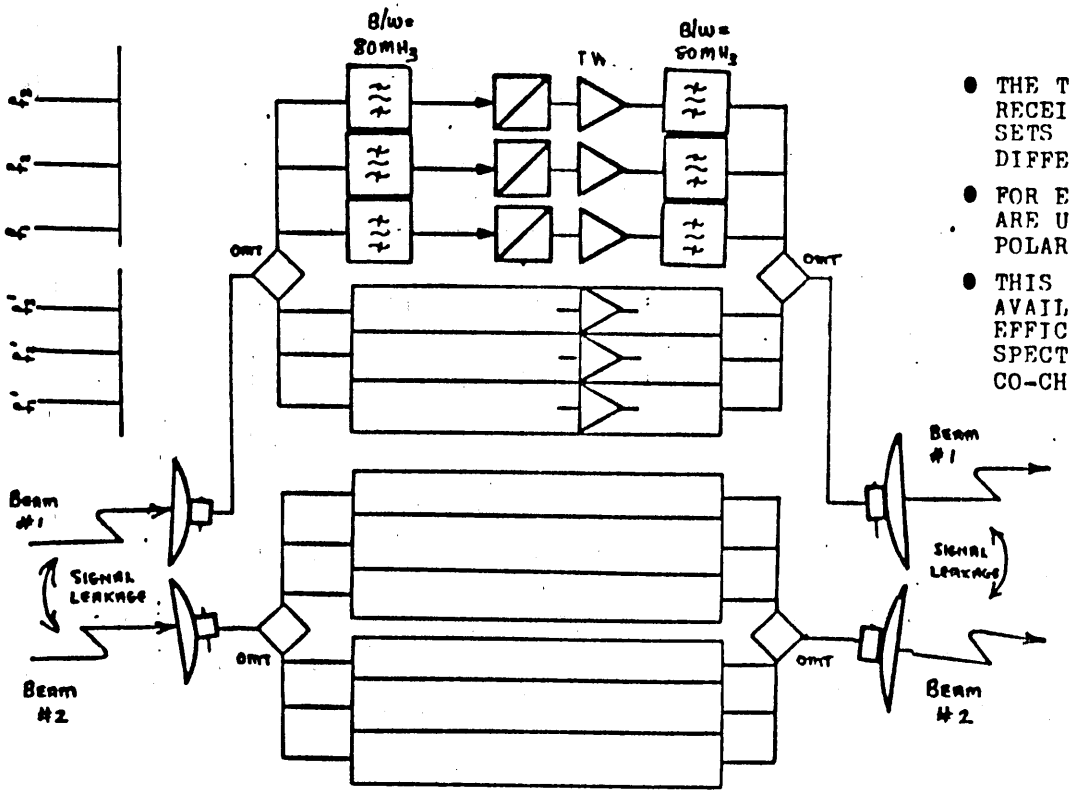

- THE TWO BANDS ARE DUPLICATED .... RECEIVE FROM, AND TRANSMIT TO, TWO SETS OF ANTENNA WHICH ILLUMINATE DIFFERENT AREAS OF THE EARTH
- FOR EACH SET OF ANTENNA, THE BANDS ARE USED AGAIN BY EMPLOYING TWO POLARIZATIONS
- THIS FOUR-FOLD REUSE OF THE AVAILABLE FREQUENCY YIELDS EFFICIENT USE OF THE AVAILABLE SPECTRUM BUT GIVES RISE TO CO-CHANNEL INTERFERENCE PROBLEMS

- CO-CHANNEL INTERFERENCE ARISES FROM IMPERFECT ANTENNA ALIGNMENT AND POLARIZATION, ATMOSPHERIC DEPOLARIZATION AND LEAKAGE BETWEEN THE SPACIALLY SEPARATED ANTENNA

FIGURE 4.2 SIMPLIFIED BLOCK DIAGRAM OF INTELSAT V SATELLITE

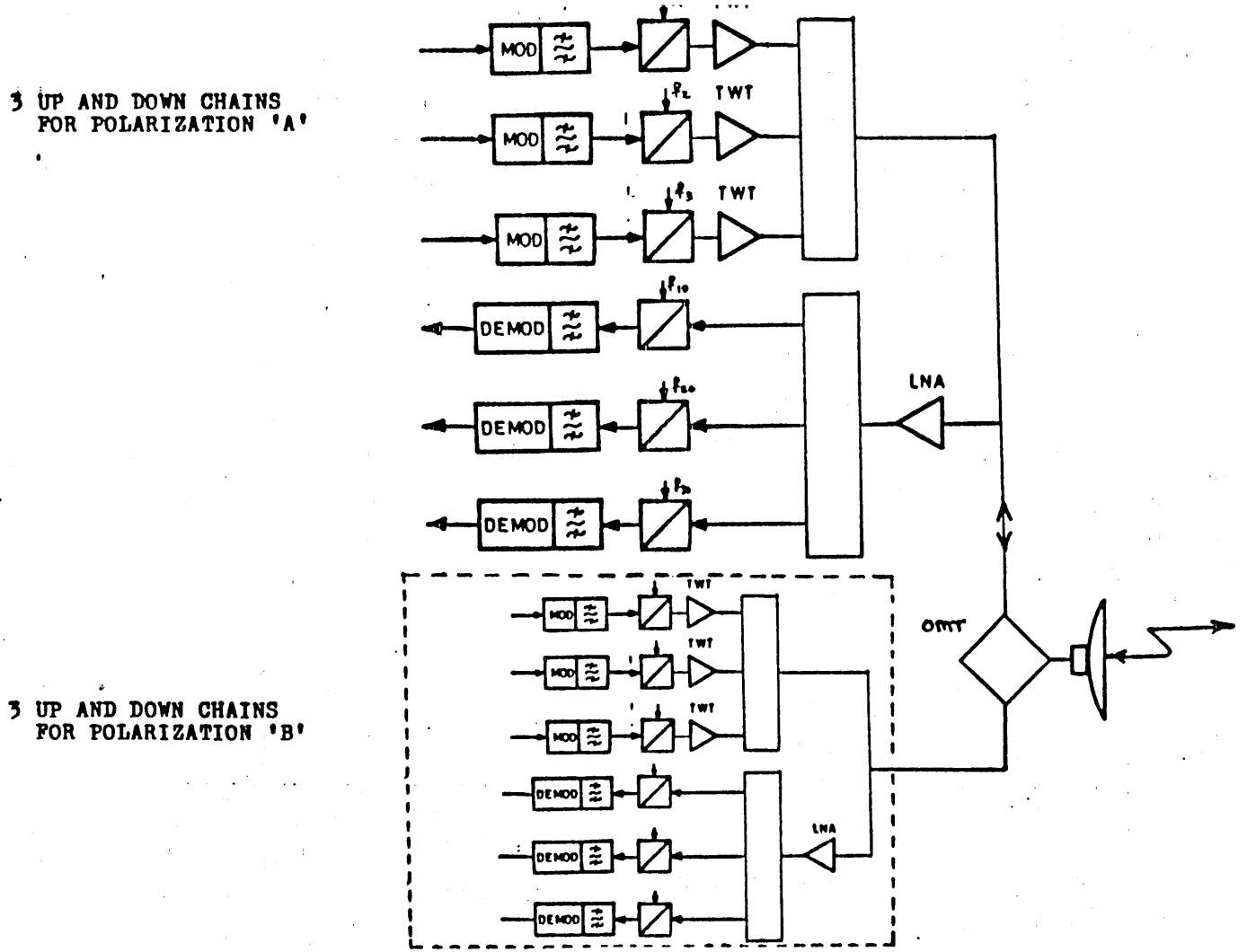

FIGURE 4.3 SIMPLIFIED BLOCK DIAGRAM
OF EARTH STATION

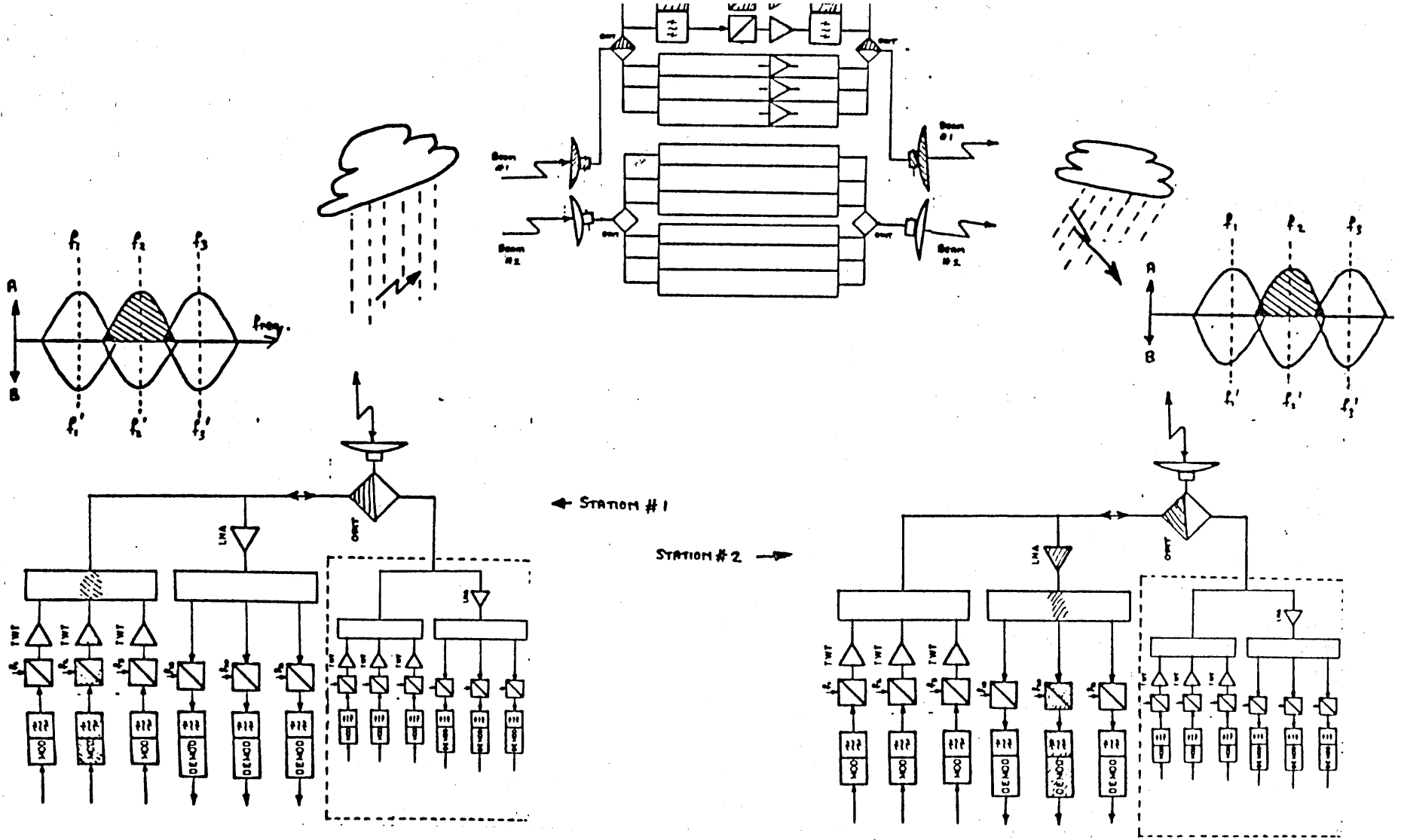

FIGURE 4.4 EARTH STATION/SATELLITE/
EARTH STATION COMBINATION

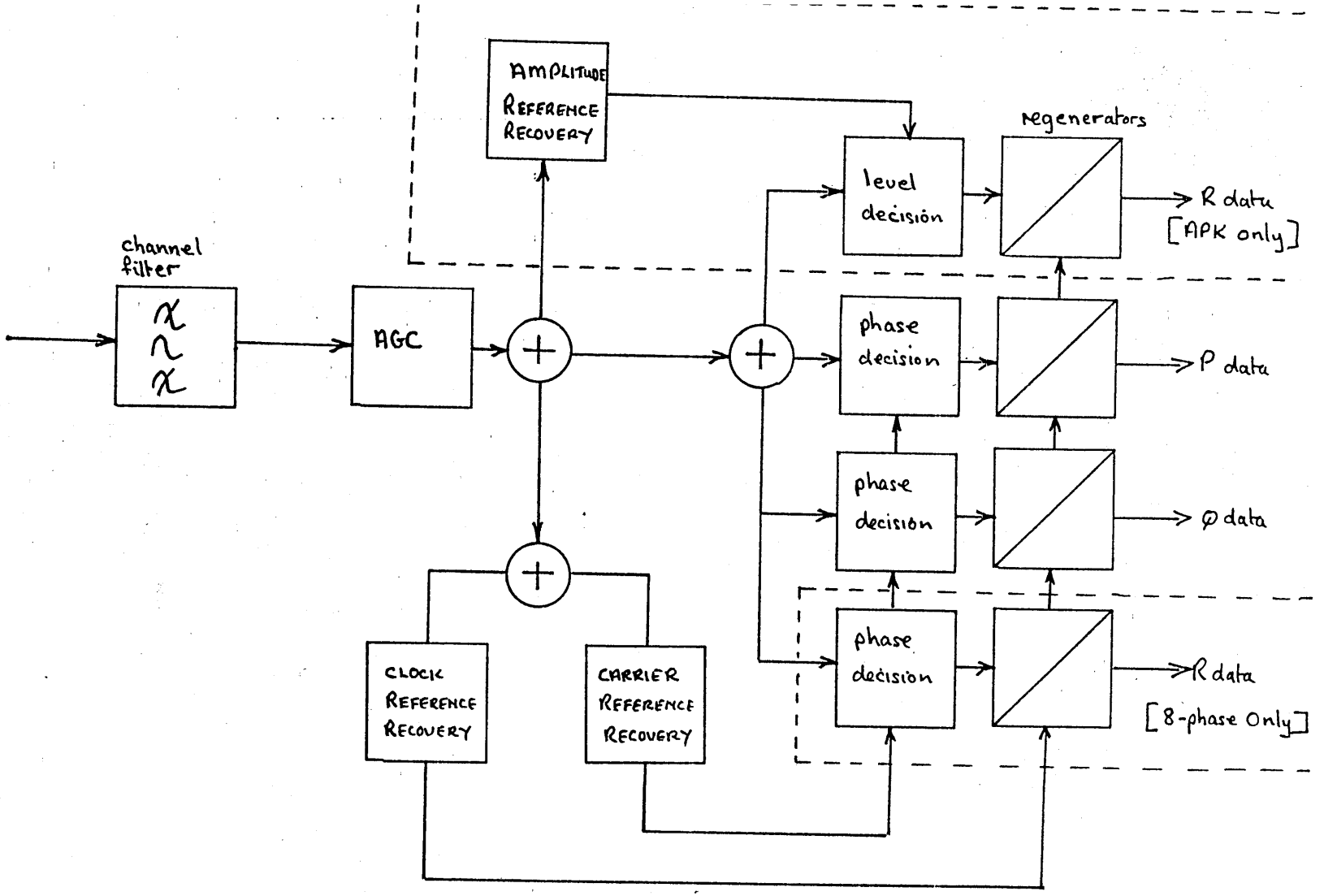

FIGURE 4.5 SIMPLIFIED PSK OR APK DEMODULATOR

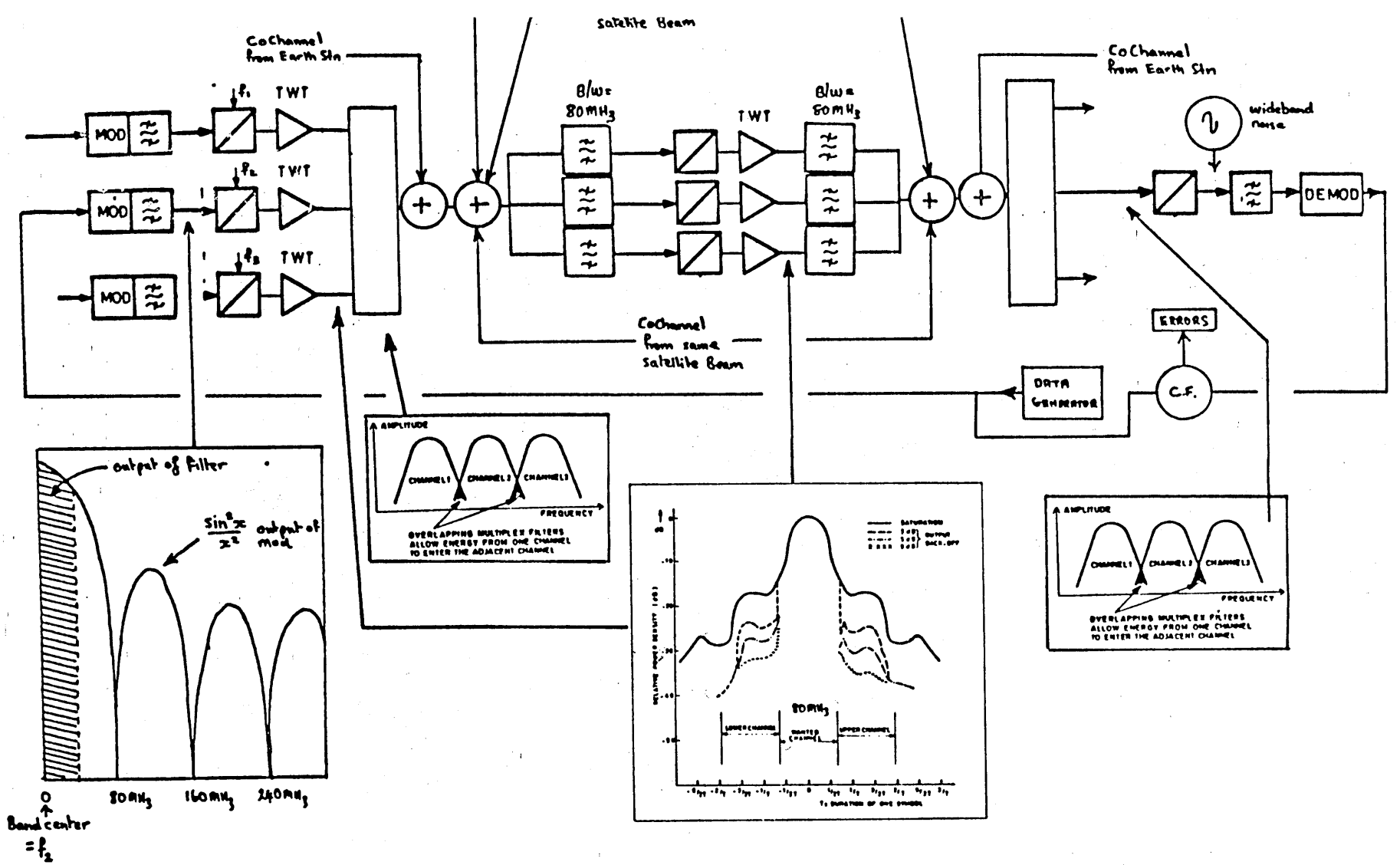

FIGURE 4.6 GENERALIZED TRANSMISSION MODEL

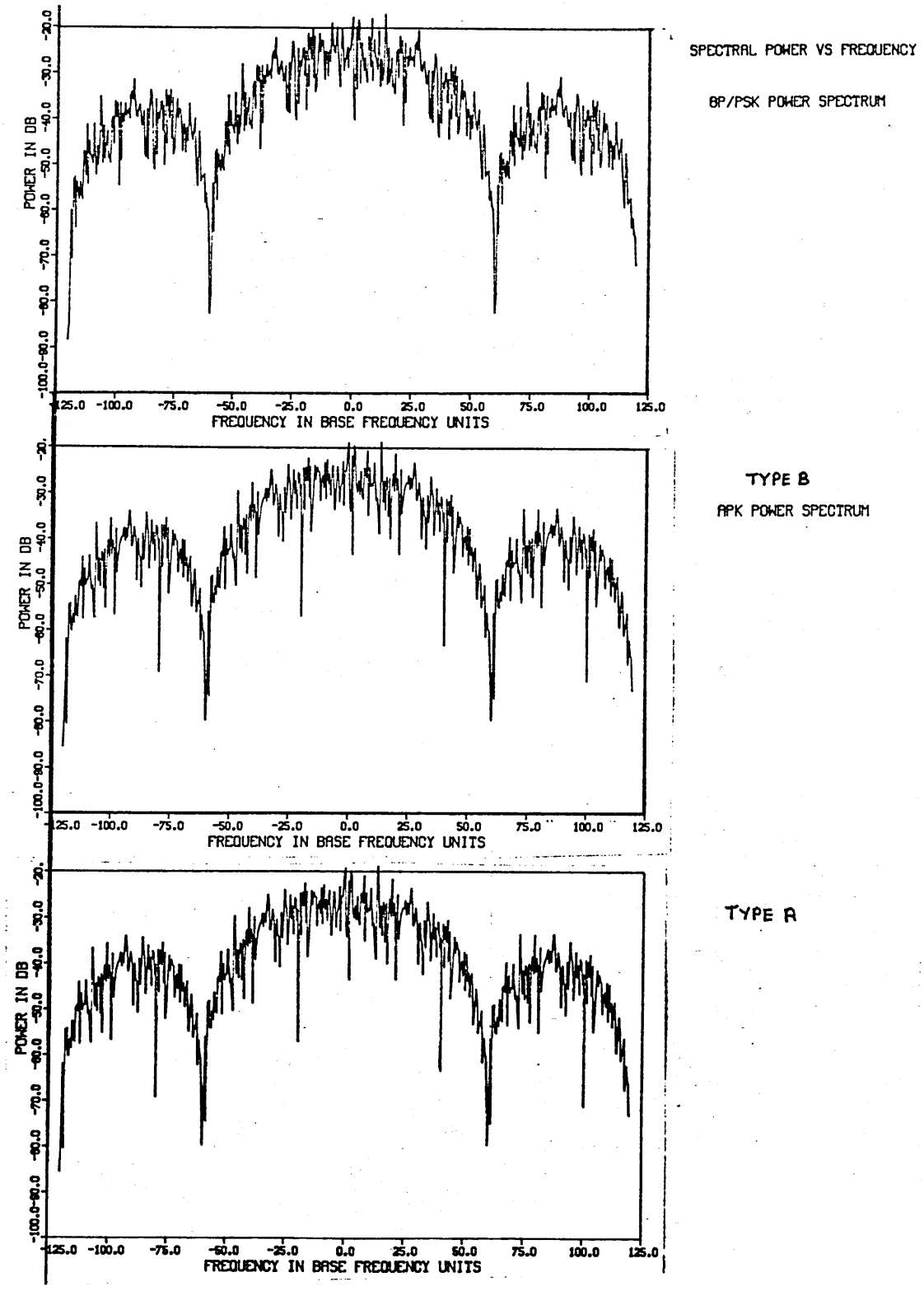

FIGURE 4.7 COMPUTER SIMULATED WIDEBAND APK AND PSK SIGNALS

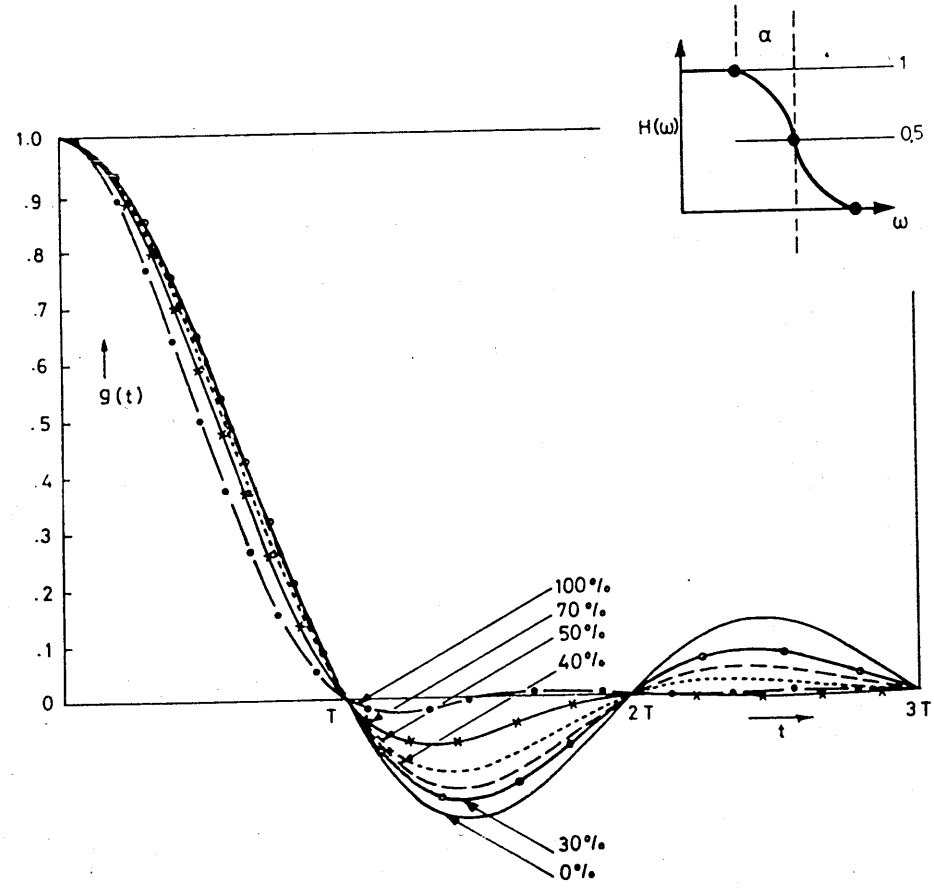

FIGURE 4.8 PULSE RESPONSE FOR A FAMILY OF COSINE ROLL-OFF FILTERS

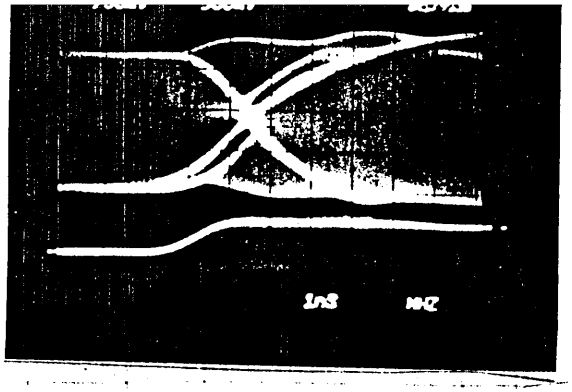

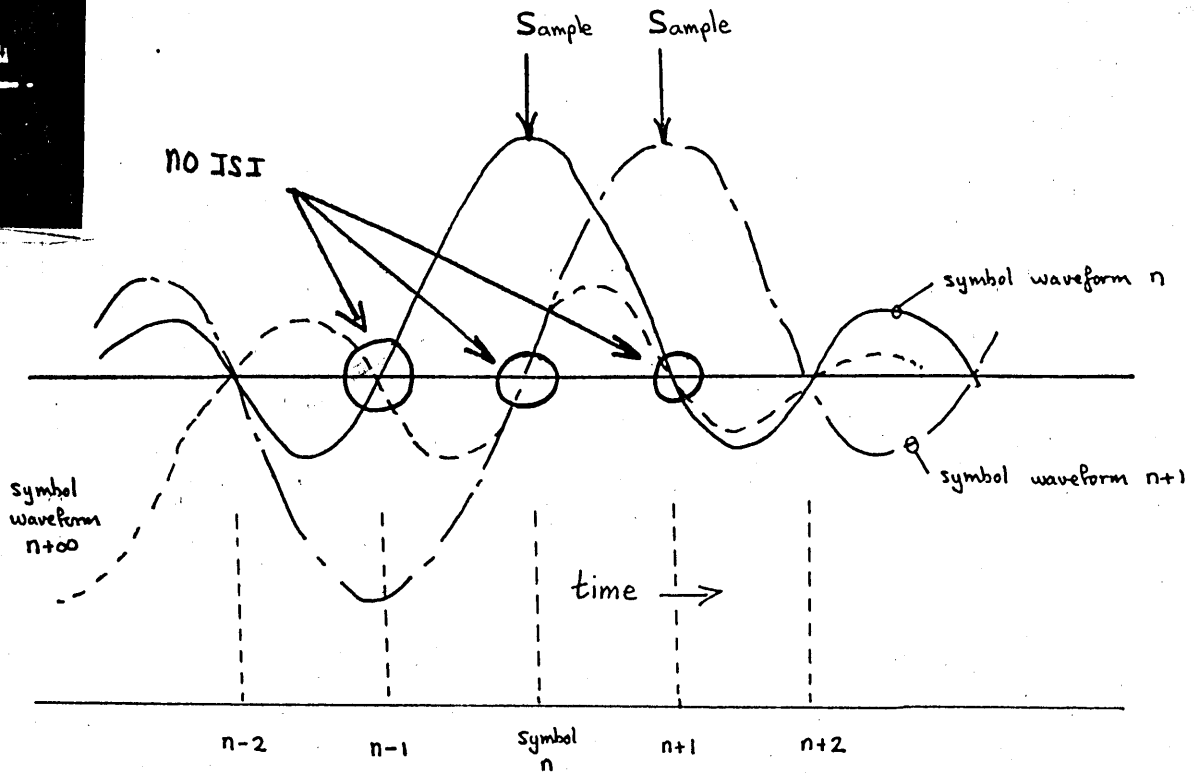

FIGURE 4.9 CONTIGUOUS NYQUIST PULSES

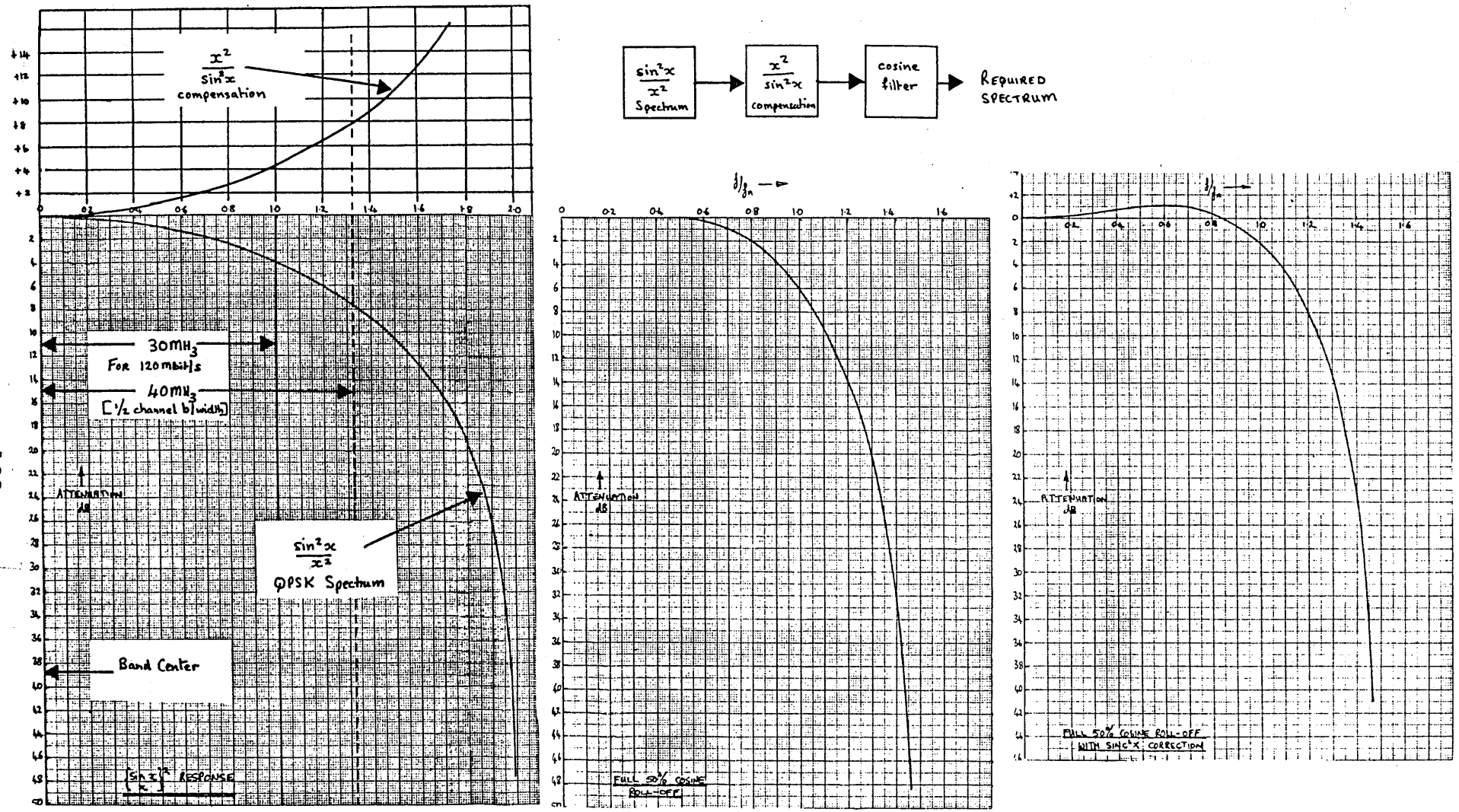

FIGURE 4.10 SINE X/X CORRECTION

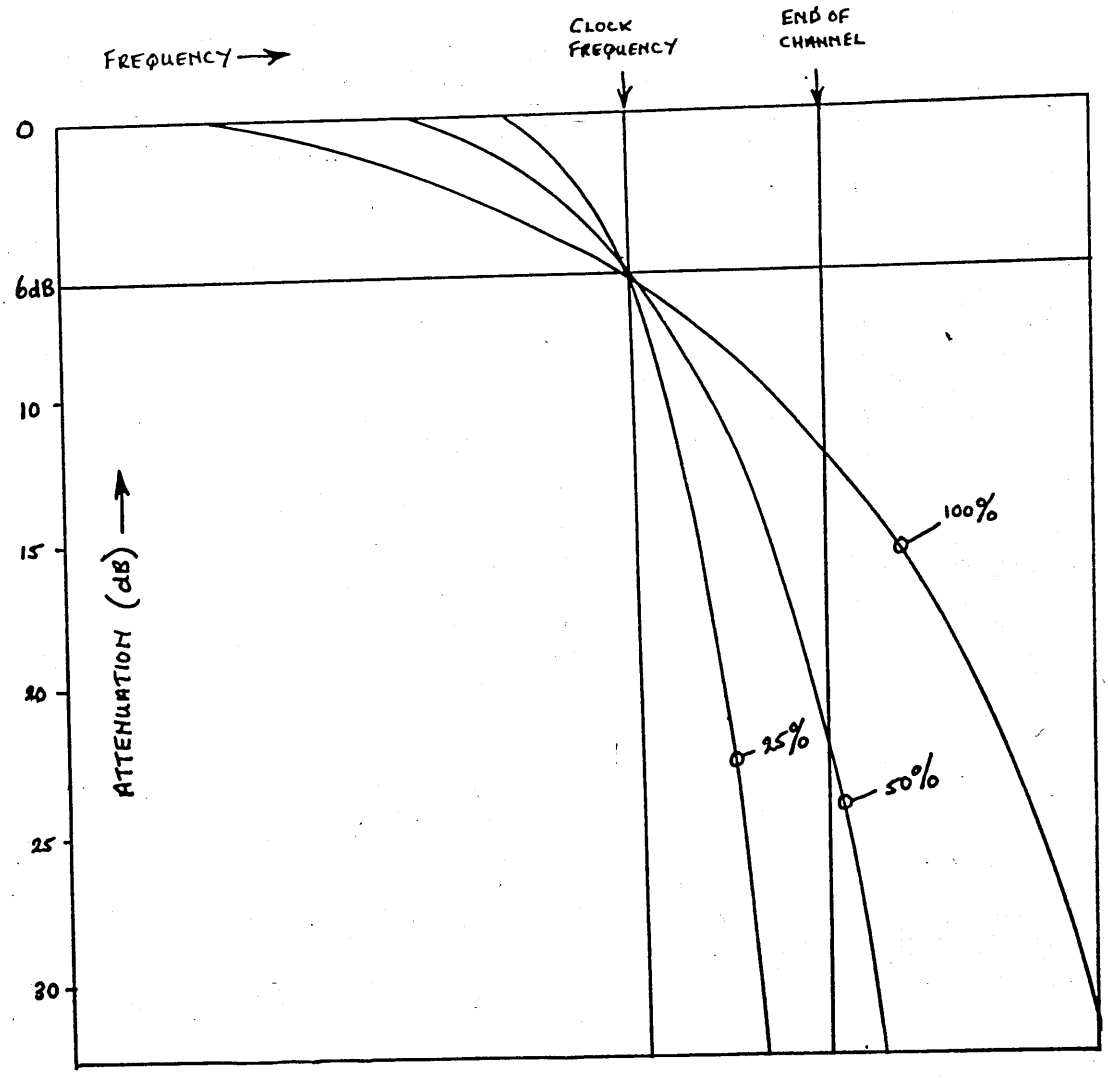

FIGURE 4.11 AMPLITUDE RESPONSE OF A FAMILY OF COSINE ROLL-OFF FILTERS

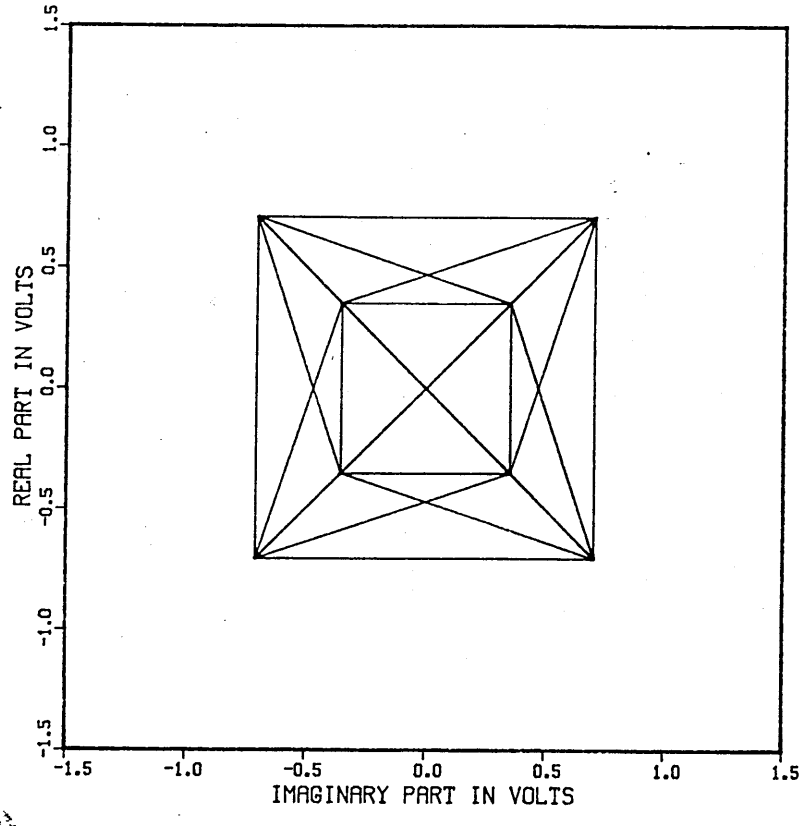

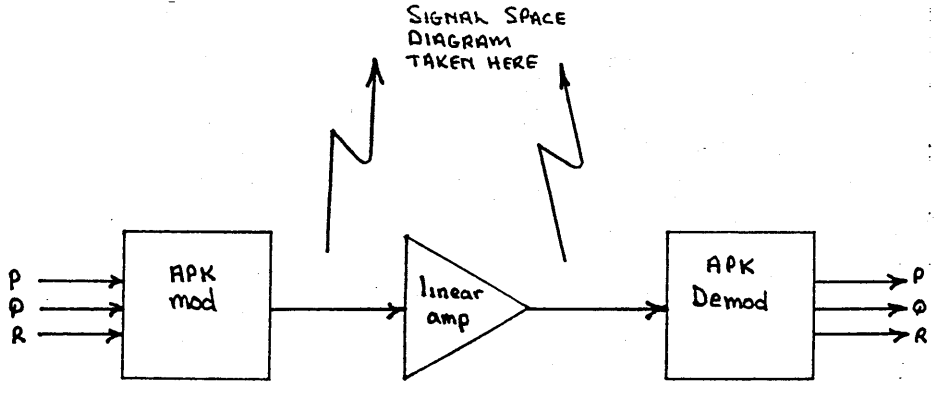

FIGURE 4.12 ELEMENTARY TYPE-A APK CHANNEL AND SIGNAL SPACE DIAGRAM

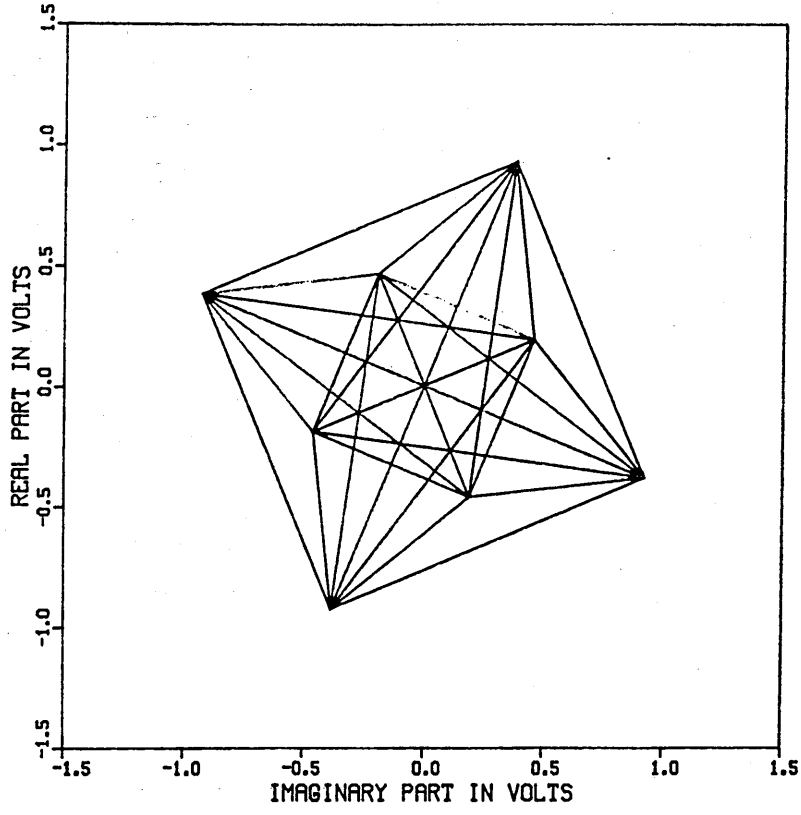

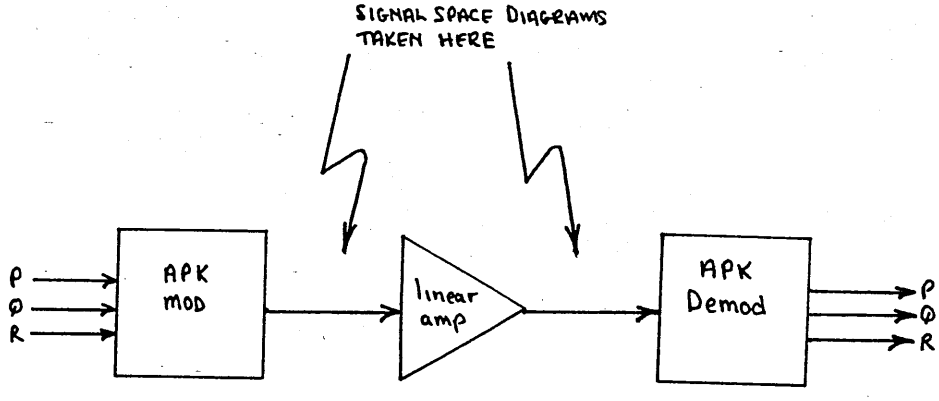

FIGURE 4.13 ELEMENTARY TYPE-B APK CHANNEL AND SIGNAL SPACE DIAGRAM

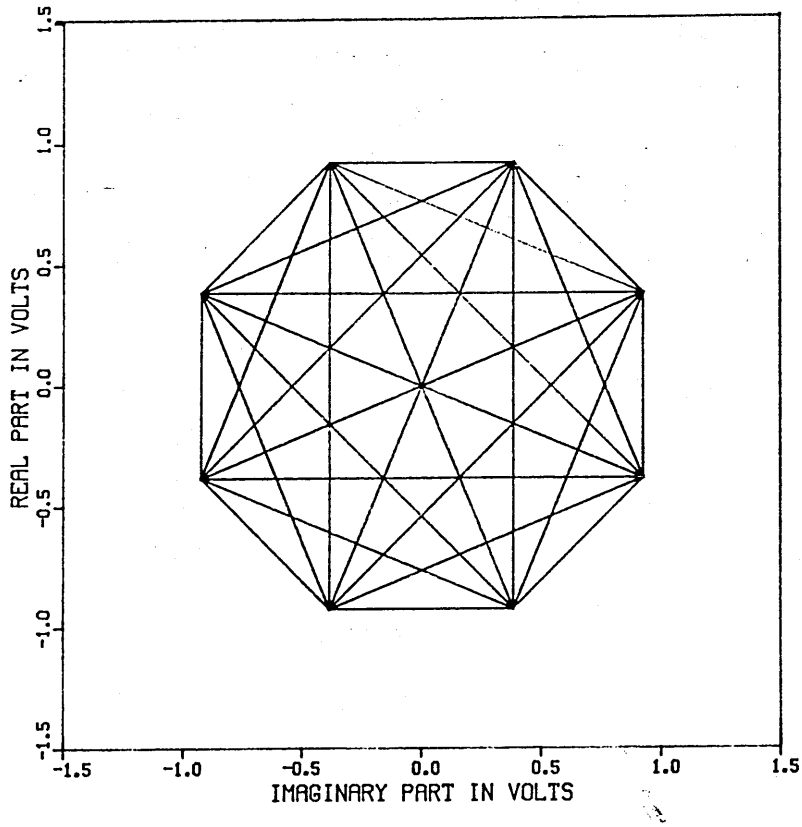

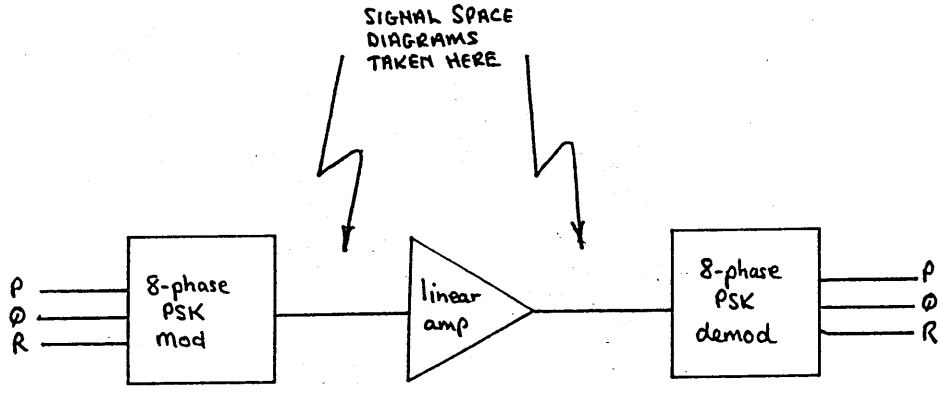

FIGURE 4.14 ELEMENTARY 8-PHASE CHANNEL AND SIGNAL SPACE DIAGRAM

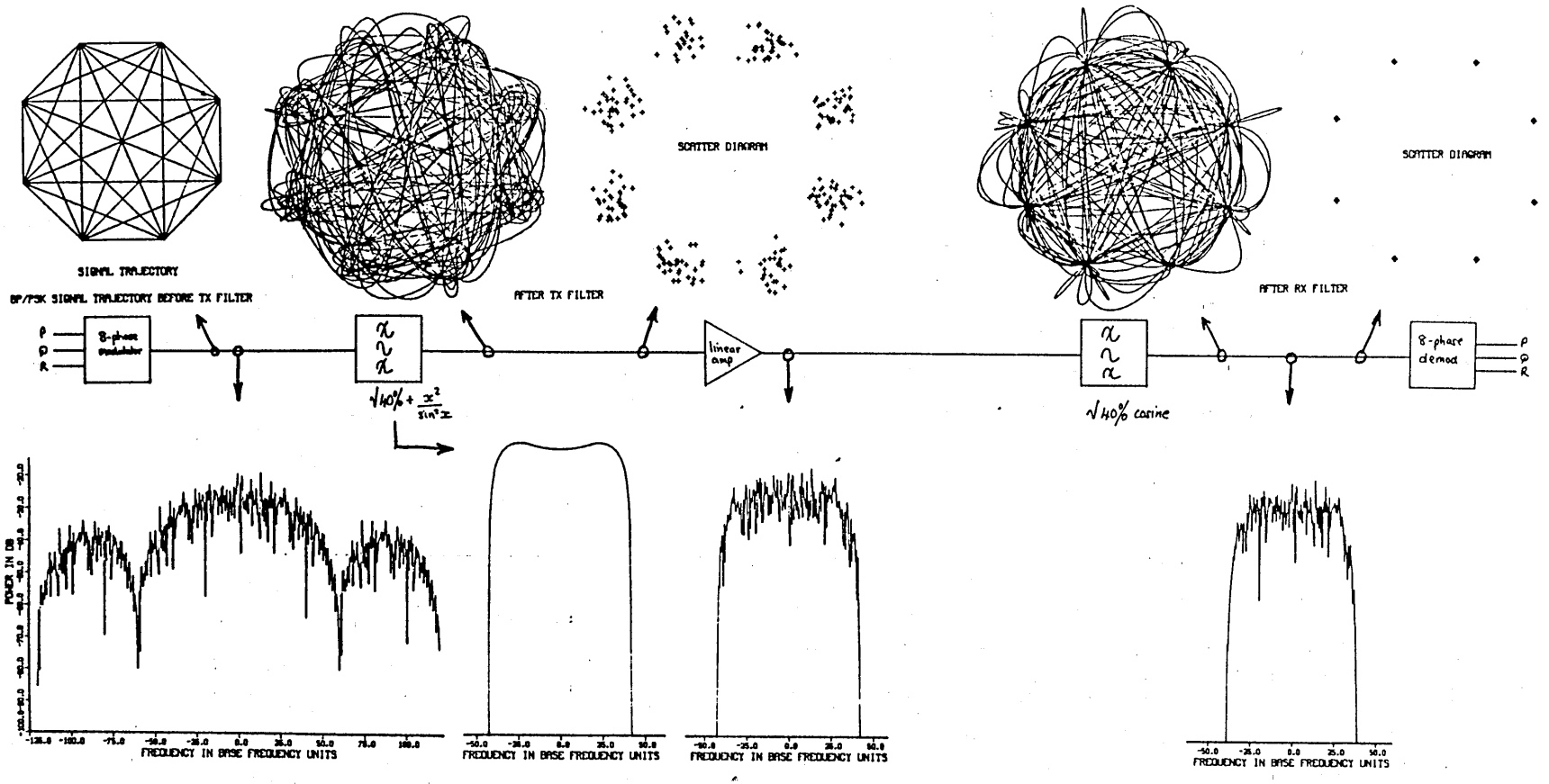

FIGURE 4.15 8-PHASE PSK LINEAR SYSTEM WITH CHANNEL FILTERING

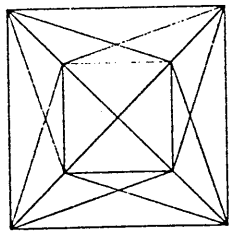

Wideband
(Input)

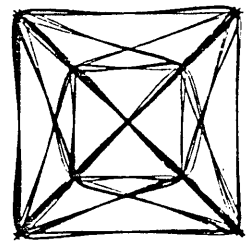

100% cosine

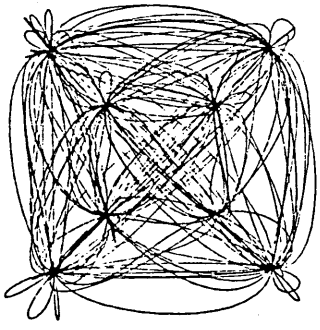

50% cosine

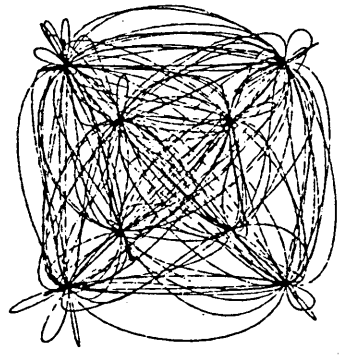

40% cosine

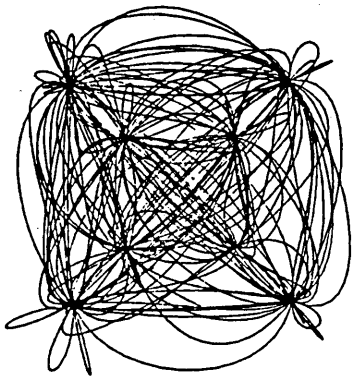

30% cosine

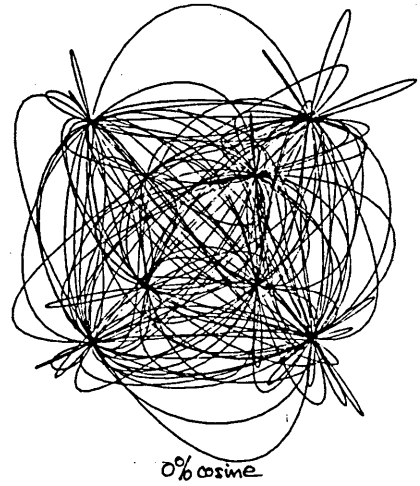

0% cosine

FIGURE 4.16 COMPUTER GENERATED SIGNAL SPACE DIAGRAMS FOR VARIOUS COSINE ROLL-OFF FACTORS IN A TYPE-A APK SYSTEM

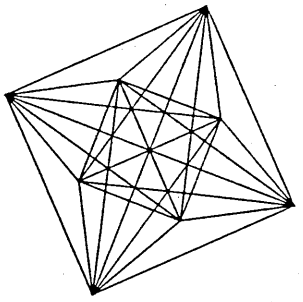

Wideband
(Input)

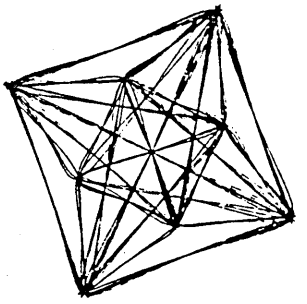

100% cosine

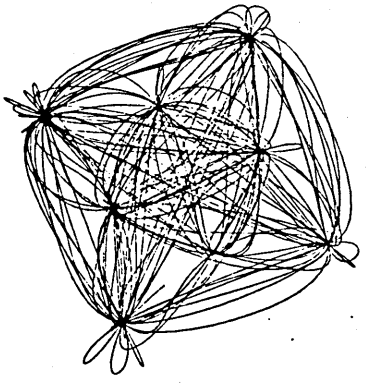

50% cosine

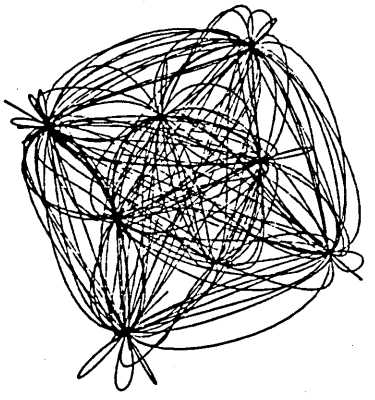

40% cosine

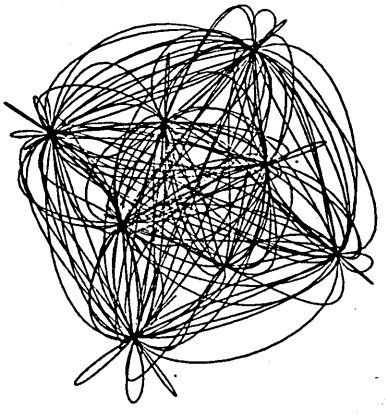

30% cosine

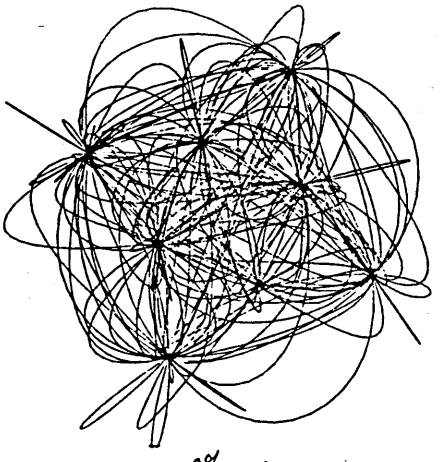

0% cosine

FIGURE 4.17 COMPUTER GENERATED SIGNAL SPACE DIAGRAMS FOR VARIOUS COSINE ROLL-OFF FACTORS IN A TYPE-B APK SYSTEM

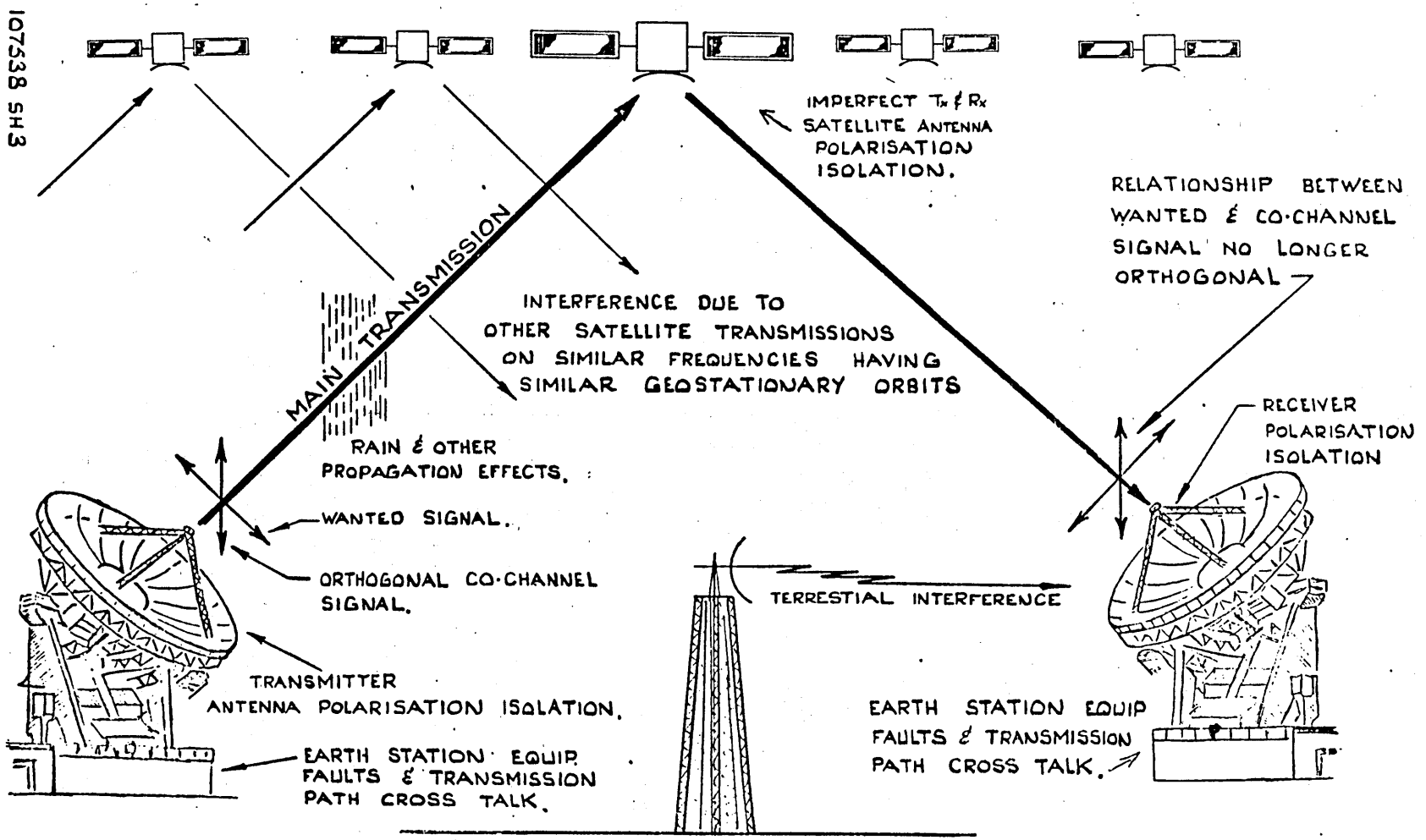

FIGURE 4.18 SOURCES OF CO-CHANNEL INTERFERENCE

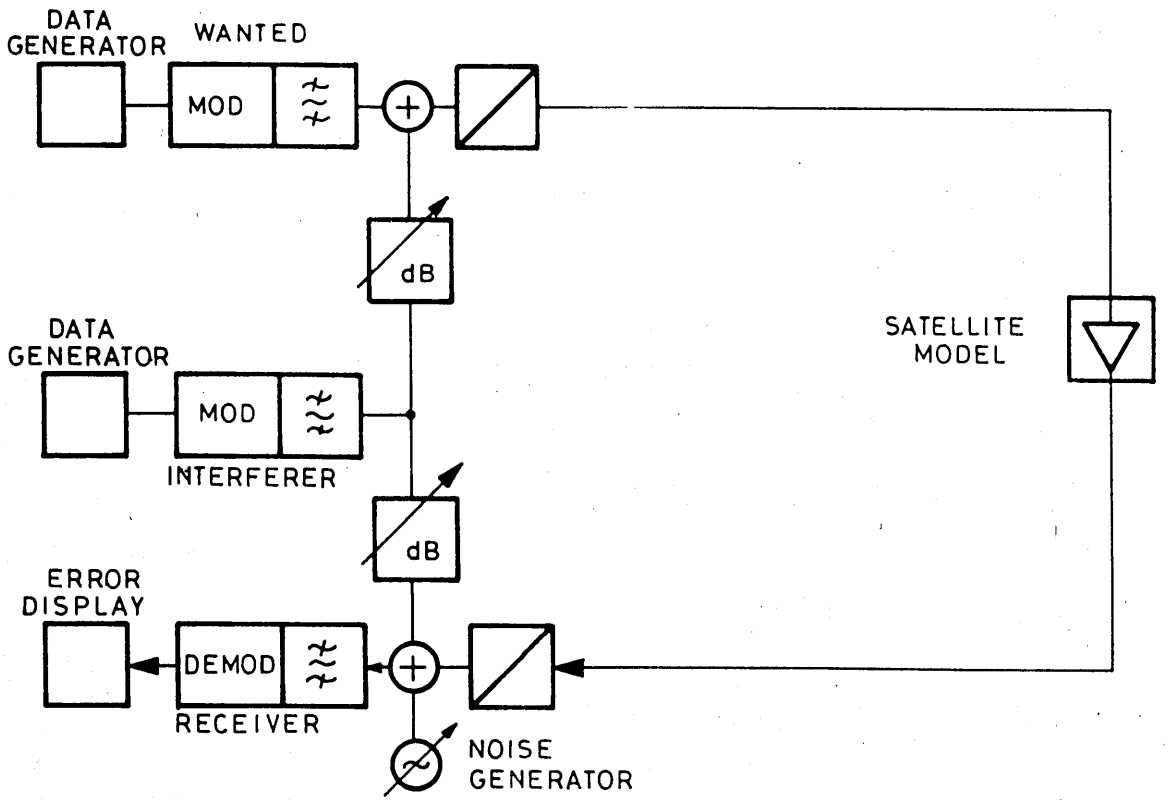

FIGURE 4.19 TRANSMISSION MODEL FOR CCI INVESTIGATIONS

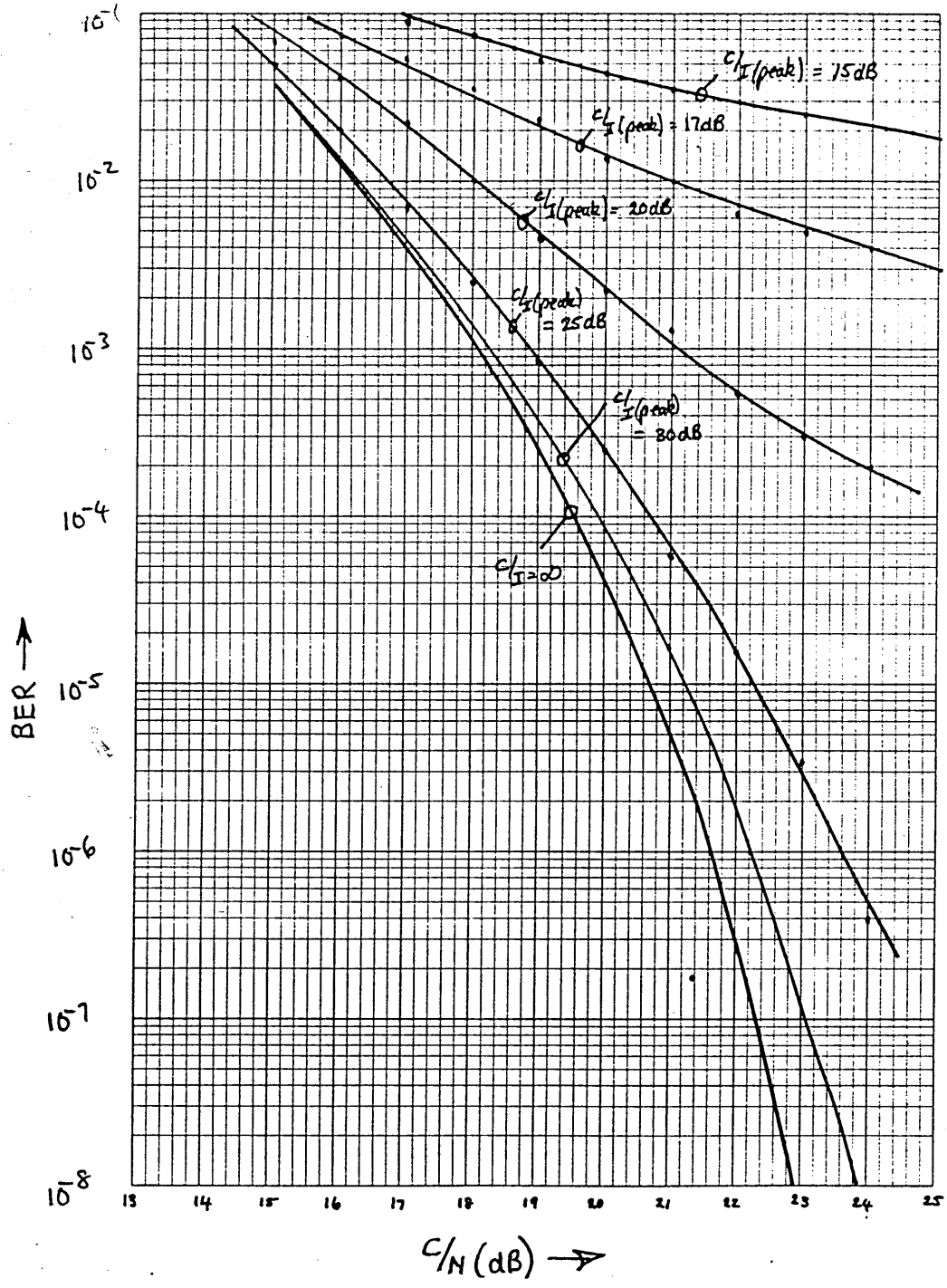

FIGURE 4.20 BER vs C/N FOR VARIOUS C/I IN AN APK-A LINEAR CHANNEL

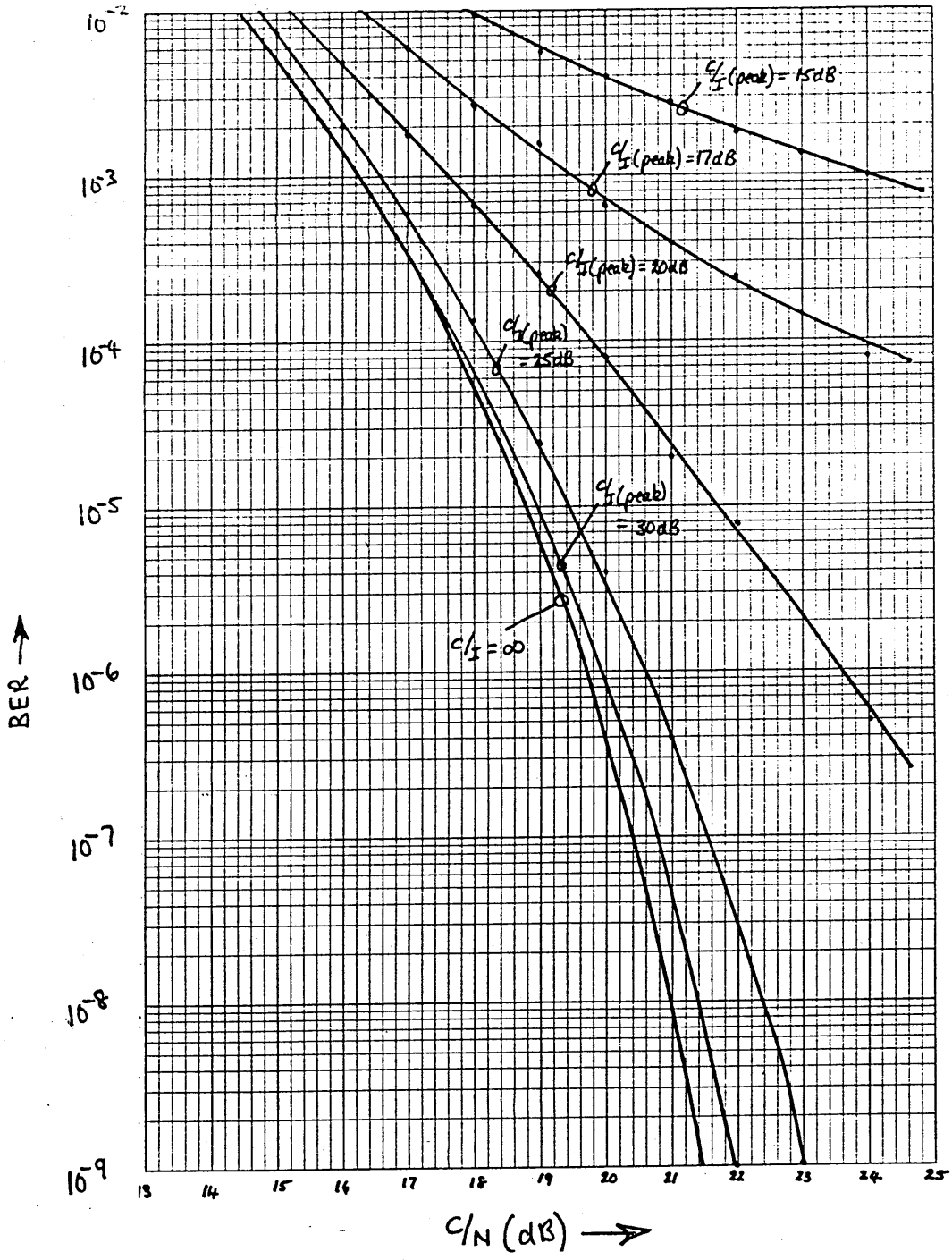

FIGURE 4.21 BER vs C/N FOR VARIOUS C/I IN AN APK-B LINEAR CHANNEL

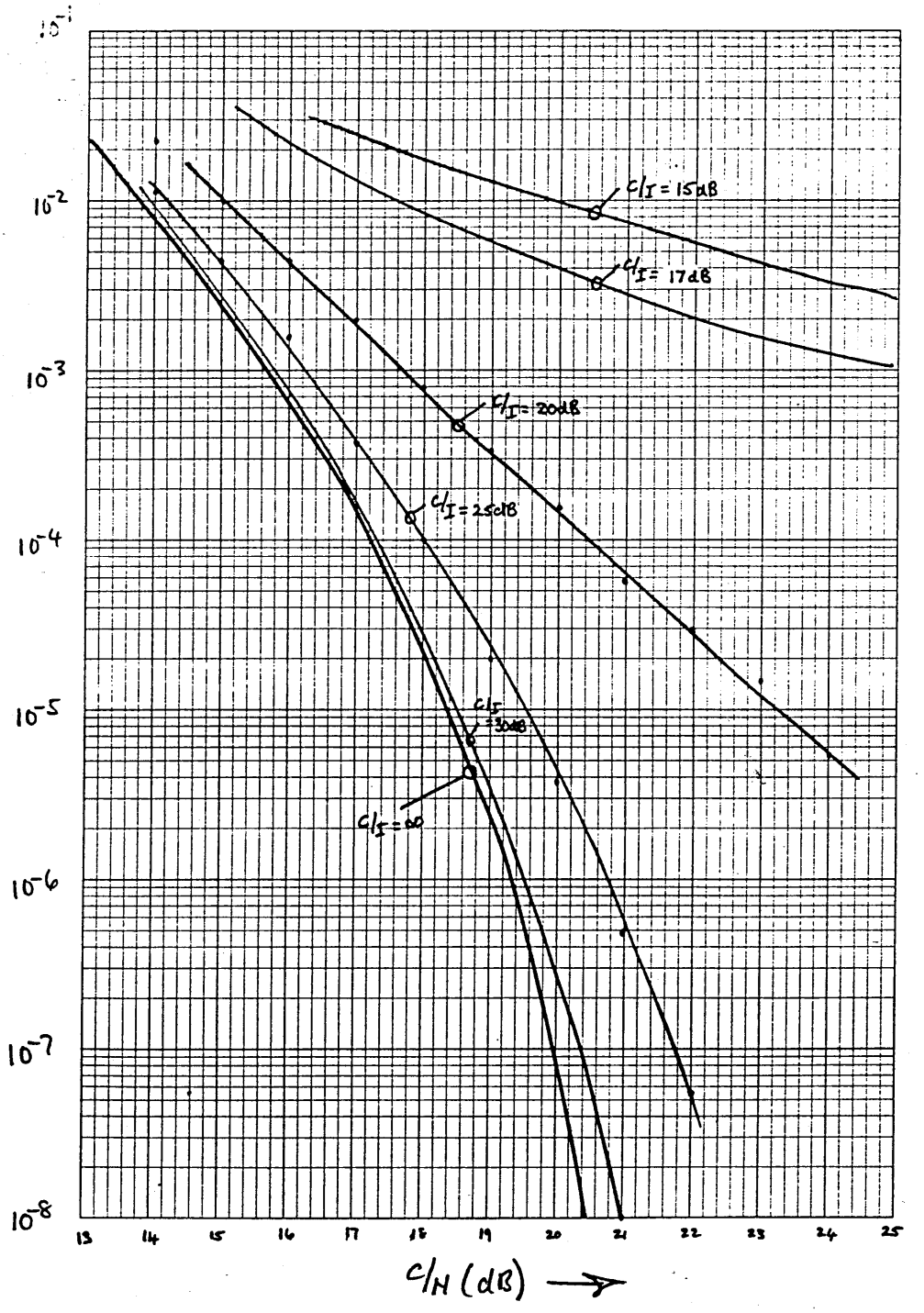

FIGURE 4.22 BER vs C/N FOR VARIOUS C/I IN AN 8-PHASE LINEAR CHANNEL

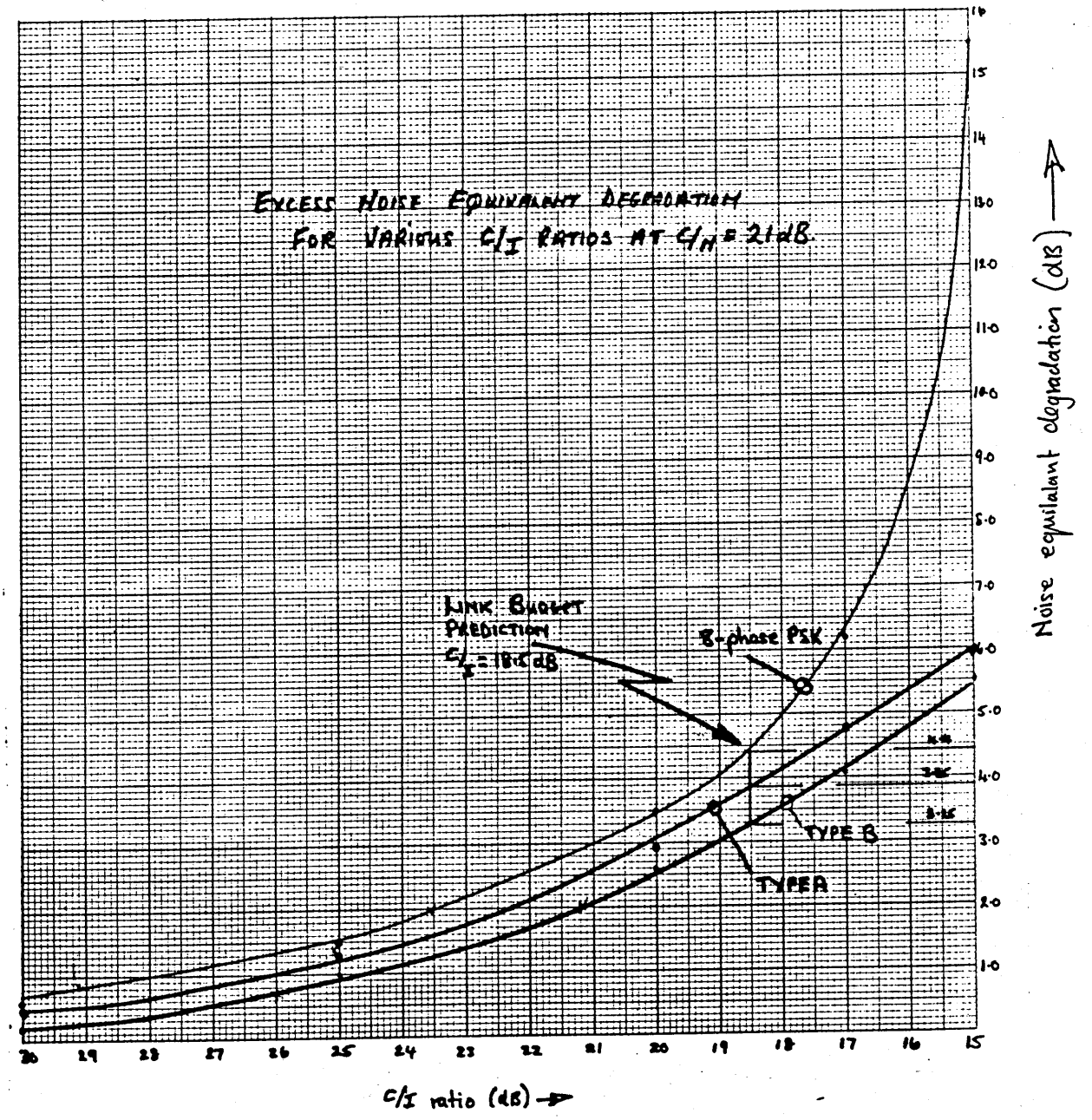

FIGURE 4.23 NOISE EQUIVALENT DEGRADATION vs C/I FOR THE THREE SYSTEMS

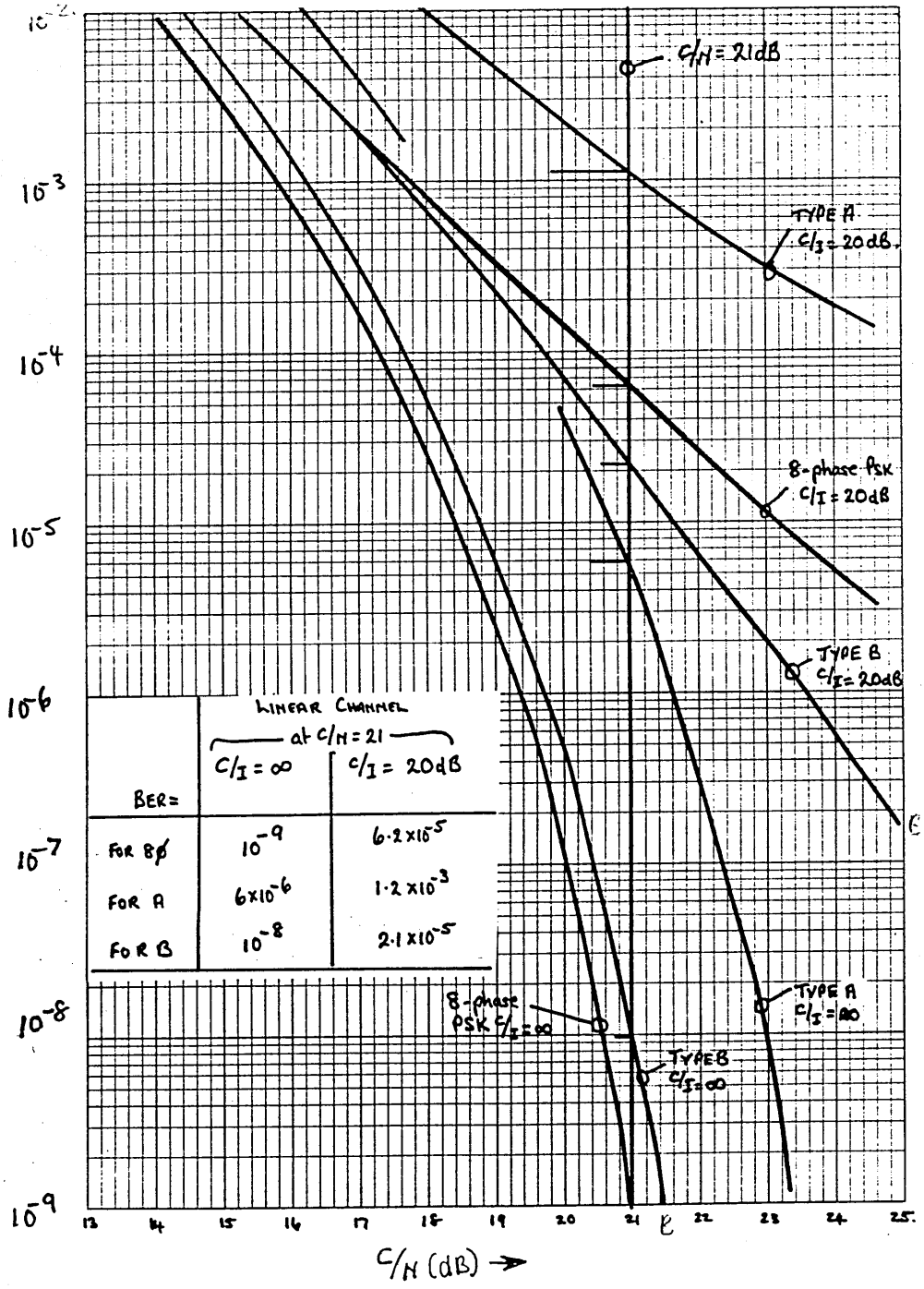

FIGURE 4.24 BER vs C/N FOR C/I =20dB
FOR THE THREE SYSTEMS

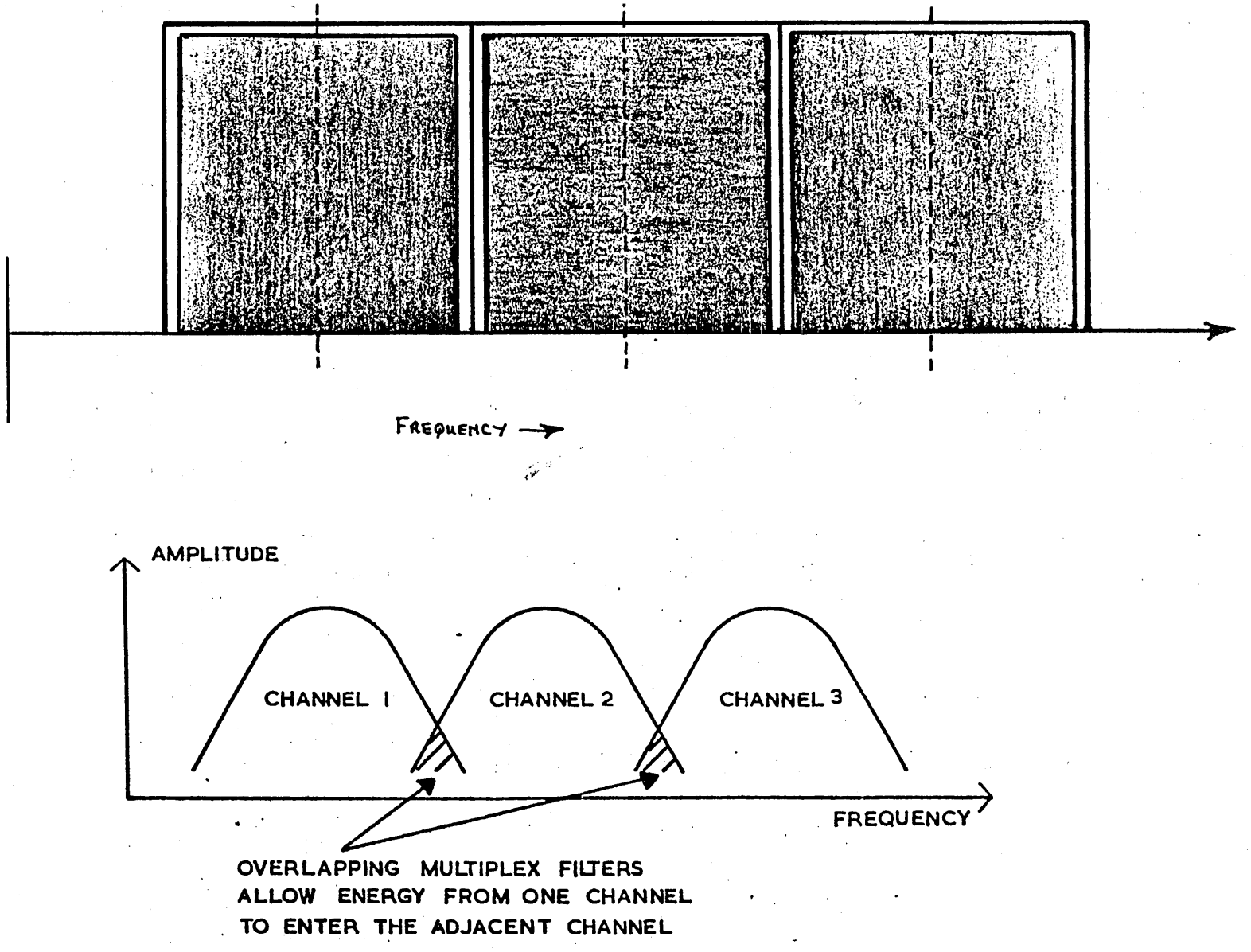

FIGURE 4.25 IDEALIZED CHANNEL SPECTRAL SHAPE AND MULTIPLEXING ARRANGEMENTS

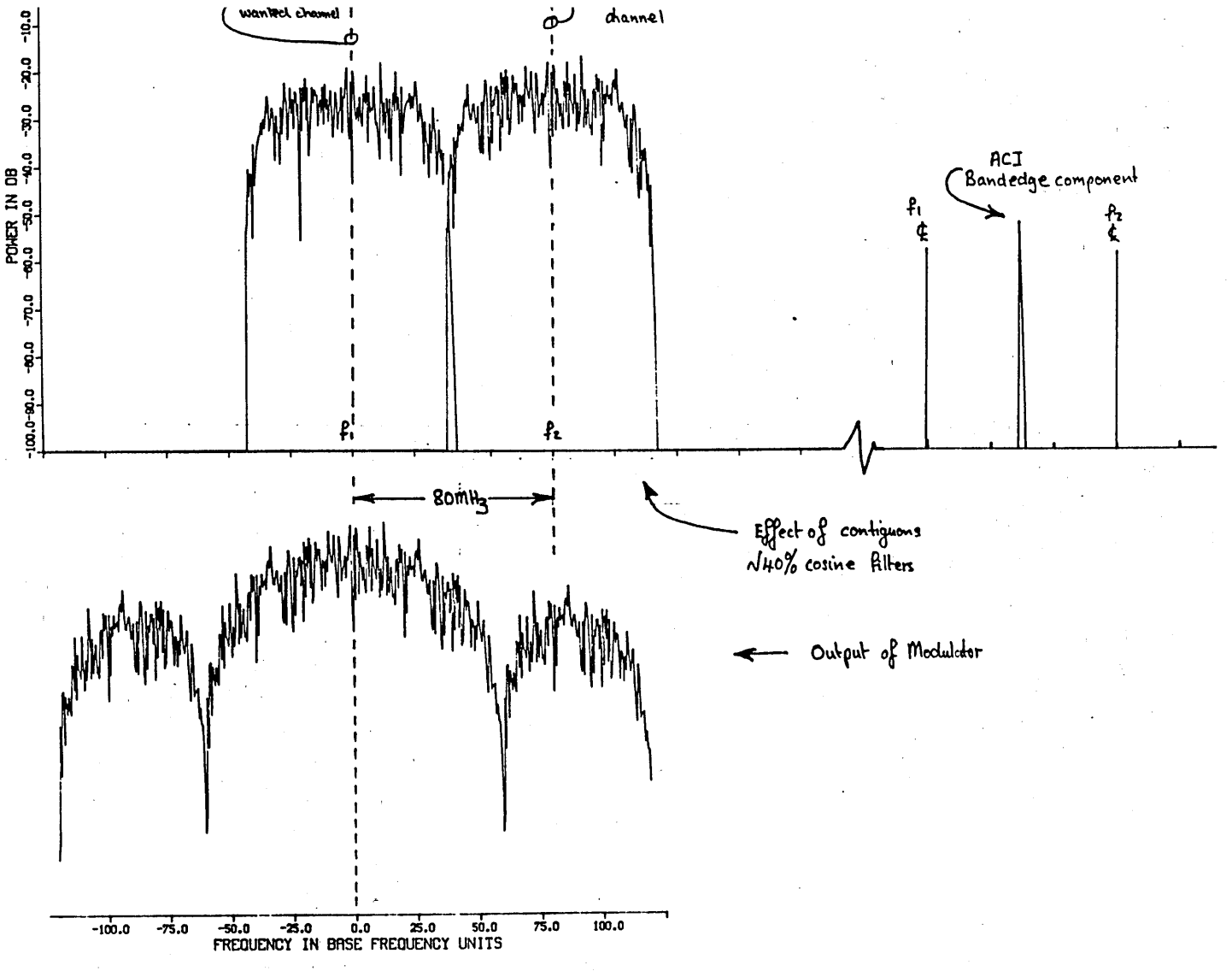

FIGURE 4.26 GENERATION OF ADJACENT CHANNEL INTERFERENCE COMPONENT

SECTION 5

NON-LINEAR CHANNEL ANALYSIS

5.1 Introduction

In the previous section, the mechanisms are examined which prevent the theoretical obtainable performance being achieved in a satellite system employing linear power amplifiers. However, this linear channel analysis is a poor approximation to the real case where the satellite TWTA will be operated close to or at saturation. Accordingly, in this section the techniques developed for the linear channel analysis will be applied to the non-linear channel in order to obtain a reliable estimate of the performance of the three candidate modulation schemes operating in a practical satellite system.

The analysis process for the non-linear channel therefore employs the same techniques as the linear channel, but becomes very much more complex because of the larger number of variables. The overall aim is to use the transmission model developed in Section 4 to analyze the performance of the three candidate modulation schemes and to seek the optimum value for those transmission

parameters not fixed by the satellite and earth station designs. For example, the Traveling Wave Tube Amplifiers (TWTA's) used in satellite power amplifiers consume the same dc input power irrespective of the power delivered to the load. If the satellite is to be used efficiently, the repeater amplifier must be operated close to, or at, the maximum output power which is termed saturation. Furthermore, overall economics may in some circumstances dictate that the ground station high power amplifier (HPA) will also have to operate non-linearly. Accordingly, the performance of the three systems must be obtained at various degrees of non-linearity in order that increasing non-linearity (increasing output power) can be properly balanced against the resulting C/N ratio improvement thus achieving the best BER.

The main problem in the system engineer's mind when dealing with a channel containing one or two gross non-linearities is the lack of established guidelines. For example, we know that in the linear channel a filter satisfying Nyquist's first criteria will give freedom from ISI at the sampling instant, but at all other times, the amplitude of the signal is influenced by the overlapping tails of the adjacent symbols. When a signal passes through a non-linear device, the waveforms can be severely modified, and the extent of the modification is dependent

upon the message content (since that determines the characteristics of the ISI "tails"). This is especially so with APK since preceeding and succeeding symbols could be substantially higher in power level. When Nyquist shaping is carried out both at the transmitter and receiver, and a non-linearity is effectively inserted between the two filter characteristics, the matched filter concept no longer applies since the spectral shape following non-linear amplification will certainly bear only a passing resemblance to the original waveform. It is therefore necessary to supplement the optimization techniques employed in the linear channel case.

5.2 Optimization of a Non-Linear Channel

Initial studies in which the author participated, performed for the European Communication Satellite (ECS) design, discovered that a major factor affecting the distortion of a QPSK signal was the rate of roll-off of the spectrum at the input of the non-linear amplifier[24]. Since that time many studies have been made to attempt to understand the behavior of the non-linear distortion mechanisms[23,26].

In Section 4, it was shown that when the rate of roll-off of the channel shaping filters is increased, the

signal space diagrams show increasing signal point overshoot because the pulse-response of the filters exhibits greater ringing (Figures 4.16 and 4.17). As a consequence, the signal envelope variations become larger and the interaction between the higher envelope variations and the non-linear TWTA will lead to greater distortion after amplification. This tends to imply that sharper roll-off filters will give greater distortion.

5.2.1 Non-Linear Distortion Mechanisms

In order to establish clearly and unequivocally that sharper roll-off filters result in greater TWTA-induced distortion, it is useful to start by again considering a linear system. Figures 4.12, 4.13 and 4.14 showed the effect of APK types A and B and 8-phase PSK systems, respectively, transmitted over an elementary linear channel. As shown in these figures, the signal space diagram is taken from the input to the demodulator (i.e., after the receive channel shaping filter) and in the ideal case should consist of eight points in vector signal space corresponding to the eight signal point positions, 000, 001, 010 ....111. When the baseband message necessitates a change in the transmitted signal, the new position in the signal space diagram will be reached by passage along one of the straight lines linking

the points. In order to judge what happens in practice, the signal space diagrams for a family of cosine roll-off filters in a linear channel was shown in Figures 4.15, 4.16 and 4.17. It will be noted that in the 100 percent cosine roll-off case, the pulse waveforms exhibit very little overshoot and the signal moves directly from point to point. As the roll-off factor is reduced, the pulse overshoot increases and the individual symbol waveform is increasingly affected by the ISI tails from the other pulses. This corrupts the trajectory of the signal vectors when moving from point to point, effectively increasing the peak-to-mean ratio of the signal (or, in other words, increasing the am component of the signal).

These changes do not affect the performance of the linear system--the ISI at the sampling instant is still theoretically zero--and whatever happens to the signal outside the sampling instant is irrelevant (at least in a wideband scheme). However, the oscillatory tendencies of the signal in the non-linear channel have a critical influence on the overall performance. A wideband TWTA non-linear amplifier produces a number of distortion mechanisms; viz: imperfect gain/frequency response, imperfect phase/frequency response, increased electrical path length with output power, and gain compression. The last two are a significant cause of degradation while the

gain frequency response and imperfect phase frequency response can be assumed to be externally equalized to the point where their contribution is negligible. The primary distortion introduced by the non-linear amplifier is gain compression. Figure 5.1 shows an elementary channel containing two non-linearities. Note that the power transfer characteristics are such as to exhibit a saturation effect beyond which a further increase in input power results in a decrease in output power. From the small power region to the full power region, the gain reduces as a function of output power. This means that the signal amplitude distribution is compressed after passing through the non-linearity which causes intermodulation between the various overlapping ISI pulse tails. The term "intersymbol intermodulation" (ISIM) has been proposed for this effect[27].

5.2.1.1 Filtering Effects in a Non-linear Channel

The reaction of a non-linear channel to sharp roll-off filters is shown by considering the signal space diagrams for the three candidates in Figures 5.2, 5.3 and 5.4 for a system containing one non-linearity. Forty percent cosine roll-off filtering has been chosen to illustrate the performance defects associated with moderately tight channel filtering arrangements. Since

channel filtering is carried out at the transmitter, its output (as shown in the Figures) has the same oscillatory trajectories in the signal space diagram as the linear channel case. These signals are now amplified by a saturated or near-saturated TWTA and so the output signal space diagrams are bounded by a circle of constant amplitude because the signal amplitude cannot exceed the maximum output of the TWTA. Distortion arises because the low amplitude signals, particularly the inner ring in APK, are amplified more than the high amplitude signals (gain compression effects). Similarly, the phase shift given to high amplitude signals is different than that given to low amplitude signals due to electrical path length variations with output power (known as amplitude modulation/phase modulation (am-pm) effect). It can be seen from the curved trajectory within the circles that considerable distortion arises from the combination of these effects. Nevertheless, since the TWTA is memoryless (very wide bandwidth) no further intersymbol interference is introduced at the sampling instant. The APK scatter diagrams show the effect of gain compression and am/pm. Note that the ring ratios are much reduced after the non-linearity and the outer ring is rotated relative to the inner ring by the am/pm effect.

In practice, some form of filtering is always necessary at the receiver for the reduction of noise and interference. Every form of filter which will satisfy the receiver demultiplexing requirement of a practical system will be sufficiently narrow to introduce significant memory into the transmission path. The signal applied to the filter is grossly distorted, but as has been said before, it contains no ISI at the sampling instant. The action of any filter after the non-linearity is to spread the distorted waveform in time which means that the sampling instant no longer contains only the wanted signal. This in turn, means that less noise power will be required to cause an error in the demodulator. Removal of these spread waveform products is possible in principal, but is very difficult in practice[27].

Accordingly, if the channel is to operate non-linearly and because of the presence of some form of filter after the non-linearity (even, for example, the satellite Output Multiplexing Filter (OMUX)), gentle spectral roll-off must be employed prior to the non-linearity in order to minimize the spread waveform effects.

5.2.2 Selection of Channel Filters

At this stage we now have five main degrees of freedom:

- Operating point of the satellite TWTA (i.e., the degree of non-linearity).

- Operating point of the ground station TWTA.

- Manner by which the channel shaping characteristic is shared between transmitter and receiver.

- Overall channel shaping characteristic.

- Signal Level Ring ratios (in the case of APK).

5.2.2.1 Operating Point of the Satellite

Satellite systems are normally down-link power limited and this leads to the conclusion that saturation would seem to be a good operating point. Of course, that is also the region of maximum distortion, and therefore it is necessary to try and design a system that is insensitive (or at least less sensitive) to in-band

distortion. Operating at saturation not only maximizes the down-link signal-to-noise ratio, but permits a small degree of variation in the up-link power, thus allowing a simple form of earth station transmit power control. (In an 11/14 GHz system, as will be seen in Section 6, operating at saturation gives good protection against up-path fading due to precipitation.) Considering all the various aspects, saturation would seem to be a good target if the attendant distortion can be accommodated. However, it is easy to forsee a problem with the gain compression effects on the amplitude decision regions of APK. This may force a re-evaluation of the satellite operating point when the overall optimization is performed.

5.2.2.2 Operating Point of the Ground Station

The ground station operating point is a little less critical under normal circumstances. In contrast to the satellite, which is power limited by well-defined aspects of design (e.g., weight, solar cell area, antenna size, etc.), the optimum choice of the ground station transmitter is far less sharply defined. The DC power input to the transmitter clearly results in increased cost for increased power, and it is also clear that large tubes cost more than small tubes. However, the ground station antennas tend to be large in order to satisfy the receive

signal-to-noise requirements and so the high gain reduces the power requirements of the transmitter. There are, in practice, two other factors. Technology tends to limit the size of 14 GHz TWTA's to around 2 kW, however, the gain of the average 11/14 GHz earth station antenna results in a backoff of around 5 dB for a 2 kW TWTA. On the other hand, for 6 GHz systems TWTA's are available up to 13 kW. Taking the average of typical earth station transmitters at around 8 kW, the average backoff in a 6 GHz TWTA may well be in excess of 13 dB. In short, a range of earth station TWTA backoff may be expected.

5.2.2.3 Method of Distributing the Overall Shaping Characteristic

Early work showed[24] that to minimize distortion, the channel shaping should be fairly evenly distributed between the transmitter and receiver. However, small differences between the sharing of transmit and receive filter characteristics does not have a large impact on overall performance. Therefore, there is some small degree of freedom in this respect, but for now a 50 percent sharing (i.e., a square root sharing) will be assumed.

5.2.2.4 Overall Channel Shaping Characteristic

We have established that sharper roll-off gives increased TWTA distortion. Figure 5.5, which gives a composite set of curves derived by the author from computer simulations performed at ESA/ESTEC, shows the behavior of a single satellite channel as the roll-off factor is altered. The satellite is assumed to be saturated, and curves are plotted for both a saturated and a linear HPA for APK types A and B and 8-phase PSK. The filtering is assumed equally shared between transmit and receive, and impulse signalling is also assumed. It is implicit in this result that means are available (for example by pre-compensation) to obviate the compression effect on the signal level rings of the APK signals. This will be justified later. As the roll-off factor is decreased, the non-linear distortion increases due to the mechanisms discussed above. This is the primary effect, but it will be noted that the degradation rises again toward the high roll-off region of the curve. This is a second order effect, and is assumed by Harris[27] on the basis of his computer simulations to be due to the action of the input and output satellite multiplexing filters. This could not be substantiated by the hardware experiments used as the basis of this work, because a variety of I/OMUX filters were not available, but is a

reasonable assumption and remains a working hypothesis. It can be seen from Figure 5.5 that the result of these opposing phenomena is a rather flat optimum in the region of 50 percent cosine roll-off, for the linear HPA. (This curve has been taken from Harris' computer simulation: except for the high roll-off section of the curve, which was derived by the author using a hardware simulation).

When the HPA is operated in the saturated region, the signal is spread far beyond its original bandwidth by a process known as spectrum spreading[20]. As will be seen later, this has a greater significance in out-of-band emission studies than on the in-band distortions. Some effects are present, however, and this centres around the reaction of the satellite IMUX to this wider spectrum. At the output of the HPA, the same distortion and amplitude limitation, as was described earlier for the satellite TWTA, has occurred. Again, this severe distortion has no significance until the IMUX is reached. This filter is generally of appreciably wider bandwidth than the channel filters, but even this filter has considerable memory and so spreads the distortion out across the pulse, causing interference at the sampling instant and reintroducing an additional degree of am to the signal. The satellite TWTA now repeats the process of amplitude limitation and causes

further distortion (although less than with the linear HPA). The receiver filter then smears even more energy across the sampling instant.

It can be seen that freedom from ISI at the TWTA input does not guarantee good performance over the non-linear channel, and it is essential to keep the overall non-linear distortion to a minimum. This can only be done by reducing the am component of the input signal to a minimum.

Before it is possible to come to a firm conclusion as to the optimum channel filter, it would be useful to check the sensitivity of various filter schemes to the TWTA operating point. By the use of this method, it should be possible to justify some of the assumptions used in the selection process.

Figure 5.6 plots the increase in distortion in the receiver as a TWTA is driven from the linear region to saturation. Two curves (which have been derived from practical measurements over a QPSK simulator) are plotted, corresponding to 50 percent and 30 percent cosine roll-off filtering characteristics. It can be seen that in the linear region both systems are unaffected by the presence of the TWTA, but as the TWTA enters saturation, the

distortion shows a marked increase. However, in the case of the 50 percent filtered system, the distortion increase only becomes significant in regions close to saturation and even at saturation the magnitude of the degradation is markedly less than the 30 percent case. Figure 5.7 translates these effects into practice for an INTELSAT V satellite system. The BER vs satellite operating point curve was derived from a combination of calculations and simulations using a linear earth station and assuming a maximum attainable C/N of 21 dB. The curves show the performance of a 40 percent cosine roll-off filtered system for 8-phase PSK, and APK types A and B. It is assumed that the gain compression effect on the signal rings have been obviated (e.g., by precompensation (5.2.3)). Clearly, the optimum is indicated by the minimum in the curves in Figure 5.7, and the 8-phase PSK system shows the optimum to be at 2 dB input backoff, whereas the APK A and B systems yield optimum performance at 6.7 and 6.5 dB satellite input backoff, respectively. This means that all three systems must be dominated by distortion since, as the satellite is driven into saturation, the distortion is rising rapidly but because of the proximity of the operating point to saturation, the down-link power and hence the receive signal-to-noise ratio is only changing slowly. In the APK cases, the

increased distortion requires a significant degree of backoff and therefore the distortion must be comparable with the degradation due to noise.

By this stage, it is clear that a cosine roll-off in the 45 percent to 60 percent range can be considered optimum and it would seem reasonable that 50 percent filtering could be considered representative of the optimum filter spread from now on.

5.2.3 Gain Compression Effects On Signal Level Rings

In Section 3, the optimum for the level decision thresholds was computed and shown in Figure 3.9. Thus, for a Type A system, an amplitude ratio of 0.43 minimized the overall BER. If this optimized ratio is now applied to a TWTA, such that the peak signal just saturates the amplifier, the ring ratio seen on the down-link is substantially reduced due to TWTA gain compression. Figure 5.8 shows this effect. The input has one ring at 0 dB and the other at the optimum (-6 dB). The output, however, is 0 dB and 1.7 dB which when converted to a linear voltage ratio and applied to Figure 3.9 shows that the error rate degrades from 10^{-8} to 10^{-2}. If the peak level is now moved from 0 dB to -3 dB input back-off, the output ratios are now -0.5 dB and -3.4 dB which gives

an error rate of 10^{-4}. However, since the full output power of the satellite TWTA is not being used, there is a 0.5 dB noise penalty to be added, since the received C/N would be degraded by this amount. This results in a further fall in BER to 2.5×10^{-4}. Table 5.1 shows these effects for a range of input back-off from +3 dB (overdrive) to -13 dB for the Type A and B systems. The results contained is Table 5.1 are plotted in Figure 5.9 for Type A, Type B and 8-phase PSK. Note that 8-phase PSK performs substantially better than Type B which in turn performs better than Type A. This is due to the near constant envelope of 8-phase PSK which is more suitable to single carrier non-linear operation. Similarly, Type B is nearer to a constant envelope signal than Type A and therefore, its performance is superior. Nevertheless, in this form, both Types A and B APK systems are not acceptable for the satellite system due to transmitted power loss stemming from their back-off requirements and it should be noted that the Type B system achieves the best error rate of about 10^{-5} at an 8 dB input back-off while the Type A system achieves approximately 10^{-4} at 6 dB input back-off. 8-phase PSK however, achieves better than 10^{-6} at saturation (maximum output power).

dB	dB=P1	dB=P2	dB (ratio)	ratio	penalty	penalty.	lower level dB=P2	P1-P2 dB(ratio)	Voltage ratio	level penalty	add power penalty	PSK
				1								
+3	-0.5	1.0	0.5	0.94	$7\,10^{-2}$	10^{-1}	(3.1) 0.5	0			0.5×10^{-1}	2×10^{-6}
+2	-0.25	1.3	1.05	0.88	10^{-2}	2×10^{-2}	0.8	0.6	0.93	10^{-1}	$7\,10^{-1}$	10^{-6}
+1												
0	0	2.3	2.3	0.77	6×10^{-3}	6×10^{-3}	1.7	1.7	0.82	10^{-2}	10^{-2}	6×10^{-7}
-1												
-2	-0.25	3.8	3.55	0.66	7×10^{-4}	8×10^{-4}	2.8	2.55	0.75	3×10^{-4}	4×10^{-4}	10^{-6}
-3	-0.5	4.6	4.1	0.62	2×10^{-4}	5×10^{-4}	3.4	2.9	0.72	10^{-4}	2.5×10^{-4}	2×10^{-6}
-4	-0.8	5.4	4.6	0.59	10^{-4}	3×10^{-4}	4.2	3.4	0.68	2×10^{-5}	7×10^{-5}	4×10^{-6}
-5	-1.2	6.3	5.1	0.56	5×10^{-5}	2×10^{-4}	5.0	3.8	0.65	5×10^{-6}	5×10^{-5}	10^{-5}
-6	-1.8	7.5	6.5	0.53	2×10^{-5}	2×10^{-4}	6.0	4.2	0.62	10^{-6}	5×10^{-5}	8×10^{-5}
-7	-2.2	8.3	6.1	0.49	7×10^{-6}	2×10^{-4}	7.0	4.8	0.58	10^{-7}	2×10^{-5}	6×10^{-5}
-8	-2.8	9.3	6.5	0.47	3×10^{-6}	5×10^{-4}	8.0	5.2	0.55	2×10^{-8}	1.5×10^{-5}	0.5×10^{-4}
-9	-3.5	10.4	6.9	0.45	2×10^{-6}	7×10^{-4}	8.8	5.3	0.54	2×10^{-8}	8×10^{-5}	4×10^{-4}
-10	-4.0	11.3	7.3	0.43	10^{-6}	10^{-3}	10.0	6.0	0.5	10^{-8}	0.5×10^{-4}	8×10^{-4}
-13	-7.0	14.3	7.3	0.43	10^{-6}		13.0	6.0	0.5	10^{-8}	8×10^{-3}	2×10^{-2}
-15	-9		7.3	0.43	10^{-6}	$7\,10^{-4}$	-15	6.0	0.5	10^{-8}	10^{-1}	10^{-1}
		TYPE A SYSTEM					TYPE B SYSTEM					

TABLE 5.1 FIXED OPTIMUM LEVEL SPACING
(A=0.43; B=0.5) BASED ON
C/N (PEAK)=21dB

5.2.3.1 Pre-Distortion Compensation

It was considered that the simplest method of obviating the compression effects would be to expand the signal level ring ratios such that, following TWTA compression, the optimum level ratios are once again presented to the down-link. In a simple system, this expansion is fixed at one output level and therefore, if the up-link power should vary, the down-link ratios will be non-optimum. Table 5.2 shows the calculated performance for the two systems. By way of example, consider a Type B system with the ratios set to achieve the optimum ratios on the down-link when the TWTA is operated at saturation (since only compression effects are to be considered, saturation is clearly the optimum region). At 0 dB input back-off (= upper ring level) the lower ring would be at -12 dB to achieve the optimum (-6 dB) on the down-link which would result in the restoration of the 10^{-8} best attainable error rate. Note however, that if the input falls to -3 dB, the upper ring level falls to -0.5 dB and the lower ring to -8.8 dB. This gives a new ring ratio of 8.3 dB which when converted to a linear voltage and applied to Figure 3.11 gives a 4×10^{-6} error rate. As before, the 0.5 dB power penalty must be "charged" to the system and accordingly, the new error rate is 10^{-5}. Table 5.2

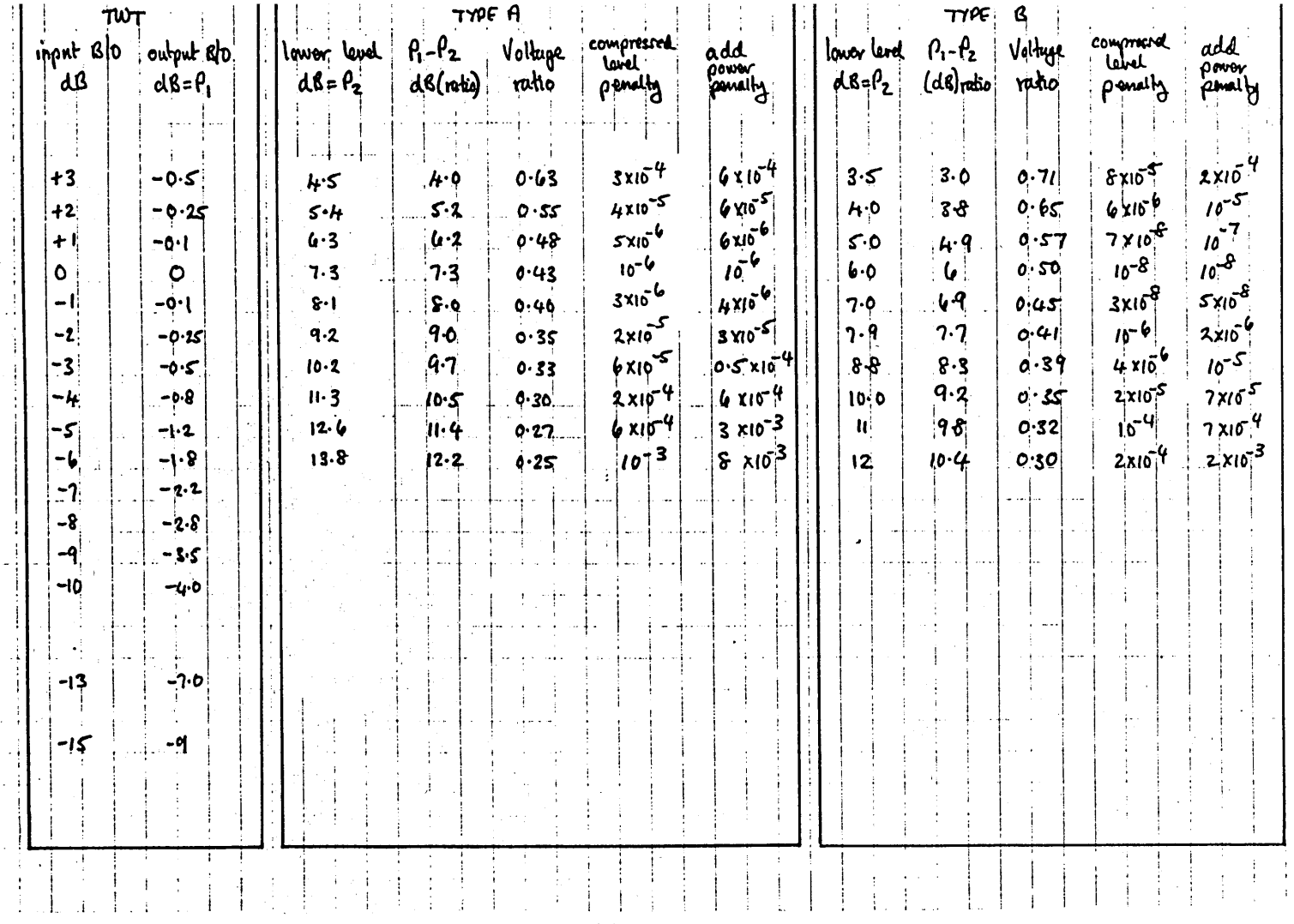

TWT		TYPE A					TYPE B				
input B/O dB	output B/O dB=P_1	lower level dB=P_2	P_1-P_2 dB(ratio)	Voltage ratio	compressed level penalty	add power penalty	lower level dB=P_2	P_1-P_2 (dB)ratio	Voltage ratio	compressed level penalty	add power penalty
+3	-0.5	4.5	4.0	0.63	3×10^{-4}	6×10^{-4}	3.5	3.0	0.71	8×10^{-5}	2×10^{-4}
+2	-0.25	5.4	5.2	0.55	4×10^{-5}	6×10^{-5}	4.0	3.8	0.65	6×10^{-6}	10^{-5}
+1	-0.1	6.3	6.2	0.48	5×10^{-6}	6×10^{-6}	5.0	4.9	0.57	7×10^{-8}	10^{-7}
0	0	7.3	7.3	0.43	10^{-6}	10^{-6}	6.0	6	0.50	10^{-8}	10^{-8}
-1	-0.1	8.1	8.0	0.40	3×10^{-6}	4×10^{-6}	7.0	6.9	0.45	3×10^{-8}	5×10^{-8}
-2	-0.25	9.2	9.0	0.35	2×10^{-5}	3×10^{-5}	7.9	7.7	0.41	10^{-6}	2×10^{-6}
-3	-0.5	10.2	9.7	0.33	6×10^{-5}	0.5×10^{-4}	8.8	8.3	0.39	4×10^{-6}	10^{-5}
-4	-0.8	11.3	10.5	0.30	2×10^{-4}	6×10^{-4}	10.0	9.2	0.35	2×10^{-5}	7×10^{-5}
-5	-1.2	12.6	11.4	0.27	6×10^{-4}	3×10^{-3}	11	9.8	0.32	10^{-4}	7×10^{-4}
-6	-1.8	13.8	12.2	0.25	10^{-3}	8×10^{-3}	12	10.4	0.30	2×10^{-4}	2×10^{-3}
-7	-2.2										
-8	-2.8										
-9	-3.5										
-10	-4.0										
-13	-7.0										
-15	-9										

TABLE 5.2 PRE-DISTORTED RESULTS
(SET FOR SATURATION)

shows a range of these calculations from +3 dB to -15 dB input back-off for the Type A and Type B systems. The results are shown plotted on Figure 5.10. Note that the best attainable performance of 10^{-8} (Type B) and 10^{-6} (Type A) have been restored by this compensation technique. Note also that the curves show a rather sharp optimum indicating a need to maintain the operating point of the satellite within rather close limits (say $\pm$1.0 dB). This compares with the less critical 8-phase PSK (+2.5 dB), which is assumed to use a predistortion technique in accordance with Reference 27, in order to make fair comparisons. Nevertheless, the Type B system is indicating a clear 1.6 dB inferior performance than 8-phase PSK.

5.2.4 AM/PM Effects

Up to this point, only the compression effects of power input/output (amplitude effects) have been considered. This is the primary distortion mechanism in TWTA satellite repeaters. It has been shown that a simple predistortion technique may obviate the gain compression effects. The secondary distortion mechanism will now be considered.

A TWTA exhibits a pronounced change in its electrical path length with changes in output power. The output/input power transfer characteristic of a typical TWTA and corresponding AM/PM characteristic is shown in Figure 5.11. The phase change through the device can be seen to change markedly over the range -15 dB to saturation. The previously successful predistortion technique was based on enhancing the level difference between the two signal rings on the up-link such that the optimum spacing was achieved on the down-link. For operation at saturation, this resulted in an up-link level ratio of 12 dB from the Type B system and 13.5 dB for the Type A system (Table 5.2). Figure 5.12 shows these enhanced level applied to the AM/PM characteristics. It can be seen that the phase difference between the lower and upper signal rings is corrupted by 34° for the Type B system and 36.5° for the Type A system. These effects are illustrated in Figure 5.13, where the upper signal ring is rotated relative to the lower ring by the am/pm action. To assess the effect of this, Figure 5.14 which was derived from computer simulation shows the noise equivalent degradation for various inter-ring phase shifts (noise equivalent degradation can be viewed as the increase in signal-to-noise ratio necessary to restore a link to the error rate that existed before the degradation was added).

It should be noted that the 34° and 36.5° phase shifts discussed above give rise to 12.5 dB and 14.8 dB noise equivalent degradation. Table 5.3 calculates the overall effect of am/pm for the two systems. Note that at saturation, the Type B system overall error rate has degraded from 10^{-8} to 10^{-1}. In a similar manner to methods used in Tables 5.1 and 5.2, the error rates are computed from a range of input back-offs and the results shown in Figure 5.15. The Type B system only achieves 5×10^{-4} at 7 dB input backoff, while the Type A system achieves 3×10^{-3} at 7.5 dB input backoff. This effect has rendered the techniques unworkable for satellite communications and some form of compensation must be sought.

The simplest form of compensation is based on equalization of the phase/amplitude response by predistortion. Figure 5.16 shows the curves of 5.11 reproduced but with the addition of a 3 degree per dB phase linearizer. The equalizer is not a perfect fit for the am/pm characteristic but has been chosen for reasons of simplicity. The residual phase remaining after equalization is also shown. Table 5.4 calculates the performance of this simple phase correction. For example, for a Type B system at saturation, one degree of residual phase error remains, which corresponds to a negligible

peak input back-off	upper ring output back-off	upper ring phase shift
+3	-0.5	49°
+2	-0.25	48.2°
+1	-0.1	47°
0	0	46°
-1	-0.1	43.5°
-2	-0.25	41.0°
-3	-0.5	38°
-4	-0.8	32°
-5	-1.2	30°
-6	-1.8	26.5°
-7	-2.2	23°
-8	-2.8	20.5°
-9	-3.5	18°
-10	-4.0	16°
-15	-9	7.5°

Common TWT effects

lower ring phase shift	$\Delta\phi$	* power HED + penalty = total
12.2°	36.8°	15 + 0.5 = 15.5
10.2°	38.0°	16.5 + 0.25 = 16.75
9.8°	37.2°	15.6 + 0.1 = 15.7
9.5°	36.5°	14.8 + 0 = 14.8
9.3°	34.8°	12.6 + 0.1 = 12.7
9.0°	32.0°	11.0 + 0.25 = 11.25
8.5°	29.5°	8.5 + 0.5 = 9.0
7.8°	24.2°	6.0 + 0.8 = 6.8
7.5°	22.5°	5.2 + 1.2 = 6.4
7.0°	19.5°	3.8 + 1.8 = 5.6
6.3°	16.7°	3.1 + 2.2 = 5.3
5.8°	14.7°	2.5 + 2.8 = 5.3
5.5°	12.5°	2.0 + 3.5 = 5.5
5.0	11.0°	1.7 + 4.0 = 5.7
3.0	4.5°	0.5 + 9.0 = 9.5

Type A results

lower ring phase shift	$\Delta\phi$	* power HED + penalty = total
13.2°	35.8°	14 + 0.5 = 14.5
13.0°	35.2°	13.8 + 0.25 = 14.05
12.6°	34.5°	13.3 + 0.1 = 13.4
12°	34.0°	12.5 + 0 = 12.5
11.8°	31.2°	10.6 + 0.1 = 10.7
11.5°	29.5°	9.5 + 0.25 = 9.75
11.2°	26.8°	6.8 + 0.5 = 7.3
10.4°	21.6°	5.0 + 0.8 = 5.8
10°	20.0°	4.3 + 1.2 = 5.5
9.5°	17.0°	3.3 + 1.8 = 5.1
8°	15.0°	2.7 + 2.2 = 4.9
7°	13.5°	2.2 + 2.8 = 5.0
6.3°	11.7°	2.0 + 3.5 = 5.5
6.0°	10.0°	1.8 + 4 = 5.8
3.5°	4.0°	0.5 + 4.0 = 9.5

Type B results

Type A BER	Type B BER
0.5×10^{-1}	0.5×10^{-1}
0.5×10^{-1}	0.5×10^{-4}
0.5×10^{-1}	5×10^{-1}
0.5×10^{-1}	10^{-1}
0.5×10^{-1}	7×10^{-2}
0.5×10^{-1}	2×10^{-2}
10^{-1}	8×10^{-3}
4×10^{-2}	0.5×10^{-3}
2×10^{-2}	10^{-3}
6×10^{-3}	7×10^{-4}
4×10^{-3}	5×10^{-4}
4×10^{-3}	6×10^{-4}
5×10^{-3}	10^{-3}
8×10^{-3}	0.5×10^{-3}
2×10^{-1}	3×10^{-2}

results in BER

notes
1) pre-distorted ring ratios used to maintain output ring ratio at optimum
2) TWT effects taken from fig
3) noise equivalent degradation taken from fig
4) noise equivalent degradation converted to BER by use of fig

* HED = noise equivalent degradation.

TABLE 5.3 AM/PM EFFECT -CALCULATION OF NOISE EQUIVALENT DEGRADATION (POWER PENALTY)

noise equivalent degradation. The table covers the standard range of input back-offs and the results are plotted in Figure 5.17. Aqain, the best attainable performance of the Type B and A system is recovered, but the performance is still inferior to 8-phase PSK, which is also assumed to be compensated. Note, however, that the optimum region has become much sharper necessitating even greater up-link control (say 0.5 dB) whereas the PSK case has improved to 3.0 dB.

One possible method to alleviate such stringent up-path power control is to use an adaptive predistortion (expansion) effect. An adaptive predistortion technique uses a feedback loop which includes the TWTA. Thus, by making observations of the ring ratios at the output of the satellite, the input ring ratios may be adjusted in order to maintain the ratio constant. Since this technique necessitates that the transmitter can also receive its own burst (global coverage) it cannot be directly applied to spot beam coverage. In this case, the cooperation of a correspondent will be required. Such a correspondent would receive the transmission, compare the ring ratios and send a coded signal to the originating transmitter in order to complete the feedback loop. Table 5.5 calculates the overall performance of a link where, irrespective of the input power level, the output signal

peak input back-off	upper ring output back-off	upper ring phase shift
+3	-0.5	6.5^0
+2	-0.25	2.5^0
+1	-0.1	1^0
0	0	0.5^0
-1	-0.1	0
-2	-0.25	-0.5
-3	-0.5	-0.6
-4	-0.8	-0.4
-5	-1.2	0
-6	-1.8	+1
-7	-2.2	+1.2
-8	-2.8	+1
-9	-3.5	+0.8
-10	-4.0	0
-15	-9	-8

lower ring phase shift	$\Delta\phi$	noise equivalent degradation	
		down link	up-link
-0.2	6.7^0	1.0	4dB
+0.3	2.2^0	0.2	1.5dB
+0.8	0.2^0	—	—
+1.0	-0.5^0	—	—
+1.0	-1.0^0	0.1	0.7dB
+0.8	-1.3^0	0.1	0.7dB
0	-0.6^0	0.1	0.7dB
-1.3	-0.9^0	0.1	0.7dB
-2.6	$+2.6^0$	0.7	3dB
-4.0	-5.0^0	0.9	3.6dB
-6.0	-7.2^0	1.2	4.8dB
-8.5	-9.5^0	1.8	6dB
-11.0	-11.8^0	2.1	6.25dB
-13.0	-13^0	2.5	7.4dB
-23^0	-31^0	10	16dB

lower ring phase shift	$\Delta\phi$	noise equivalent degradation	
		down link	up link
-0.8^0	7.3^0	1.25	5dB
-0.4^0	2.9^0	0.4	2.3dB
0^0	1^0	—	—
$+0.8^0$	-0.3^0	—	—
$+1.0^0$	-1.0	0.1	0.7dB
$+1.0^0$	-1.5^0	0.1	0.7dB
$+0.8^0$	-1.4^0	0.1	0.7dB
$+0$	-0.4^0	—	—
$+1.0^0$	$+1.0^0$	0.1	0.7dB
-2.0^0	$+1.0^0$	0.1	0.7dB
-3.5^0	-2.3^0	0.6	2.8dB
-5.0^0	-6.0^0	1.0	4dB
-8.0^0	-8.5^0	1.5	5dB
-10^0	-10^0	1.8	6dB
2ϕ	-28^0	8	14dB

Type A BER	Type B BER
7×10^{-2}	5×10^{-2}
10^{-3}	2×10^{-3}
6×10^{-6}	10^{-7}
10^{-4}	10^{-8}
10^{-5}	8×10^{-8}
6×10^{-5}	2×10^{-6}
3×10^{-4}	6×10^{-5}
10^{-3}	8×10^{-5}
6×10^{-2}	2×10^{-3}
2×10^{-1}	7×10^{-3}
5×10^{-1}	10^{-1}
5×10^{-1}	0.5×10^{-1}
5×10^{-1}	0.5×10^{-1}
5×10^{-1}	0.5×10^{-1}
5×10^{-1}	0.5×10^{-1}

notes
1) pre-distorted rings set at saturation (ie do not track)
2) straight line 3°/dB equalizer used
3) TWT effects shown on figure
4) noise equivalent degradation shown in figure
5) noise equivalent degradation converted to BER using figure

NED = noise equivalent degradation.

TABLE 5.4 PRE-DISTORTION (SET AT SATURATION) AND PHASE EQUALIZATION

Common TWT effects			Type A results			Type B results			results in BER	
+3	-0.5	6.5^0	3.0^0	9.5^0	1.3 +0.5 = 1.8	1.0^0	7.5^0	1.2 + 0.5 = 1.7	4×10^{-5}	2×10^{-6}
+2	-0.25	2.5^0	3.5^0	6.0^0	1.0 +0.25 = 1.25	1.2^0	3.7^0	0.5 +0.25 = 0.75	2×10^{-5}	10^{-7}
+1	-0.1	1^0	3.8^0	4.8^0	0.8 +0.1 = 0.9	1.3^0	2.3^0	0.3 +0.1 = 0.4	10^{-5}	3×10^{-8}
0	0	0.5^0	4^0	4.5^0	0.7 +0 = 0.7	1.5^0	2.0	0.35 +0 = 0.35	5×10^{-6}	2×10^{-8}
-1	-0.1	0	4.2^0	4.2^0	0.6 +0.1 = 0.7	1.7^0	1.7^0	0.25 +0.1 = 0.35	5×10^{-6}	2×10^{-8}
-2	-0.25	-0.5	4.5^0	4.0^0	0.5 +0.25 = 0.725	2.0^0	1.5^0	0.2 +0.25 = 0.45	5×10^{-6}	3×10^{-8}
-3	-0.5	-0.6	5.2^0	4.6^0	0.7 + 0.5 = 1.2	2.5^0	1.9^0	0.35 + 0.5 = 0.85	2×10^{-5}	10^{-7}
-4	-0.8	-0.4	5.8^0	5.4^0	1.1 +0.8 = 1.9	3.2^0	2.8^0	0.45 +0.8 = 1.25	6×10^{-5}	5×10^{-7}
-5	-1.2	0	6.2^0	6.2^0	1.2 +1.2 = 2.4	4.0^0	4.0^0	0.6 +1.2 = 1.8	10^{-4}	2×10^{-6}
-6	-1.8	+1	8.0^0	9.0^0	1.3 +1.8 = 3.1	4.5^0	5.5^0	0.9 +1.8 = 2.7	3×10^{-4}	0.5×10^{-5}
-7	-2.2	+1.2	9.5^0	10.9^0	2.0 +2.2 = 4.2	6.2^0	7.4^0	1.2 + 2.2 = 3.4	0.5×10^{-3}	7×10^{-5}
-8	-2.8	+1	11.3^0	12.3^0	2.3 +2.8 = 5.1	8.0^0	9.0^0	1.3 + 2.8 = 4.1	4×10^{-3}	2×10^{-4}
-9	-3.5	+0.8	13.0^0	13.8^0	2.5 +3.5 = 6.0	10^0	10.8^0	1.5 + 3.5 = 5.0	10^{-2}	6×10^{-4}
-10	-4.0	0	14.5^0	14.5^0	2.8 +4.0 = 6.8	11^0	11.0^0	1.8 + 4.0 = 5.8	3×10^{-2}	0.5×10^{-3}
-15	-9	-8	29^0	21.0^0	4.5 +9 = 13.5	25^0	17^0	3.0 + 9 = 12.0	5×10^{-1}	10^{-1}

notes
1) pre-distorted ring ratios used to maintain output ring ratio's at optimum (adaptive technique)
2) straight line 3^0/dB phase equalizer modeled.
3) TWT effects derived from figure
4) noise equivalence degradation derived from figure
5) noise equivalent degradation converted to BER using figure

* NED = noise equivalence degradation.

TABLE 5.5 ADAPTIVE PRE-DISTORTION AND FIXED PHASE EQUALIZATION

level ratios are maintained constant. The results are shown in Figure 5.18 and while in general, the best attainable performance is still met, the output power control requirements may be relaxed to 1.5 dB.

Finally, Figure 5.19 shows the summary curves for the Type B system. Note the poor performance due to the use of the predistortion technique alone and note also the best obtainable performance displayed by the combination of predistortion and phase compensation. It is clear that the adaptive method gives a much wider optimum region than the fixed predistorted method.

5.3 In-Band Optimization

The in-band characteristics of a digital satellite system employing APK or 8-phase PSK have now been thoroughly examined. It is concluded that careful optimization of the single channel characteristics can bring about very significant improvements in overall performance. The main conclusions are best summarized, but before doing so, it is important to stress once again that this is for the single channel case operating in isolation. All the other effects will be discussed in the order given in the introduction.

The main results from the study of in-band distortion are as follows:

a) The satellite TWTA should operate at or near saturation.

b) The overall channel shaping characteristics should be shared approximately equally between the transmitter and the receiver.

c) The overall channel shaping should approximate to a cosine roll-off characteristic in the 45 percent to 60 percent range.

d) The transmit filter should include an x/sin x full compensation network if square wave signalling is employed.

e) The earth station may be operated over the range of 3 dB output backoff to the linear region without significant additional degradation.

f) Pre-distortion must be used to compensate for the gain compression effects of the satellite TWTA in APK system.

g) Phase equalization must be used to alleviate the am/pm effects of the satellite TWTA.

5.4 Co-Channel Interference Effects

5.4.1 Sources of Co-Channel Interference (CCI) and Associated Effects in the Non-Linear Channel

The sources of Co-Channel Interference (CCI) in the non-linear channel are the same as those described for the linear channel. The non-linear environment does not normally materially affect the characteristics or the source of interference. However, the effect of a given level of interference may be different in a non-linear channel and if predistortion is employed, the up-link signals will be at a lower average power than on the down-link.

5.4.2 Co-Channel Interference Degradation Effects

Co-Channel Interference (CCI), as its name implies is associated with interference from a channel

possessing the same (or similar) frequency and usually a similar bandwidth. In attempting to quantify the effects of such interference, the various sources of interference can be placed in two main classifications: uplink and downlink. The classification is important because signals present on the uplink will be subject to intermodulation with the wanted signal due to the non-linear operation of the satellite TWTA. No intermodulation should occur on the downlink since only linear elements will be encountered.

The overall objective is to use the generalized transmission model to derive the results necessary to allow design rules to be produced to predict the degradation resulting from various CCI power levels and numbers of CCI signals in the practical satellite system. In addition it is necessary to assess the sensitivity of the system to CCI under different channel filtering conditions in order to decide if the general in-band results derived earlier need to be modified when CCI effects are considered.

Figure 5.20 shows the transmission model configured for CCI investigations. The method of measuring the bit error rate (BER) degradation proceeds by establishing the reference performance of the channel in the presence of various levels of added down-link noise,

but in the absence of other forms of disturbance. These BER vs C/N reference curves would normally be obtained for various cosine roll-off factors. However, this would have resulted in a very large requirement for computer simulation time which was unavailable. Accordingly, definitive studies of the behaviour of 8-phase PSK and APK systems are planned, but have not been executed, pending additional funding. In consequence, other techniques have been adopted based on an extensive QPSK test series conducted by the author on a hardware satellite simulator at ESA/ESTEC and reported in Reference 30. From these curves, the noise equivalent degradation will be extracted at an error rate of 10^{-4}. It is stressed that these results are estimates which will probably be proved to be slightly pessimistic, since as shown in Reference 30 noise is a good model for bandlimited modulated interference only when the number of interferers is large. To evaluate the degradation due to interferers, known levels of interference are injected in the system at points chosen to simulate the real interference sources. A wholly digital environment will be considered and the interferers are thus 8-phase PSK and/or APK modulated. Unlike the linear channel case, these interferers are added to the up-link (with no additional interference in the down-link), down-link (with no additional interference in the up-link) and to the up-link and down-link,

simultaneously. Clearly, interference added to the up-link will also be present in the down-link. However, these signals will have passed through a highly non-linear TWTA simultaneously with the wanted signal. Two opposite effects of this co-amplification can be postulated. On the one hand, when two signals are present in the non-linear amplifier an additional degradation due to intermodulation can be expected. On the other hand, the dissimilar power levels may cause a reduction in overall degradation because the non-linear TWTA small signal suppression effects will reduce the power level of the interference in the receiver. In practice, both effects are present and the dominance of one effect over the other depends to some degree on the satellite operating point and the channel filter roll-off characteristics.

5.4.3 Co-Channel Interference Results

Figure 5.21 shows the BER vs C/N reference curves for QPSK with the satellite TWTA operating in the saturated region and the earth station TWTA operating at 6 dB output backoff. These results were obtained using channel filters employing 50% cosine roll-off using a combination of measured results from Reference 30 and computer simulation.

For each case, curves of up-link CCI obtained for carrier to interference (C/I) ratios of 15, 17, 25 and 30 dB are shown. The process is then repeated for down-link and up + down-link cases as shown in Figures 5.22 and 5.23.

Generalized conclusion can be drawn from an examination of these results. Up-link CCI contributes more degradation for a given level of interference than down-link CCI. [Similarly, although not shown here, sharper roll-off filters produce greater degradation for a given level of interference than more gentle roll-off.] Without further processing, any further analysis would be very difficult. A more convenient method of assessing the degradation associated with CCI is shown in Figure 5.24. This is derived from the previous results, but replotted to show degradation as a function of C/I for the 10^{-4} error rates case. This figure clearly shows the rapid rise in distortion associated with C/I ratios in the region of 15 dB. Comparing this figure with the linear channel case for QPSK with noise-like interferers shows that a good fit may be obtained for the case:

$$C/I\ (QPSK) + 9.5\ dB = C/I\ (8\text{-phase PSK})$$

Similarly, for APK Type A:

$$C/I\ (QPSK) + 7.3\ dB = C/I\ (APK\text{-}A)$$

and for APK Type B:

$$C/I\ (QPSK) + 6.3\ dB = C/I\ (APK\text{-}B)$$

Using these results, the case for 8-phase PSK is shown in Figure 5.25, while the case for the wholly APK environment is shown in Figure 5.26 for Type A and Figure 5.27 for Type B. The down-link C/I ratios are de-rated by the same amounts as in the linear case (2 dB for Type B and 2.3 dB for Type A). However, on the up-link consideration must be given to the effect of predistortion. For operation at saturation, it was shown that the optimum predistortion up-link amplitude (ring) ratio was 12 dB (Type B) and 13.5 dB (Type A). This increases the de-rating factors (as explained in Section 4) to 2.74 dB (Type B) and 2.749 dB Type A. Thus, the up-link C/I ratio becomes 24.74 dB (Type B) and 24.749 dB (Type A). These effects are shown plotted in the Figures.

A number of conclusions can be drawn from consideration of these results. For the up-link co-channel case, it is apparent that the degradation is

greater than in the equivalent down-link case when the interference level is high. This is due to intermodulation with the wanted signal when both are passing through the non-linearity of the satellite TWTA. It would seem that intermodulation only becomes of significance when the interference increases to a C/I ratio of 20 dB or worse. At 15 dB C/I ratio, a sufficiently large increase in degradation occurs to give rise to concern because under operational conditions in 14/11 GHz system up-link depolarization can approach these levels, as will be seen later. The effect must certainly be included in system power budgets if a premature system failure is to be avoided. This effect will be discussed more fully in the section dealing with overall optimization and, in particular, up-link power control.

It should also be noted that a significant improvement in the overall system performance arises when APK is operated in a wholly APK (homogenous) environment (i.e., all the interferers are also APK). In an interference limited environment such as INTELSAT V TDMA, this advantage will have a major impact on the overall performance.

Finally, using the results in Figures 5.25, 5.26 and 5.27, it becomes apparent that a noise equivalent

degradation of 2.0 dB, 1.8 dB and 5.25 dB must be accommodated in the link budget for APK-A, APK-B and 8-phase PSK on the uplink and 2.1 dB, 2.0 dB and 4.8 dB on the down-link, respectively, at C/I(up) = C/I(down) = 22.0 dB (The expected INTELSAT V case shown in Table 2.2).

5.5 Adjacent Channel Interference

Adjacent Channel Interference (ACI), as the name implies, is caused by a spill-over of energy from the adjacent channel(s) in the frequency spectrum. The causes of ACI were discussed in the Linear Channel Analysis (Section 4). Unlike the results obtained in that section, the inclusion of non-linear travelling wave tubes for the ground station transmitter and satellite transponders, tends to increase the power of the energy which falls into the wanted channel. This process is known as spectrum spreading. In particular, because of the interaction of the spectrum spreading, multiplexing filters, and the proximity of the adjacent channels, the multipath component may be very much more severe than in the linear channel case. To evaluate these effects, a comprehensive series of tests and simulations have been conducted by the author using QPSK and a hardware satellite simulator. These results are reported in References 26 and 35.

5.5.1 The Generation of ACI

The generalized transmission model in Figure 4.6 can be used to assess the effect of ACI in a non-linear channel. APK signals are generated and suitably arranged in the frequency bands in order to load the three channels.

Figure 4.25 showed the idealised channel spectral shape and multiplexing arrangements, and under these arrangements no ACI can occur. However, when the real situation is substituted, the interaction of the out-of-band characteristics of channel shaping filters and multiplexing filters shows that some of the energy from the adjacent transmission can fall into the wanted channel, thereby causing interference. This is also shown in Figure 4.25. When non-linear TWTA's are employed, the transformed signal characteristic gives rise to a spectral modification which is known as spectrum spreading. The degree of spectrum spreading varies as a function of operating point (backoff) as shown in Figure 5.28. It is shown in Reference 35 that spectrum spreading produces a considerable increase in adjacent channel interference.

It should not be overlooked that the spectrum of the wanted signal will be similarly spread and, apart from causing adjacent channel interference to its neighbouring

channel, this out-of-band signal will considerably enhance the multipath effect. This effect is examined in detail in the next section, but it is important to note that all adjacent channel results contain an element of multipath interference.

Although not shown in the generalized transmission model, it should also be noted that channels 1 and 3 contain phase shifters. In section 2, it was shown that multipath always accompanies ACI measurements and in order to assess the multipath component (and thus to determine the true ACI degradation) use can be made of the coherent nature of the multipath interferer. As the phase shifters are rotated through 360 degrees, a well defined maximum and minimum occurs in the resulting degradation. This corresponds to the additive and destructive effects of the vectorial recombination of the multipath signal with the wanted signal as shown in Figure 5.29. At some point in the rotation of the phase shifters, the multipath signal will neither be aiding or degrading the error performance of the wanted signal. This "neutral" point allows the true ACI degradation to be obtained.

5.5.2 Up-Link Adjacent Channel Interference Mechanisms

We have seen that the partially or completely filtered APK or 8-phase PSK signal presented to the earth station high power amplifier (HPA) exhibits a significant degree of amplitude modulation. When the HPA is operated in a non-linear mode, the signal is distorted, and energy is spread beyond the original frequency band. The degree of spectrum spreading is mainly determined by the amplitude non-linearity rather than the phase non-linearity of the amplifier[20]. As the amplifier is driven towards saturation, the spread-spectrum power increases until at saturation when most of the amplitude modulation has been removed, the spectrum approaches $(\sin x)^2/x^2$ form (Figure 5.28). Whatever the HPA operating point, up-link ACI will be worse than in the linear channel because of this effect.

The output spectrum can conveniently be divided into two parts, an inband part which is essentially the input spectrum, and a separate spread-spectrum component. The former is clearly determined by the roll-off characteristic of the transmit pulse-shaping filter, but the latter appears from simulation-results conducted at ESA/ESTEC to be relatively independent of it[24]. This is somewhat surprising in view of the asssumed connection

with amplitude modulation. It is however postulated that it is due to the presence of phase-reversals which are always present in APK or 8-phase PSK signal, whatever the roll-off factor or ring ratio.

Normally, when a significant proportion of the overall channel shaping is located at the transmitter, up-link ACI will be determined almost entirely by the spread-spectrum component. This must be controlled by HPA backoff or linearization, by post HPA filtering, or by a combination of these techniques. Therefore, unless the transmit pulse-shaping filter is very wide or has a low cut-off rate, the choice of the channel shaping filter is not determined by ACI. Accordingly, we may proceed with the analysis of ACI without further concern for the type of channel filtering employed.

5.5.3 Down-Link Adjacent Channel Interference

Under normal conditions, the satellite TWTA's will be operated at, or close to, saturation, and the output spectrum will be largely determined by the TWTA amplitude non-linearity. The resulting spectrum spreading is therefore independent of conditions before the satellite TWTA. The received down-link adjacent channel interference is then mainly determined by the satellite

output multiflexing filter (OMUX) characteristic and the receive channel shaping characteristic. As with up-link ACI, Harris[27] shows that the interference spectrum can be split into a band-edge term and a spread-spectrum term. The minimum bandwidth of the satellite output filter is determined by distortion and insertion loss considerations and will nominally be fixed by the satellite designers before a specific modulation method is selected. This is an unfortunate by-product of the very long lead time of a satellite. For INTELSAT V with a channel spacing of 80 MHz, the rejection of the band-edge interference component is high for all but the slowest roll-off receiver pulse-shaping filters. Therefore, like up-link ACI, down-link ACI will be due mainly to the spread spectrum term which is controlled by the out-of-band attenuation of the satellite output filter. Again, ACI does not significantly affect the choice of receive pulse-shaping filter, but down-link ACI will be worse than in the linear channel.

5.5.4 Examination of Spectra

As an aid to understanding the nature of ACI, several photographs were recorded at the output of a typical satellite output multiplexer and in the receive IF of the demodulation system. These are reproduced from Reference 35.

Figure 5.30 shows a series of photographs. All these photographs were obtained with PSK modulation as the stimulus. In the first, the output of the satellite is shown when the three 80 MHz bandwidth transponders are loaded with unmodulated carriers, while in the second, the spectral overlap is shown when the three channels are loaded with long-sequence Pseudo-Random Binary Sequence (PRBS) Modulation. From left to right the channels are denoted as channels 1, 2 and 3.

In the third photograph, the effect of channel 1 and 2 modulated with long sequence PRBS, whilst channel 3 is switched off is shown with the phase shifter in channel 1 set to yield the maximum degradation. The fourth was taken under identical conditions, except that the minimum degradation is shown. Examination of the overlapping region between the two channels shows distinct evidence of a "gap" under maximum interference conditions. This confirms the reasoning that multipath induced degradation results from destruction of the received signal energy at the band edges. It will be noted that under minimum interference conditions, the amplitude of the signals present at the band edges is increased, indicating constructive interference (additive interference) of the wanted and interfering signals.

Figure 5.31 shows a series of photographs taken at the receive IF following the receive channel shaping filter. The first two are recorded under the same conditions, but the second photograph was recorded with the addition of two adjacent channels. It will be noted that a significant modification to the band edges of the received signal has occurred. This is much more readily seen if the wanted transmission is removed. In the third photograph, the ACI in the receive IF due to the presence of channel 1 loaded with a PRBS is shown. The effect of channel 3 falling into channel 2 is shown in the fourth photograph while the fifth photograph was derived from both adjacent channels being loaded. From examination of these photographs, it is thus a simple matter to understand the band-edge spectral modification suffered by the wanted channel interference conditions.

5.5.5 Expected Noise Equivalent Degradation Due to ACI

Figure 5.32 shows the degradation resulting from channels 1 into 2, 3 into 2 and 1 + 3 into 2 under maximum and minimum interference conditions for QPSK. For the purposes of estimating a link budget, the noise equivalent of these interferers was assessed for APK-A, APK-B and 8-phase PSK.

This was accomplished in the following stages:

1) Determine noise equivalent degradation at 10^{-4} for the QPSK case (example 0.8 dB from 5.31).

2) Use Figure 5.4 to convert to a C/I power ratio (e.g., 0.8 dB Ξ 21 dB C/I)

3) Derate where appropriate for average power ratio of signal sets; i.e.,

uplink: 8-phase PSK = 0, APK-A = 2.75 dB, APK-B = 2.7 dB.

downlink: 8-phase PSK = 0, APK-A = 2.3 dB, APK-B = 2.0 dB.

Example: downlink ACI for APK-B

2.0 dB + C/I(QPSK) = 21 dB + 2 dB = 23 dB = C/I APK-B

4) Use appropriate C/I vs noise equivalent degradations to give NED for the ACI interference (Example: APK-B given in Figure 5.27; from figure 23 dB = 2.5 dB degradation).

The results of these transformations show that 2.4, 2.5 and 5.7 dB degradations must be accommodated in the link budget for APK-A, APK-B and 8-phase PSK, respectively.

5.6 Adjacent Channel Multipath

For two reasons the multipath problem is potentially more severe in some satellites which are not specifically designed for TDMA operation (e.g., INTELSAT V). Firstly, operation of the satellite TWTA's close to saturation when the signals are present means that the silent channel (unloaded adjacent channel) gain to small signals such as multipath will be of the order of 7 dB higher than normal. This condition must be accommodated. Secondly, if overlapping antennas coverage areas exist, unfavourable gain-differences (as high as 4 dB in some locations) may result[27]. A multipath-gain of 11 dB relative to the wanted signal must thus be accepted. Because the multipath signal is partially coherent with the wanted signal, the degradation it produces will depend on the relative path delays experienced by the two signals and the precise phase-distortions experienced by each. It is, therefore, extremely difficult to calculate the precise degradation which will be experienced in a given situation. It will however, be obvious that the worst

case of degradation produced by a multipath component of a given power will be considerably greater than that due to noise or non-coherent interference of the same power.

For multipath purposes, the transmission path can be regarded as linear in the sense that up-link and down-link spectrum spreading can be ignored. The multipath power is then determined by, on the one hand the combined wanted channel transmit and receive pulse-shaping characteristics, and on the other, the adjacent channel IMUX and OMUX responses. Both of these vary rapidly with frequency in the overlap region, and either can be used to control multipath.

5.6.1 Method of Determining Multipath Degradations

The transmission model shown in Figure 4.6 is suitable for multipath investigations if phase shifters are inserted prior to the TWT's of the adjacent channels. It has three contiguous 80 MHz bandwidths. A hardware simulator with this configuration was used to obtain the results that follow, which are reported fully in Reference 35. The results are useful to illustrate the optimization technique, but specific to the hardware used in the simulator. However, it should be remembered that the multipath component is critically dependent on the actual

band edge effects of the filters employed. Therefore, the amount of multipath interference will vary significantly between sets of hardware.] If the centre transponder is considered (channel 2), it is evident, from Figure 5.33 that a wide band signal, such as that associated with a normal 8-phase PSK or APK transmission, may be passed by the filter band-edges into the adjacent transponders and after being amplified by the TWT, will recombine in the output multiplex. Thus a signal component at the channel band-edges may be amplified by the Channel 2 TWT (the wanted channel) in the normal manner but also to some lesser extent by the adjacent channels 1 and 3.

The signal component amplified by the adjacent channel(s) re-enters the wanted channel via the output multiplex filter's overlapping band-edges. When this signal appears in the wanted band, it can cause destructive corruption of the wanted signal, thus increasing the bit error rate for a given C/N ratio.

The amplitude of this multipath component, which is amplified by the adjacent channel(s), depends on the following factors:

1) The width of the spectrum in the wanted channel.

2) The roll-off slope (and its position) of the multiplex filter(s).

3) The gain of the adjacent channel(s) amplifier.

The first two factors, having been optimized by the satellite designers, may have to be considered constant. The last factor is variable since the apparent gain of the satellite repeater containing a TWT depends on the TWT input level. Examination of Figure 5.8, which shows the power transfer characteristics of the TWT used in the satellite model in channel 2, shows that the gain of the device displays a well defined minimum. This minimum, known as saturation, is a point beyond which an increase in input power yields a decrease in output power. At some 15 dB below this point, the gain is effectively linear and is known as the small signal region. Since the level of multipath depends on the gain of the adjacent channel, this in turn depends on the operating point of the adjacent channel. The operating point is thus set by the TWT input power of the main signal occupying the adjacent channel. The multipath component has too small an amplitude to be significant in power setting mainly because of the attenuation through the input multiplex filter. The level of the multipath component in the wanted channel then varies as a function

of the power of the adjacent channel signal; being a maximum when the adjacent signal is not present.

Figure 5.34 shows the result of the basic C/N vs BER reference curve for the wanted channel 2. Figure 5.34 also shows the degraded curves due to multipath interference via the unloaded channel 1. The effect of varying the phase shift between the wanted and interfering channels is clearly demonstrated. A 180 degrees change of phase can result in the equivalent of a 2 dB additional degradation. The phase shift corresponding to the minimum degradation (50°) yields only 0.2 dB degradation. This is presumed to be the additive vectorial condition, whilst the maximum degradation corresponds to the destructive addition. These curves clearly show that the multipath effect is potentially a source of severe degradations with an unloaded adjacent channel. The degradation at C/N = 15 dB considerably exceeds any other single form of degradation in the link. Figure 5.35 shows similar effects to those in Figure 5.34, but although indicating lower maximum degradations than channel 1 into channel 2, the maximum and minimum degradations are seen to occur at similar relative phase shifts. It is considered that the phase shifters setting is arbitrary since the different electrical length (i.e., phase) depends not only on the physical length of the transponder paths, but on the

particular phase shifts within the elements (especially the TWT) in the amplifier chains. The maximum degradation is approximately 0.6 dB. Figure 5.36 was derived by the multipath interference effects of two silent adjacent channels (1 and 3). Two phase shifters were employed in the adjacent channels and preliminary investigations showed that a maximum degradation occurred when the channel 1 phase shifter was at 220° and channel 3 at 260°. (These are close to the previous single channel case of 210° and 270° respectively, and are assumed to be the same. This assumption is justified by the slope of the phase/BER characteristic being essentially flat in both the maximum and minimum regions). The maximum degradation resulting is seen to be about 1.8 dB at 15 dB C/N, whilst in the minimum case, an improvement of 0.2 dB is noted. The minimum case is obtained with a phase shifter setting of 55° in channel 1 and 45° in channel 3. (The corresponding single channel case gave channel 1 at 50° and channel 2 at 65°. As in the case of the maximum degradation, these are considered to be essentially the same).

5.6.2 Modifications Necessary to Obviate Multipath Interference

The very long lead times associated with the deployment of a satellite (typically 7 years) often results in the transmission characteristics being determined before the modulation method is selected. Accordingly, it is often necessary to manipulate bandwidths and/or signalling speeds to "fit" a modulation method to the predetermined channel characteristics. However, in this case, the results obtained from the multipath measurements (reported in Reference 35) were sufficiently serious to force a redesign of the satellite input and output multiplexing filters and the center frequency of the transponders. These changes were reported in Reference 27. The author had no further opportunity to evaluate the changes, but understands that the effect was to reduce the multipath induced degradation to a negligible level ($<$0.2 dB).

The objective of this study is to assess the performance of a 8-phase PSK, APK-A and APK-B through an INTELSAT V satellite. To this end, the QPSK measurements are used as the basis of the comparison. The eventual aim being to produce a link budget based on realistic predictions of the link degradations. However, the author

feels that it would be unduely pessimistic to use the multipath effect from the "pre-changes" ECS model to determined the clear weather performance of the INTELSAT V. Accordingly, the link budget will first compute the error rate without multipath and then for illustrative purposes include this effect to support the author's decision.

5.6.3 Noise Equivalent Degradation for Multipath Interference

In the same way that the noise equivalent degradations (NED) were obtained for CCI and ACI, it is necessary to assess the degradation due to multipath. Accordingly, the following steps were used to obtain the NED's due to multipath:

1) Determine NED at 10^{-4} for the QPSK case (Example: 1.5 dB from Figure 5.36).

2) Subtract NED for ACI obtained in Section 5.5, since silent channel multipath and loaded channel multipath cannot occur simultaneously. (Example: 1.5 dB - 0.8 dB = 0.7 dB).

3) Use Figure 5.24 to convert to a C/I power ratio (e.g., 0.7 dB $\equiv$ 22 dB C/I for QPSK).

4) Derate where appropriate for average power ratio of signal sets; i.e.,

uplink: 8-phase PSK = 0, APK-A = 2.75 dB, APK-B = 2.7 dB.

downlink: 8-phase PSK = 0, APK-A = 2.3 dB, APK-B = 2.0 dB.

Example, uplink multipath (via silent channel)

22 dB C/I(QPSK) + 2.7 dB = APK-B equivalent C/I = 24.7 dB.

5) Use appropriate C/I vs NED curve to give NED for multipath interference power; e.g., Figure 5.27 gives APK-B results, $\therefore$ 24.7 dB = 1.7 dB NED.

Using this technique, worse case margin of 2.2 dB, 2.0 dB and 3.6 dB are assigned for Type A, Type B and 8-phase PSK, respectively.

5.6.4 Examination of Baseband Spectra

The difference between the two channels is clearly seen in the photographs in Figure 5.37. The first shows the multipath signal spike caused by channel 3 and 2 overlapping. By comparison with the second photograph (channel 1 to 2 multipath), it can be seen that the amplitude difference between the signals is of the order of 8 dB. This can be accounted for by a difference in the manufacturing tolerance of the multiplexed filter both in roll-off slope and position. The third photograph shows the compression of the channel 3 to 2 multipath signal by the loading of channel 3 with an unmodulated carrier, while the fourth shows the same effect on channel 1 to 2 multipath. The higher amplitude of the channel 1 to 2 multipath signal is clearly seen relative to the channel 3 to 2 multipath. The decrease in gain when the channels are loaded is seen to depress the interfering spikes by some 10 dB, but the presence of an inter-modulation component should also be noted.

5.7 Overall Optimization

In assessing the performance of a digital communications system, it is common to study each source of performance degradation separately and to establish a

noise equivalent degradation factor (in dB) for each. These are then added to estimate the total performance degradation for the complete system. This approach has the disadvantage that each degradation factor strictly only applies at one bit-error-rate and that the effect of a given impairment (distortion, noise, interference) depends to some degree on the other impairments present. This approach gives a good idea of the relative importance of the different impairments and of areas where improvements would be beneficial and enables the estimated link budget shown in Section 1 to be refined. However, it is possible that some individual impairments are poorly modelled by Gaussian noise and certainly this technique is not appropriate when one such impairment alones causes a large performance degradation. Fortunately, in the case of INTELSAT V, several independent non-Gaussian components are combined and none of them is dominant. Thus, the Central Limit Theorem indicates that their joint distribution will tend towards Gaussian form. In the INTELSAT system, therefore, the individual impairments are fairly well characterized as Gaussian noise, at least over a limited range, and the Central Limit Theorem applies quite well.

5.7.1 Link Budget

In Section 2, a tentative link budget was presented based on estimates of the degradations associated with Co-channel and Adjacent Channel Interference levels. With the analysis of the 6/4 GHz non-linear channel now complete, it is now possible to refine the link budget by substituting the various noise equivalent degradations obtained in this section for the estimates previously used. These are shown in Tables 5.6, 5.7 and 5.8. The following table summarizes the results obtained for the candidates:

Noise Equivalent Degradation (NED)

	CCI up	CCI down	ACI	Multipath*
8-phase PSK	5.25 dB	4.8 dB	5.7 dB	3.6 dB
APK-A	2.0 dB	2.1 dB	2.4 dB	2.2 dB
APK-B	1.8 dB	2.0 dB	2.5 dB	2.0 dB

* Additional degradation: must be added to the ACI NED's to give overall silent channel multipath results.

The link budgets for the three candidates are constructed in the same way. Lines 1 through 5 calculate the up-link carrier to noise (C/N) power ratio while lines 6 through 11 calculate the down-link C/N ratios.

Lines 12 through 14 use the up-link C/N ratio from line 5 and subtract the up-link CCI noise equivalent degradation shown in the table above to give the total C/(N+I) for the up-link. Similarly, the total C/(N+I) for the down-link is calculated in lines 15 through 18 using the down-link CCI and ACI NED's in the table above. Finally, the up-link C/(N+I) line 14 and down-link C/(N+I) line 18 are added linearly to give a combined C/(N+I) which after substracting 1 dB for miscellaneous losses, gives the total available C/(N+I). This is converted to an equivalent Bit Error Rate (BER) by using an appropriate BER vs C/N curve (e.g., 5.18).

The degradation associated with multipath is treated separately (in lines 23 through 25), because as indicated in Section 5.6, the degradations are unacceptably high and in consequence the satellite I/OMUX filters and the center frequency of the transponders must be changed to obviate this effort. It will be noted that the addition of the multipath degradations in the link budgets does result in unacceptable performance as was

predicted in Section 5.6. [Furthermore, the improvements necessitated by the multipath performance are likely to substantially improve the adjacent channel performance, since the degradation mechanism are similar in both cases. For this reason, an estimated 1.2 dB improvement in the ACI has been incorporated in the BER shown in parenthesis after the "corresponding BER"].

These results from the link budgets are best summarized in the form of a table, viz:

Summary of BER Results

Clear Sky 6/4 GHz, Atlantic Satellite, UK to USA Beam

	Original OMUX Loaded Channel Multipath	Original OMUX Silent Channel Multipath	Estimated Performance with new OMUX
8-phase PSK	1×10^{-2}	--	1×10^{-3}
APK-A	3×10^{-3}	1×10^{-2}	6×10^{-6}
APK-B	1×10^{-5}	8×10^{-3}	2×10^{-7}

TABLE 5.6

APK-A Clear-Sky 6/4 GHz Link Budget
UK to USA East-Hemi to West-Hemi

No Terrestrial or Inter-network Interference Included
Atlantic Satellite Longitude: 335.5°E
Single Carrier

Up-Beam 6 GHz UK
Down-Beam 4 GHz USA
Occupied Bandwidth 72 MHz

Line #	Up-Link (noise only)	Units	Parameters	Remarks
1	Saturation Flux Density	(dBW/m^2)	-72.0	Nominal high-gain specs
2	G/T of Satellite	(dB/K)	-11.6	Min. G/T specs
3	C/N at Saturation	(dB)	30.0	Elevation: 25.2°
4	Input Backoff	(dB)	1.0	6.175 GHz
5	C/N	(dB)	29.0	Path Loss: 200.3 dB
	Down-Link (noise only)			
6	Saturation e.i.r.p.	(dBW)	29.0	Min. specified e.i.r.p.
7	Earth-Station G/T	(dB/K)	40.7	Elevation: 28.2°
8	Pathloss	(dB)	196.3	3.95 GHz
9	C/N at Saturation	(dB)	24.2	
10	Output Backoff	(dB)	0.1	From Figure 5.8
11	C/N	(dB)	24.1	
	Up-Link (noise + interference)			
12	C/N	(dB)	29.0	From Line 5 (noise only)
13	C/I loss estimate 22 dB	(dB)	2.0	
14	C/N + C/I = Net C/(N+I)	(dB)	27.0	Combine Lines 12 & 13
	Down-Link (noise + interference)			
15	C/N	(dB)	24.1	From Line 11 (noise only)
16	C/I loss estimate 22 dB	(dB)	2.1	
17	Adjacent Channel Interference Loss Estimate	(dB)	2.4	HPA input backoff: 10 dB
18	C/N + C/I = Net C/(N+I)	(dB)	19.6	Combine Lines 15, 16, 17
	Combined Up-Link & Down-Link			
19	Overall C/(N+I)	(dB)	18.9	Combine Lines 14 & 18
20	Miscellaneous Loss	(dB)	1.0	Modem performance variation; antenna tracking error, etc.
21	Total Available C/(N+I)	(dB)	17.9	
22	Corresponding BER		3×10^{-3}	Adjacent channels loaded. (6×10^{-6}, with modified OMUX)
23	Silent Channel Multipath		1.9	
24	Total available C/(N+I)	(dB)	16.0	
25	Corresponding BER		10^{-2}	Adjacent channels not loaded. (6×10^{-6}, with modified OMUX)

TABLE 5.7

APK-B Clear-Sky 6/4 GHz Link Budget
UK to USA East-Hemi to West-Hemi

No Terrestrial or Inter-network Interference Included
Atlantic Satellite Longitude: 335.5°E
Single Carrier

	Up-Beam		6 GHz	UK
	Down-Beam		4 GHz	USA
	Occupied Bandwidth		72 MHz	
Line #	Up-Link (noise only)	Units	Parameters	Remarks
1	Saturation Flux Density	(dBW/m^2)	-72.0	Nominal high-gain specs
2	G/T of Satellite	(dB/K)	-11.6	Min. G/T specs
3	C/N at Saturation	(dB)	30.0	Elevation: 25.2°
4	Input Backoff	(dB)	0.5	6.175 GHz
5	C/N	(dB)	29.5	Path Loss: 200.3 dB
	Down-Link (noise only)			
6	Saturation e.i.r.p.	(dBW)	29.0	Min. specified e.i.r.p.
7	Earth-Station G/T	(dB/K)	40.7	Elevation: 28.2°
8	Pathloss	(dB)	196.3	3.95 GHz
9	C/N at Saturation	(dB)	24.2	
10	Output Backoff	(dB)	0.0	From Figure 5.8
11	C/N	(dB)	24.2	
	Up-Link (noise + interference)			
12	C/N	(dB)	29.5	From Line 5 (noise only)
13	C/I loss estimate 22 dB	(dB)	1.8	
14	C/N + C/I = Net C/(N+I)	(dB)	27.7	Combine Lines 12 & 13
	Down-Link (noise + interference)			
15	C/N	(dB)	24.2	From Line 11 (noise only)
16	C/I loss estimate 22 dB	(dB)	2.0	
17	Adjacent Channel Interference Loss Estimate	(dB)	2.5	HPA input backoff: 10 dB
18	C/N + C/I = Net C/(N+I)	(dB)	19.7	Combine Lines 15, 16, 17
	Combined Up-Link & Down-Link			
19	Overall C/(N+I)	(dB)	19.06	Combine Lines 14 & 18
20	Miscellaneous Loss	(dB)	1.0	Modem performance variation; antenna tracking error, etc.
21	Total Available C/(N+I)	(dB)	18.06	
22	Corresponding BER		10^{-5}	Adjacent channels loaded. (2×10^{-7}, with modified OMUX)
23	Silent Channel Multipath		1.7	
24	Total available C/(N+I)	(dB)	16.36	
25	Corresponding BER		8×10^{-3}	Adjacent channels not loaded. (2×10^{-7}, with modified OMUX)

TABLE 5.8

8-phase PSK Clear-Sky 6/4 GHz Link Budget
UK to USA East-Hemi to West-Hemi

No Terrestrial or Inter-network Interference Included
Atlantic Satellite Longitude: 335.5°E
Single Carrier

	Up-Beam		6 GHz UK	
	Down-Beam		4 GHz USA	
	Occupied Bandwidth		72 MHz	
Line #	Up-Link (noise only)	Units	Parameters	Remarks
1	Saturation Flux Density	(dBW/m^2)	-72.0	Nominal high-gain specs
2	G/T of Satellite	(dB/K)	-11.6	Min. G/T specs
3	C/N at Saturation	(dB)	30.0	Elevation: 25.2°
4	Input Backoff	(dB)	0.5	6.175 GHz
5	C/N	(dB)	29.5	Path Loss: 200.3 dB
	Down-Link (noise only)			
6	Saturation e.i.r.p.	(dBW)	29.0	Min. specified e.i.r.p.
7	Earth-Station G/T	(dB/K)	40.7	Elevation: 28.2°
8	Pathloss	(dB)	196.3	3.95 GHz
9	C/N at Saturation	(dB)	24.8	
10	Output Backoff	(dB)	0.1	From Figure 5.8
11	C/N	(dB)	24.7	
	Up-Link (noise + interference)			
12	C/N	(dB)	29.5	From Line 5 (noise only)
13	C/I loss estimate 22 dB	(dB)	5.25	
14	C/N + C/I = Net C/(N+I)	(dB)	24.25	Combine Lines 12 & 13
	Down-Link (noise + interference)			
15	C/N	(dB)	24.2	From Line 11 (noise only)
16	C/I loss estimate 22 dB	(dB)	4.8	
17	Adjacent Channel Interference Loss Estimate	(dB)	5.7	HPA input backoff: 10 dB
18	C/N + C/I = Net C/(N+I)	(dB)	13.7	Combine Lines 15, 16, 17
	Combined Up-Link & Down-Link			
19	Overall C/(N+I)	(dB)	13.3	Combine Lines 14 & 18
20	Miscellaneous Loss	(dB)	1.0	Modem performance variation; antenna tracking error, etc.
21	Total Available C/(N+I)	(dB)	12.3	
22	Corresponding BER		10^{-2}	Adjacent channels loaded. (10^{-3}, with modified OMUX)
23	Silent Channel Multipath		5.25	
24	Total available C/(N+I)	(dB)	7.05	
25	Corresponding BER		----	Adjacent channels not loaded. (10^{-3}, with modified OMUX)

5.8 Summary

Using the techniques developed within the linear channel analysis section, this section has enabled a prediction of the BER performance of the candidate 8-phase PSK, APK-A and APK-B modulation methods to be obtained for a realistic INTELSAT V 6/4 GHz environment. The linear channel analysis techniques have been extended to include the mechanisms which arise (or are affected by) non-linear operation of the earth station or satellite TWTA's.

At an early stage in the analysis, it became apparent that design rules based on the Nyquist criteria cannot be directly applied in this case mainly because a non-linearity is inserted between the two filters which together constitute the overall required Nyquist channel (pulse) shaping. Non-conformance with the Nyquist criterion means that freedom from ISI at the sampling instant can no longer be obtained. Furthermore, by the use of computer generated signal space diagrams, the interaction between the non-linearity and any subsequent filtering was shown to cause a "time smearing" of the pulse waveforms, further increasing the interfering ISI signal power at the sampling instant. This composite interfering signal acts as a power elevating "pedestal" for the noise effectively decreasing the noise power

required to cause a given error rate. The power of the ISI signal was reasoned to be related to the TWTA non-linearity, which increases as the output power increases. Thus, a balance point is established in which the improvement in down-link C/N no longer dominates the increased distortion caused by the increased signal power demanded from the TWTA. Accordingly, the performance of the three candidates was evaluated as a function of TWTA back-off. The analysis shows the optimum operating point of the TWTA to be 2 dB, 6.7 dB and 6.5 dB for 8-phase PSK, APK-A and APK-B, respectively. This confirmed that the PSK was more tolerant of the distortion than the APK systems and in consequence was able to use more power on the down-link to improve the receive C/N. This was reflected in the best attainable BER's of 6×10^{-5}, 4×10^{-3} and 5×10^{-4} for 8-phase PSK, APK-A and APK-B, respectively.

The relatively large back-off required for the APK signal sets was shown upon examination of the non-linear characteristics of the TWTA's to be due to the am-am power transfer non-linearity compressing the APK ring ratios. Accordingly, these calculations were repeated but this time only the TWT compression effects were used and results were obtained on the assumption that the APK ring ratios could be maintained at the optimum

setting irrespective of the operating point on the non-linear power transfer curve of the TWTA. This time the optimum operating points for 8-phase PSK, APK-A and APK-B were shown to be 0.2 dB, 0 dB and 0.1 dB, respectively, giving BER's of 10^{-9}, 10^{-8} and 10^{-6}. Two different forms of compensation were compared: fixed predistortion and an adaptive technique using a closed feedback loop encompassing the TWTA. The adaptive technique was shown to maintain optimum performance over a 2 dB variation in transmitted power. In contrast, a much simpler fixed predistortion method yielded optimum performance over a 0.5 dB range. Nevertheless, for a 4/6 GHz system where fades are infrequent and e.i.r.p.'s are easily set and maintained, it was concluded that the fixed method was more desirable. When the predistortion was set for the optimum operating point, the ring ratios on the up-link became 13.5 dB and 12 dB for the APK-A and APK-B schemes, respectively.

Next, the effect of the am/pm conversion was considered. The calculations showed that all three methods gave unsatisfactory performance and indicated that some form of compensation would be necessary. A simple linear phase equalizer of 3°/dB was tried. The combination of predistortion and phase equalization

restores the optimum BER performance of the three candidates to 10^{-6}, 10^{-8} and 10^{-9} for APK-A, APK-B and 8-phase PSK, respectively.

Since INTELSAT V is known to be an interference limited spacecraft, considerable emphasis was placed on the effect of Co-channel Interference. Using results obtained by the author on a QPSK satellite simulator, estimates were made of the performance degradation at the anticipated interference C/I levels of 22 dB in the up-link and down-link. The results obtained show that a performance degradation of 2.0 dB, 1.8 dB and 5.25 dB on the up-link and 2.1 dB, 2.0 dB and 4.8 dB on the down-link must be expected for APK-A, APK-B and 8-phase PSK, respectively. It was noted that in this case the APK systems perform better than PSK due to the lower average power of the APK signal sets which was considered to be a major advantage in an interference limited environment.

To complete the study, Adjacent channel and Multipath interference effects were assessed under the sprectrum spreading conditions associated with non-linear operation of the TWTA's. The results were obtained by the author using a hardware simulator and PSK modulation. The calculated results showed additional performance degradations of 2.4 dB, 2.5 dB and 5.7 dB together with

2.2 dB, 2.0 dB and 3.6 dB for APK-A, APK-B and 8-phase PSK, under adjacent channel and multipath interference conditions, respectively.

Finally, the various noise equivalent performance degradation were incorporated in the tentative 6/4 GHz link budget shown earlier to give the predicted link budgets for the three candidates. The result shows that the APK-B system at expected BER of 10^{-5} out-performs 8-phase PSK and APK-A at 3×10^{-3} and 10^{-2}, respectively. [Note that the silent channel multipath effect have been accounted separately. This is because, as explained in Section 5.6, these effects are expected to be obviated by redesigning the satellite OMUX filters and slightly shifting the center frequency of the adjacent transponders so as to remove the overlapping region of the filters. Failure to remedy the multipath effects can be seen to raise the error rates to unacceptable regions. These changes can be expected to improve the adjacent channel performances for the same reasons and new estimates of the overall BER are provided in the parenthesis after the "corresponding BER entry" in the Link Budget]. It is concluded that although the single channel performance of PSK is superior to APK, in a heavily interference limited environment, the lower

average power requirement of APK-B leads to an overall improvement in the error rate of almost two orders of magnitude over the 8-phase PSK case in 6/4 GHz environment.

In the next section, the performance of the three candidates will be evaluated in a 14/11 GHz environment where deep fades and associated depolarization are common occurrences.

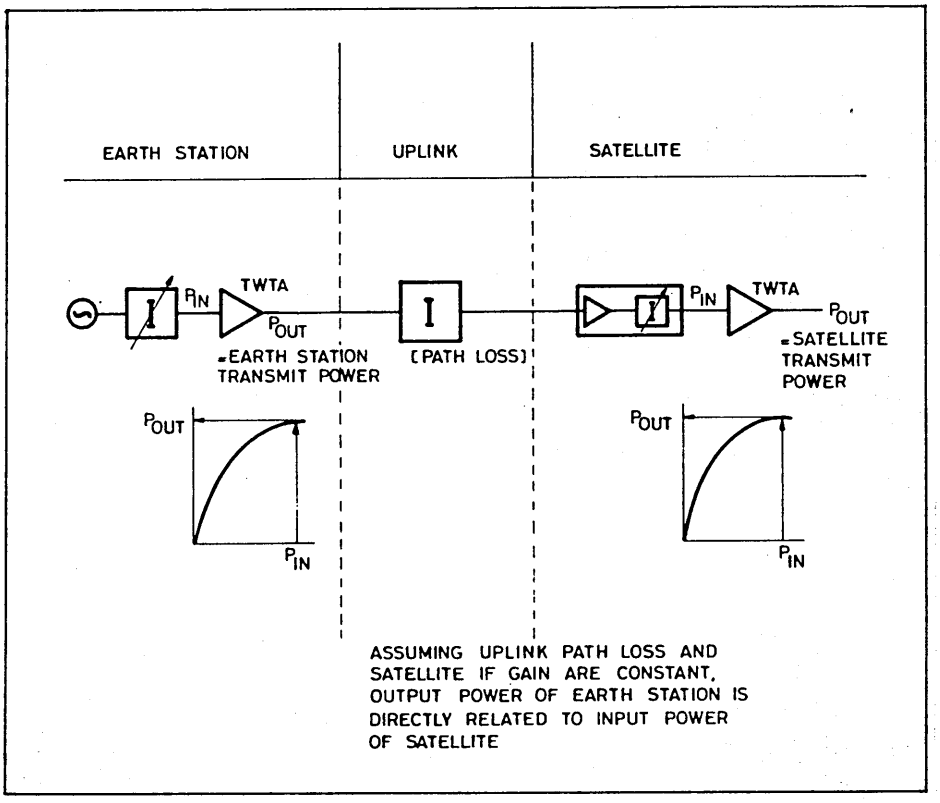

FIGURE 5.1 ELEMENTARY NON-LINEAR CHANNEL

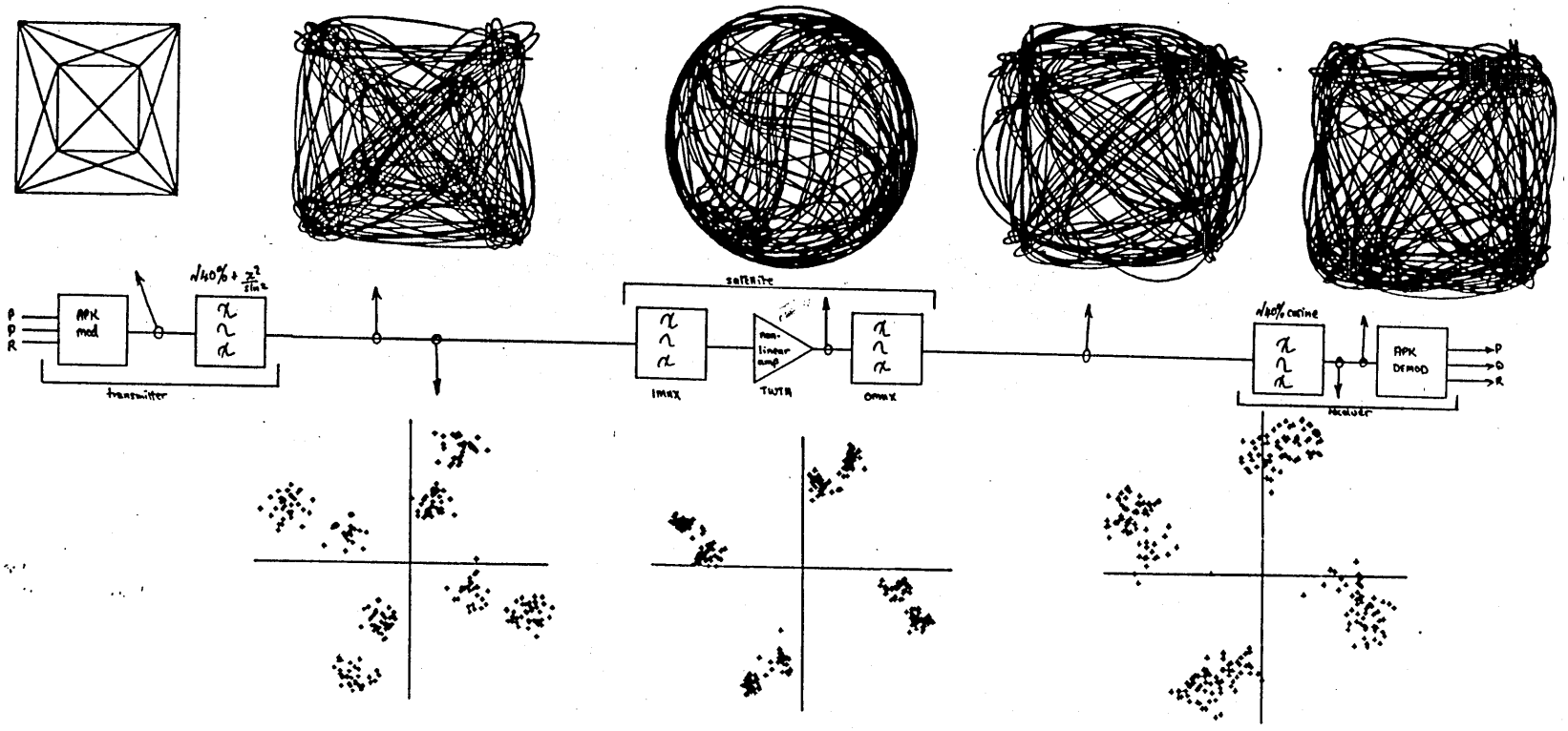

FIGURE 5.2 NON-LINEAR SIGNAL SPACE DIAGRAMS FOR APK TYPE-A

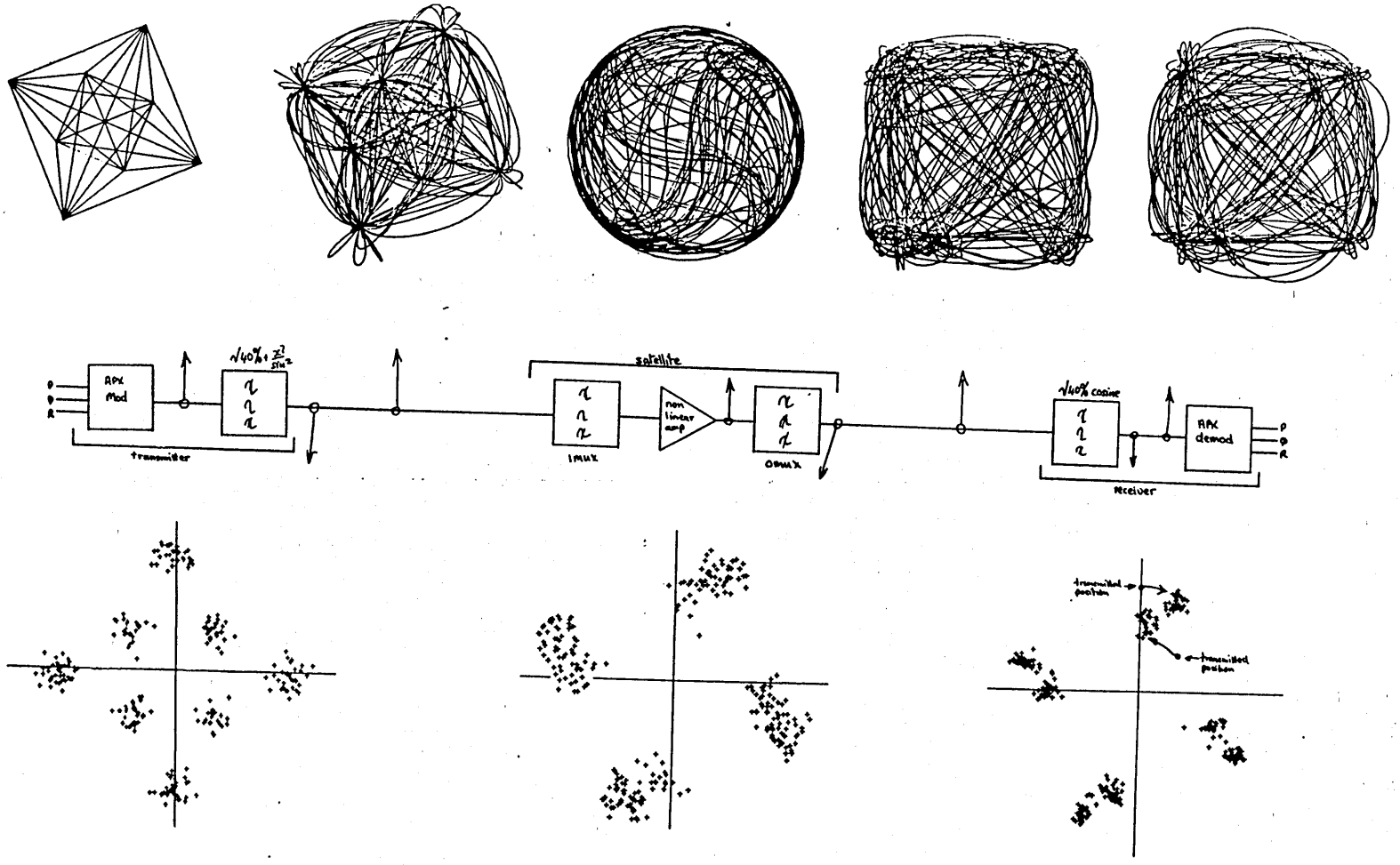

FIGURE 5.3 NON-LINEAR SIGNAL SPACE DIAGRAMS FOR APK TYPE-B

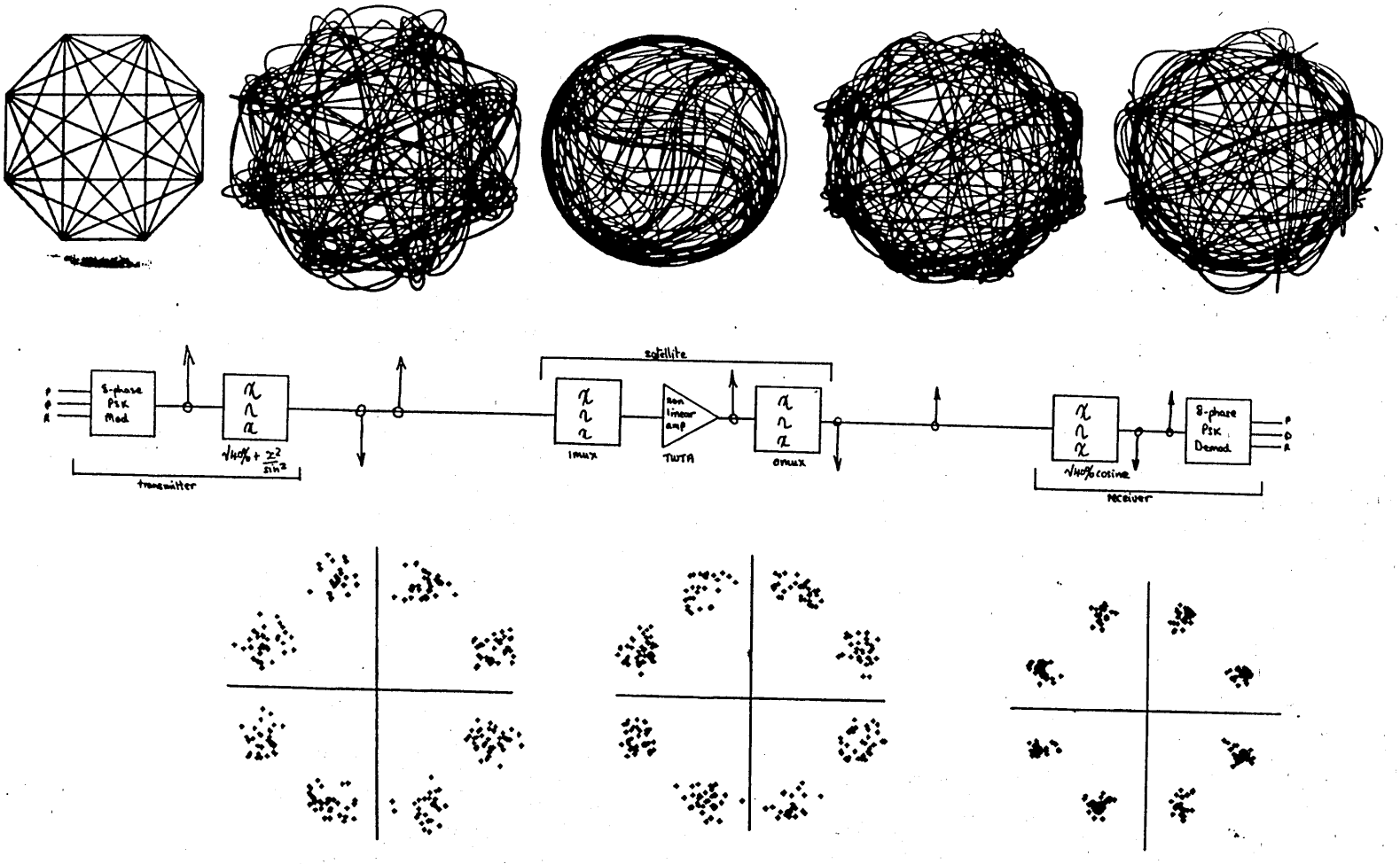

FIGURE 5.4 NON-LINEAR SIGNAL SPACE DIAGRAMS FOR 8-PHASE PSK

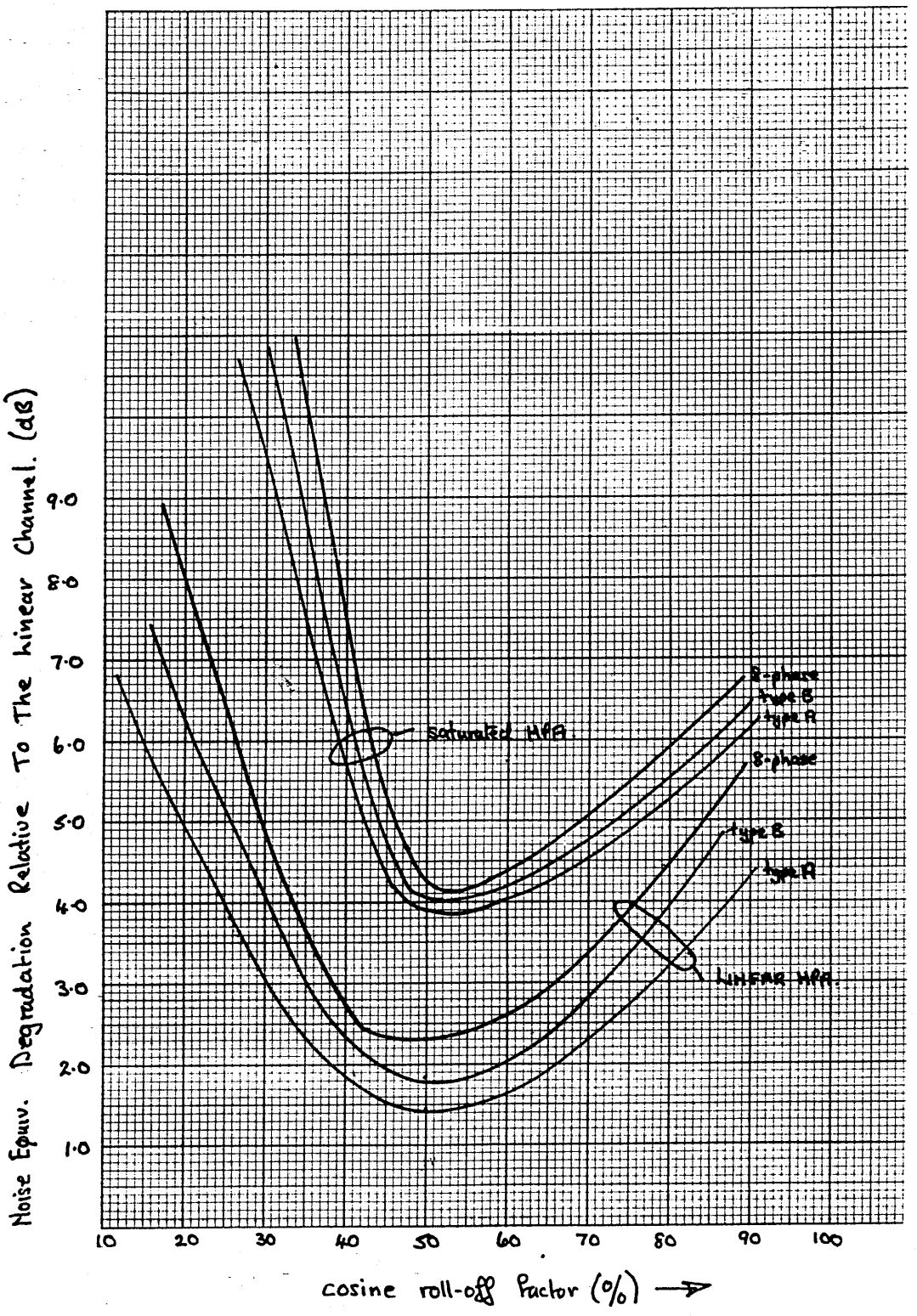

FIGURE 5.5 NOISE EQUIVALENT DEGRADATION
vs COSINE ROLL-OFF FACTOR

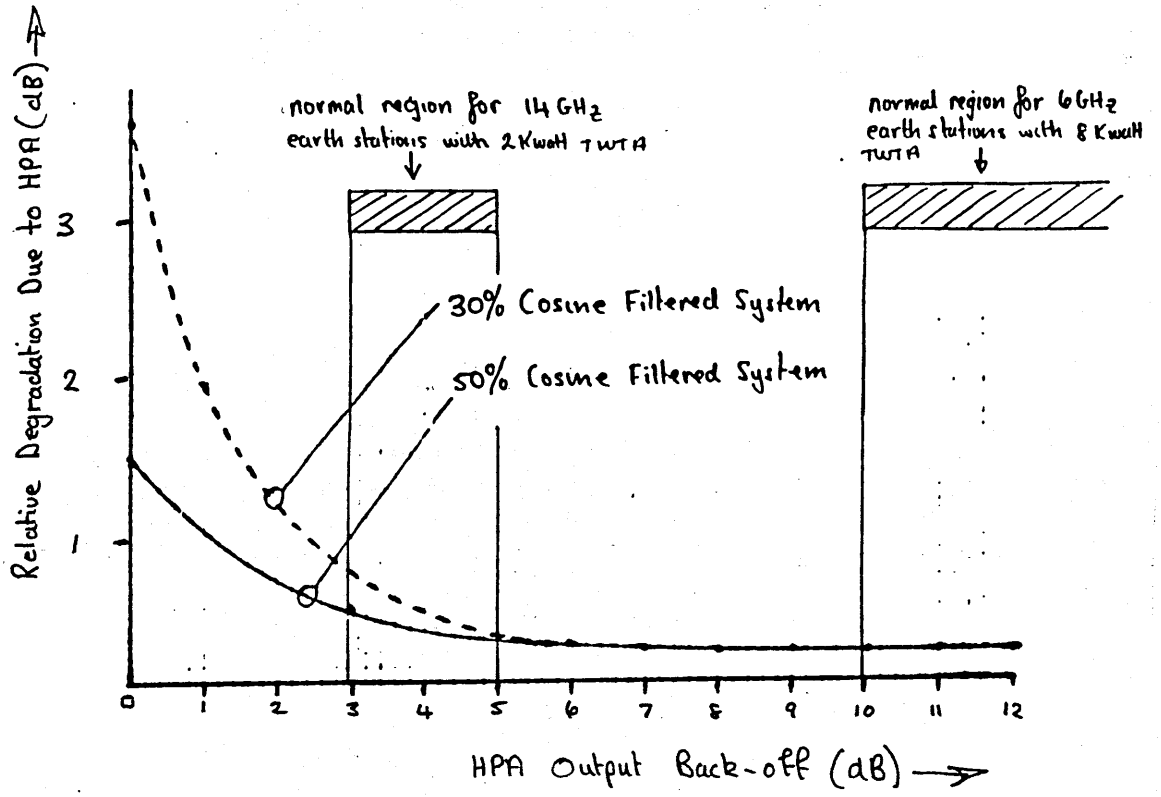

FIGURE 5.6 VARIATION IN LINK DEGRADATION WITH HPA OPERATING POINT FOR 30% AND 50% COSINE ROLL-OFF FILTERS

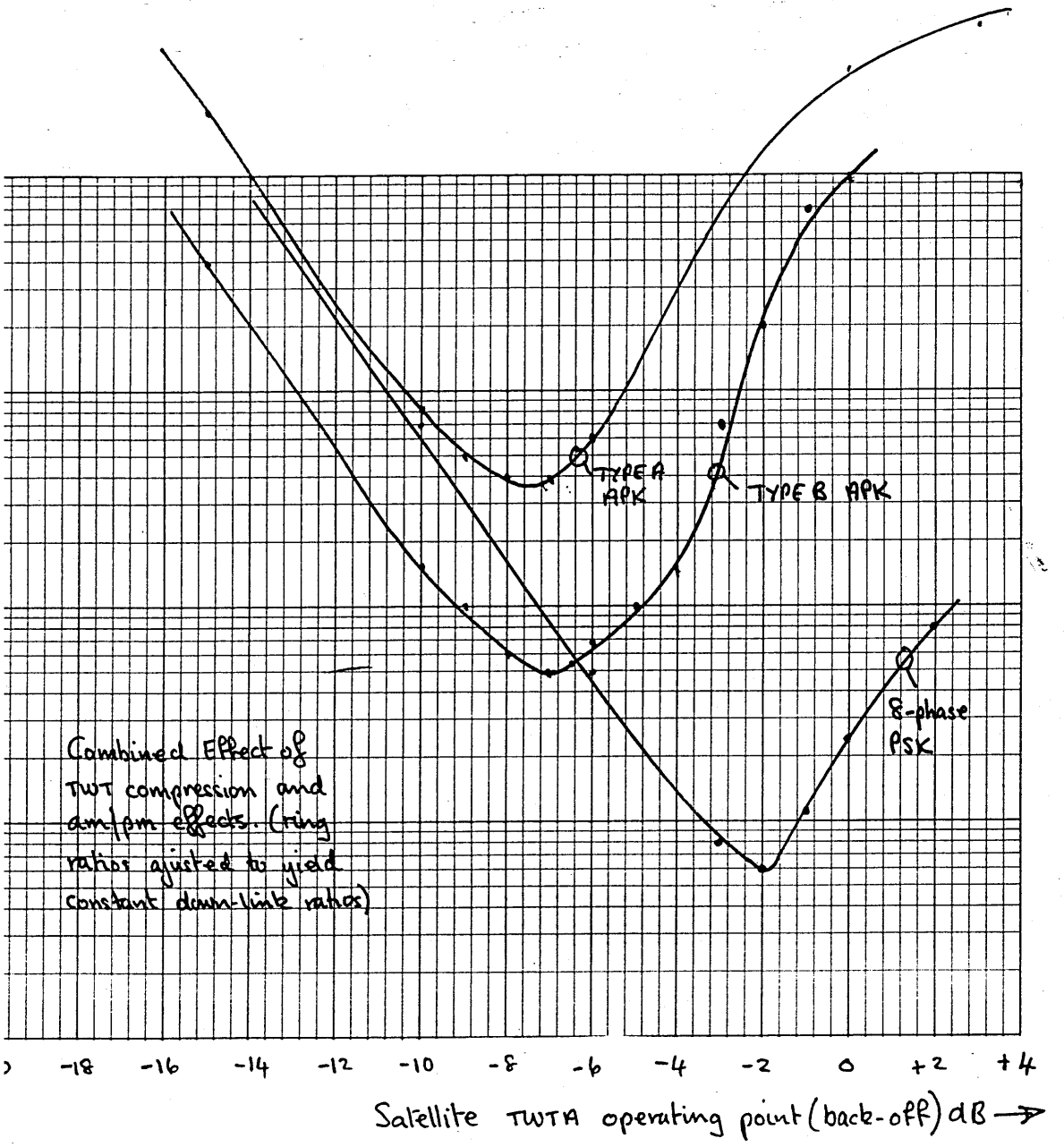

FIGURE 5.7 BER vs TWT OPERATING POINT

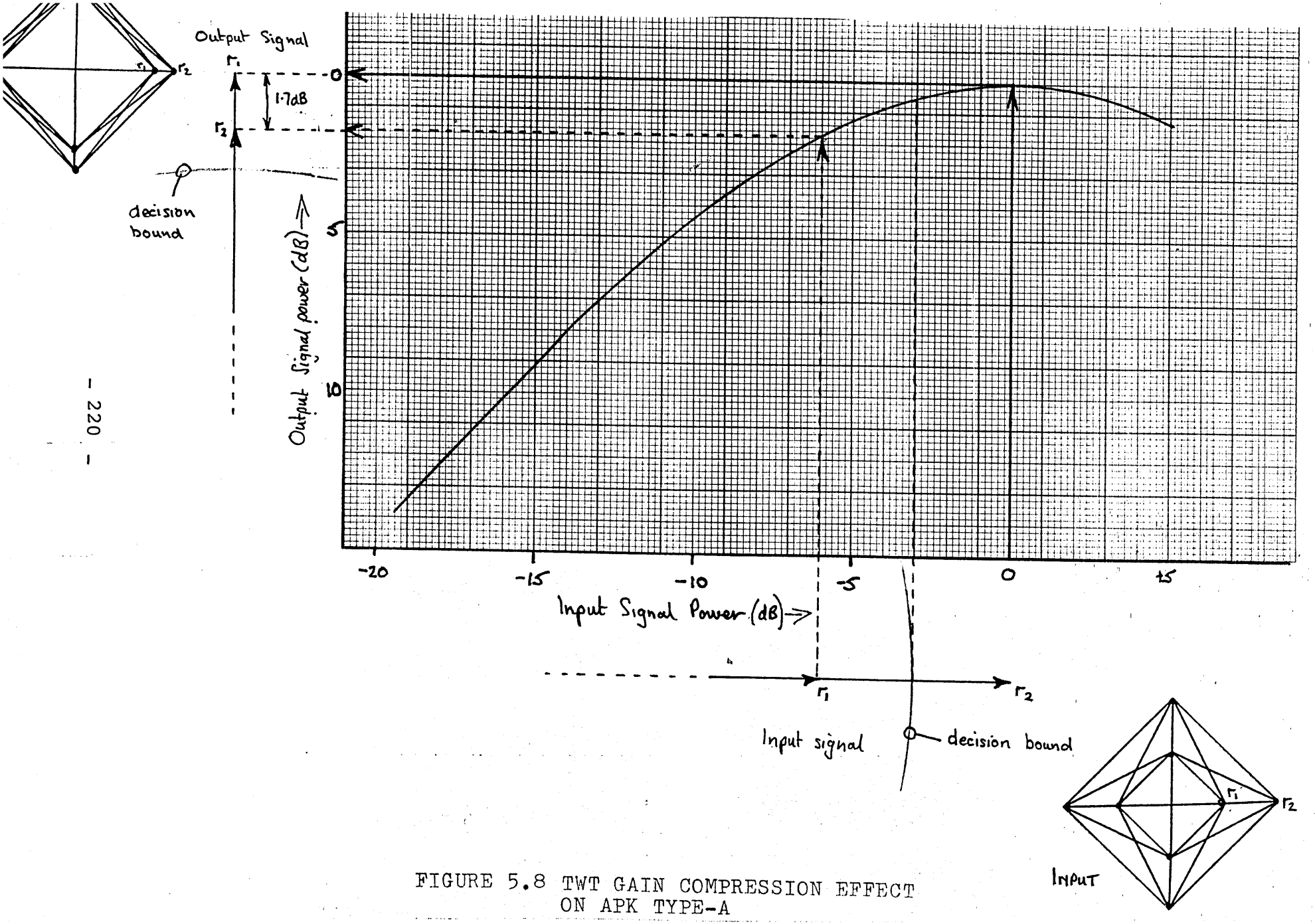

FIGURE 5.8 TWT GAIN COMPRESSION EFFECT ON APK TYPE-A

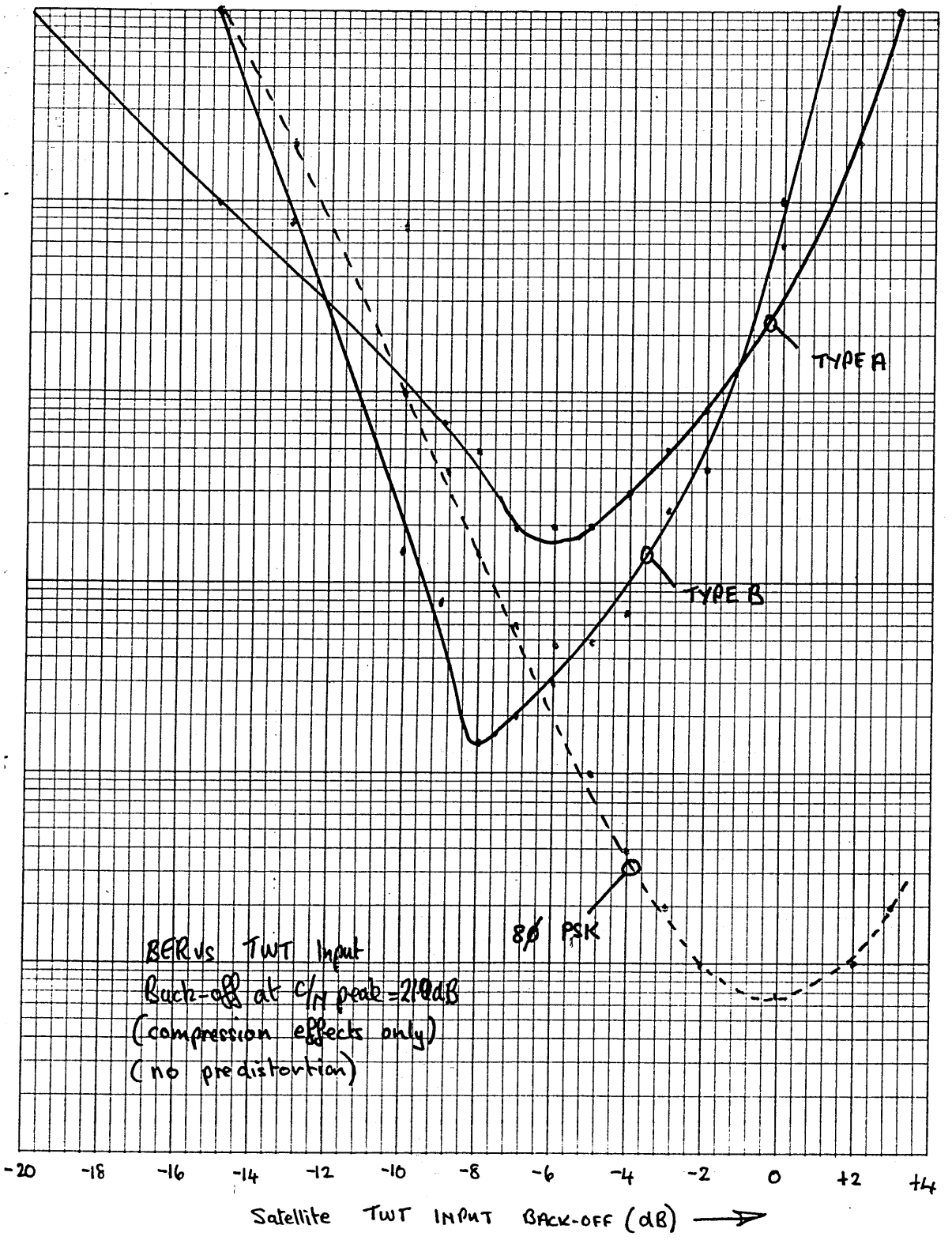

FIGURE 5.9 BER vs TWT BACK-OFF WITH NO COMPENSATION

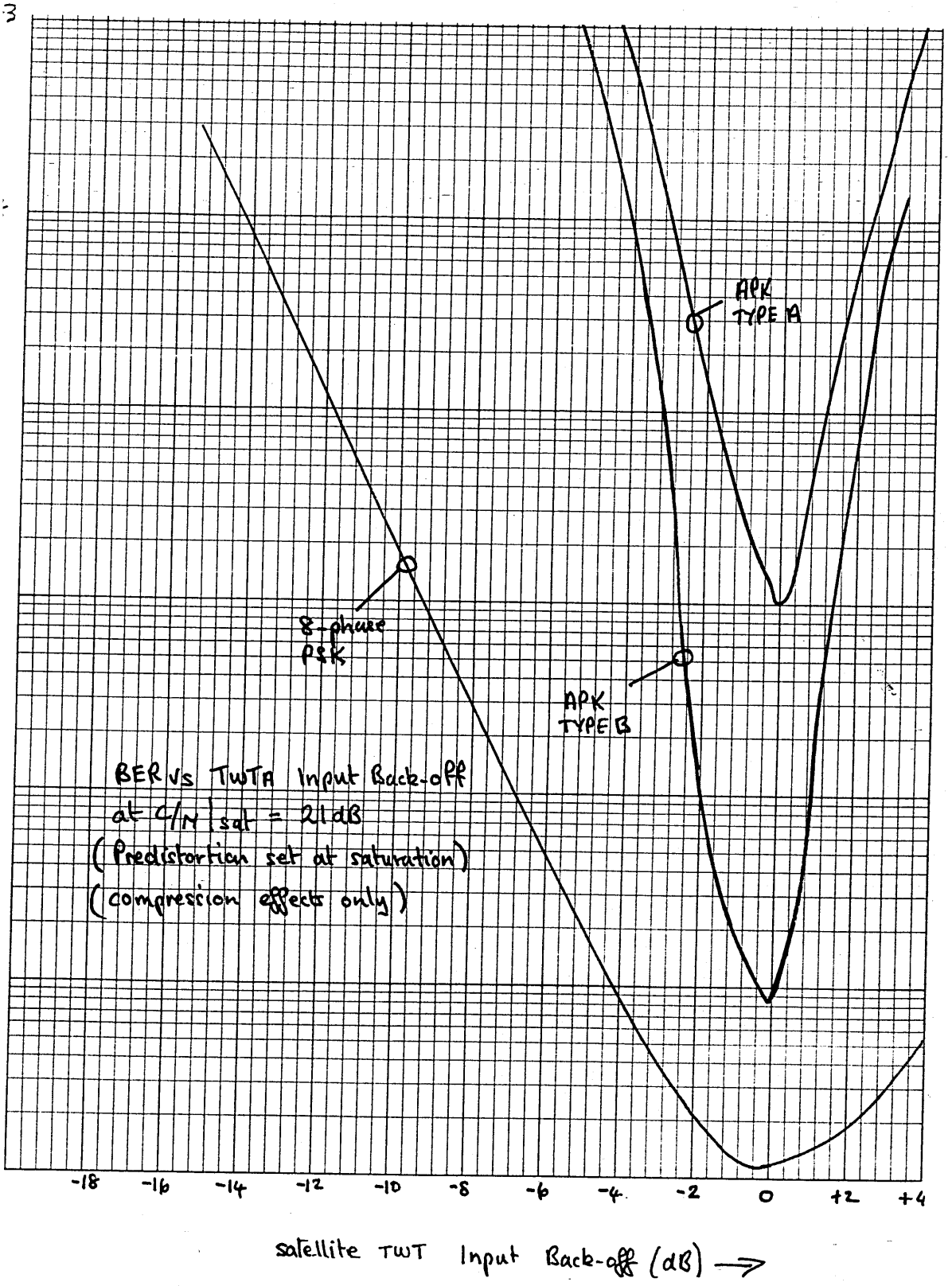

FIGURE 5.10 BER vs TWT BACK-OFF WITH AMPLITUDE PREDISTORTION

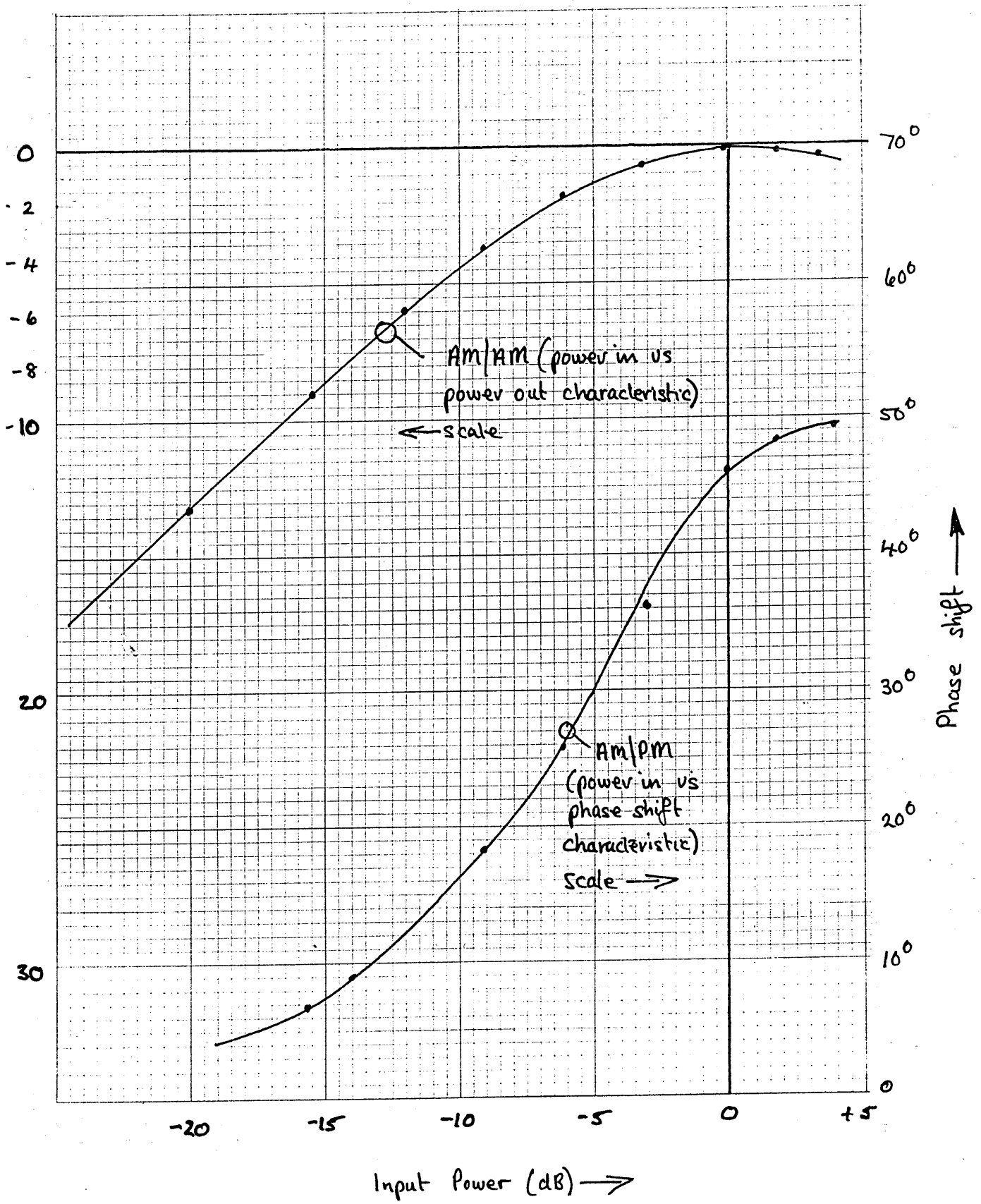

FIGURE 5.11 TWT AM/AM AND AM/PM CHARACTERISTICS

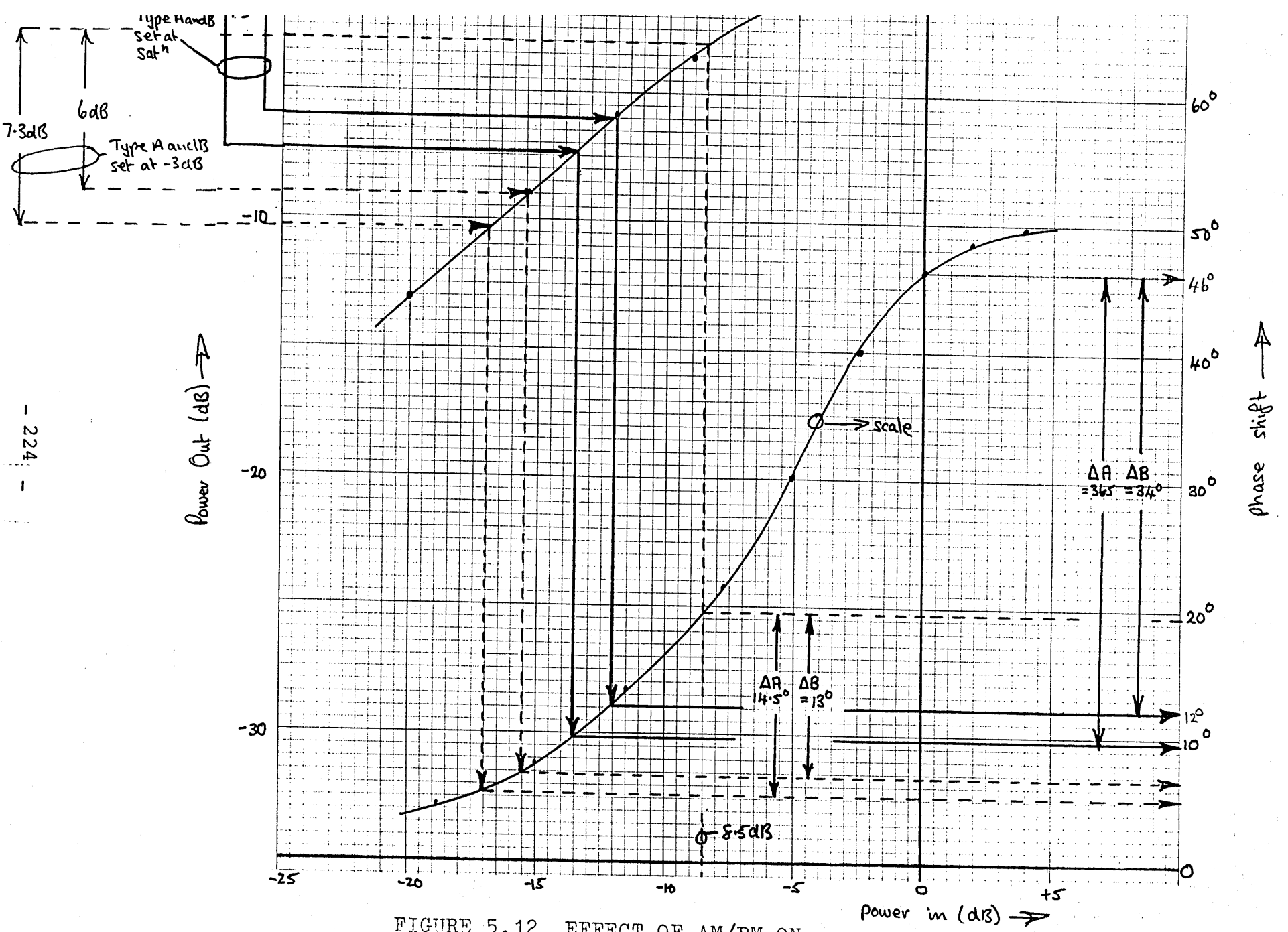

FIGURE 5.12 EFFECT OF AM/PM ON TYPE A AND B APK

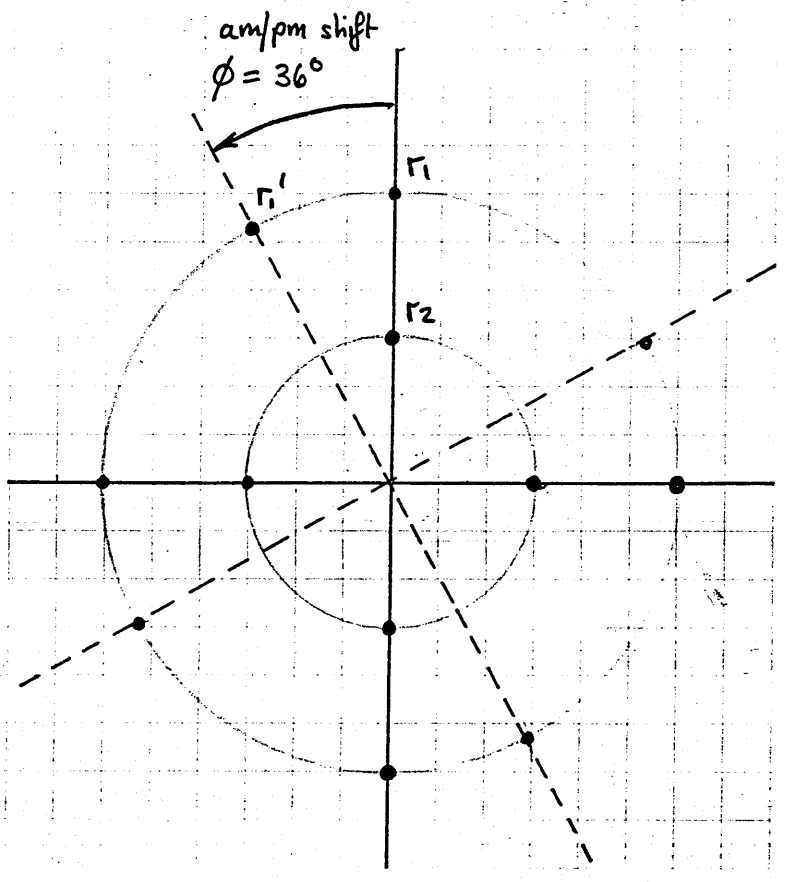

FIGURE 5.13 SHIFT OF OUTER SIGNAL RING DUE TO AM/PM EFFECTS FOR A TYPE-A SYSTEM

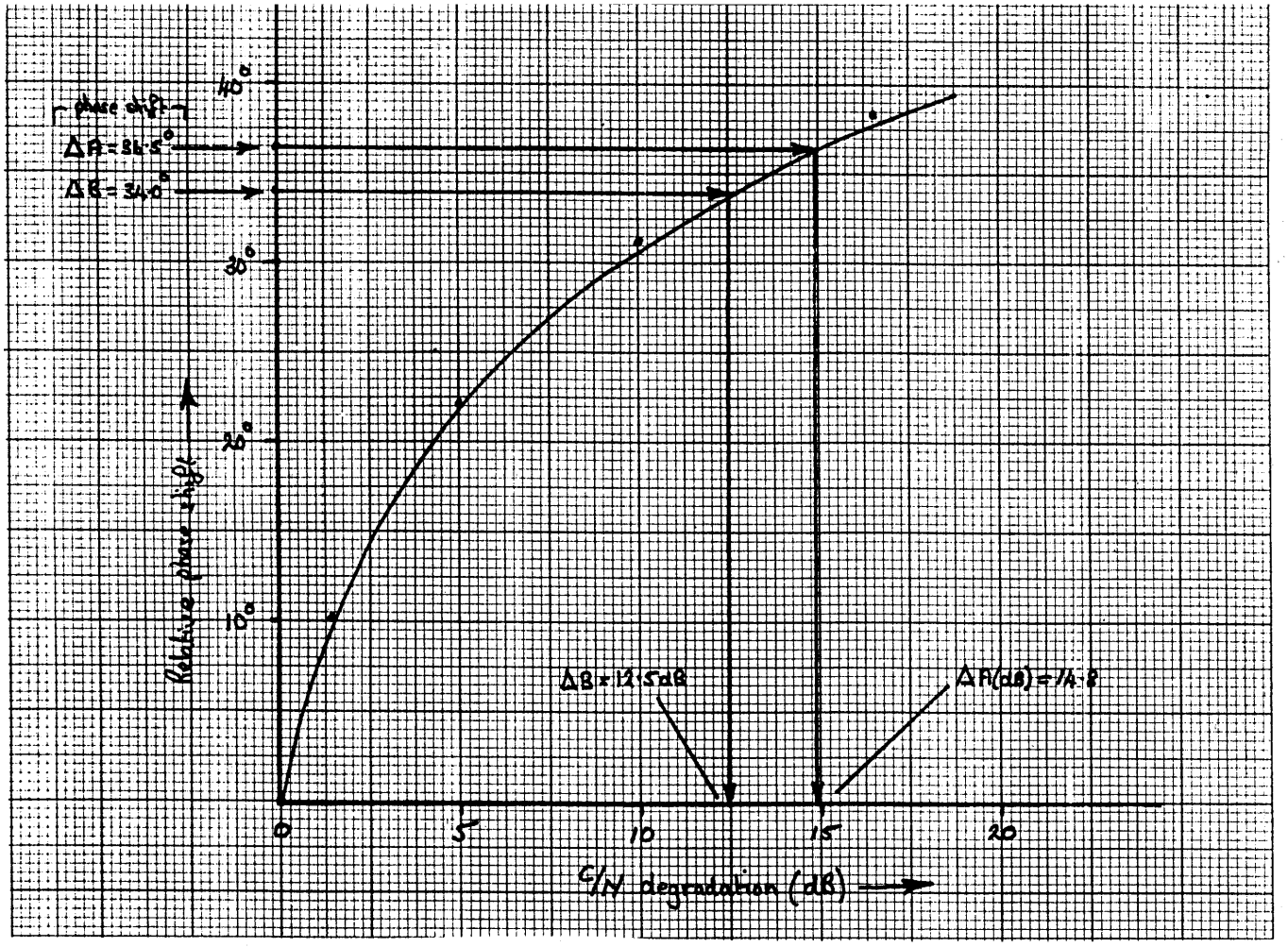

FIGURE 5.14 NOISE EQUIVALENT DEGRADATION FOR VARIOUS INTER-RING PHASE SHIFTS

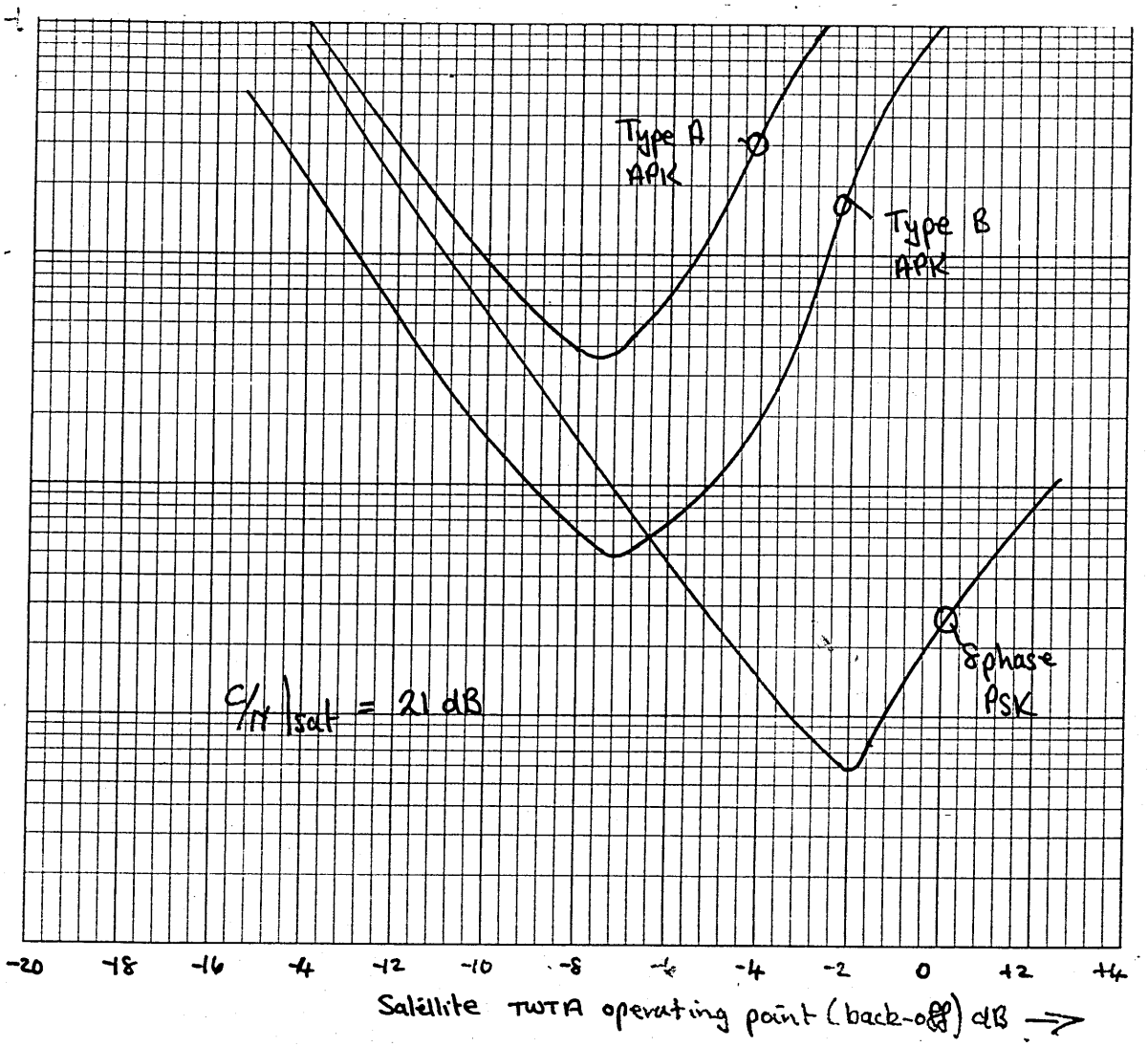

FIGURE 5.15 BER vs TWT BACK-OFF WITH AM/PM EFFECTS

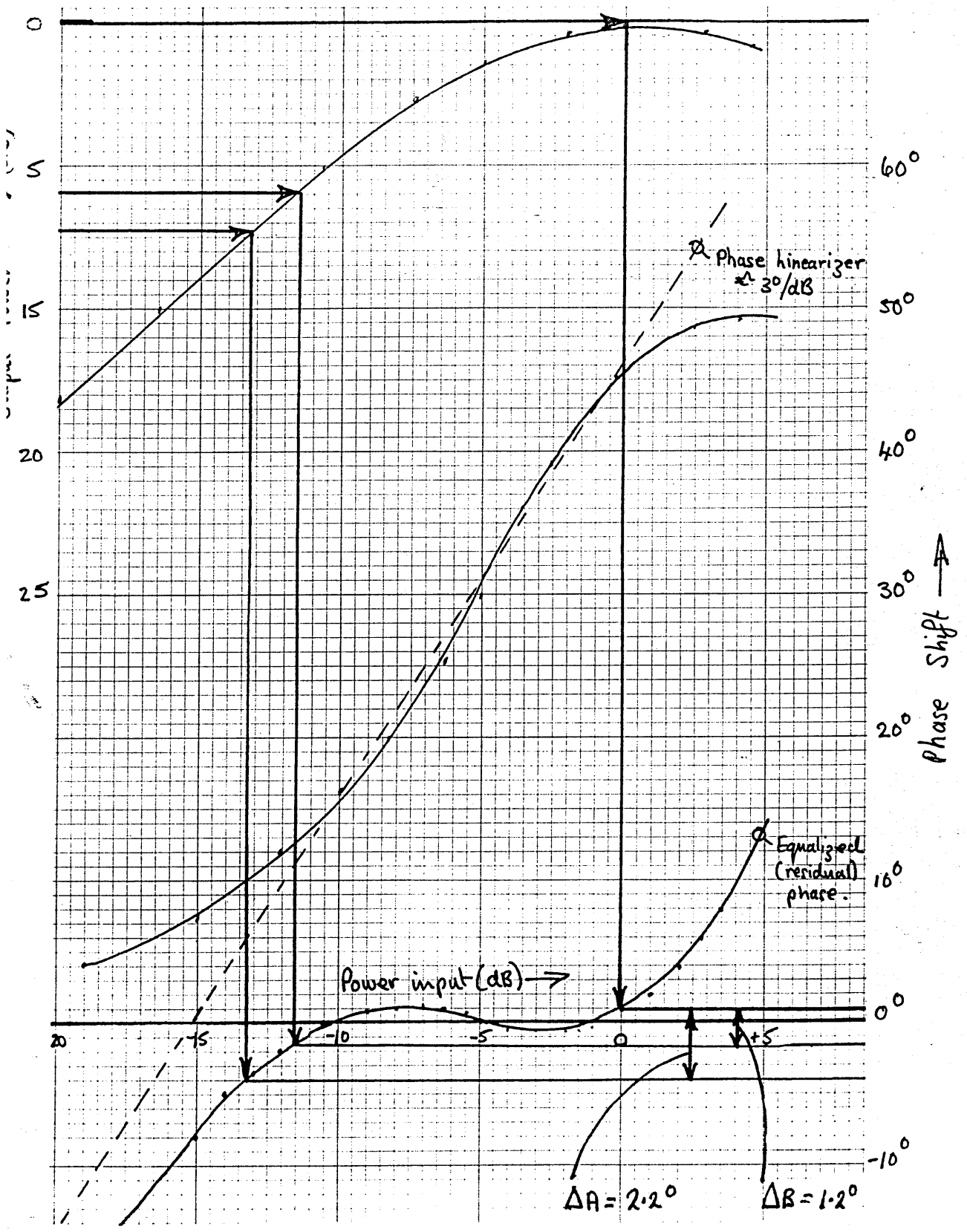

FIGURE 5.16 PHASE EQUALIZATION TECHNIQUE

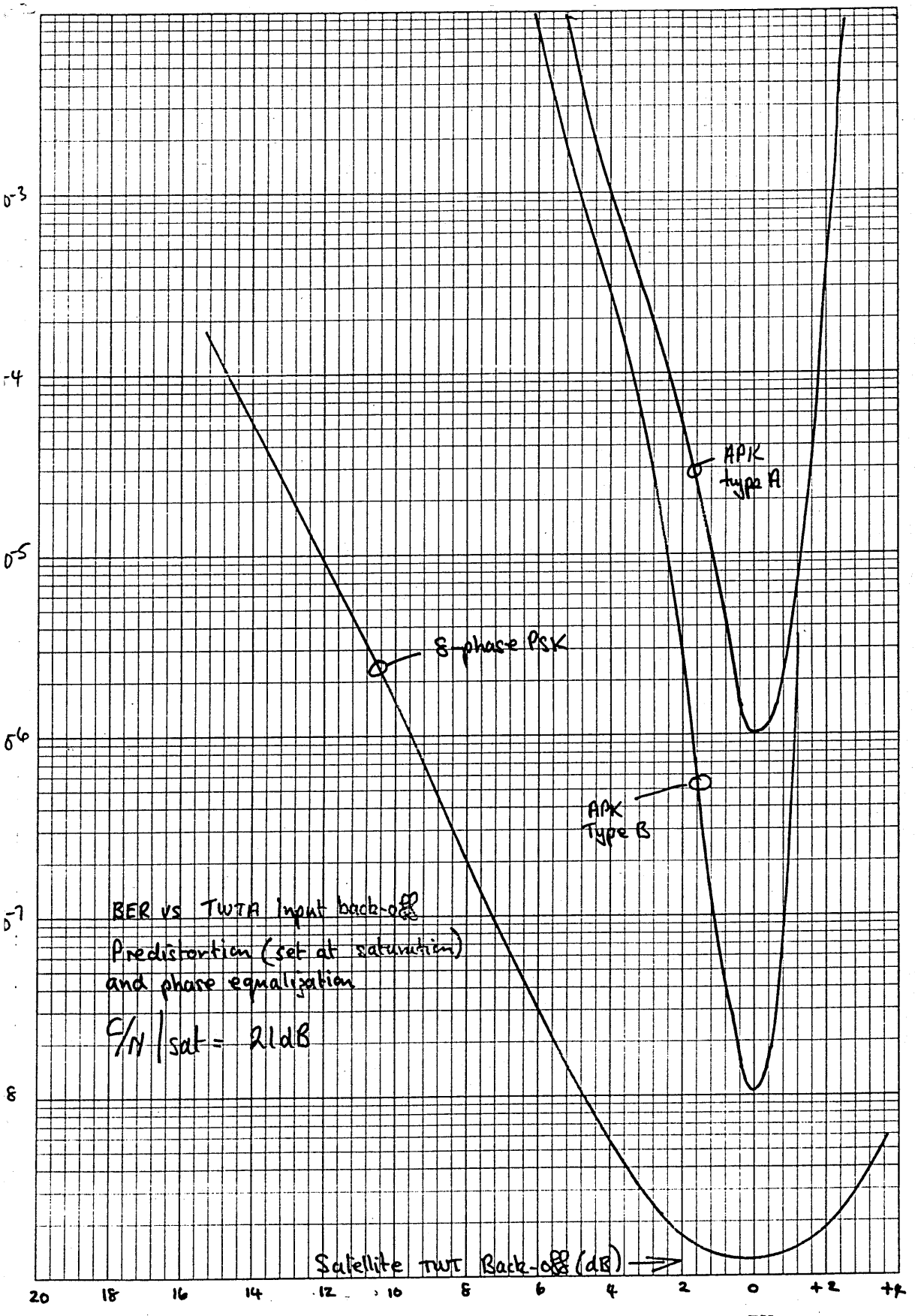

FIGURE 5.17 BER vs TWT BACK-OFF WITH AMPLITUDE AND PHASE COMPENSATION

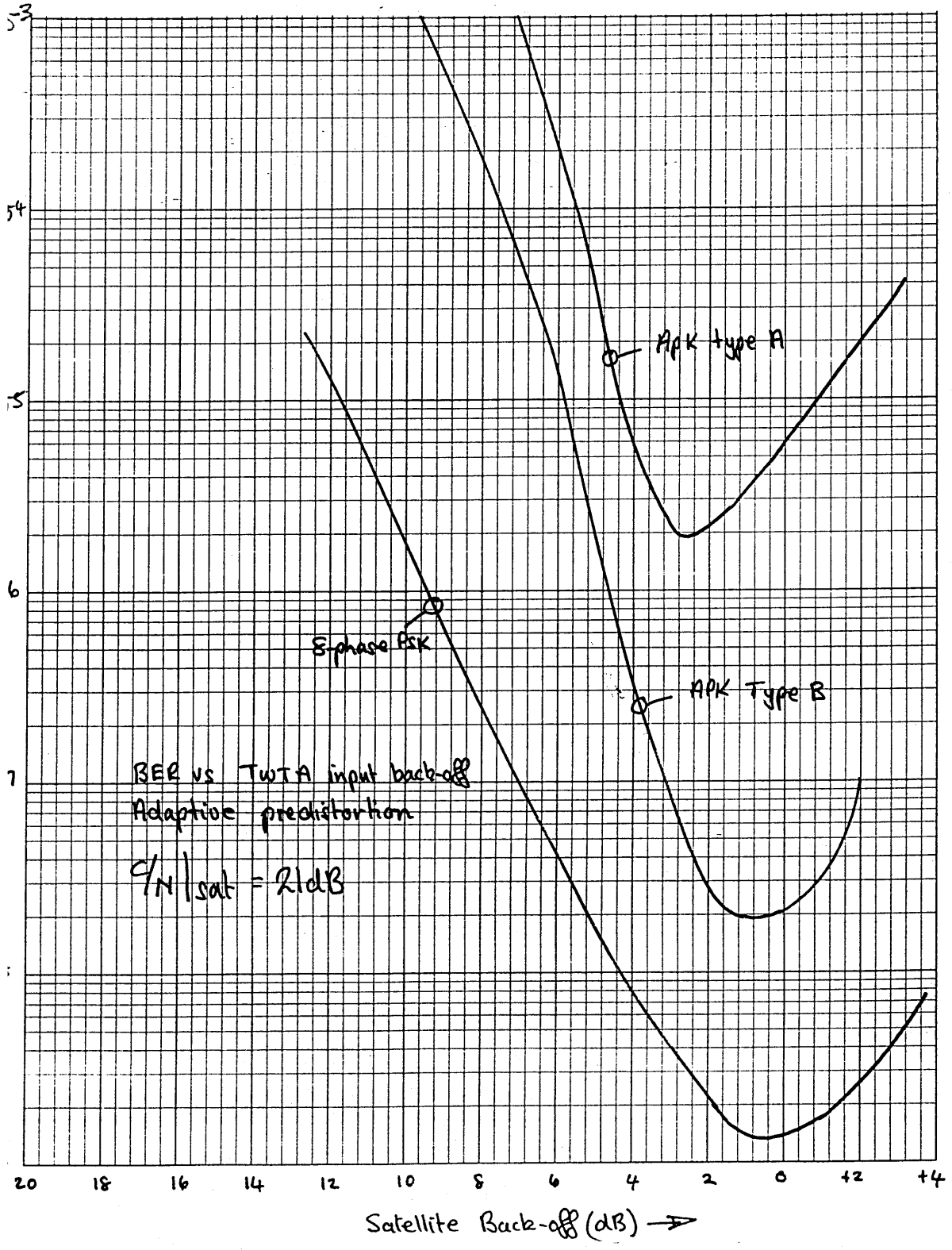

FIGURE 5.18 BER vs TWT BACK-OFF FOR ADAPTIVE AMPLITUDE AND PHASE PREDISTORTION

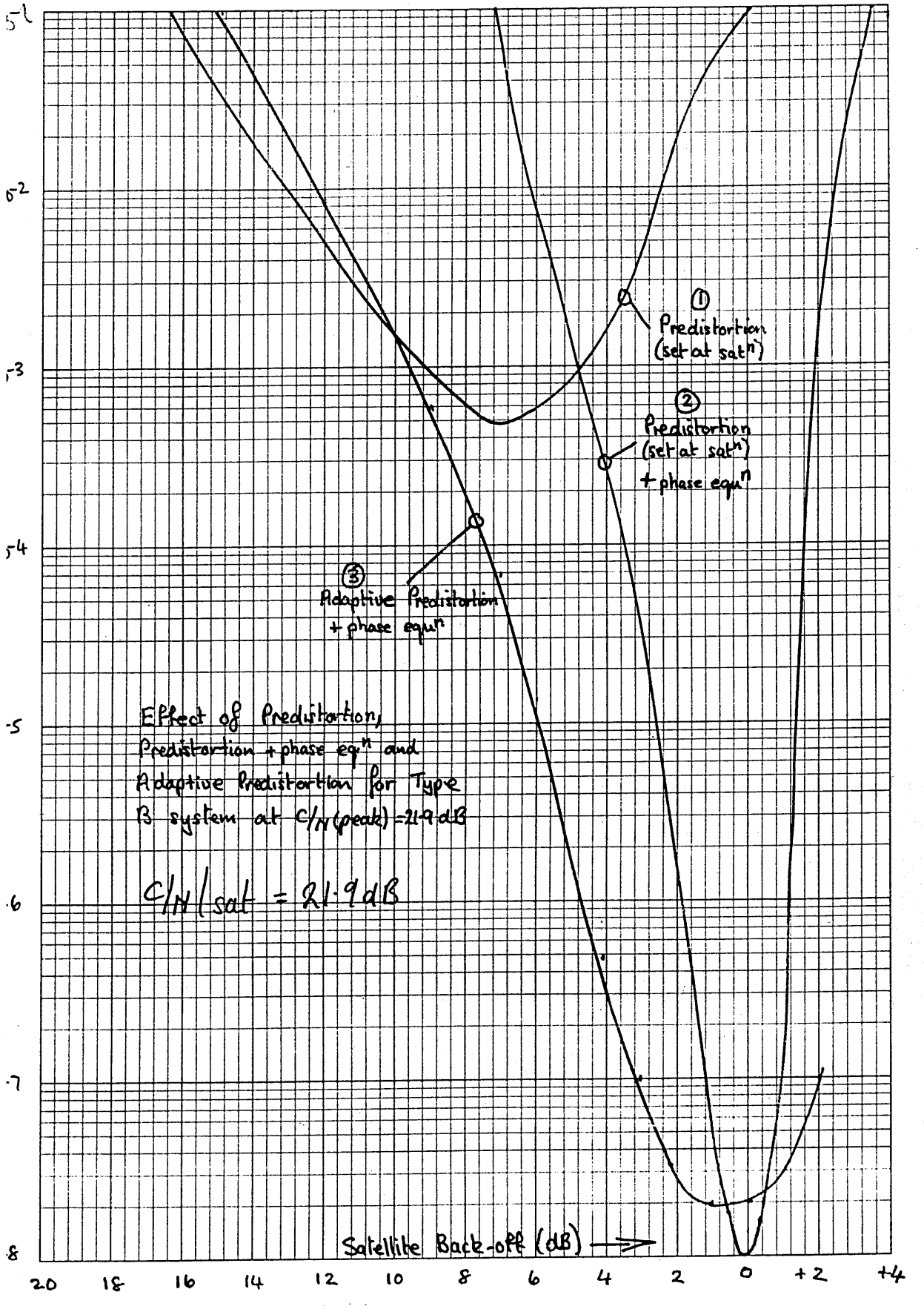

FIGURE 5.19 SUMMARY PERFORMANCE CURVES

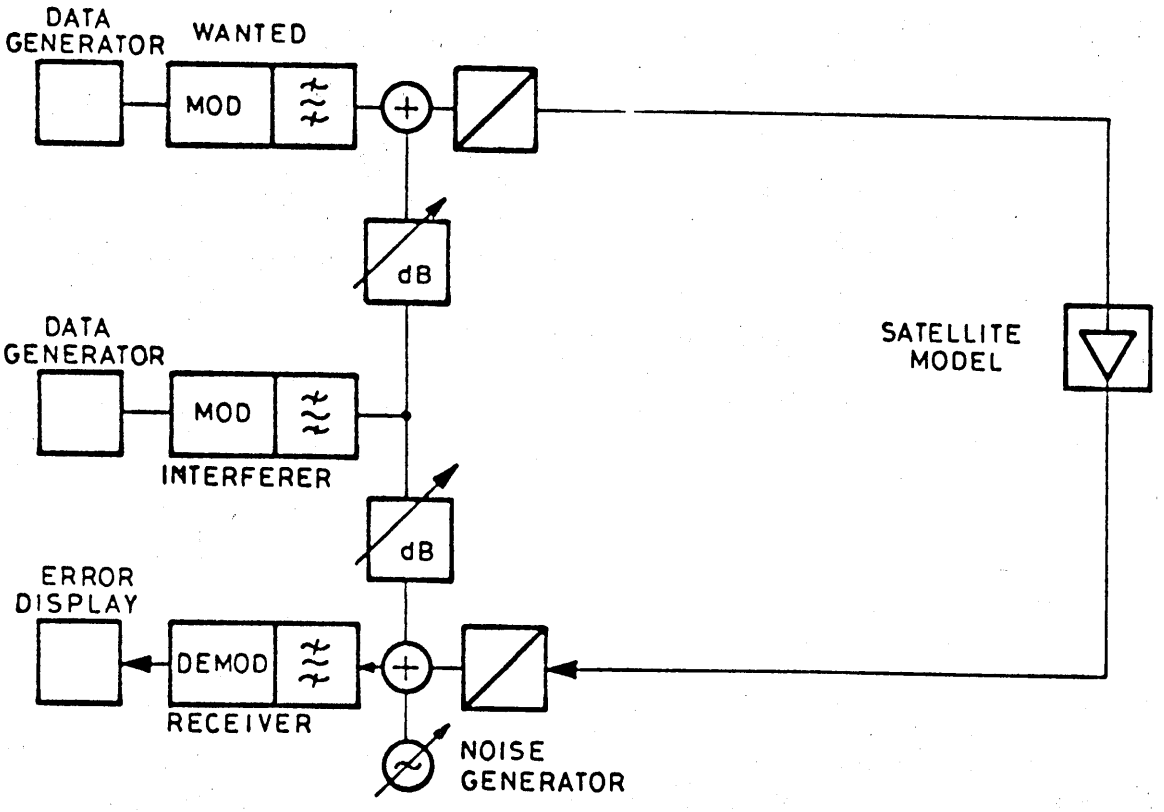

FIGURE 5.20 TRANSMISSION MODEL FOR CCI INVESTIGATIONS

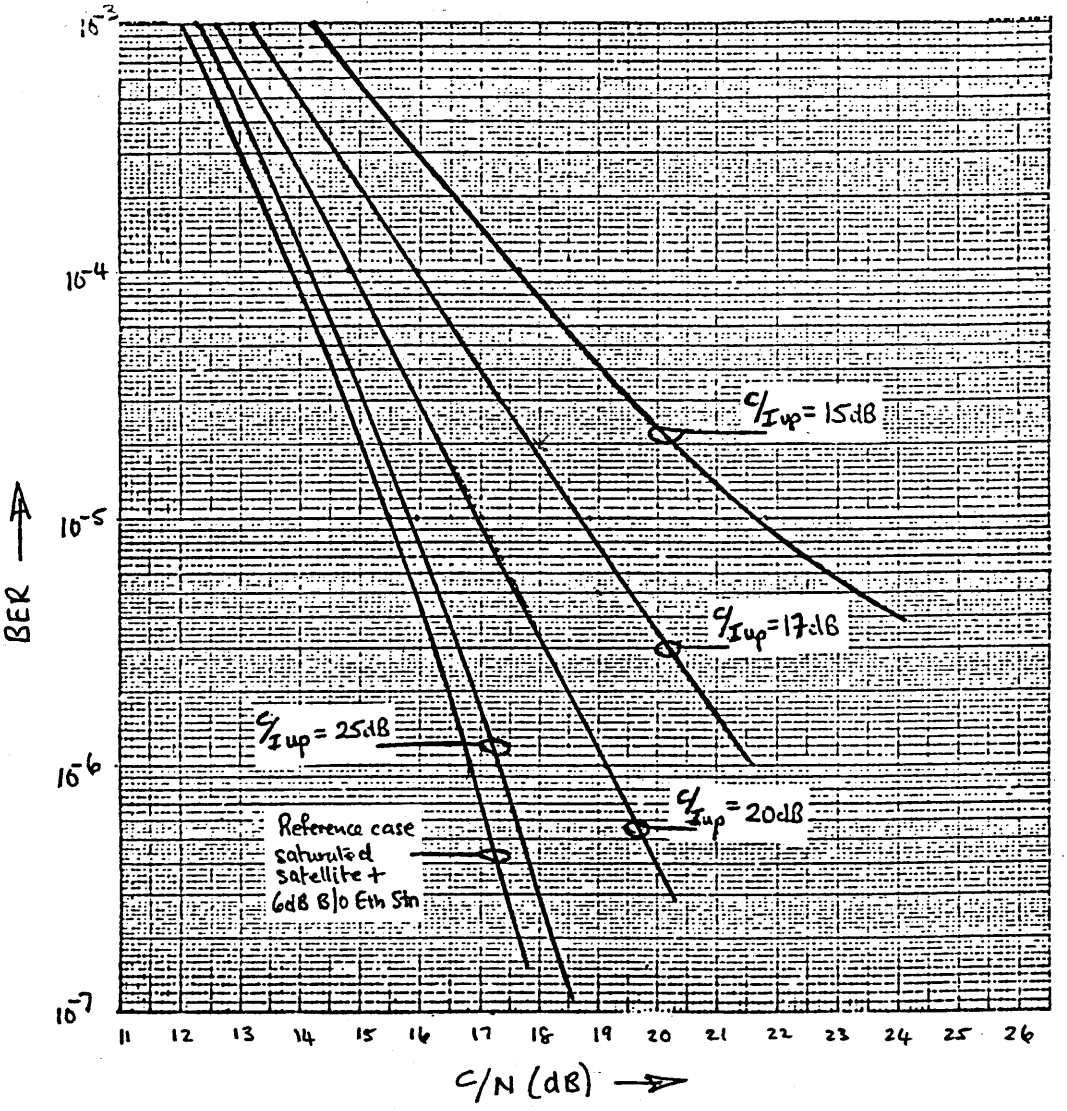

FIGURE 5.21 BER vs C/N FOR VARIOUS UP-LINK C/I RATIOS

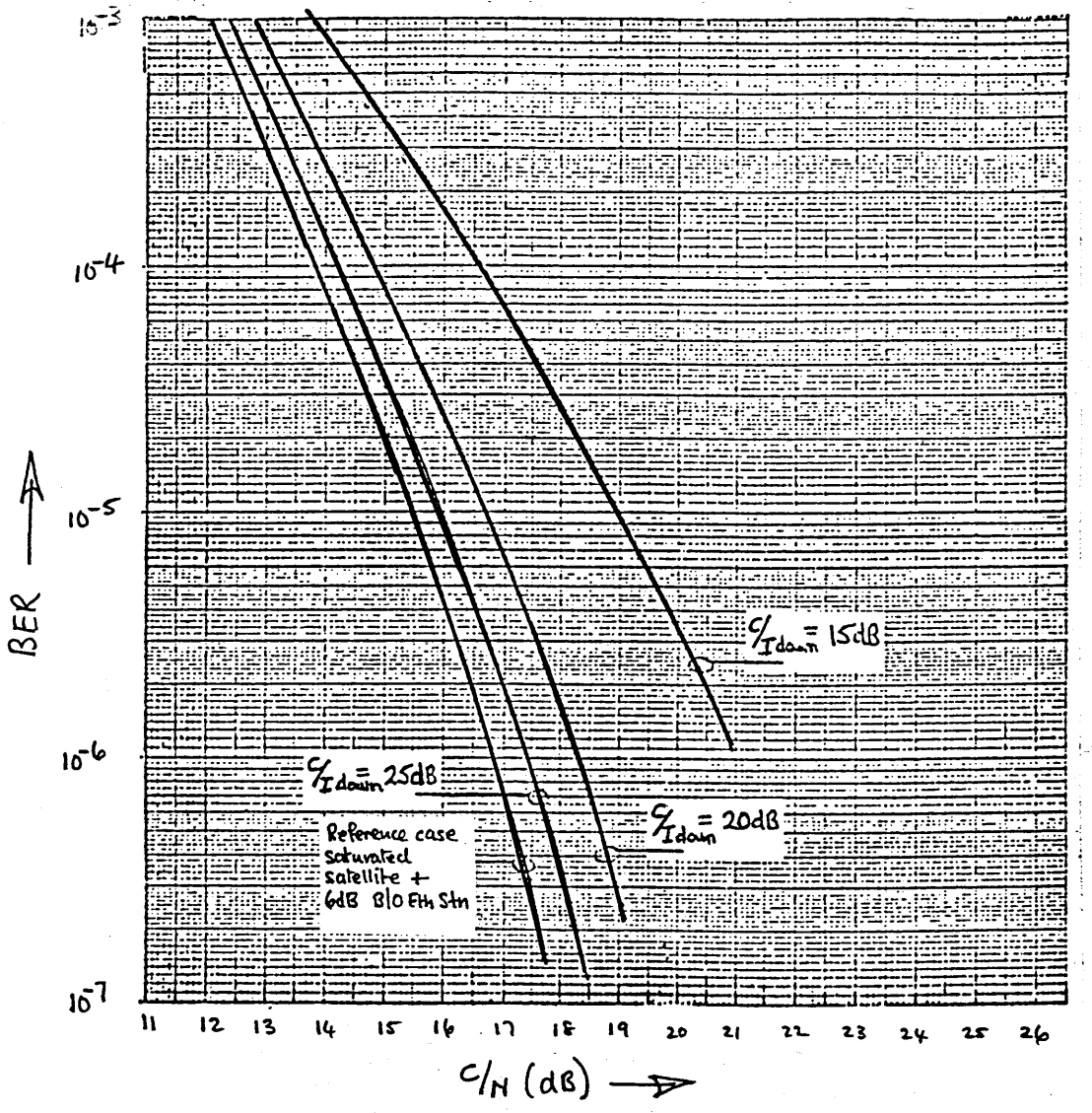

FIGURE 5.22 BER vs C/N FOR VARIOUS DOWN-LINK C/I RATIOS

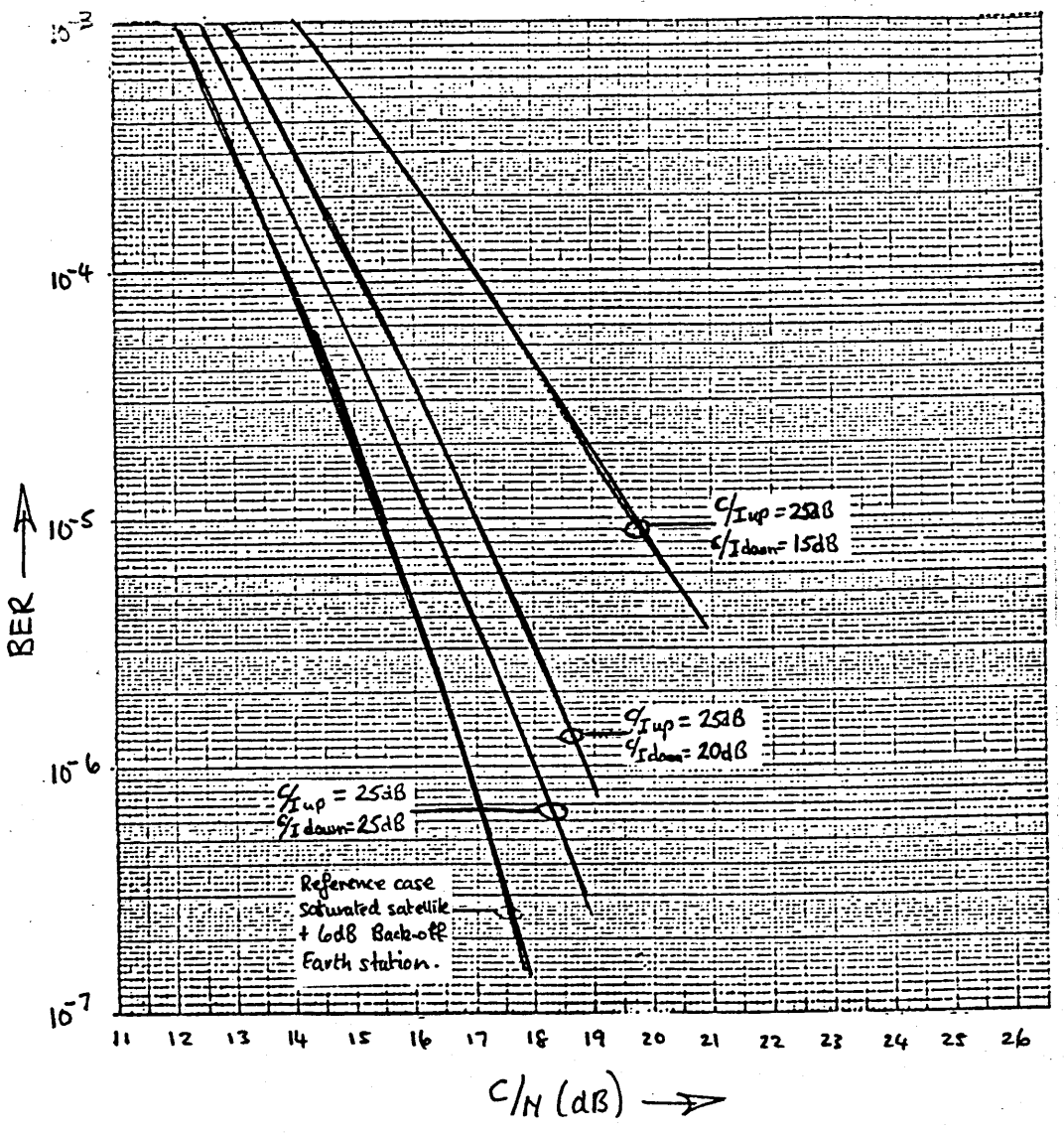

FIGURE 5.23 BER vs C/N FOR VARIOUS UP-LINK AND DOWN-LINK C/I RATIOS

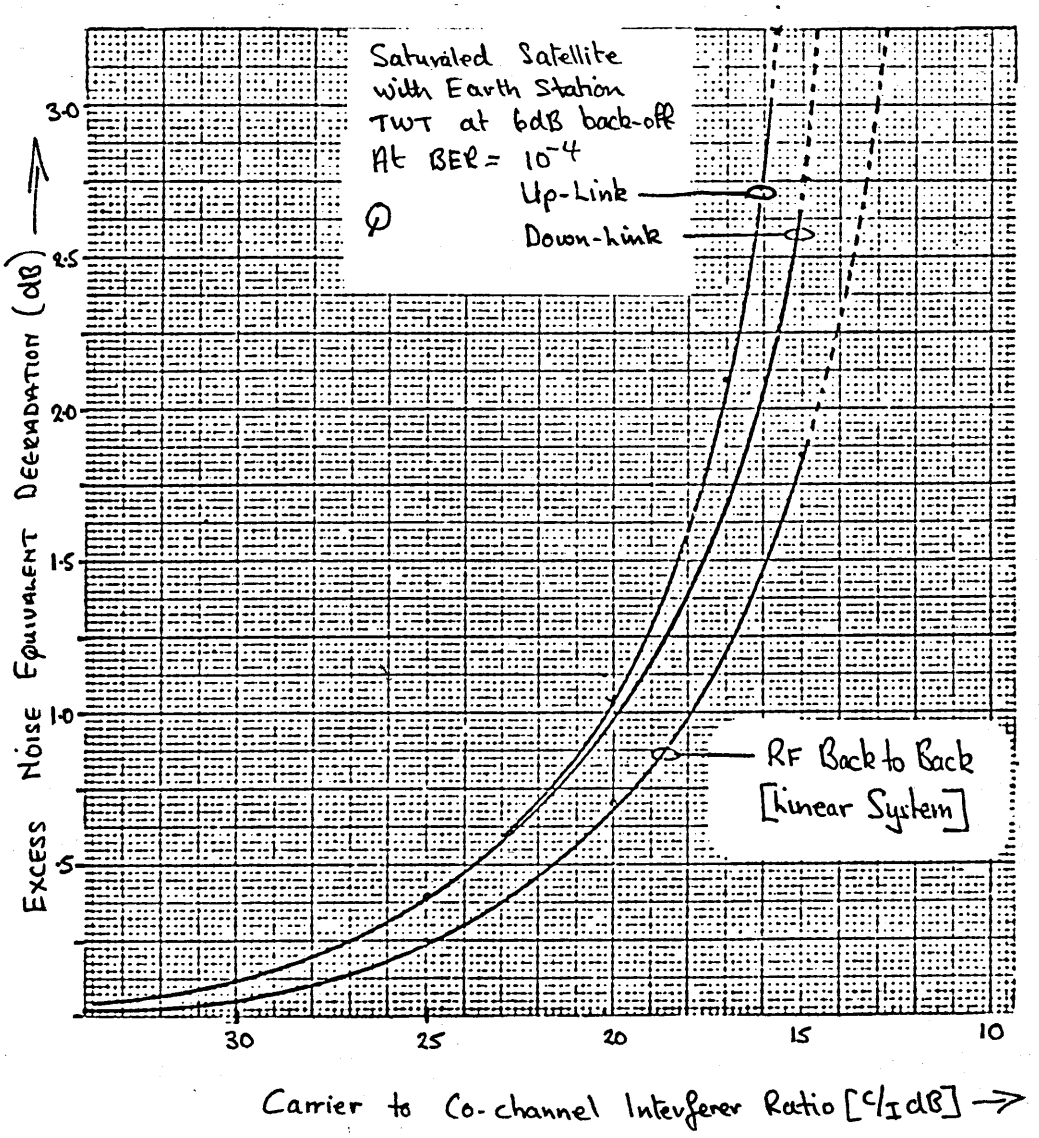

FIGURE 5.24 NOISE EQUIVALENT DEGRADATION vs C/I RATIO

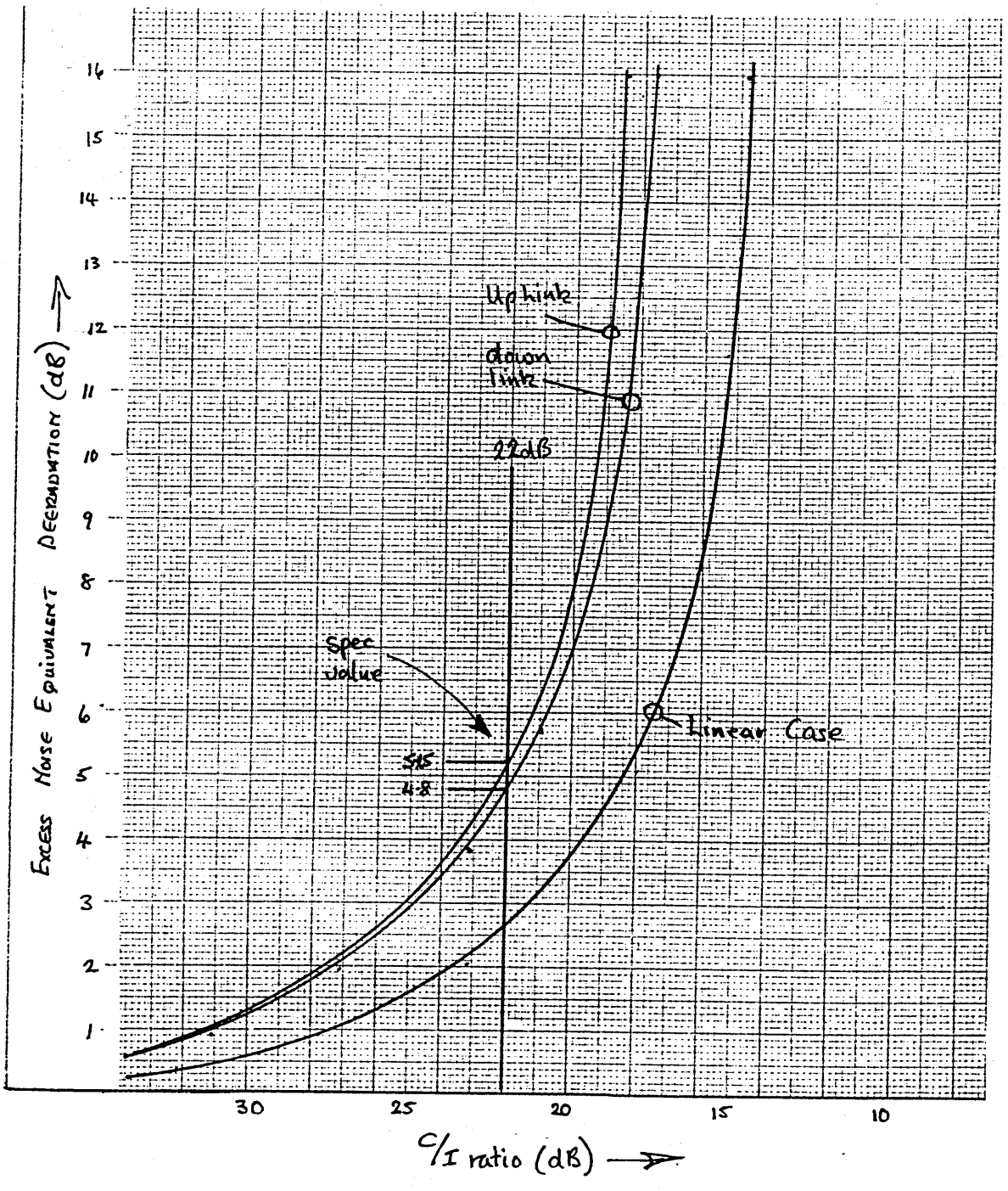

FIGURE 5.25 NOISE EQUIVALENT DEGRADATION vs C/I RATIO FOR 8-PHASE PSK

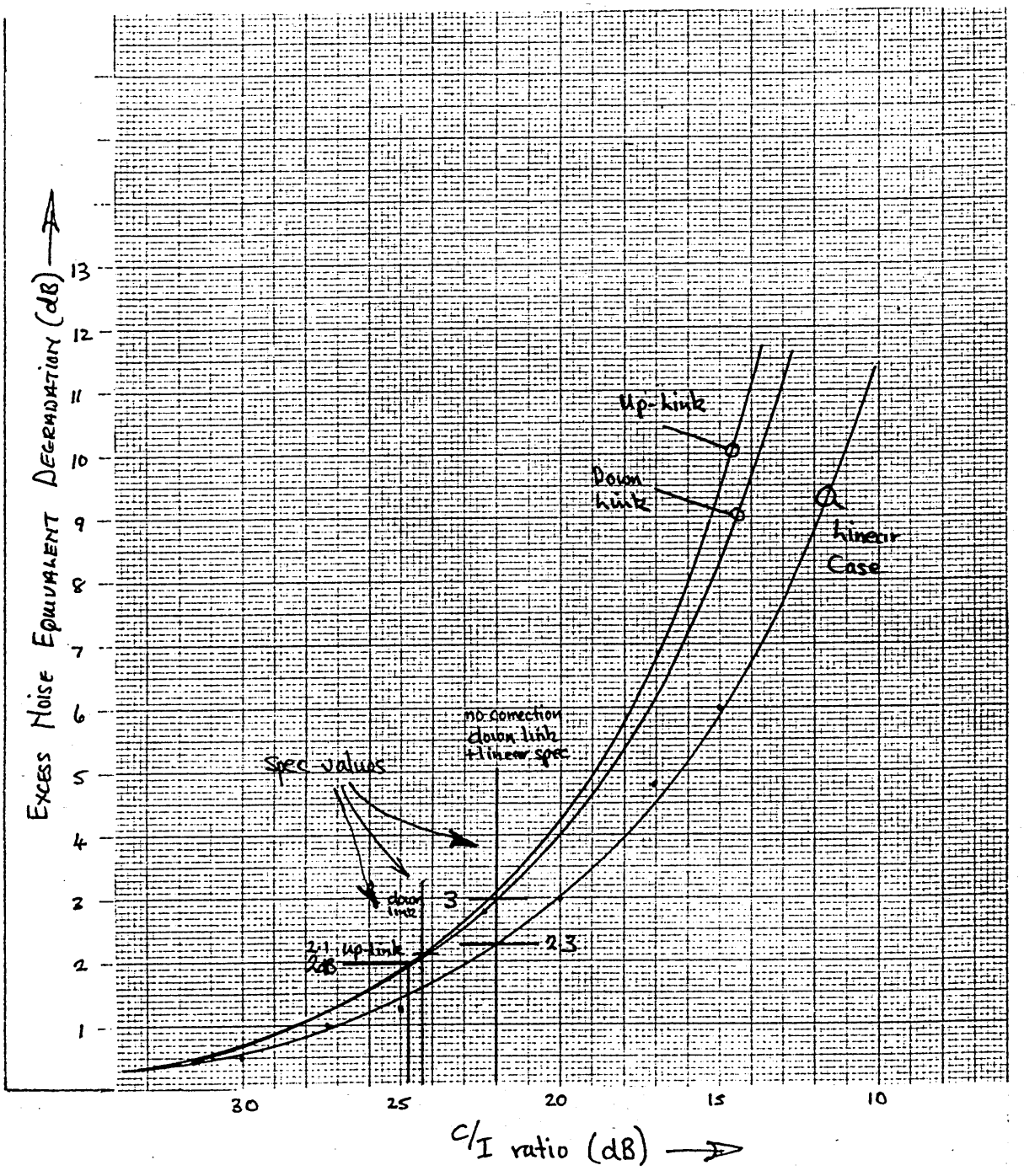

FIGURE 5.26 NOISE EQUIVALENT DEGRADATION vs C/I RATIO FOR APK TYPE-A

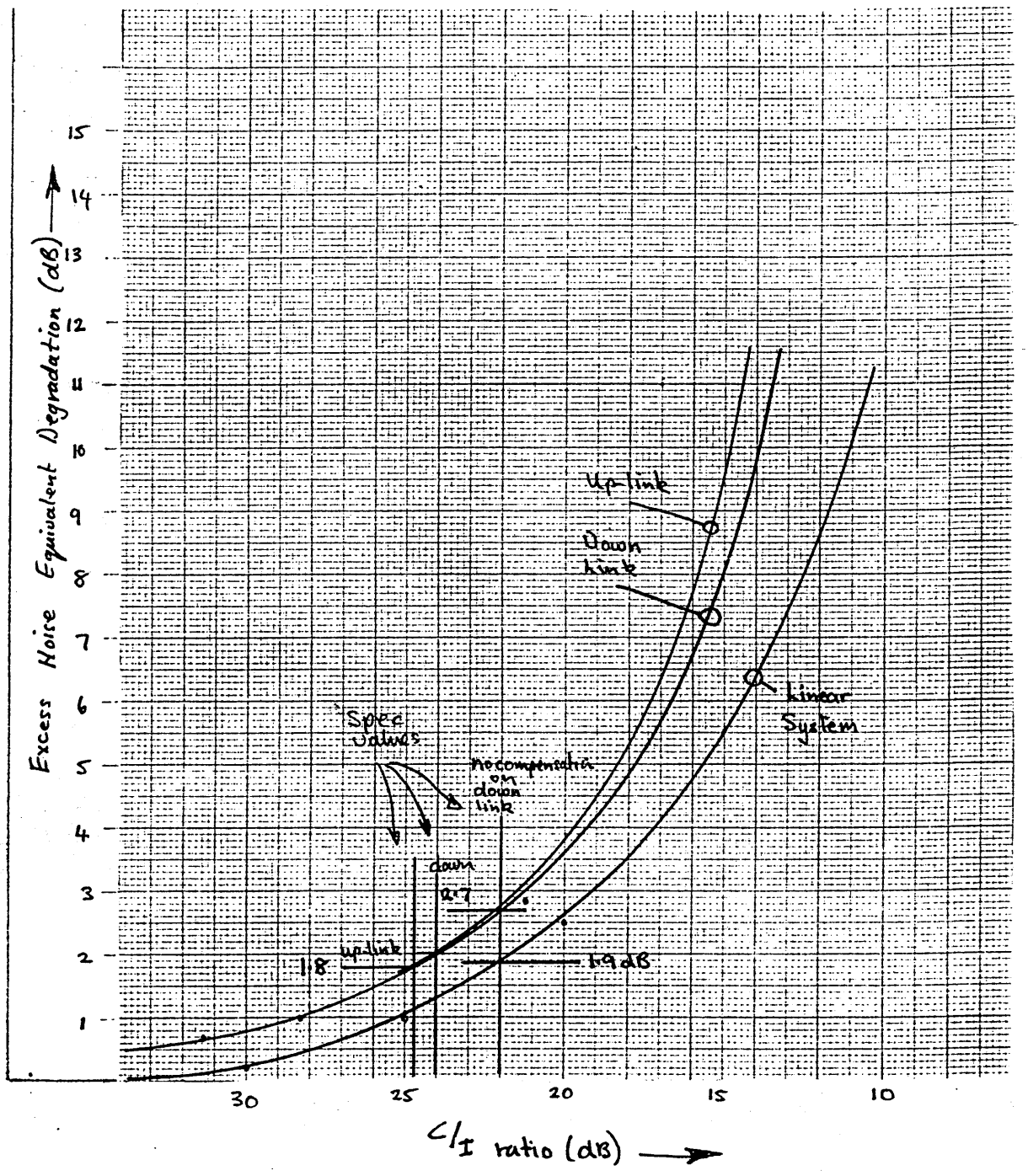

FIGURE 5.27 NOISE EQUIVALENT DEGRADATION vs C/I RATIO FOR APK TYPE-B

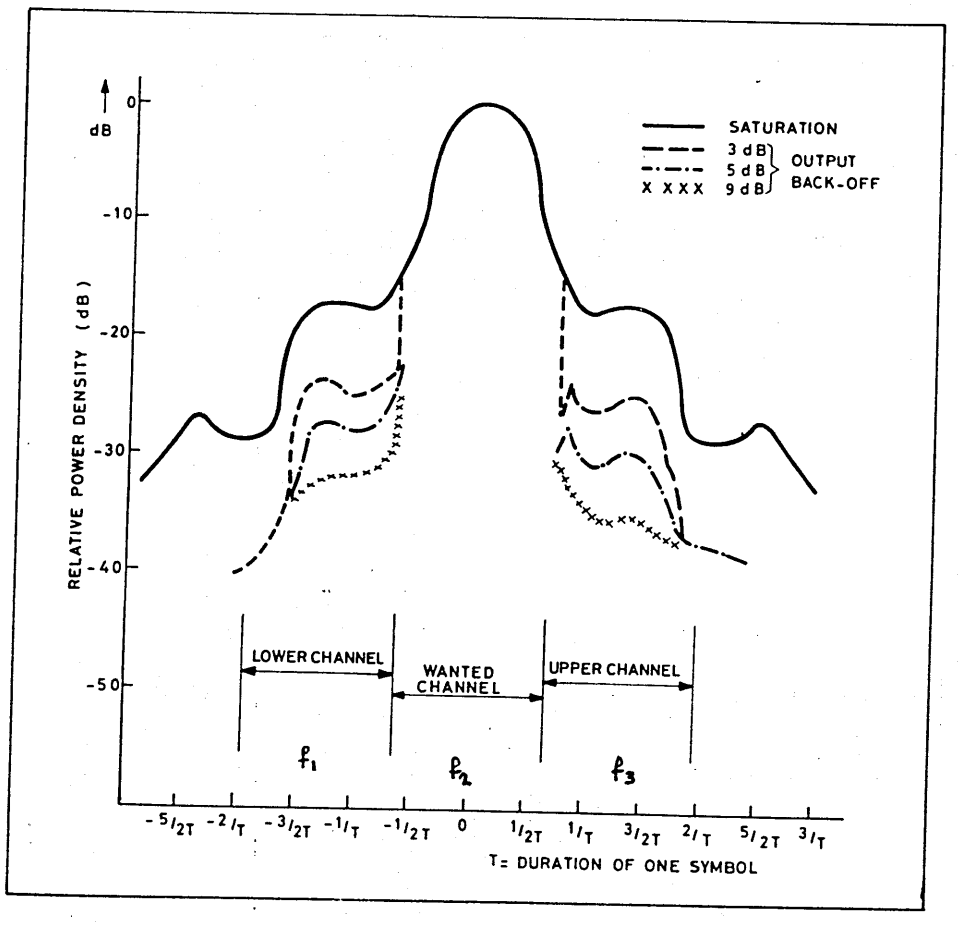

FIGURE 5.28 SPECTRUM SPREADING AS A FUNCTION OF HPA OPERATING POINT

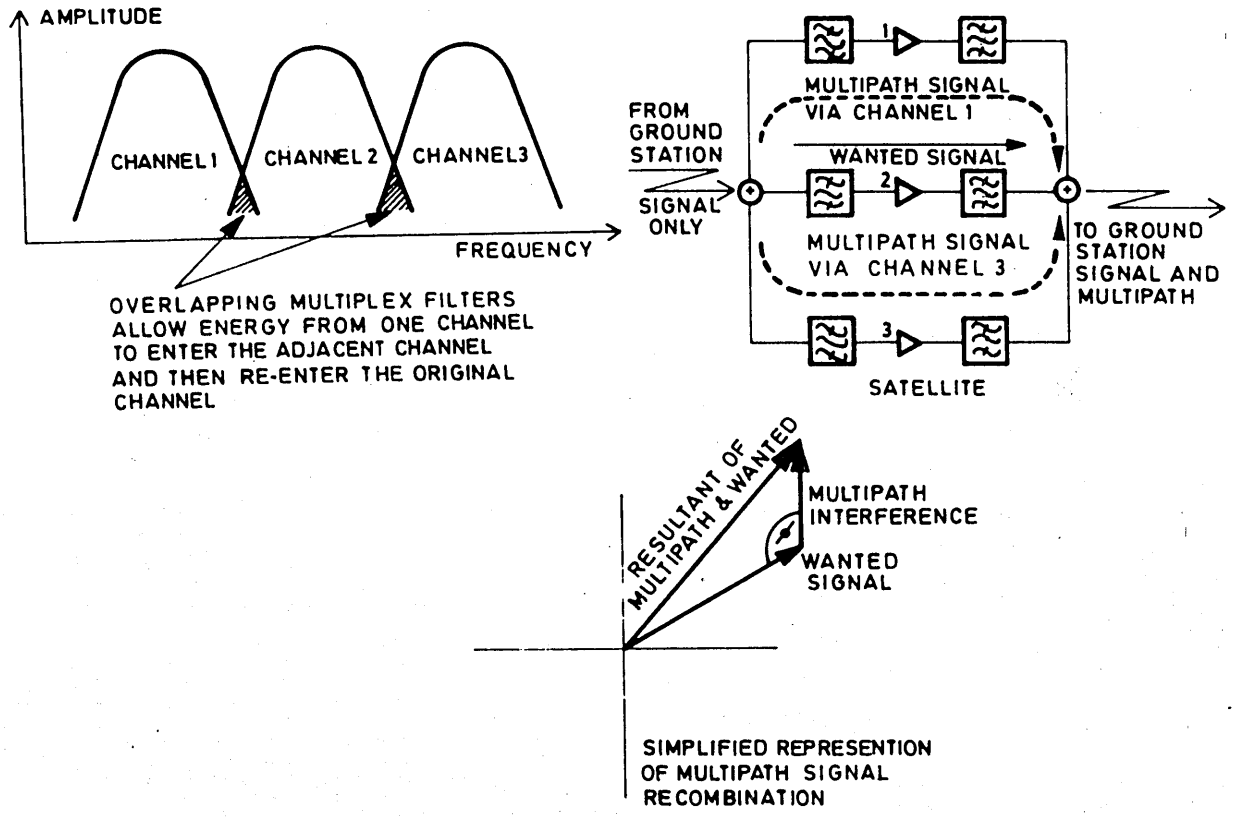

FIGURE 5.29 MULTIPATH GENERATION

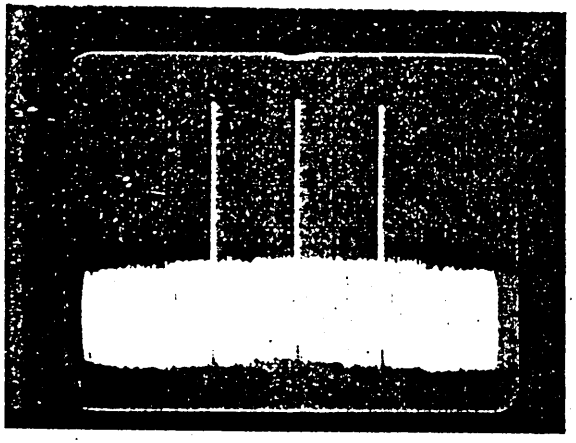

1 RF Output Spectrum showing all three transponders loaded by unmodulated carrier

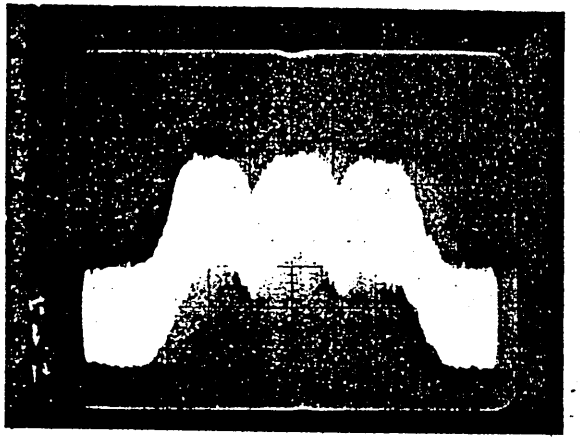

2. RF Output Spectrum showing all three transponders loaded by PRBS modulated carrier

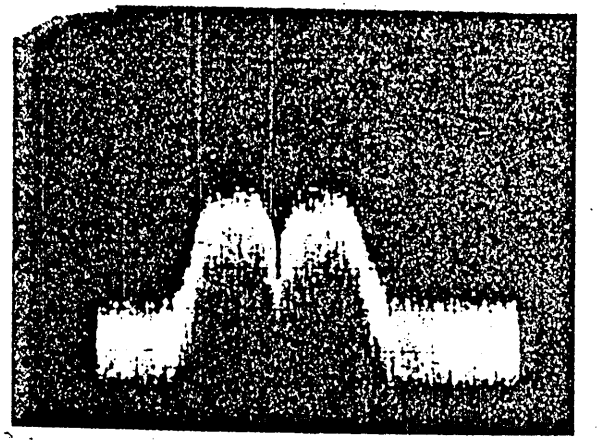

3 Channel 1 phase shifter at 270°
TWT 3 off.

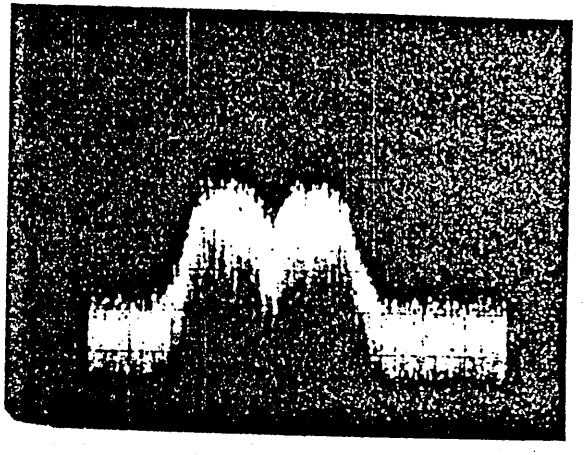

4 Channel 1 phase shifter at 110°
TWT 3 off.

FIGURE 5.30 RF OUTPUT SPECTRA OF SATELLITE

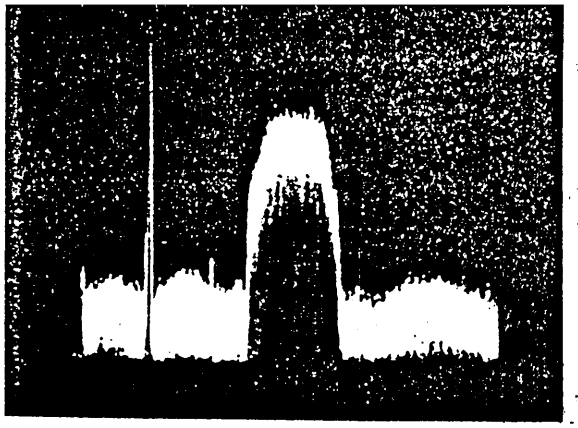

1 IF output of receiver following channel shaping filter.

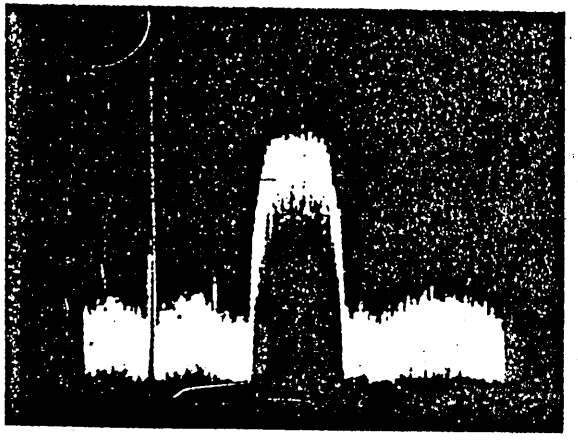

2. Channel 2 spectrum shown with the addition of two adjacent channel interferers from channels 1 and 3,

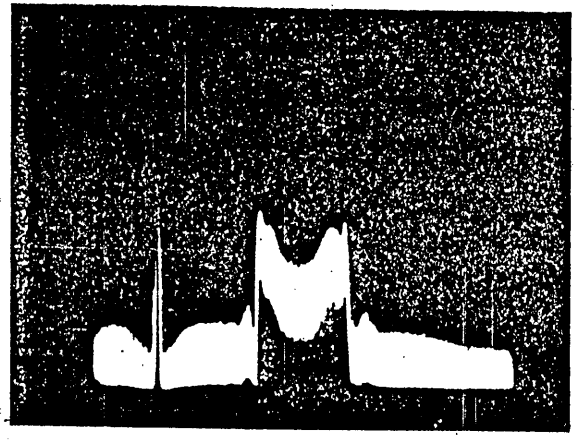

5 Channels 1 and 3 adjacent channel interferers shown in the channel 2 TWT 2 switched off,

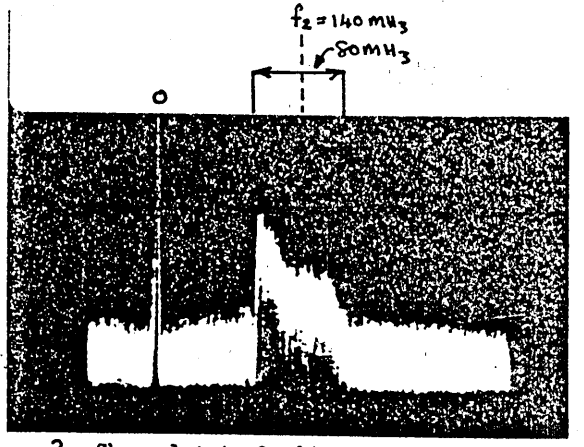

3 Channel 1 to 2 adjacent channel interferer shown in the channel 2 TWT 2 switched off.

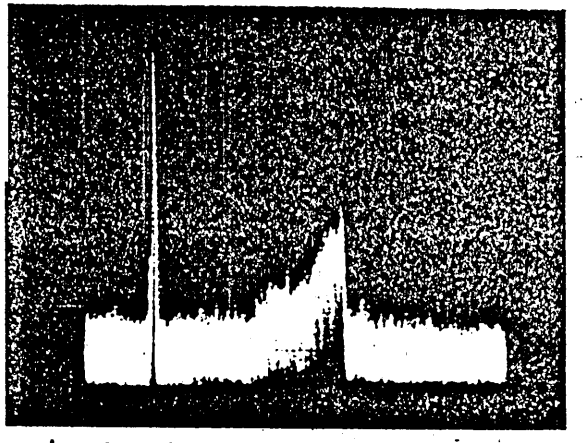

4 Channel 3 to 2 adjacent channel interferer shown in channel 2 TWT 2 switched off

FIGURE 5.31 IF SPECTRA AT RECEIVER

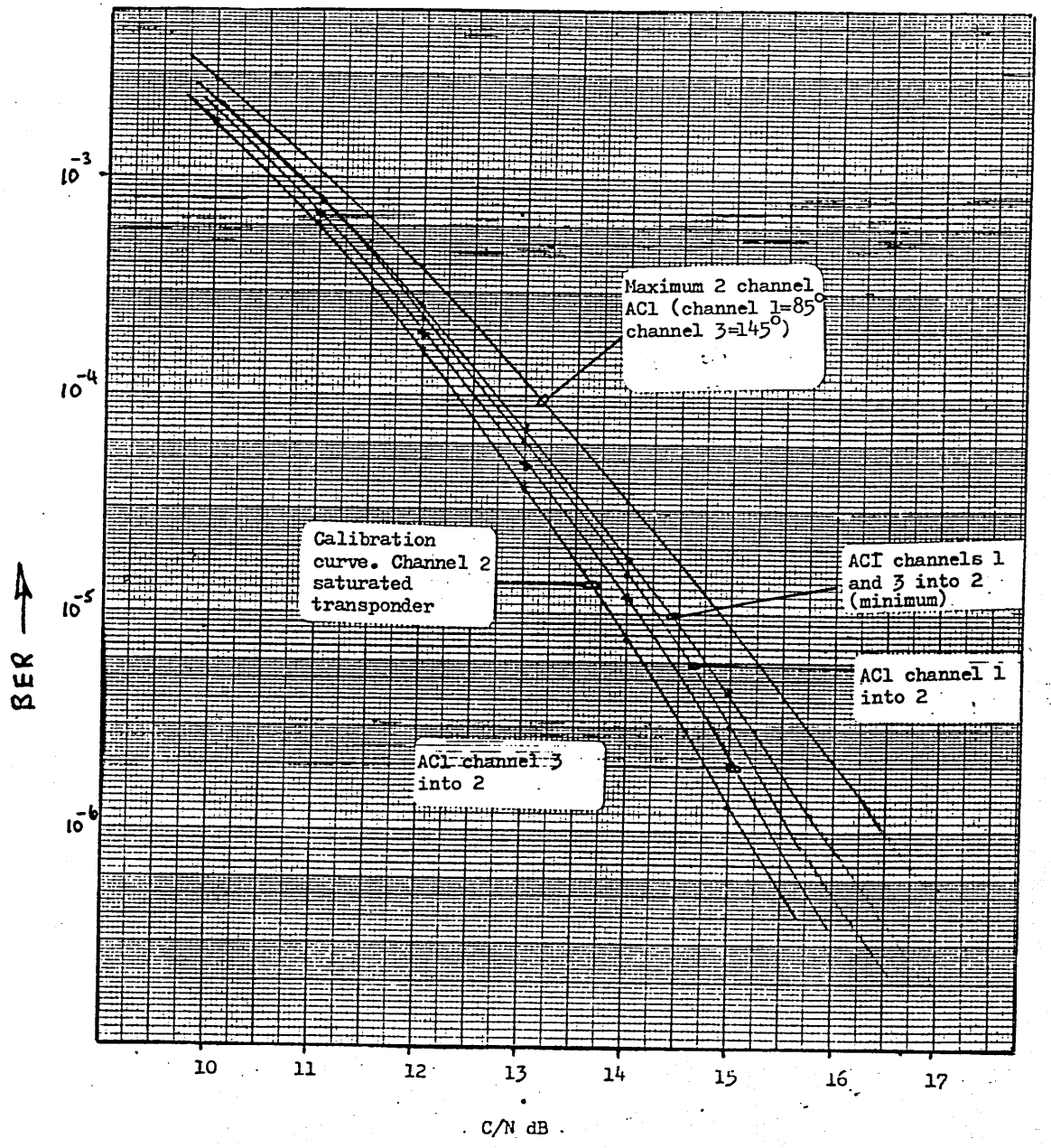

BER vs C/N
Continuous mode 50% roll off filter
Adjacent channel interference
Channel 1 into 2 (wanted)
Channel 3 into 2
Channels 1+3 into 2 (minimum)
Channels 1+3 into 2 (maximum)

FIGURE 5.32 DEGRADATION DUE TO ACI

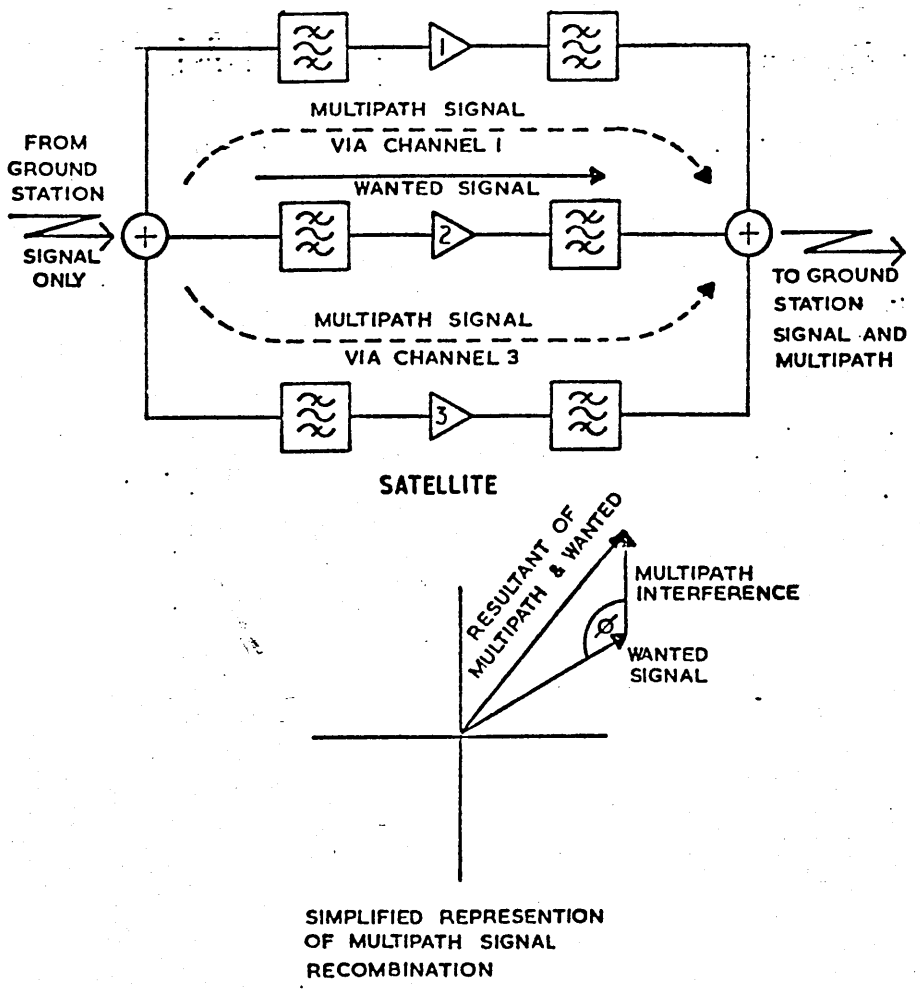

FIGURE 5.33 THE GENERATION OF MULTIPATH INTERFERENCE

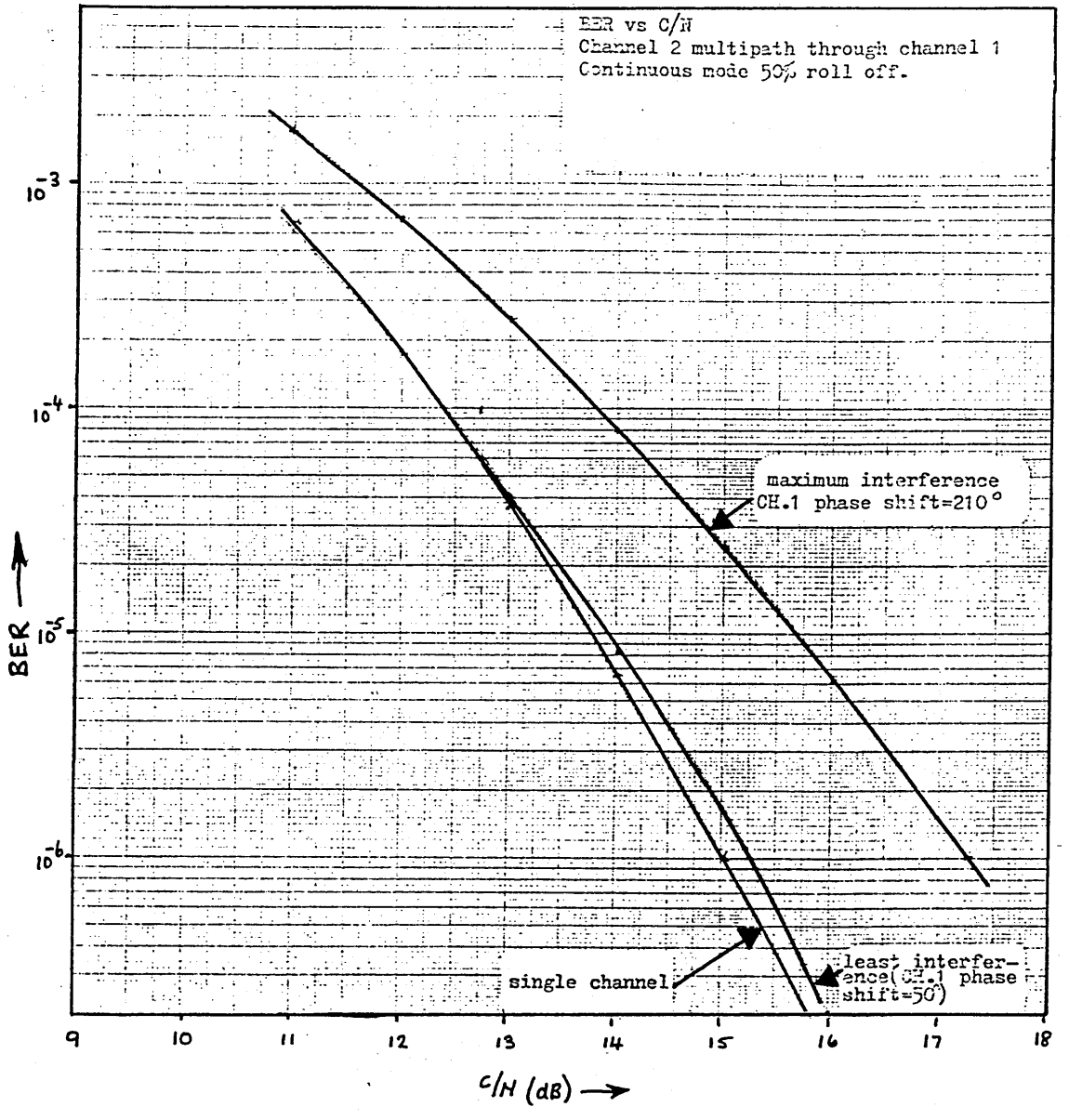

FIGURE 5.34 MULTIPATH FROM CHANNEL 1 INTO CHANNEL 2

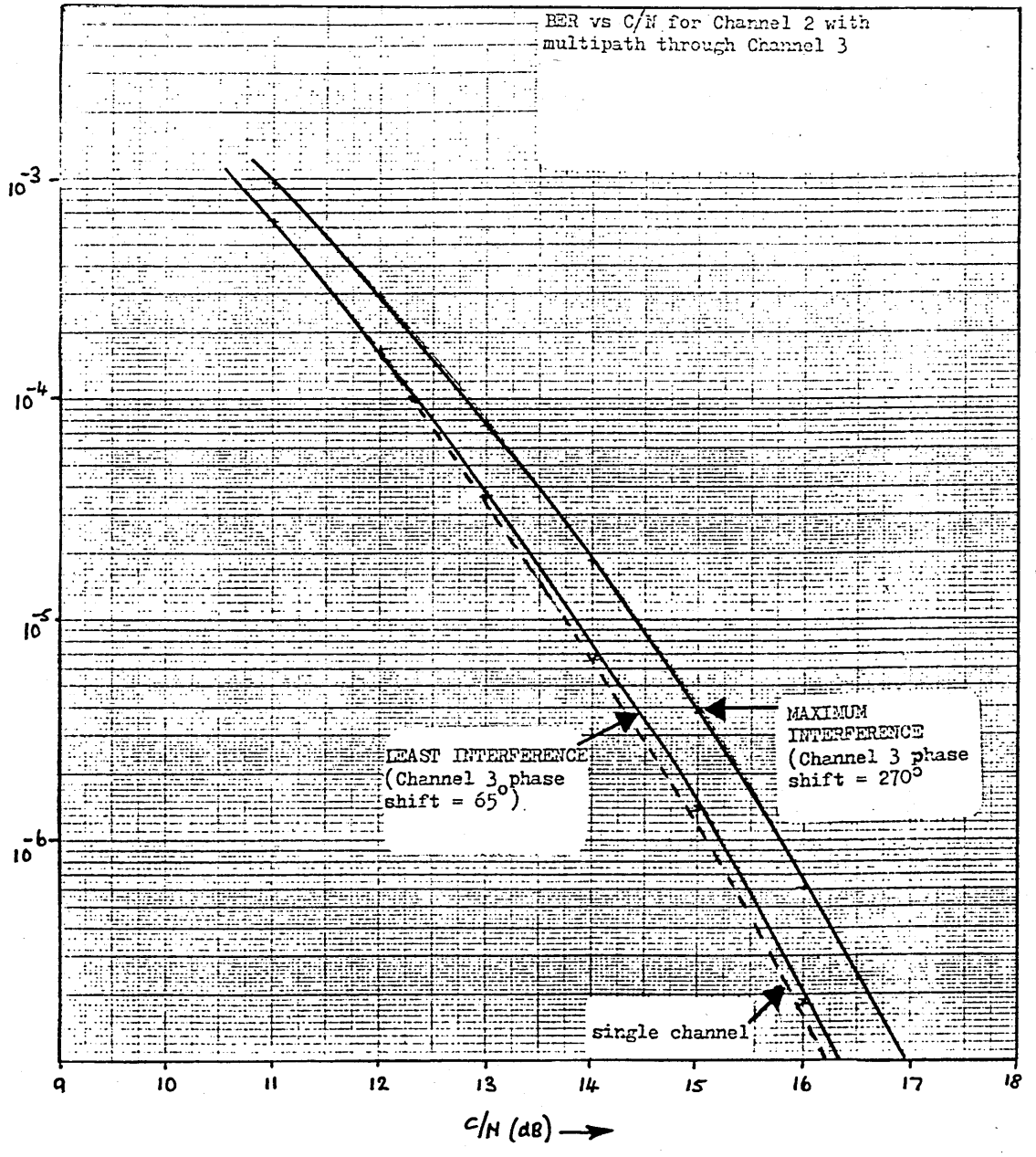

FIGURE 5.35 MULTIPATH FROM CHANNEL 3 INTO CHANNEL 2

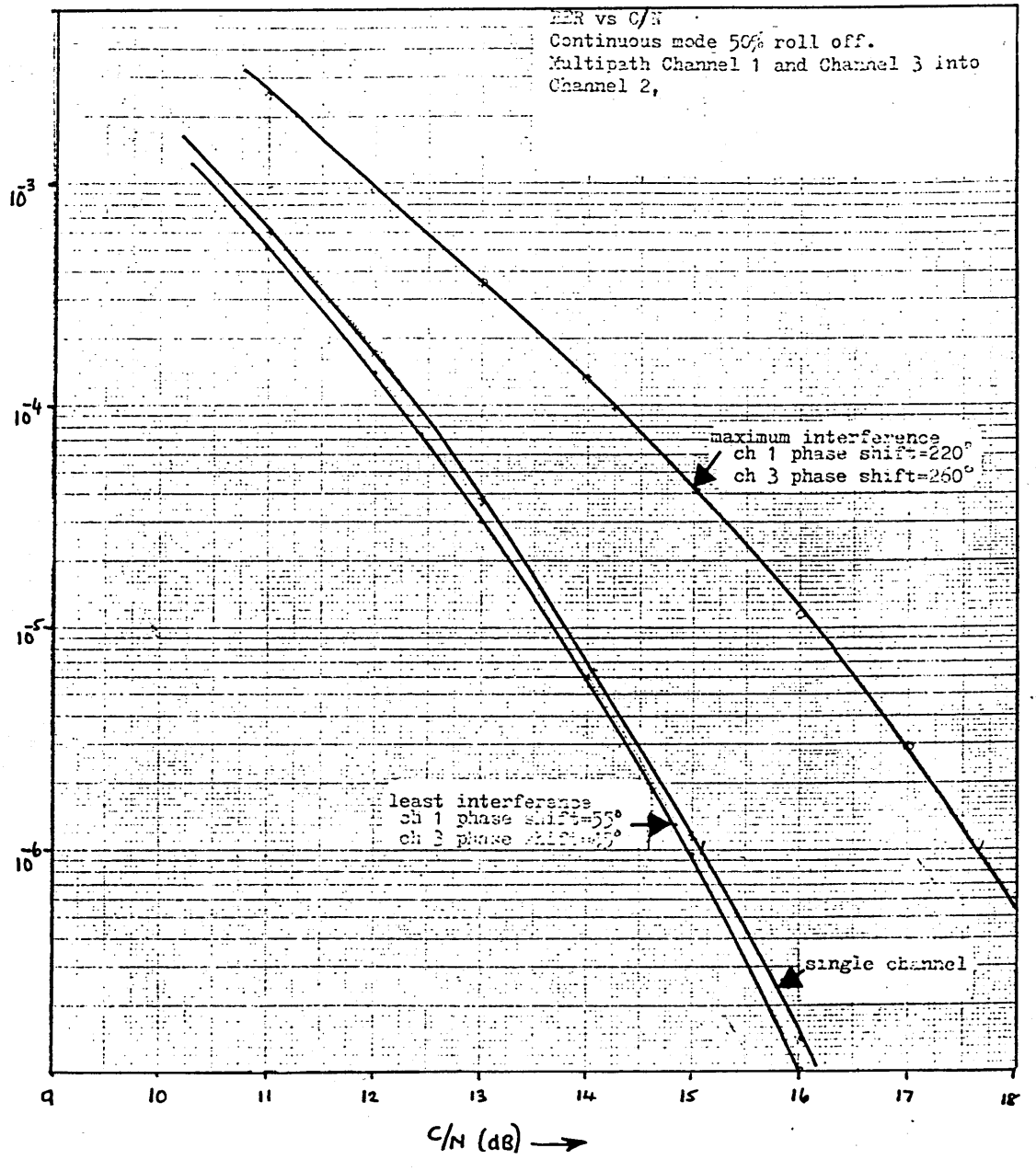

FIGURE 5.36 MULTIPATH FROM CHANNEL 1 +3 INTO CHANNEL 2

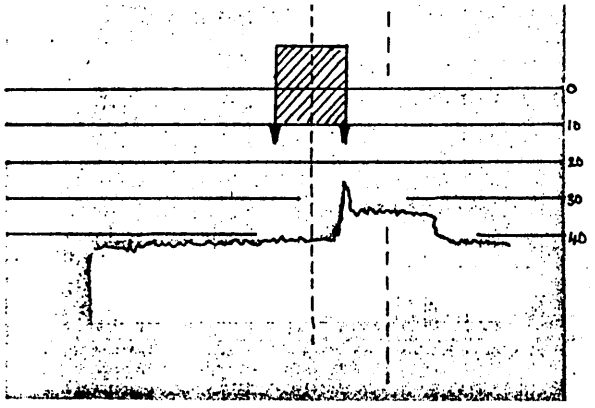

Channel 3 to Channel 2
Adjacent Channel multipath interference.
Unloaded channel 2

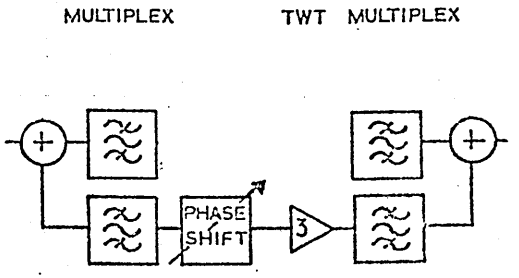

Channel 3 to Channel 2
Adjacent channel multipath interference.
Channel 3 loaded by unmodulated carrier.

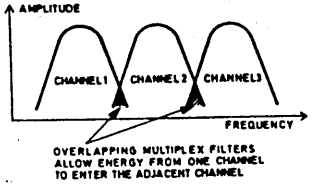

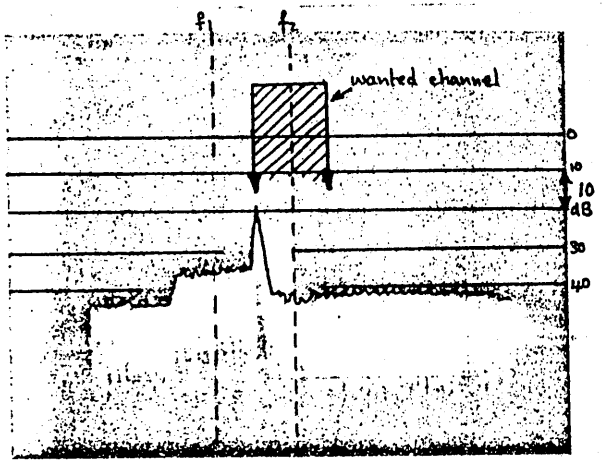

Channel 1 to Channel 2
Adjacent Channel Multipath Interference.

Unloaded Channel 1

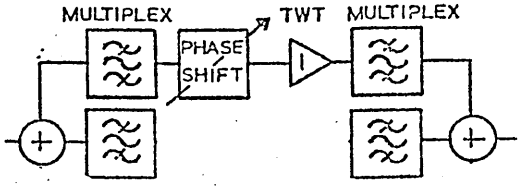

Channel TWT 2 switched off
input loaded with PRBS

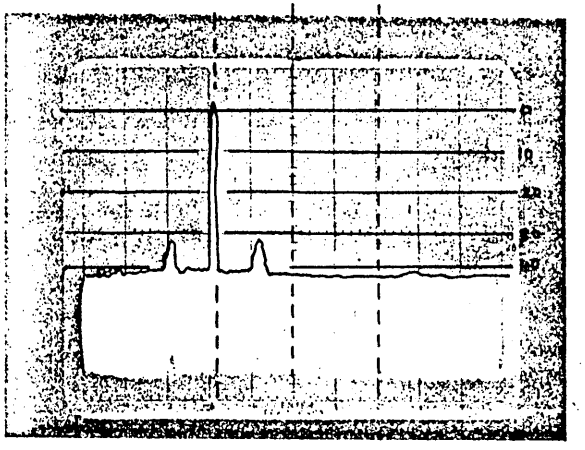

Channel 1 to Channel 2
Adjacent Channel Multipath Interference.
Channel 1 loaded by unmodulated carrier.

FIGURE 5.37 MULTIPATH SPECTRA FOR CHANNELS 1 INTO 2 AND 3 INTO 2

SECTION 6

OPERATION AT 11/14 GHz

6.1 INTRODUCTION

The analysis and performance estimates presented so far in this dissertation have been concerned exclusively with operation using the 6/4 GHz bands. As explained in Section 1, the satellites scheduled for TDMA applications are also equipped with a limited number of transponders operating in the 11/14 GHz bands.

At the time of writing, no firm decision has been made as to when (or if) TDMA operation will start in these new bands. Nevertheless, the author considered it useful to perform some preliminary analysis and make estimates of the behavior of candidate modulation methods in these bands. This motivation was two-fold. Firstly, the use of the higher frequencies permits the use of narrower beam width antenna which significantly increases the available carrier to noise (C/N) power ratios available at the receiver relative to that available in the 6/4 GHz transponders and this can be exploited by using modulation methods that are capable of higher symbol rates for a given error rate. Secondly, one of the main reasons

delaying the use of the 11/14 GHz bands is the problem created by precipitation-induced fading, primarily the increase in co-channel interference. However, as has been seen in the 4/6 GHz analysis, APK systems are more tolerant of co-channel interference than phase modulation systems. Accordingly, the combination of higher available C/N power ratios and greater tolerance to interference suggests that application of APK techniques to the 11/14 GHz band may be worthwhile.

To make the estimates of the performance of 8-phase PSK, APK-A and APK-B in the 11/14 GHz bands, the techniques developed in the earlier sections will be used. Specifically, this section will use the results from a series of tests carried out by the author on a realistic hardware simulation of the European Communications Satellite System conducted at the laboratories of ESA/ESTEC and reported in Reference 38. QPSK was used during these tests, but it was possible to extrapolate the performance of 8-phase PSK, APK-A and APK-B and from these estimates, a link budget has been prepared for INTELSAT V operating at 11/14 GHz.

6.2 System Configuration

The majority of the points to be made in this section are applicable to many digital satellite systems employing PSK or APK modulation schemes operating the 14/11 GHz band. However, for the system on which the tests were performed, the symbol rate was 30 Mbaud/s using 40 MHz nominal transponder bandwidths.

The satellite transponders employ 20 watt travelling wave tube amplifiers (TWTA) in the 11 GHz band, whilst most earth stations may be expected to use 2 kW TWTA's in the 14 GHz band.

As in the 6/4 GHz system, the analysis starts from the tentative link budget (Table 6.1). A cursory inspection shows that operation with the higher gain "spot beam" antenna has afforded a considerable increase in carrier to noise ratio ($\gtrsim$4 dB) and a substantial clear weather interference improvement ($\gtrsim$8 dB).

TABLE 6.1

Clear-Sky 14/11 GHz Link Budget
UK to USA East-Spot to West-Spot

No Terrestrial or Inter-network Interference Included
Atlantic Satellite Longitude: 335.5°E
Single Carrier

	Up-Beam		14 GHz UK	
	Down-Beam		11 GHz USA	
	Occupied Bandwidth		72 MHz	
Line #	Up-Link (noise only)	Units	Parameters	Remarks
1	Saturation Flux Density	(dBW/m^2)	-80.3	Nominal high-gain specs
2	G/T of Satellite	(dB/K)	3.3	Min. G/T specs
3	C/N at Saturation	(dB)	29.3	Elevation: 25.2°
4	Input Backoff	(dB)	1.0	
5	C/N	(dB)	28.3	Path Loss: 200.3 dB
	Down-Link (noise only)			
6	Saturation e.i.r.p.	(dBW)	42.0	Min. specified e.i.r.p.
7	Earth-Station G/T	(dB/K)	41.0	Elevation: 28.2°
8	Pathloss	(dB)	205.4	
9	C/N at Saturation	(dB)	28.5	
10	Output Backoff	(dB)	0.1	From Figure 5.8
11	C/N	(dB)	28.4	
	Up-Link (noise + interference)			
12	C/N	(dB)	28.3	From Line 5 (noise only)
13	C/I Clear Sky	(dB)	29.7	
14	C/N + C/I = Net C/(N+I)	(dB)	25.9	Combine Lines 12 & 13
	Down-Link (noise + interference)			
15	C/N	(dB)	28.4	From Line 11 (noise only)
16	C/I Clear Sky	(dB)	29.7	
17	Adjacent Channel Interference Loss Estimate	(dB)	1.0	HPA input backoff: 10 dB
18	C/N + C/I = Net C/(N+I)	(dB)	24.99	Combine Lines 15, 16, 17
	Combined Up-Link & Down-Link			
19	Overall C/(N+I)	(dB)	22.4	Combine Lines 14 & 18
20	Miscellaneous Loss	(dB)	1.0	Modem performance variation; antenna tracking error, etc.
21	Total Available C/(N+I)	(dB)	21.4	

6.3 Up-Link Power Control

The performance of satellite links using frequencies above 10 GHz can be seriously degraded by heavy precipitation. Degradation is caused by the increased path loss due to absorption by precipitation and, where there is a dual polarization frequency reuse, the depolarizing effect of precipitation which degrades the cross-polar channel by introducing Co-Channel Interference (CCI). Table 6.2, which is based on a long term measurement programm using radiometers at 9 locations in Europe[28], shows the excess path attenuation not exceeded for more than a given percentage of time in the worst month of an average year.

TABLE 6.2

Recommended Design Values for Atmospheric Attenuation in 11/14 GHz Bands

Frequency	10.95–11.7 (GHz) (downlink)	14.0–14.5 (GHz) (uplink)
Percentage time	Attenuation not exceeded for more than % time in worst month of average year (dB)	
20	0.4	0.6
5	0.6	1.0
1	1.2	1.8
0.3	1.9	2.9
0.1	3.5	5.3
0.03	7.7	11.8

Interpolation of these measured values indicate that in an average year, fades on the 14 GHz up-link of 7.0 dB or greater may occur for 0.06% of the worst month (about 25 minutes) and fades of 3 dB or greater for 0.3% of the worst month (about 2 hours). One method of improving the overall network reliability under these circumstances is based on increasing the transmitted power from an earth station to compensate for an up path fade. This technique is called Up-link Power Control (ULPC).

In establishing whether the use of up-link power control (ULPC) would materially improve the performance of a multi-channel satellite system in fading conditions, it is necessary to determine not only the increased in-band distortion which will be caused by driving the earth station HPA into saturation, but also the effect that the increase in HPA output power will have on co-channel and adjacent channel interference. In order to assess whether the potential benefits of ULPC outweigh the possible disadvantages, these various effects are examined in detail in Reference 38.

6.3.1 In-Band Distortion

It has already been established that in-band distortion increases as the earth station HPA is driven

into saturation. If the system degradation caused by operating the HPA at saturation under up-link power control is greater than that due to the effects of a fade, then there is clearly no advantage in providing such control. The measured in-band distortion performance of the simulated satellite system, with and without ULPC, under up-link fading conditions is shown in the Reference. The clear weather operating point of the earth station HPA is 3 dB output back-off, while the satellite TWTA is operated at the saturation point. Without ULPC, as the up-link fade deepens, initially the in-band performance marginally improves and then degrades almost linearly. For an up-link fade of 7 dB, a 2 dB increase in overall channel degradation is experienced at the receiving earth station. The initial marginal improvement in performance arises because the optimum operating point of the satellite TWTA for QPSK is actually at 1 dB input back-off rather than at saturation. Thus, for a constant earth station HPA output power adjusted to saturate the satellite TWTA, an up-link fade initially causes the satellite TWTA to pass through its optimum operating point.

When up-link power control is applied to the system under consideration, the earth station HPA output power is assumed to increase in direct proportion to the depth of the fade. However, since the HPA output back-off

in clear weather is only 3 dB, full compensation can only be provided for fades up to this level. Fades in excess of 3 dB, cause the satellite TWTA to experience an input back-off corresponding to the excess fade depth. In the Reference, it can be seen that over the first 3 dB range of the fade (which is fully compensated for by up-link power control) the overall degradation at the receiving earth station is slightly worse than that for a similar fade without power control. In contrast, for fades in excess of 3 dB, a clear advantage results from the use of ULPC, such that for a 7 dB fade an improvement in system performance of more than 1 dB is obtained. This argument however, does not form a complete basis for deciding whether power control is advantageous, especially since deep fades (which yield an improvement under ULPC) are less probable than shallow fades (which do not yield an improvement). Furthermore, for an operational satellite system employing frequency reuse techniques, it is also necessary to determine the effect of ULPC on co-channel and adjacent channel interference, since protection of the wanted channel by this method would not be justified if, in so doing, excessive degradation was caused to the transmission in the adjacent and cross-polar transponders.

6.3.2 Co-Channel Interference

Precipitation causes both excess path attenuation and reduced cross-polar discrimination (XPD) in dual polarization systems. An empirical relationship between these two effects has been derived from system measurements[29,30] and this relationship has been used in the Reference to model the result of precipitation-induced wanted channel fades on the cross-polar interference signal level. The relationship is:

$$XPD = 30 - 20 \log_{10} A \text{ dB}$$

where A is the excess path attenuation (dB) due to precipitation.

Two general classes of Co-channel interference are addressed in the Reference corresponding to whether the cross-polar channel is originated at the same or different locations. The distinction is important because it is assumed that fading and associated depolarization is a local event and therefore another location is not liable to be experiencing a significant simultaneous fade. Tne two cases are shown in Figures 6.1 and 6.2.

The Reference considers first the case of a signal and a co-channel cross-polarized signal, radiated from different locations and received at the satellite (under clear weather conditions) at the same carrier level (C). The wanted signal is then subjected to excess path attenuation due to precipitation, whilst the cross-polar signal is unaffected. Under these conditions, the level of interference (I) in the cross-polar channel (due to depolarization of the wanted signal) can be related to the excess path attenuation (A) and the cross-polar discrimination (XPD) by the expression:

$$I = C - (XPD + A) \text{ dB}$$

Hence, the carrier to cross-polarization interference ratio (C/I) causing co-channel interference, is directly related to (XPD + A) and as A increases, XPD decreases but eventually A will tend to dominate, resulting in a fairly well-defined maximum value of co-channel interference due to fading. When this interference model described above is examined, it is shown that, in the absence of up-link power control, the cross-polarization C/I ratio falls to a minimum of about 20 dB for up-link fades of about 7 dB.

If a simple up-link power control system is inserted in the model (i.e., one which will linearly increase the wanted signal power by up to 3 dB from the onset of the fade), it is evident that the level of the co-channel interference in the cross-polar channel will increase by the same amount.

For the case where the co-polar and cross-polar transmission originate from the same earth station, both can assume to suffer heavy precipitation. It is therefore only necessary to examine one transmission, since the condition of the orthogonal transmission will be identical.

In the absence of ULPC, the excess attenuation will reduce the power of the transmission at the satellite by (A) dB.

$$\text{i.e., } C_{(\text{faded})} = C_{(\text{normal})} - A \text{ dB}$$

Simultaneously, the cross-polar interference component (I) from the other transmission will be increased by (XPD -A) dB as discussed above. Thus, from the above, it is clear that this situation is more serious than the case where the transmissions originate from different locations, since the overall carrier to

interferer ratio is degraded by the depolarization factor, XPD. In the earlier case, the system is only degraded by (XPD + A) since the carrier power is not reduced in the cross-polar transponder. The Reference shows that for an up-link fade of, say, 8 dB the C/I ratio is nearly 9 dB worse when both the cross-and-co-polar transponders are loaded by the same station.

The application of the simple ULPC system used previously, increases the carrier and interferer levels by the same amount, since it is assumed that both transmitters in the earth station will be identically equipped and respond in an identical manner to the common increase in attenuation. Thus, the co-channel-induced degradation in the receiving station will be almost constant over the range of up-link power control and its use will not cause an additional penalty in the orthogonal channel.

6.3.3 Adjacent Channel Interference

In practical satellite systems adjacent channels will exist side by side with the 'wanted' channel, and in a correctly designed system, the adjacent channel interference (ACI) will have been reduced to an acceptably low level by the correct choice of channel shaping filter,

satellite input and output multiplexing arrangements, and by the use of frequency guard bands. However, the degree of spectrum spreading has been shown to be mainly influenced by the amplitude non-linearity and so it follows that the amount of energy falling into adjacent satellite channels due to spectrum spreading, is dependent on the operating point of the earth station HPA. Based on practical measurements, the Reference shows that as the output back-off of the HPA is reduced from 3 dB to 0 dB, the corresponding degradation in the wanted channel increases by approximately 1.6 dB. However, as the adjacent channel HPA Moves into saturation in response to a fade, the resulting degradation in the wanted channel rises more rapidly than the increase in attenuation, which results in increasing ACI degradation. As the fade continues the ACI level (and thus the degradation) follows the excess attenuation linearly, until at a fade depth of about 8 dB the ACI level is the same as the normal clear weather case. Thereafter, the ACI level is determined solely by the fade and so for fades in excess of 8 dB, the ACI degradation reduces below the normal clear weather value.

6.4 Summary of Findings

i) In the clear weather the "average" earth station TWTA will operate at about 3 dB output back-off.

ii) At this operating point, only moderate in-band distortion (0.4 dB) over the linear earth station case will be experienced.

iii) Under up-link fade conditions both the wanted (co-polar) and the cross-polar channels are degraded, especially when the orthogonal transmissions originate from the same location.

iv) Up-link power control can degrade the system performance for fades up to 3 dB, but improves the performance during the deeper fades, which statistically, have a lower probability of occurrence.

v) During moderate fades (say 3 dB) with ULPC, the wanted channel is degraded by a further 0.75 dB due to the spectrum spreading effects caused by the adjacent channel

saturated earth station TWTA. Additionally, during deep fades the non-faded cross-polar channel is degraded by up to 2 dB over the non-ULPC case, due to the enhanced cross-polar interference signal.

The summary of findings for the 4/6 GHz case is presented in graphical form in Figure 6.3 which has been obtained by plotting the difference between a fade with and without ULPC. It clearly shows that for fades up to 3 dB a simple ULPC system degrades the performance, but that improved wanted channel performance under deeper fades may be obtained principally at the expense of the cross-polar channel.

Having obtained the results of hardware simulator measurements for the application of up-link power control to the QPSK channel, it is necessary to convert these results into the equivalent 8-phase PSK, APK-A and APK-B using the methods described in Section 5. Table 6.3 shows the stages involved in converting the adjacent channel, cross-polar channel and wanted channel effects. For a given excess attenuation (fade depth) shown in column 1, an equivalent QPSK C/I power ratio is obtained (column 2) from the QPSK curve (Figure 5.24).

① excess attenuation (dB)	② Interferer level from QPSK curve	③ 8-phase HED from 5.25	④ APK-A derated C/I ② − 2.75dB	⑤ APK-A HED from 5.26	⑥ APK-B derated C/I ② − 2.7dB	⑦ APK-B HED from 5.27
← Adjacent Channel →						
0	26dB	2.6 dB	28.75 dB	0.9 dB	28.0dB	1.1dB
1	25dB	3.0 dB	27.55 dB	1.0 dB	27.5dB	1.2dB
2	23dB	4.4dB	25.75dB	1.6 dB	25.7 dB	1.5dB
3	21dB	6.0 dB	23.75 dB	2.3 dB	23.7dB	2.2dB
4	22dB	5.2 dB	24.75 dB	2.0 dB	24.7dB	1.8dB
5	23dB	4.4 dB	25.75 dB	1.6 dB	25.7dB	1.5dB
6	24dB	3.6 dB	26.75 dB	1.3dB	26.7dB	1.3dB
7	25dB	3.0 dB	27.75 dB	1.0 dB	27.7dB	1.2dB
8	26 dB	2.6 dB	28.75 dB	0.9 dB	28.7 dB	1.0dB
9	27dB	2.2 dB	29.75 dB	0.7dB	29.7dB	0.8dB
10	28 dB	1.8 dB	30.75 dB	0.6dB	30.7 dB	0.7dB
11	29 dB	1.6 dB	31.75 dB	0.55dB	31.7dB	0.6dB
12	30 dB	1.4dB	32.75 dB	0.5dB	32.7dB	0.5dB
← Cross-Polar Channel →						
0						
1	30 dB	1.3dB	32.75dB	0.4 dB	32.7 dB	0.4dB
2	26.7dB	2.2 dB	29.45 dB	0.8 dB	29.4 dB	0.9dB
3	24.8dB	3.1 dB	27.55dB	1.2 dB	27.5 dB	1.2dB
4	22 dB	4.3 dB	24.55dB	2.0 dB	24.7dB	1.8dB
5	21 dB	4.3 dB	23.75dB	2.3 dB	23.7dB	2.2dB
6	20.8dB	5.6dB	23.55dB	2.4 dB	23.2dB	2.4dB
7	20.5dB	7.0 dB	23.55dB	2.5 dB	23.5dB	2.2 dB
8	20.0dB	7.8 dB	22.75 dB	2.7 dB	22.7dB	2.5dB
9	20.2dB	7.6dB	22.95 dB	2.6dB	22.9dB	2.3dB
10	20.4dB	7.1dB	23.15 dB	2.5dB	23.1dB	2.2dB
Wanted Channel (In band distortion)						
0	35dB	−0.5dB	same as ⑤	−0.2dB	same as ⑥	−0.2dB
1	27dB	−2.2dB		−1.3dB		−1.3dB
2	26dB	−2.5dB		−1.5dB		−1.5dB
3	24.8dB	−2.2dB		−1.3dB		−1.3dB
3.3	∞	0		0		0
4	26.8dB	+2.2dB		+1.3dB		+1.3dB
5	22.0dB	+5.5dB		+3.0dB		+2.8dB
6	20.0dB	+7.8dB		+4.2dB		+3.8dB

TABLE 6.3

The noise equivalent degradation (NED) for 8-phase PSK, APK-A and APK-B can now be obtained by using the C/I curves given in Figures 5.25, 5.26 and 5.27, respectively for the wanted channel case (in-band distortion). Similarly, the adjacent channel and cross-polar channel results can be directly obtained for the 8-phase PSK by the use of Figure 5.25. However, for APK-A and APK-B, these results must be obtained by derating the C/I ratios in column 2 by 2.75 dB (APK-A) or 2.7 dB (APK-B) and then using Figure 5.26 and 5.27, respectively. The derating, as explained in Section 5, is necessary to reflect the lower average power of the APK signals on the up-link.

These results are shown in the summary Figure 6.4, which has been drawn in the same way as the QPSK case (Figure 6.3). It should be noted that the same behavior is apparent, i.e., that the wanted channel performance degrades before an improvement is affected and that the cross-polar and adjacent channels are degraded by the use of up-link power control (ULPC). Accordingly, the same overall determination can be made and ULPC can be said to offer no advantage. An interesting effect is illustrated by the figure. The amount of degradation suffered by the 8-phase PSK modulation system is always greater than the

corresponding APK case. This further supports the contention that APK performs better in an interference limited environment than the equivalent 8-phase PSK system.

6.5 Overall Performance of 8-phase PSK, APK-A and APK-B using 11/14 GHz.

It has been concluded that ULPC does not offer significant advantages and thus the overall performance will disregard this technique. Using the margins and results contained in Section 5, together with the link budget shown earlier in this Section, the overall link budgets for the three candidates can be determined (Tables 6.4, 6.5 and 6.6).

The results show that all three candidate methods will operate satisfactorily in the 11/14 GHz environment, while increasing the transmission capacity of the link by 50% relative to the QPSK system. The link budgets show that the available clear weather C/N is greatly in excess of that needed for a threshold error rate of 10^{-4} (C/N margin). Specifically, 8-phase PSK, APK-A and APK-B show C/N margins of 6 dB, 8 dB and 10 dB, respectively when multipath is not considered. For the multipath cases, the margins reduce to 4 dB, 5 dB and 7 dB, respectively. These margins provide protection against precipitation

induced fades. Accordingly the higher margins associated with APK-B would result in the satellite system being useable for a greater fraction of the year. Using the fade depth/% of year curves contained in Reference 38, shows that APK-B would be useable for 99.99% of the year (1 hour outage), while 8-phase PSK would be useable 99.94% of the year (about a 5 hour outage). For the high cost INTELSAT circuits, these differences are judged very significant and further indicate the robustness of the APK-B system in a heavily interference limited environment.

TABLE 6.4

APK-A Clear-Sky 14/11 GHz Link Budget
UK to USA East-Spot to West-Spot

No Terrestrial or Inter-network Interference Included
Atlantic Satellite Longitude: 335.5°E
Single Carrier

Up-Beam 14 GHz UK
Down-Beam 11 GHz USA
Occupied Bandwidth 72 MHz

Line #	Up-Link (noise only)	Units	Parameters	Remarks
1	Saturation Flux Density	(dBW/m^2)	-80.3	Nominal high-gain specs
2	G/T of Satellite	(dB/K)	3.3	Min. G/T specs
3	C/N at Saturation	(dB)	29.3	Elevation: 25.2°
4	Input Backoff	(dB)	1.0	
5	C/N	(dB)	28.3	Path Loss: 200.3 dB
	Down-Link (noise only)			
6	Saturation e.i.r.p.	(dBW)	42.0	Min. specified e.i.r.p.
7	Earth-Station G/T	(dB/K)	41.0	Elevation: 28.2°
8	Pathloss	(dB)	205.4	
9	C/N at Saturation	(dB)	37.9	
10	Output Backoff	(dB)	0.1	From Figure 5.8
11	C/N	(dB)	37.8	
	Up-Link (noise + interference)			
12	C/N	(dB)	28.3	From Line 5 (noise only)
13	C/I loss estimate 27 dB	(dB)	0.7	
14	C/N + C/I = Net C/(N+I)	(dB)	27.6	Combine Lines 12 & 13
	Down-Link (noise + interference)			
15	C/N	(dB)	37.8	From Line 11 (noise only)
16	C/I loss estimate 27 dB	(dB)	0.8	
17	Adjacent Channel Interference Loss Estimate	(dB)	2.4	HPA input backoff: 6 dB
18	C/N + C/I = Net C/(N+I)	(dB)	34.6	Combine Lines 15, 16, 17
	Combined Up-Link & Down-Link			
19	Overall C/(N+I)	(dB)	26.8	Combine Lines 14 & 18
20	Miscellaneous Loss	(dB)	1.0	Modem performance variation; antenna tracking error, etc.
21	Total Available C/(N+I)	(dB)	25.8	
22	Corresponding BER		2×10^{-12}	Adjacent channels loaded.
23	Silent Channel Multipath		1.9	
24	Total available C/(N+I)	(dB)	23.9	
25	Corresponding BER		1×10^{-9}	Adjacent channels not loaded.

TABLE 6.5

APK-B Clear-Sky 14/11 GHz Link Budget
UK to USA East-Spot to West-Spot

No Terrestrial or Inter-network Interference Included
Atlantic Satellite Longitude: 335.5°E
Single Carrier

Up-Beam		14 GHz	UK
Down-Beam		11 GHz	USA
Occupied Bandwidth		72 MHz	

Line #	Up-Link (noise only)	Units	Parameters	Remarks
1	Saturation Flux Density	(dBW/m^2)	-80.3	Nominal high-gain specs
2	G/T of Satellite	(dB/K)	3.3	Min. G/T specs
3	C/N at Saturation	(dB)	29.3	Elevation: 25.2°
4	Input Backoff	(dB)	0.5	
5	C/N	(dB)	28.8	Path Loss: 200.3 dB
	Down-Link (noise only)			
6	Saturation e.i.r.p.	(dBW)	42.6	Min. specified e.i.r.p.
7	Earth-Station G/T	(dB/K)	40.7	Elevation: 28.2°
8	Pathloss	(dB)	205.4	
9	C/N at Saturation	(dB)	37.9	
10	Output Backoff	(dB)	0.0	From Figure 5.8
11	C/N	(dB)	37.9	
	Up-Link (noise + interference)			
12	C/N	(dB)	28.8	From Line 5 (noise only)
13	C/I loss estimate 27 dB	(dB)	0.8	
14	C/N + C/I = Net C/(N+I)	(dB)	28.0	Combine Lines 12 & 13
	Down-Link (noise + interference)			
15	C/N	(dB)	37.9	From Line 11 (noise only)
16	C/I loss estimate 27 dB	(dB)	0.9	
17	Adjacent Channel Interference Loss Estimate	(dB)	2.4	HPA input backoff: 6 dB
18	C/N + C/I = Net C/(N+I)	(dB)	34.4	Combine Lines 15, 16, 17
	Combined Up-Link & Down-Link			
19	Overall C/(N+I)	(dB)	26.9	Combine Lines 14 & 18
20	Miscellaneous Loss	(dB)	1.0	Modem performance variation; antenna tracking error, etc.
21	Total Available C/(N+I)	(dB)	25.9	
22	Corresponding BER		10^{-14}	Adjacent channels loaded.
23	Silent Channel Multipath		1.7	
24	Total available C/(N+I)	(dB)	24.2	
25	Corresponding BER		10^{-11}	Adjacent channels not loaded.

TABLE 6.5

8-phase PSK Clear-Sky 14/11 GHz Link Budget
UK to USA East-Spot to West-Spot

No Terrestrial or Inter-network Interference Included
Atlantic Satellite Longitude: 335.5°E
Single Carrier

Up-Beam 14 GHz UK
Down-Beam 11 GHz USA
Occupied Bandwidth 72 MHz

Line #	Up-Link (noise only)	Units	Parameters	Remarks
1	Saturation Flux Density	(dBW/m^2)	-80.3	Nominal high-gain specs
2	G/T of Satellite	(dB/K)	3.3	Min. G/T specs
3	C/N at Saturation	(dB)	29.3	Elevation: 25.2°
4	Input Backoff	(dB)	0.5	
5	C/N	(dB)	28.8	Path Loss: 200.3 dB
	Down-Link (noise only)			
6	Saturation e.i.r.p.	(dBW)	42.0	Min. specified e.i.r.p.
7	Earth-Station G/T	(dB/K)	40.7	Elevation: 28.2°
8	Pathloss	(dB)	205.4	
9	C/N at Saturation	(dB)	37.9	
10	Output Backoff	(dB)	0.1	From Figure 5.8
11	C/N	(dB)	37.8	
	Up-Link (noise + interference)			
12	C/N	(dB)	28.8	From Line 5 (noise only)
13	C/I loss estimate 27 dB	(dB)	2.3	
14	C/N + C/I = Net C/(N+I)	(dB)	26.5	Combine Lines 12 & 13
	Down-Link (noise + interference)			
15	C/N	(dB)	37.8	From Line 11 (noise only)
16	C/I loss estimate 27 dB	(dB)	2.2	
17	Adjacent Channel Interference Loss Estimate	(dB)	2.4	HPA input backoff: 6 dB
18	C/N + C/I = Net C/(N+I)	(dB)	30.8	Combine Lines 15, 16, 17
	Combined Up-Link & Down-Link			
19	Overall C/(N+I)	(dB)	25.1	Combine Lines 14 & 18
20	Miscellaneous Loss	(dB)	1.0	Modem performance variation; antenna tracking error, etc.
21	Total Available C/(N+I)	(dB)	24.1	
22	Corresponding BER		10^{-10}	Adjacent channels loaded.
23	Silent Channel Multipath		5.25	
24	Total available C/(N+I)	(dB)	18.85	
25	Corresponding BER		10^{-8}	Adjacent channels not loaded.

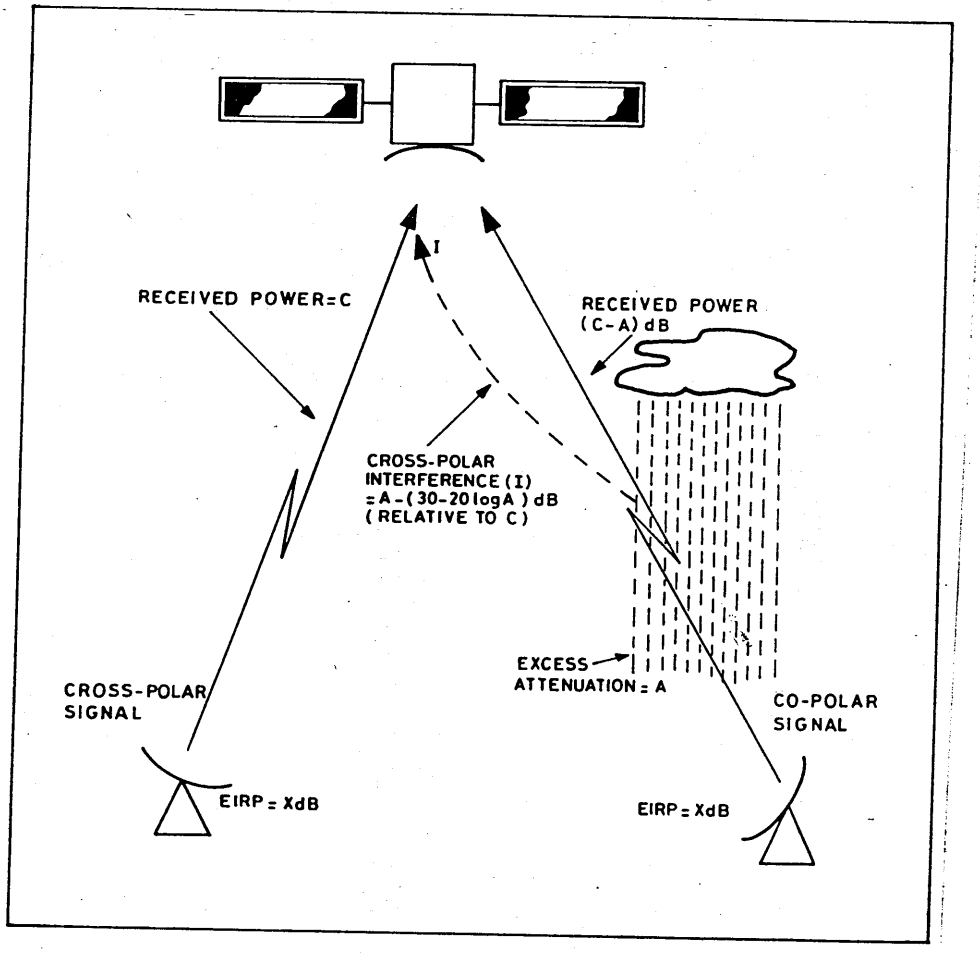

FIGURE 6.1 TWO EARTH STATIONS (DIFFERENT SITES) LOADING TWO ORTHOGONAL SATELLITE CHANNELS

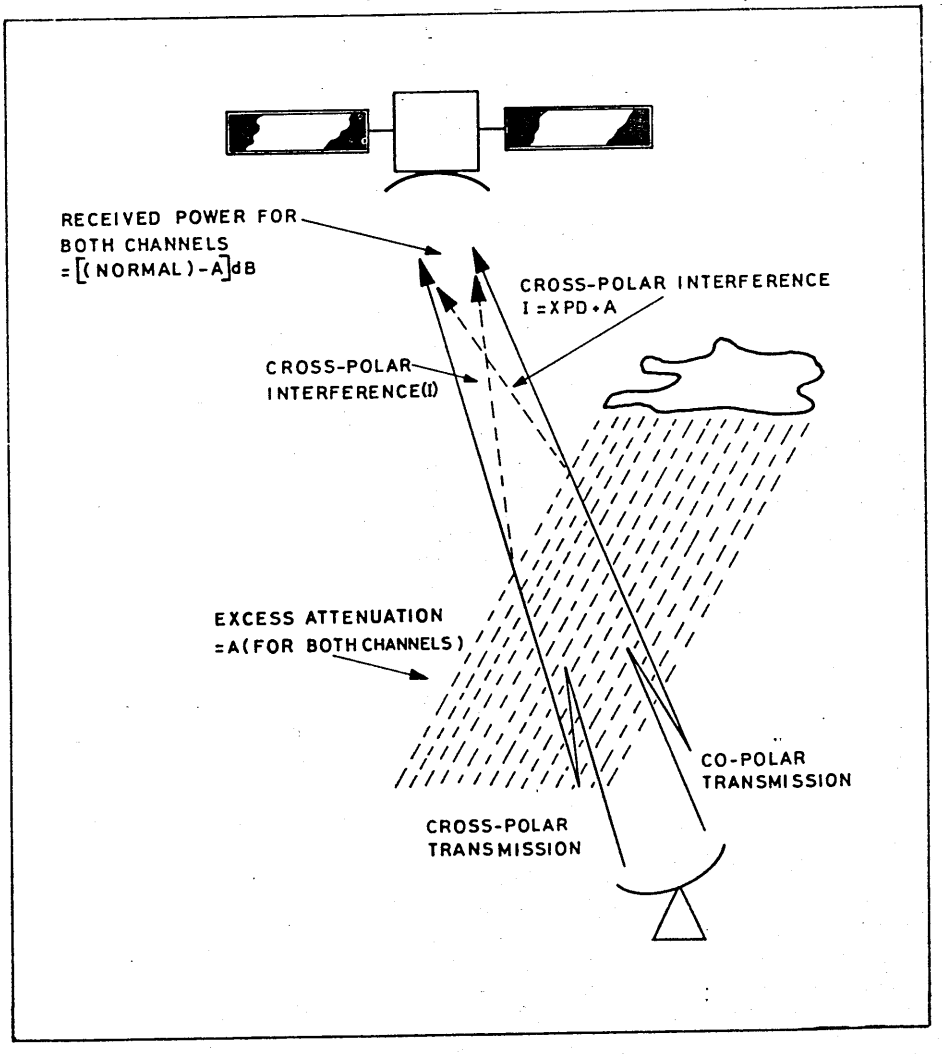

FIGURE 6.2 ONE EARTH STATION LOADING TWO ORTHOGONAL CHANNELS

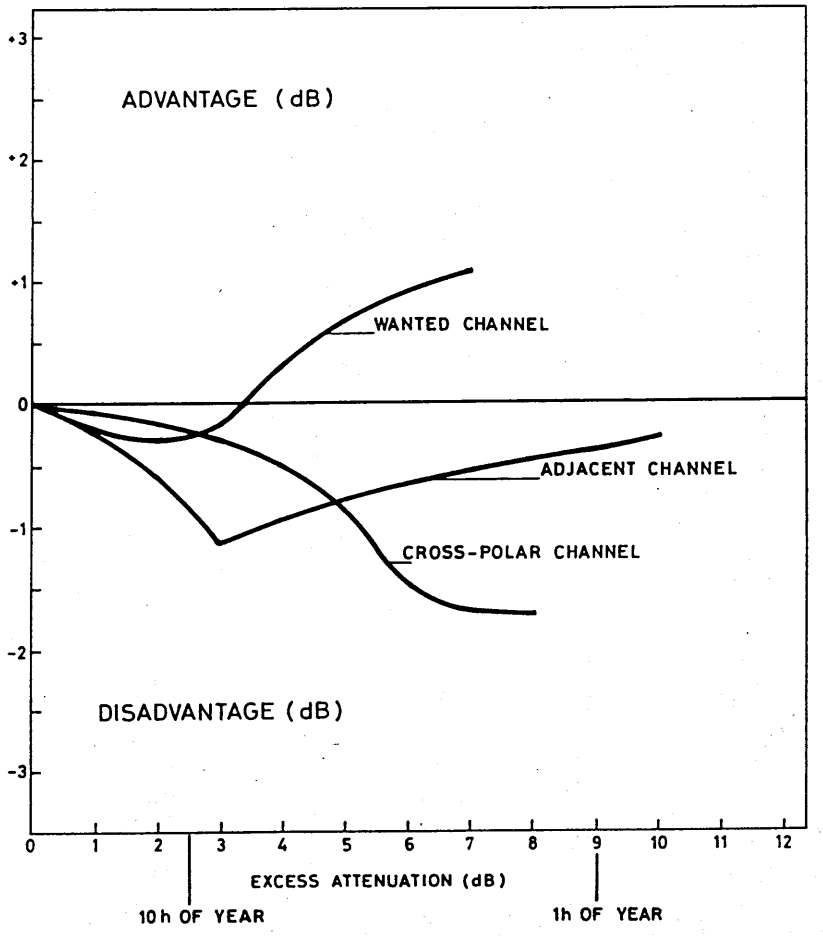

FIGURE 6.3 SUMMARY OF EFFECTS OF ULPC ON WANTED, CROSS-POLAR AND ADJACENT CHANNELS

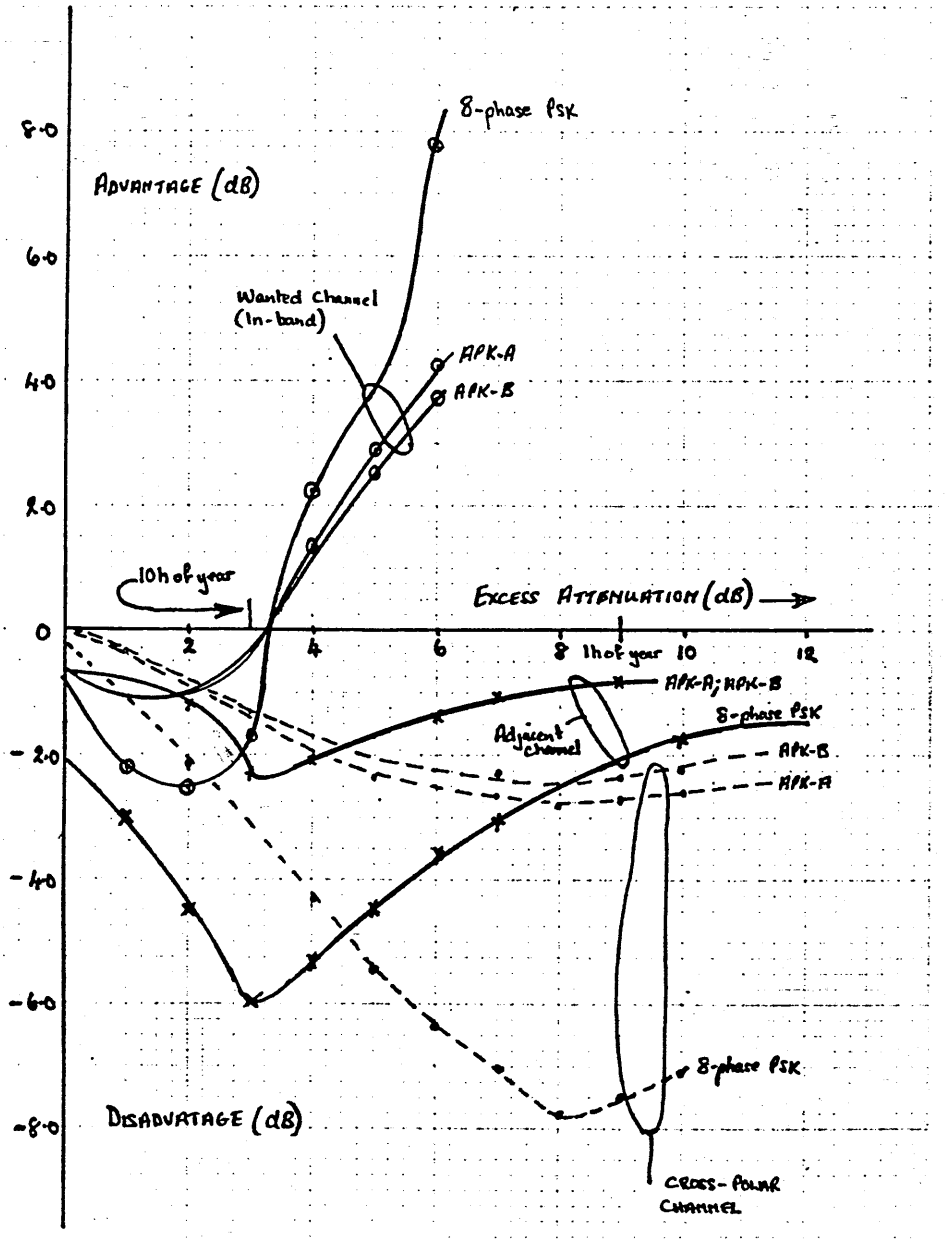

FIGURE 6.4 SUMMARY OF EFFECTS FOR THE THREE CANDIDATES

SECTION 7

MODEM CONSIDERATIONS

7.1 INTRODUCTION

The link budgets, derived in Sections 4 and 5, contain elements which are estimates of the performance degradation likely to be experienced under realistic conditions. For the most part, these estimates have been based on practical measurements using QPSK simulators. This in turn means that the measured QPSK performance degradation contains contributions from the QPSK modulator/demodulator (modem) imperfections. As explained in the earlier sections, the QPSK noise equivalent degradations (NED) are scaled or converted into 8-phase PSK, APK-A and APK-B NED's by a process involving the creation of an equivalent C/I power ratio. This technique is suitable for such preliminary estimates of performance. However, there remains the possibility that the candidate modulation methods may require distinct differences in the mechanization of the modems, perhaps necessitating a greater carrier power than might be indicated from the QPSK results. In this case, an additional amount of carrier power must be allocated in the link budget. It will be remembered that a 1 dB margin

was added to link budget for such contingencies and it is the purpose of this section to determine if this margin is adequate.

This will be done in two ways. Firstly, the general characteristics of high speed, burst mode modems will be considered, including the need for and the performance of, the modem reference recovery circuits. Secondly, the development and performance of an experimental APK modem built by the author will be described.

7.2 Background

The design and construction of high speed, burst-mode digital modulators and demodulators (modems) is a complex specialized field. In the first part of this section, an attempt will be made to highlight the critical areas and to provide an appreciation of the subject.

A modulator can be viewed as being a device which translates the message signal from its original form to a form suitable for transmission over the connecting medium. The demodulator executes the complementary operation and translates the signal back into its original form. Digital modulators and demodulators have existed

for some considerable time, especially the 4 phase or 8 phase modems commonly employed in inland microwave links. However, operation in the TDMA mode and the need to attain near theoretical performance places unusual demands on the synchronization circuits. Ordinarily, synchronizers for continuous mode systems (e.g., inland networks) do not have a requirement for fast acquisition of synchronization and some form of narrow band phase-locked loop is commonly used to establish local carrier and clock reference at the receiver.

However, TDMA operation is in the burst mode. Each transmitting station sends data for short lengths of time and then stops, allowing the next station to send a short burst of data. In most systems, there is no phase coherence from one burst to the next. This dictates that the receiver must re-synchronize itself at the start of each burst. In order to achieve good frame efficiency, only a small portion of each burst can be devoted to synchronization. In consequence, fast synchronization is essential if the data capacity of the link is not to be wasted. It would be a simple matter to obtain fast acquisition at the expense of degraded error rate using wide bandwidth recovery loops. However, the link budgets in TDMA satellite systems do not, in general, have sufficient excess carrier to noise ratio to support such a

simple trade-off. It is, therefore, necessary to seek techniques and mechanizations which minimize steady-state error rate whilst permitting very fast acquisition.

The methods and results in this section are extensively based on those obtained from the QPSK studies in this area conducted by, participated in and observed by the Author. Examples of these studies are given in References 26, 39 and 40.

7.3 General Modem Considerations

The elementary non-linear channel is shown in Figure 7.1. In this concept, as explained in Section 4, channel shaping filters are concatenated with the modulator and demodulator in order to contain the transmitted spectrum (without introducing inter-symbol interference) and to exclude noise and interference at the receiver.

Figure 7.2 shows the basic APK modem scheme. The incoming signal is applied to a phase modulator via a bit regenerator to "clean up" the bit shapes and allow the transmitted bit transition times to be independent of the incoming bit stream. The phase modulators are supplied with quadrature carrier supplies such that the output of

the phase modulators consist of in-phase or quadrature carriers. Consequently, when both phase modulators are combined four possible phase states 90° apart can be selected under the control of the P and Q synchronous bit streams. The output of the combiner is then subjected to the R stream modulator. In a Type A system, this is a simple binary amplitude modulator. In a Type B system, this takes the form of an amplitude and phase modulator in order that the outer signal level ring is shifted in phase by 45° relative to inner level. Finally, the last element in the modulator is the channel shaping filter.

The Type A demodulator in many ways, is the mirror image of the modulator. The incoming signal after channel shaping splits into three arms. In the R stream demodulator the signal is amplitude demodulated and the resulting analogue waveform is regenerated and fed out to the receive line. The other two lines contain P and Q phase detectors fed with quadrature carrier signals. The analogue outputs of these two detectors are also regenerated and fed to line. The clock source to time the regenerators (sampler) and the carrier source to perform detection must be accurately phase synchronized. In the Figure, these are shown conceptually as being obtained from the transmitter (often called "cheat links"). Clearly, this is not a practical solution and accordingly

means must be established to produce (recover) local references which yield a near theoretical performance.

The design of 8-phase PSK modulators has historically been based on methods involving synthesizing the required signals by the selection (under baseband signal control) of appropriate quantized orthogonal carriers. Figure 7.3 shows one simple method of achieving this. The incoming signals are applied to two D/A coverters via a logic selection map. The resulting quantized amplitudes are fed to two quadrature modulators the outputs of which are summed, and then passed through the channel shaping filter. An 8-phase PSK demodulator is shown in Figure 7.4. The incoming signal is first passed through the channel shaping filter and then split to feed four phase detectors and the carrier and bit timing recovery arms. The phase detectors are fed with reference carriers which are mutually shifted by 45°. The output of the phase detectors is passed through a logic network and hence to the P, Q and R data stream regenerators. Note that the carrier recovery system uses a X8 multiplier, but otherwise is of a standard form.

7.4 Reference Recovery

The design of the reference recovery system determines to a large extent the performance of any digital demodulator. In consequence, recovery circuits will now be considered in some depth.

Reference recovery circuits, as the name implies, recovers from the incoming signal the various references against which the signal will be demodulated and regenerated. A general reference recovery circuits is shown in Figure 7.5 and must perform 6 functions:

1) Non-Linear Regeneration
2) Filtering
3) Signal Amplitude Control
4) Frequency Tracking
5) Phase Control
6) Amplitude Decision Control

Non-linear regeneration is required because the modulation is of the suppressed carrier type and contains no directly usable clock information. The carrier and clock information is therefore regenerated by means of some form of non-linear operation on the received signal. The non-linear regeneration will produce a wanted signal

component (carrier or clock) together with significant perturbation due to additive noise and modulation-induced disturbances (called pattern noise). The wanted signal which is of a very narrowband form is selected out of the noise by the use of a narrowband filter. It will be seen that the choice of this filter entails a compromise between fast acquisition and good noise suppression. This narrow band filter also dictates that some form of automatic frequency (AFC) control will be required in order that the filter may remain accurately centered over the wanted signal component while the incurring signal drifts due to doppler shift and various oscillator drifts. Furthermore, it was demonstrated in Section 3 that the Nyquist filtering concept gave rise to a condition of no ISI at the sample instant. This implies some degree of control of the phase of the clock and carrier signals in order that this minimum ISI condition may be located. Finally, in the APK system, an amplitude decision threshold must be established and maintained. If an automatic levelling device can be employed prior to the amplitude detector, a fixed amplitude decision can be employed. In the absence of the leveling device, an adaptive level threshold must be used. In a practical system, the received signal may be subject to considerable variations in amplitude over the longer term. In general,

phase and especially amplitude detectors within the demodulator are sensitive to these fluctuations, and some form of automatic gain control (AGC) will be required.

7.5 Carrier Recovery

The receiver must regenerate a reference carrier to permit coherent demodulation. There are many sources of interference to this reference recovery process. The TDMA system is characterized by a repetative sequence of short bursts. Guard times are established between bursts to accommodate imperfect synchronization. However, these could be zero under some circumstances and significant inter-burst interference may be expected. We can assume that the differential doppler shift between adjacent bursts is about one part in 10^8, but because the transmissions originate from different transmitters inter-burst frequency differences of about 1 part in 10^7 may be experienced.

Carrier Recovery branches can be implemented using either a phase-locked-loop (PLL) or tuned filter approach (TF). At the time of writing, the PLL approach is discredited primarily due to a weakness termed "hang-up" whereby the PLL equivocates and does not settle quickly to its steady state value[31]. However, the

tuned filter approach has been proven to be very successful[32]. The elements of both types of recovery chains are shown in Figure 7.6. Most of the elements are self explanatory, however, the non-linear regenerator deserves some further description.

The reference must be recovered from a signal which contains no discrete spectral component at the carrier or clock frequencies since the modulator suppresses the carrier and the data format (NRZ) does not contain a discrete clock. Therefore, a linear network cannot be used . Instead, a non-linear device is necessary to operate on the information contained in the sidebands. This can be viewed as an inter-modulation process where one IM product is the carrier. Reference 31 evaluates many non-linear devices and concludes that a 4th power law device may be optimum.

The filter bandwidth is determined by a trade-off between increasing noise and increasing synchronization time requirements. Figure 7.7 derived from reference[32] shows the noise equivalant degradation as a function of filter for various filter bandwidths. Whereas Figure 7.8 shows the effect on carrier acquisition times under the same conditions. A performance loss is inevitable for all practical cases for each element in the

demodulator. An allowance of 0.25 dB noise equivalent degradation for carrier recovery is common and tolerable, and using Figure 7.8 this represents a filter bandwidth of the order of 100 KHz.

7.6 Clock Recovery

Many techniques are available to extract the suppressed clock component from the APK or PSK signal. Full descriptions of all methods are not appropriate to this report and an excellent presentaion of available techniques can be found in Reference 31. By way of example, a common method, envelope detection, will be described, in order to arrive at the mini-link budget contribution for clock recovery.

Envelope detection uses a form of rectifier operating on the modulated signal, typically at the IF input point after the AGC device (as was shown in Figure 7.5). The term rectifier is meant to include any zero-memory device with an even non-linearity. Commonly, this device would be a square-law rectifier with an input/output characteristic of the form:

$$V_{out}(t) = V_{in}^2(t)$$

The amplitude modulation (a.m.) present on the received signal is due to the reaction of the narrowband filters to the phase transitions demanded by the baseband signal. The a.m. is thus directly baseband related and hence clock related. In consequence, nothing more complicated than conventional a.m. recovery techniques need be used, although Reference 31 shows that this approach is not optimum.

Whichever technique is employed, a narrowband filter is required after the detector. The filter shown in Figure 7.8 selects the wanted component, rejects the accompanying noise and stores energy. The latter function is necessary because the modulated signal may contain significant periods where no clock related information can be recovered. Consider a simple QPSK non-differentially encoded transmission system by way of example. If the baseband signal contains contiguous identical bits, no change in transmitted phase will result and therefore no clock recovery amplitude modulation will be present on the signal. Similarly, if the baseband signal dictates that +90° or -90° phase rotations be transmitted, no clock component can be recovered by a simple envelope detector due to the asymmetrical spectral nature of the phase modulated signal. When all these effects are considered, it is evident that in a suitably long message only 25% of

the data bits provide significant clock recovery information. In practice, relatively long periods can elapse (100 symbols). When the clock recovery signal must be obtained by the energy stored in the tank filter, Figure 7.9 shows a series of photographs taken at the output of a clock recovery tank circuit (obtained during the study reported on References 39 and 40). In the first, the variation in the amplitude of the signal in the filter may be seen. The Horizontal scale of 500 nS means that 15 symbols are present per division. In the second a larger section is examined (60 symbols/division). Very considerable variations in amplitude are apparent, and in the lower trace, careful examination of the data sequence shows very few data transitions. Finally, the third trace expands a particularly interesting region of the second photograph data sequence showing very few data transitions and correspondingly a very significant reduction in the recovered clock amplitude.

The need to accept very large amplitude variations in the recovered clock ampitude is now apparent. It will be recalled that the need for this clock signal arises from the need to regenerate the analogue signals out of the phase detectors. As explained earlier, the timing of the regenerator/sampler decision is initially linked to the need to minimize the ISI by

sampling at the optimum time in a symbol. For this reason, a limiter must be employed after the filter. This limiter must have a very large dynamic range (>30 dB) and a very low a.m./p.m. convertion (<0.1°/dB). Even so, the combination of amplitude variation and the limiter yields an addition source of non-ideal modem performance.

Before finally assigning a noise equivalent degradation to the clock recovery branch, another effect must be considered. The non-linear clock regenerator will produce an output which, although dominated by the wanted clock component, will also consist of significant amounts of in-phase and quadrature pattern noise. The vectorial sum of these components will result in a phase uncertainty (phase jitter) which has the effect of producing non-optimum sampling and thus ISI and ultimately errors. Reference 31 shows that the in-phase component will be removed by the post-filter limiter, but that the quadrature component dominates the jitter. Fortunately, the spectrum of the two compenents is different. Figure 7.10 shows the distribution of the two components. Note that the damaging quadrature component can be controlled by tight filtering. Naturally, this filter bandwidth must be compatible with acceptable acquisition performance. In general, such a balance may be achieved when the bandwidth of the filter is about 100 KHz. Figure 7.11 shows the

effect of clock error on the BER performance. Note that a 10% error in timing yields a 1 dB noise equivalent performance. Reference 31 suggests that a 0.3 dB noise equivalent degradation should be allocated for the effect of clock errors.

7.7 Amplitude Reference Recovery

In APK system, an amplitude reference must be recovered and maintained. As in the PSK, and the carrier and clock recovery branches, the reference must be established during the preamble. For this purpose, it is proposed to use a modified version of the INTELSAT Preamble, shown in Figure 7.12 together with the original preamble. During the first 48 symbol pure carrier (phase unmodulated) region the amplitude is varied at the maximum rate (101010) of the R stream. This region has been chosen because the crosstalk between the APK and PSK recovery loops will be minimized. Two interacting peak level sensors are proposed to establish the references with separate integrators operating on the two outputs. These outputs will also contain pattern and thermal noise effects in the same way as the carriers and clock recovery branches. Figure 7.13 shows the noise equivalent degradations as a function of amplitude error. For the purposes of the demodulator link budget another 0.3 dB is assigned to this effect.

7.8 DESIGN AND PERFORMANCE OF AN EXPERIMENTAL APK MODEM

The general characteristics of modem design set forth in the first part of this section were applied to the design of practical equipment. A simple low speed 8-phase 2-amplitude modem was built using a low speed transistor-transistor (coupled) logic family (TTL). TTL was chosen for reasons of simplicity of construction and served to validate basic principles, but limited the symbol rate to 0.5 M Symbols/s. Nevertheless, the construction of this modem fully met its design goal. The block diagram of the modulator and demodulator and the form of channel shaping filter employed is shown in Figures 7.14 and 7.15, respectively.

Consider Figure 7.14. An oscillator operating at sixteen times the required IF frequency of 1 MHz is applied to a four stage binary counter. A series of 8 4-input logic gates are connected across the four Q outputs of counter. By appropriately connecting these outputs to the inverting or non-inverting input of the gates, an 8-phase time relationship can be established between the outputs of the gates. These outputs set and reset 4 bistable elements. Together the Q and $\overline{Q}$ outputs of these elements form 8 binary waveforms mutually offset

by 45 degrees. These waveforms are then applied to a logic map which selects one phase in accordance with the three signalling bit streams and the required signal space diagram. (The 8-phase waveforms are also provided to demodulator in a "cheat link" arrangement). The fourth bit stream controls a binary amplitude modulator to provide the two signal rings. Finally, an IF channel shaping filter is provided to bandlimit the transmitted signal.

Figure 7.15 shows the partner demodulator. The incoming modulated signal is filtered and then applied to a five-way power splitter supplying four phase detectors and an amplitude detector. Each phase detector uses one of the four phase references from the demodulator. The output of the amplitude and phase detectors is next applied to level triggers to square the waveforms. Finally, the phase outputs are routed through a logic decoder map to reconstruct the original three data streams.

Once the basic principles had been established, the more representative high speed modem was planned. By this stage, the accompanying study had begun to focus on a system which was an ajunct or overlay to the existing QPSK/TDMA system. The hardware effort, in consequence, was re-directed to develop the necessary elements to

convert QPSK to APK. At the time the hardware development was initiated, 60 Mbit QPSK through 40 MHz channels was under intensive development. In particular, equipment sponsored by the British Post Office and developed by Marconi Research Laboratory (MRL) was chosen as the baseline equipment[33]. This equipment proved to be an excellent choice since it performed with near-theoretical performance and was extremely well characterized by an extensive series of tests[30,34,35,36].

The extra equipment was built to the author's design by an undergraduate student who was attached to the Author's section at Goonhilly Earth Station[37].

7.8.1 Configuration of APK Modem

To support the work in the main body of the text, the APK modem consisted of two parts: a QPSK center section and an ASK overlay. Consider Figure 7.16. The output of a conventional QPSK modulator is fed to an ASK modulator input. The output of the ASK modulator is fed via a channel shaping filter to the transmission channel. At the receiver, the incoming signal is first passed through the receive channel shaping filter and is then fed to a power splitter. One output of this splitter is fed to the input of the ASK demodulator and the other is fed

via an AGC device to a QPSK demodulator. In essence, therefore, the modification necessary to convert QPSK into Octonary APK is placed in series with the transmitter but in parallel with the demodulator. The exception being the AGC device. In general, as explained, all high performance QPSK demodulators will contain some form of automatic power leveling element. This is necessary to prevent burst-to-burst amplitude variations within the TDMA frame from adversely affecting the sensitive phase detectors within the QPSK demodulator. When a QPSK demodulator is used as part of an APK system, the same amplitude protection must be extended against the AM modulation. Failure to do this would result in severe cross-talk between the AM channel and the two PSK channels via the amplitude sensitivity of the phase detectors. However, the AGC commonly employed in such modems is deliberately designed with a relatively slow (>50 symbol) time constant largely to obviate any attempt to respond to the AM introduced to QPSK signals by passage through the narrow bandwidth channel shaping filters. In contrast, the AGC device must be very fast in order to protect the phase demodulators against the amplitude modulation in an APK system. The techniques selected in the experimental equipment will be discussed later.

Before discussing the developed APK equipment it seems helpful to review the salient features of QPSK modulator and demodulators. Figure 7.17 shows a modulator and demodulator connected back-to-back. The modulator consists of two 2-phase PSK modulators whose carrier supplies are in quadrature and whose outputs are summed to produce the 4 phase modulation.

At the demodulator, the filtered signal passes through an agc device and is split into three branches: the phase detectors, the carrier recovery branch and the clock recovery branch. The phase detectors perform the reciprocal functions to the phase modulators and are supplied with accurately phase synchronized reference carriers in quadrature. The output of the phase detectors is sampled at a point midway through the symbol to determine which of the binary levels the current symbol represents. The phase synchronized reference carrier is derived by the carrier recovery branch which performs a non-linear operation on the incoming signal. This non-linear operation consists of raising the incoming waveform to the fourth power which removes the phase modulation and then the result is filtered by a narrow band filter whose center frequency is at four times the center frequency of the incoming signal. Finally, the frequency of the filter output is divided by 4 to recreate

the carrier frequency. The clock or symbol timing recovery path consists of an envelope detector which detects the filter induced AM on the QPSK signal followed by a narrow band filter. Finally, the output of the filter is amplitude limited to give a square wave to drive the regenerators.

7.8.2 ASK Modulator

Throughout these discussions, the two data streams entering the PSK modulator will be labeled the 'P' and 'Q' streams. The data stream applied to the APK modulator will be labeled the 'R' stream.

The function of the ASK modulator is amplitude modulate a QPSK signal under the control of the 'R' data stream. Figure 7.18 shows the idealized arrangement. It can also be seen that the P, Q and R streams will have to be synchronized and be transmitted at the same symbol rate. The basic design requiremnts for the AM modem are as follows:

1) A 70 MHz center frequency QPSK Modulated signal was to be used as the carrier.

2) The baseband data rate was 30 Mbits.

3) The modulation depth must be variable enabling various signal level ring tests to be performed.

Additionally, other factors are relevant due to design practices and circuit construction.

i) Maximum available bandwidth = 36 MHz

ii) Phase changes in the composite envelope, due to the PSK carrier, should be accommodated.

iii) All stages were to be directly coupled in order to maintain the IF baseband response down to dc.

iv) The system was to have a characteristic impedance of 50 ohms with interconnections between individual circuits using 50 ohms co-ax cable.

v) Strategically placed monitor points were required.

vi) The complete system was to operate from coarse ±30 volt supply rails. (Therefore, it was necessary to provide regulated power supplies on the modular boards).

7.8.2.1 Design of the Modulator

The operation of the modulator depicted in Figure 7.19 is as follows. The 70 MHz source, which when in the hybrid mode will contain the P and Q streams of information, is split into 2 paths using 50 ohms matched resistive networks. The Y path is fed via a 70 MHz phase shifter into a switch circuit which is driven from the R stream. The device used for this switch was a double balanced mixer which provided appproximately 23 dB isolation when working at 30 Mbit/s. The X and Y paths are then combined in phase using a resistive adding circuit, resulting in the carrier being amplitude modulated by the R stream information. The attenuators were introduced into the circuit so that a variable depth of modulation was available. Some initial problems were found in the design due to the overheating of components, however, these were cured by optimizing voltage supply levels. The overall performance of the modulator was promising, having rise and fall times of approximately 3 ns when operating at 30 Mbits (maximum modulating signal

1010) (Figure 7.20). The modulated output is shown in Figures 7.21 through 7.24 for various modulating bit patterns also shown.

7.8.3 Demodulator Development

At a very early stage in the development of the demodulator, it was clear that it was necessary to use the superior low C/N performance of a coherent amplitude demodulator for the ASK detector. One major complication is that this is a very phase-sensitive method. If the carrier recovery branch signal were to be used to demodulate the composite ASK/QPSK signal, severe cross-talk from the QPSK channels to the ASK channel would result. It was also clear that this problem would be obviated by the use of an amplitude limited QPSK signal as a reference carrier supply. This is available at the output of the AGC device. In this manner, Figure 7.25 shows the general arrangement of the first APK demodulator constructed. As shown in Figure 7.25, the synchronous detector is supplied with the bandlimited incoming signal and an amplitude limited version of the same signal. The output of the detector is then applied to a regenerator to extract the R data stream. The regenerator is an identical design to that used in the QPSK demodulator and is supplied with the same symbol timing signal. In this

first design development of two items were necessary: the synchronous detector and the AGC device. These will be considered in turn.

7.8.3.1 Synchronous Detector

It was explained earlier that the superior noise performance of the synchronous (homodyne) technique lead to it selection for the ASK detector. However, in contrast to the normal application of this techniques, the sinusoidal carrier is replaced by an amplitude limited QPSK signal. In this configuration, the "local oscillator" can be exactly sychronized to the incoming signal, facilitating detection of the amplitude modulation without the cross talk from the phase transitions within the QPSK envelope.

The product detection device is the most important part of the synchronous demodulator. A reliable and well-established technique is to use double-balanced mixers such as those employed in conventional switching modulation. Figure 7.26 shows the basic circuit for such a switching device. To simplify the description at this stage, the carrier and "local oscillator" inputs are assumed to be constant phase sinusoids. In the half-cycle when the local oscillator signal is highly positive with

respect to the incoming signal, the outer diodes (D_1 and D_2) are switched hard-on while the inner diodes (D_3 and D_4) are held hard-off. The reverse situation exists during the next half cycle of the carrier. Thus, switching occurs at twice the carrier frequency, the output being related to the product of the input signal and "local oscillator" signal levels. As the latter is constant, the output follows the input envelope. The output is however, contaminated with a twice carrier frequency signal which is rejected by low pass filtering.

Reliable balanced mixer packages are readily available and the type extensively used within the Marconi demodulator was chosen for convenience. This highly balanced 50 ohm port device is known as a MCL-SRA-1. Balanced mixers are sensitive to the power level of the applied signals. Accordingly, having selected the device the next step is to select the average drive level. Figure 7.27 shows the input-output power level relationship for the SRA-1 at various levels of local oscillator input and indicates that the manufacturer's recommendation of +7 dBm for the local oscillator level allows the input of -7 dB to lie in the center of the linear region. The scales are plotted in dBm (i.e., dB with respect to 1 mW into 50 ohms). Figures 7.28 and 7.29 show photographs of the product detector output before and

after the low-pass filter, respectively. In both cases the carrier frequency is 70 MHz and the baseband signal is 30 M symbols/sec. with a 1010 sequence. Note that in Figure 7.28 the twice carrier frequency component is apparent and that after filtering a clean analogue baseband signal is obtained. (This signal is applied to the regenerator to be sampled and squared).

7.8.3.2 AGC Limiter Device

A combination automatic gain control (AGC)/limiter device was considered necessary to strip the AM modulation from the APK composite signal such that only QPSK remains to be applied to the QPSK demodulator. Figure 7.30 shows this. The combination operates on a symbol by symbol basis and in consequence is very much faster that the agc devices commonly employed.

AGC and limiter devices can be formed using a variety of techniques. Many of these techniques use a non-linear element which has an AM/PM characteristic similar to a TWTA. This implies that a signal will suffer a phase change the magnitude of which is related to the signals amplitude. Clearly, this is imcompatible with subsequent QPSK demodulation. Furthermore, the output of

the limiter will be of sin x/x form and the signals passing through the device will be subjected to intermodulation. This will be seen later.

7.8.4 Construction and Performance of the Prototype Equipment

The amplitude modulator, amplitude detector, low pass filter and limiter (regenerator) were constructed in separate boxes (Figure 7.31). Each unit was built into a cast lead-alloy box with appropriate power and access points (BNC 50 ohm). The signal processor which follows the ASK detector is also shown in Figure 7.31 and the attenuation/frequency response of the low pass filter is shown in Figure 7.32. Each module used on board regulators for the various local supply voltages and operated off a $\pm$25 volt common rail.

The ASK modem was first tested in isolation using the circuit configuration shown in Figure 7.33. A "cheat link" between the transmitter and receiver was used instead of a recovered reference. The resulting BER C/N performance curves are shown in Figure 7.34 together with the theoretical performance curves for ASK. As can be seen from the curve the modem offers an implementation

margin of 1.3 dB over theoretical at 10^{-6}. This is considered high but acceptable for such experimental equipment.

However, when the cheat link was removed and the equipment connected in its normal configuration, the best attainable performance gave an implementation margin over theoretical of 4.6 dB Figure 7.35. In addition, the QPSK performance degraded by 0.8 dB relative to its normal (i.e., non-APK) performance. Accordingly, reasons for the poor APK performance were investigated. It will be recalled that a limited version of the input signal was used as the "local oscillator". Therefore, it was considered that the source of the degradation was the imperfect matching between the local oscillator (LO) and input port of the AM detector. This would result in a considerable increase in effective noise power. It was considered that this effect together with the AM/PM effect of the limiter was responsible for the excess degradation.

The method of supplying the "local oscillator" input was therefore, re-examined. The need, it will be recalled, was to provide a constant level QPSK signal to the amplitude detector in order that the effect of the phase transitions may be matched and therefore obviated.

The final approach adopted was to use the regenerated P and Q data streams to QPSK modulate the recovered carrier reference signal (Figure 7.36) in a "remodulation" technique. By this method, the noise doubling effect was much reduced since the P and Q data streams are subjected to the non-linear regenerator process which removes most of the noise. Occasionally, the P and Q data streams are in error in accordance with the error rate. When an error occurs, some cross-talk will be experienced by the APK channel. This is one source of discrepancy between the practical results and the theoretical performance.

This promising technique required that a QPSK modulator be built. Accordingly, a wholly digital phase selection modulator was built (Figure 7.37) and the same style of construction was used (Figure 7.38) as the other APK elements. The signal space diagram for the QPSK modulator output is also shown in Figure 7.39. The performance of this method is shown in Figure 7.40. In this case, the implementation margin has fallen to 2.4 dB. This would be considered rather high by normal commercial standards, but more than adequate for a low budget practical realization of this nature.

A series of photographs were taken to illustrate the waveforms of the system. In Figure 7.41, two pictures are shown. In the first, an APK 1010 modulated input signal is shown with the QPSK P and Q streams loaded with long sequence psuedo-random noise. Also shown in this picture is the recovered carrier and baseband signals. In the second picture, which was taken at the same monitor points, all three channels were loaded with a long sequence PRBS of which only a small part is seen.

7.9 SUMMARY

The link budget estimates used throughout this study are based on extending various QPSK results to the 8-phase PSK, APK-A and APK-B cases. Since these results were obtained using QPSK modems, it was considered important to compare the methods that may be employed in the candidate modulation methods' modems. The overall aim being to ensure that no further link degradation must be accommodated due to the differences in attainable modem performance. To this end, basic modem designs have been examined and those elements identified which may result in degraded performance. At an early stage, the importance of the reference recovery circuits was recognized, and some considerable time was spent on examining the elements within these cicuits. To this end, the carrier and clock

recovery circuits were examined separately. In the carrier recovery circuit, it was concluded that a "tuned filter" (TF) form of implementation was superior to a phase locked loop (PLL), due to the occasional occurrence within the PLL of an equivocating hang-up condition. After examining the various mechanisms, it was concluded that degradation margin of 0.25 dB should be included in the link budget to accommodate carrier recovery effects. It was also concluded that clock recovery circuits should be constructed using a tuned filter design for the same reason as in the carrier recovery case. In this case, however, it was noted that the clock signal recovered from the incoming signal (typically by an envelope detector) would display considerable variations in signal level corresponding to the message content in the incoming signal and that some form of amplitude limiter would be required. When all these assessments were made, it was decided to include 0.3 dB margin in the link budget to the degradation associated with clock recovery. The assessment of the recovery loops was completed by investigating the techniques available to establish an amplitude reference for the APK systems. Again, it was decided to allocate 0.3 dB for degradations experienced in this loop.

The next stage was to build a simple 8-phase phase-selection modem using low speed logic. Having gained some confidence from this exercise, attention was directed towards the final APK modem. This was designed to be an overlay to an existing QPSK modem, which resulting in the need to developed only a small number of addition units: an am modulator, a.g.c. device, and an am demodulator/regenerator.

The modulator used a double balanced mixer as a current controlled attenuator and the technique worked well. The demodulator also used mixers but this time in a synchronous demodulator mode. Originally, the demodulator was connected across a fast a.g.c. device which stripped the am from the APK incoming waveform. This gave rise to an implementation margin of 4.6 dB over theoretical. This high margin was traced to a noise penalty resulting from this type of connection. Accordingly, the circuit was redesigned with a QPSK remodulator supplying the demodulator. In this configuration, the margin fell to 2.4 dB.

Within the tight confines of available budget and manpower, the combined APK technique has been verified, although much could be refined. It is hoped that a

commercial development of these ideas will ensue, in which case a considerable improvement in implementation margin may be expected. However, the 1 dB margin allocated for modem uncertainties in the link budget can be considered, since the calculated loop margins (given by Carrier (0.25 dB) + Clock (0.3 dB) + Amplitude (0.3 dB) amount to 0.85 dB.

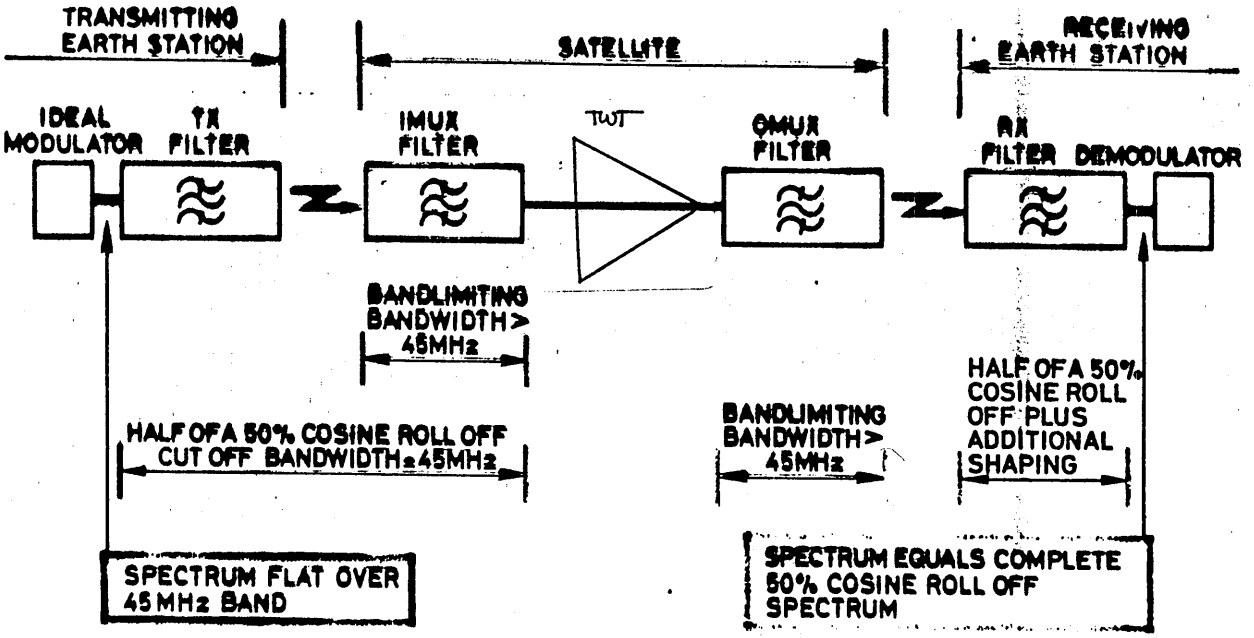

DESIRED CHANNEL DESIGN FOR MINIMUM DEGRADATION

FIGURE 7.1 ELEMENTARY NON-LINEAR CHANNEL

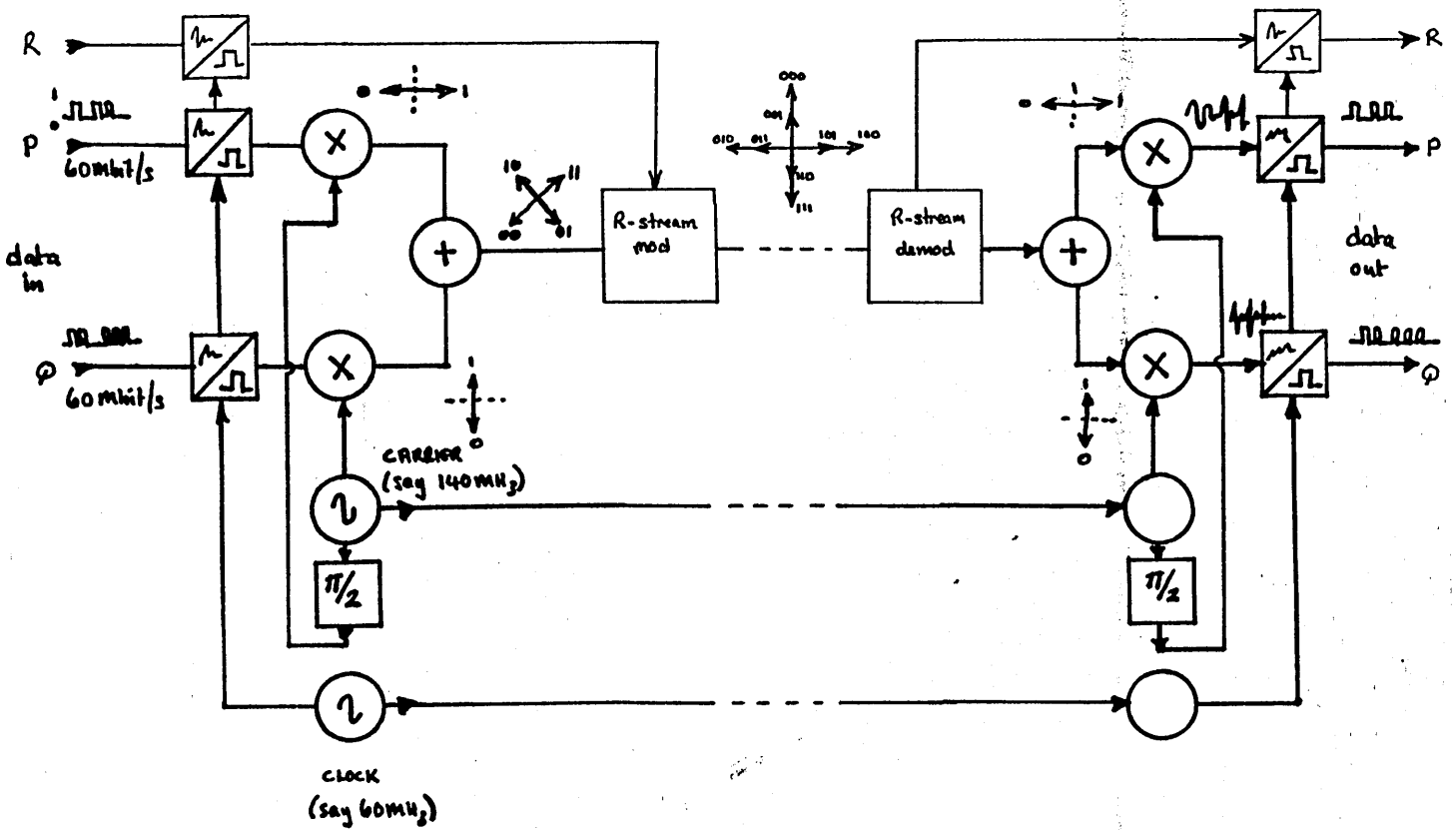

FIGURE 7.2 BASIC APK MODEM SCHEME

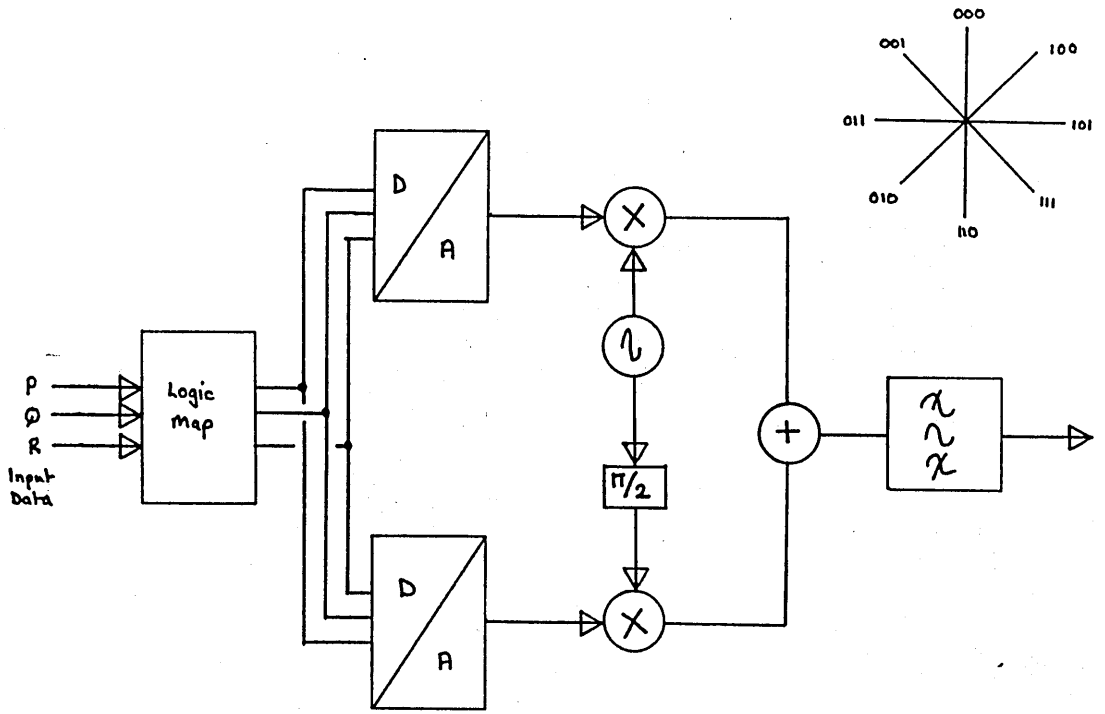

Input Data P	Q	R	Output Phase
0	0	0	0
0	0	1	$-\pi/4$
0	1	1	$-2\pi/4$
0	1	0	$-3\pi/4$
1	1	0	$-4\pi/4$
1	1	1	$-5\pi/4$
1	0	1	$-6\pi/4$
1	0	0	$-7\pi/4$

FIGURE 7.3 8-PHASE PSK MODULATOR

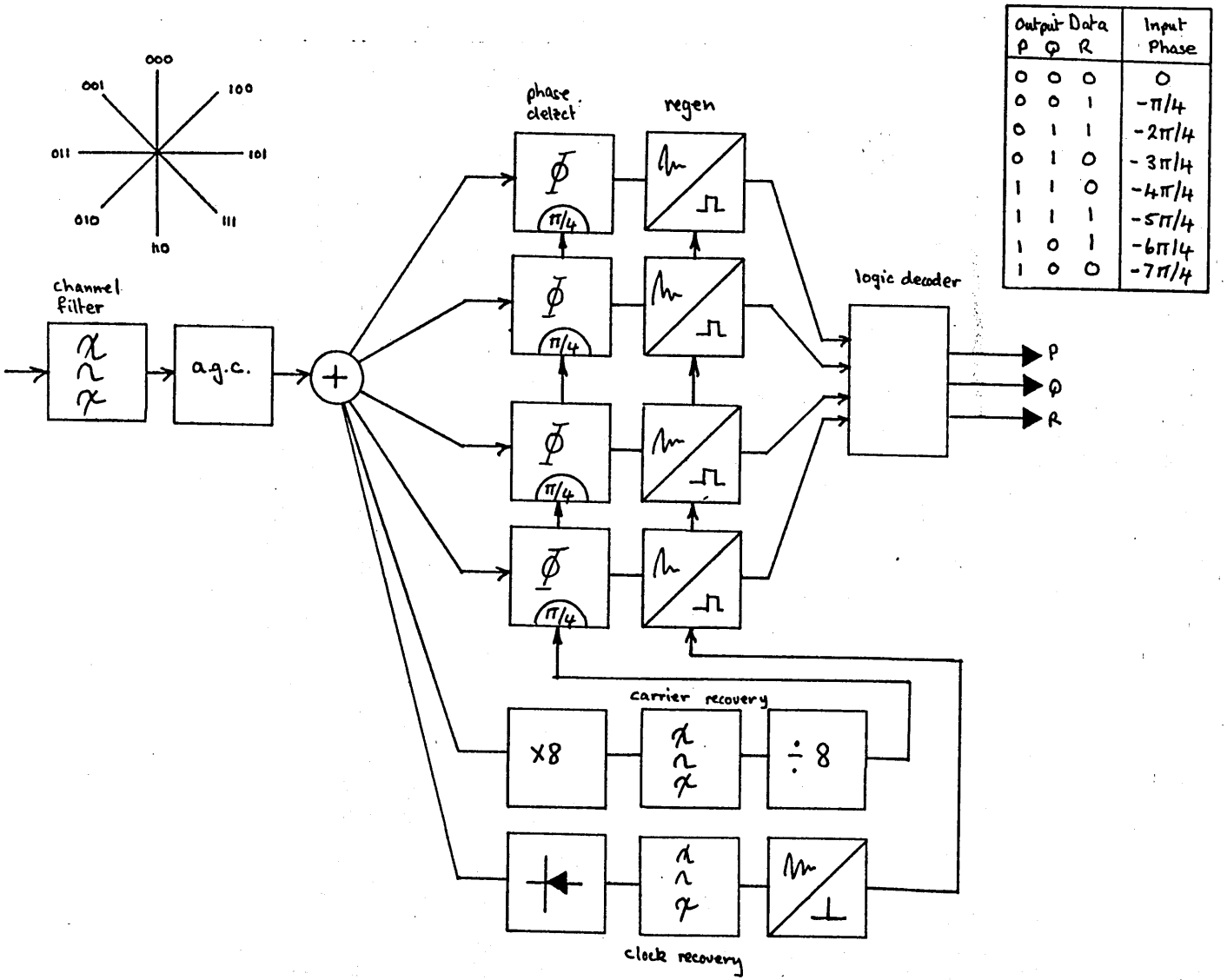

Output Data P	Q	R	Input Phase
0	0	0	0
0	0	1	$-\pi/4$
0	1	1	$-2\pi/4$
0	1	0	$-3\pi/4$
1	1	0	$-4\pi/4$
1	1	1	$-5\pi/4$
1	0	1	$-6\pi/4$
1	0	0	$-7\pi/4$

FIGURE 7.4 8-PHASE PSK DEMODULATOR

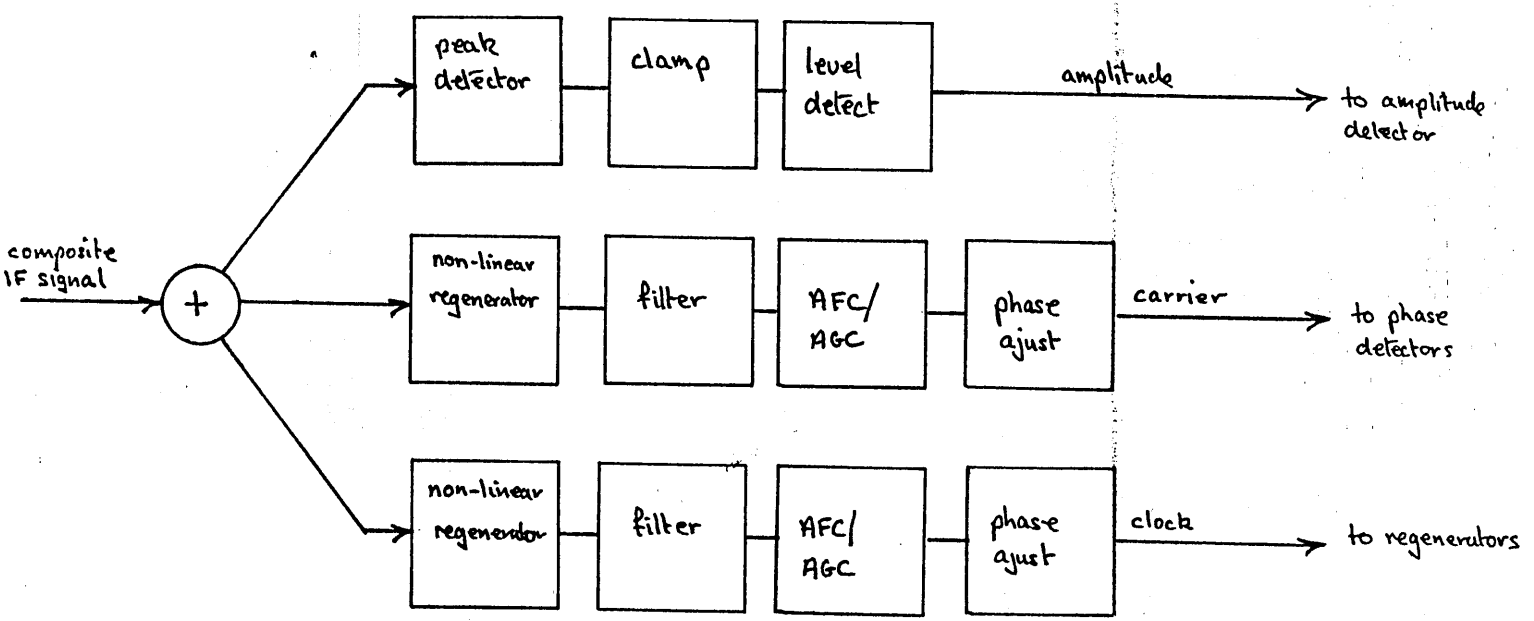

FIGURE 7.5 REFERENCE RECOVERY CIRCUIT

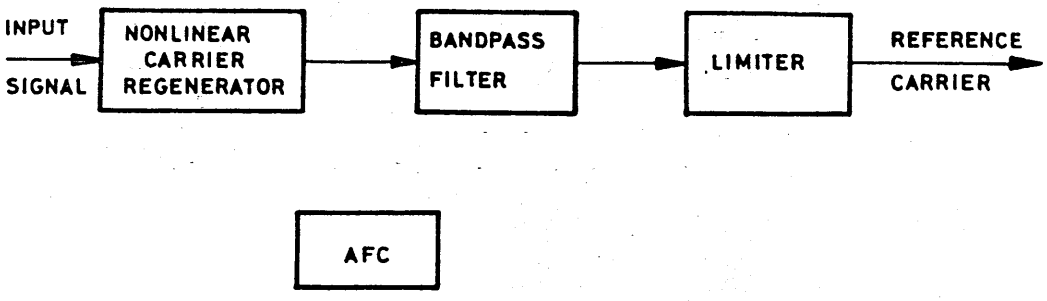

TUNED-FILTER MECHANIZATION OF CARRIER RECOVERY.

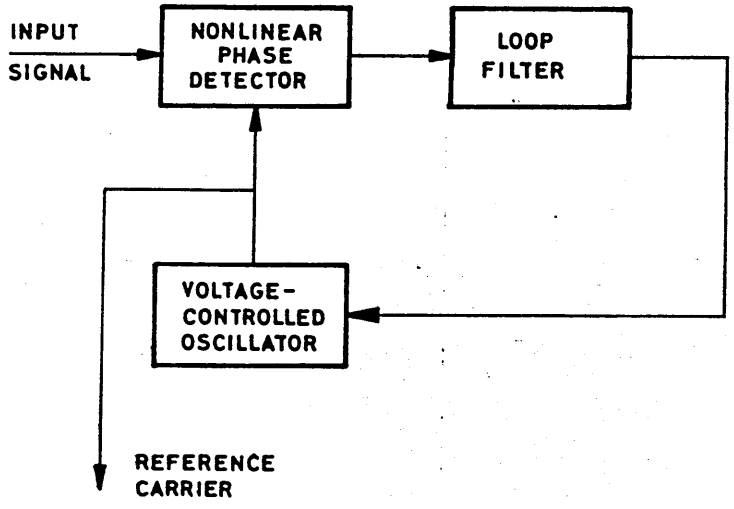

PHASE LOCK LOOP MECHANIZATION OF CARRIER RECOVERY.

FIGURE 7.6 CARRIER RECOVERY METHODS

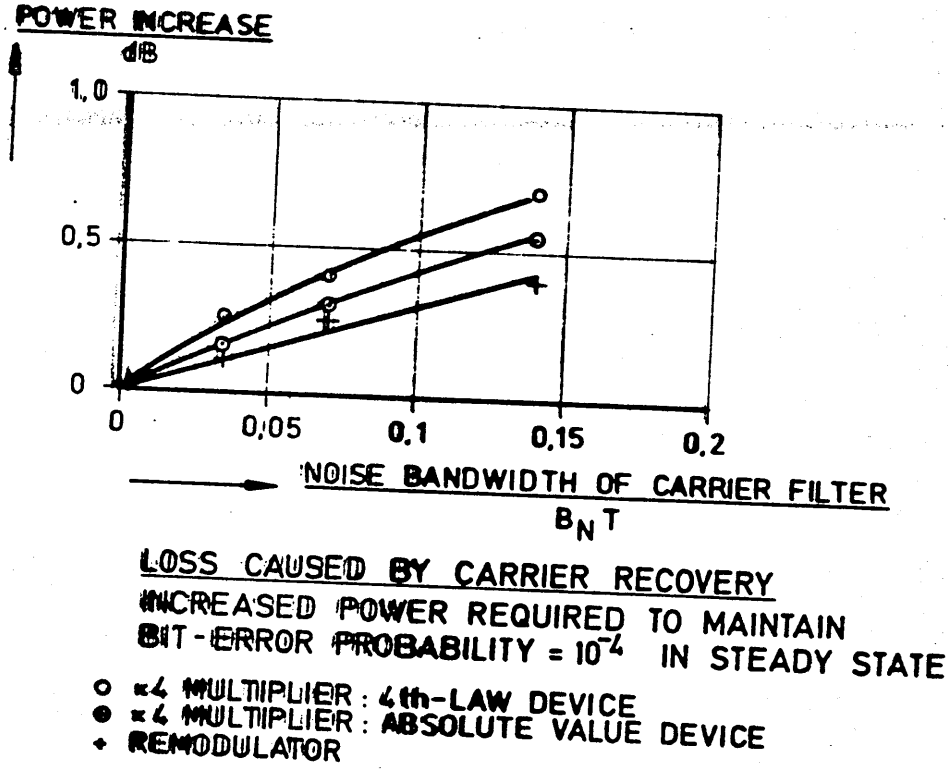

FIGURE 7.7 CARRIER FILTER BANDWIDTH DEGRADATION TRADE-OFF

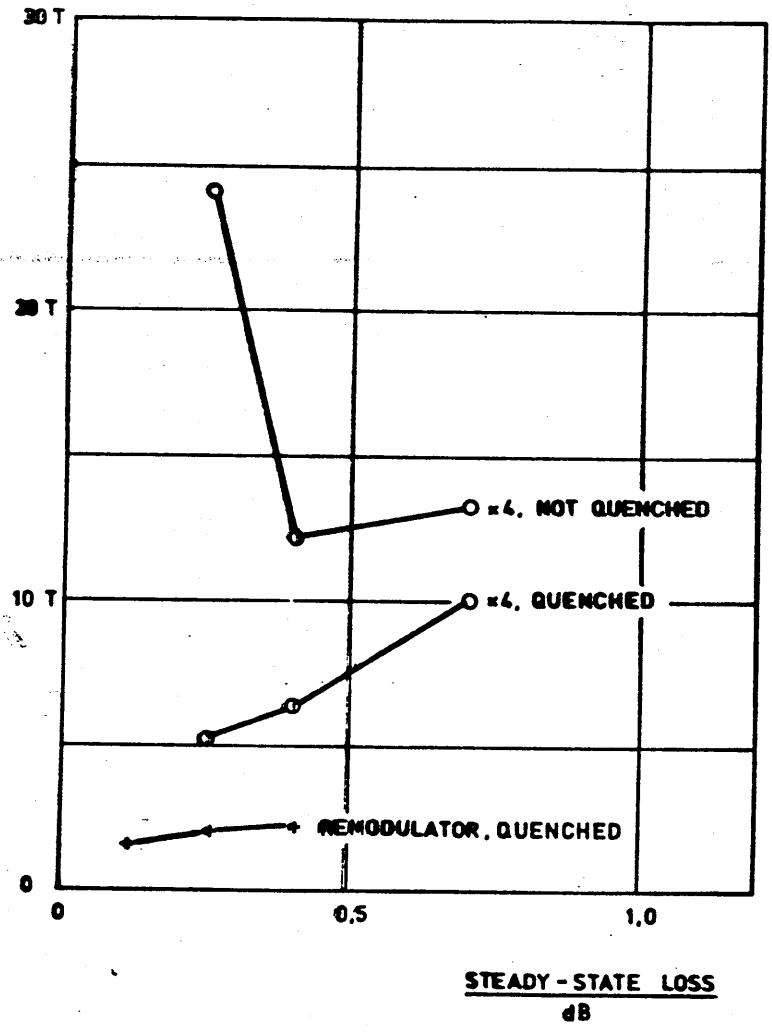

FIGURE 7.8 CARRIER RECOVERY FILTER:
EFFECT ON AQUISITION TIME

(1)

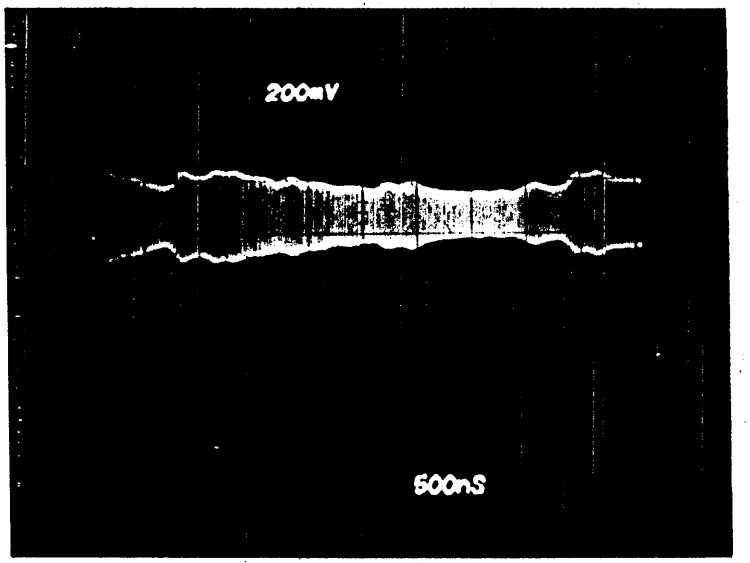

(2)

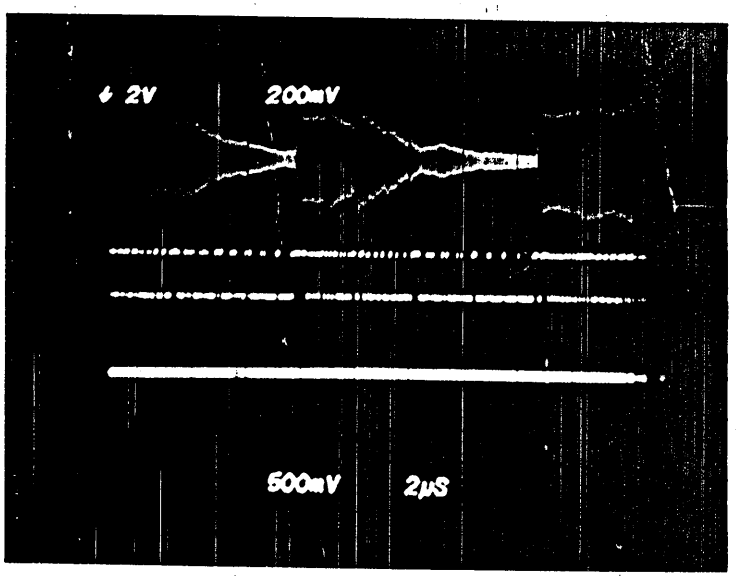

(3)

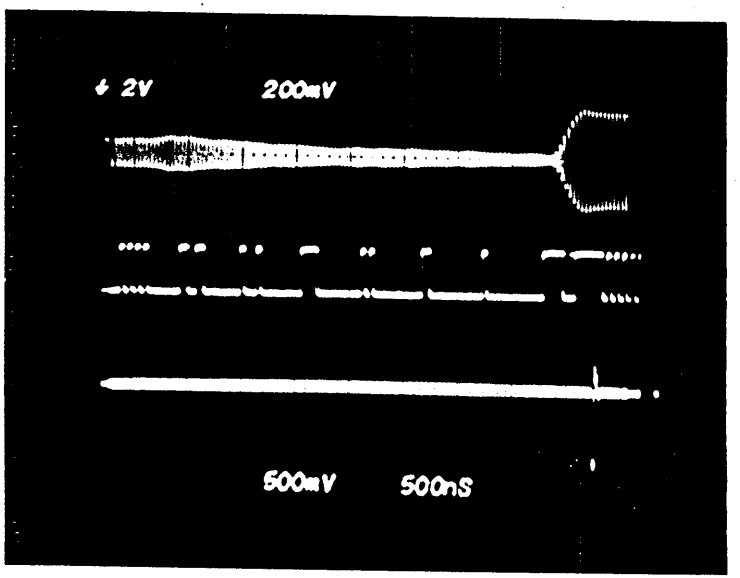

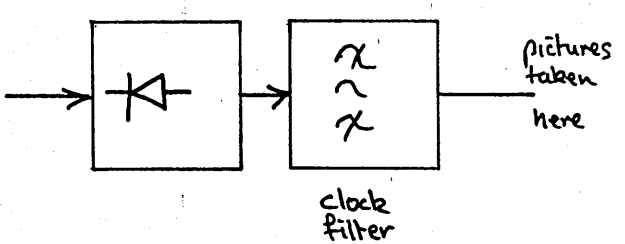

FIGURE 7.9 OUTPUT OF CLOCK FILTER

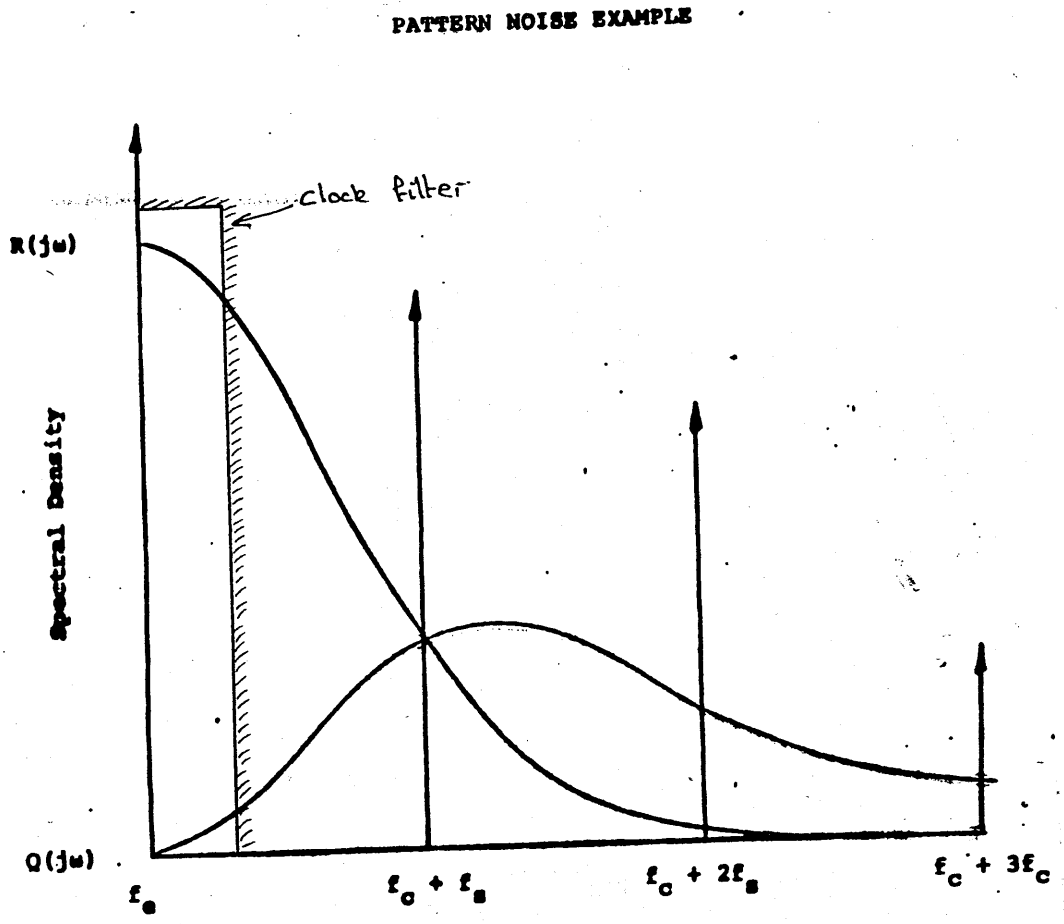

FIGURE 7.10 IN-PHASE AND QUADRATURE PATTERN NOISE

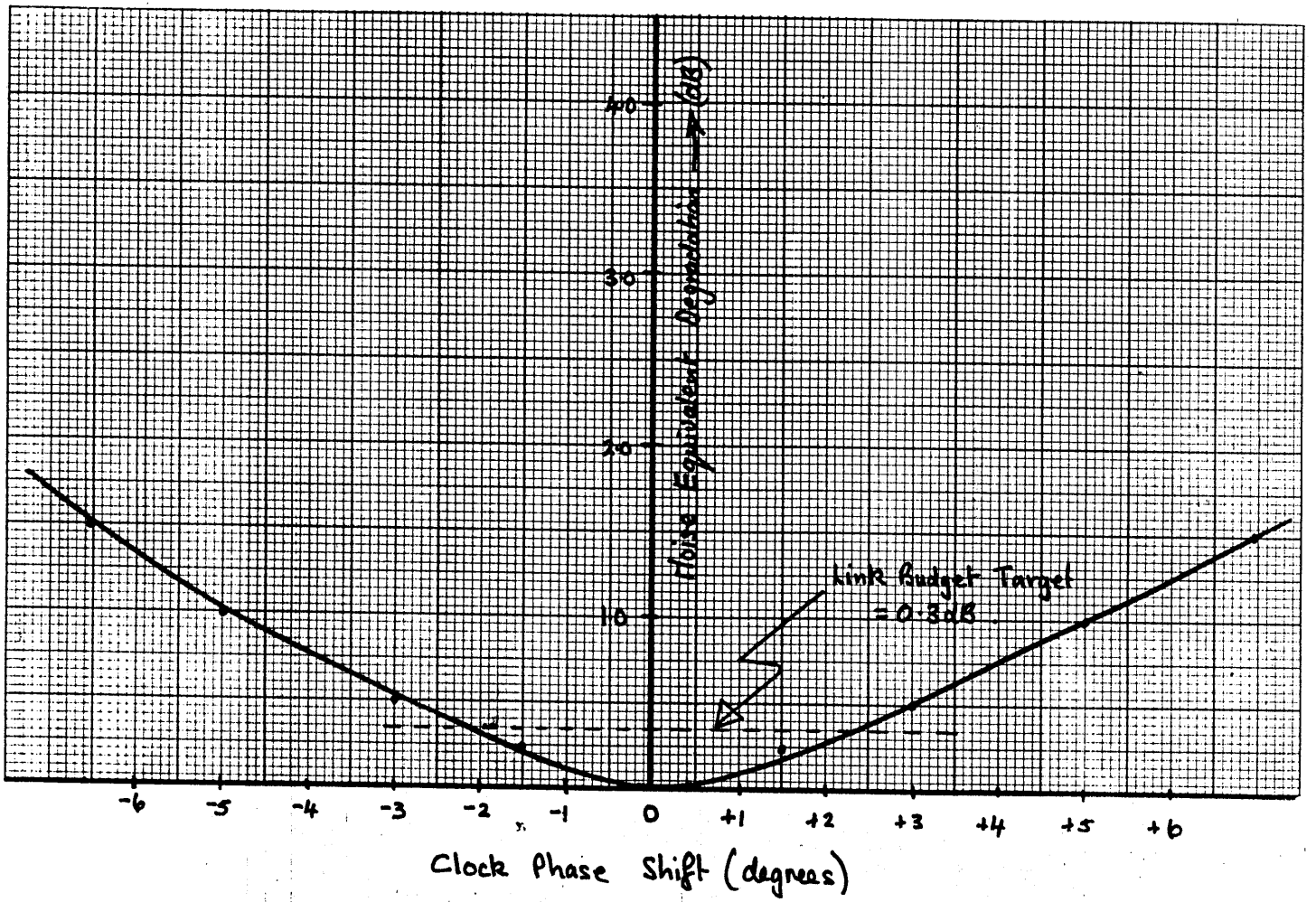

FIGURE 7.11 CLOCK TIMING ERROR

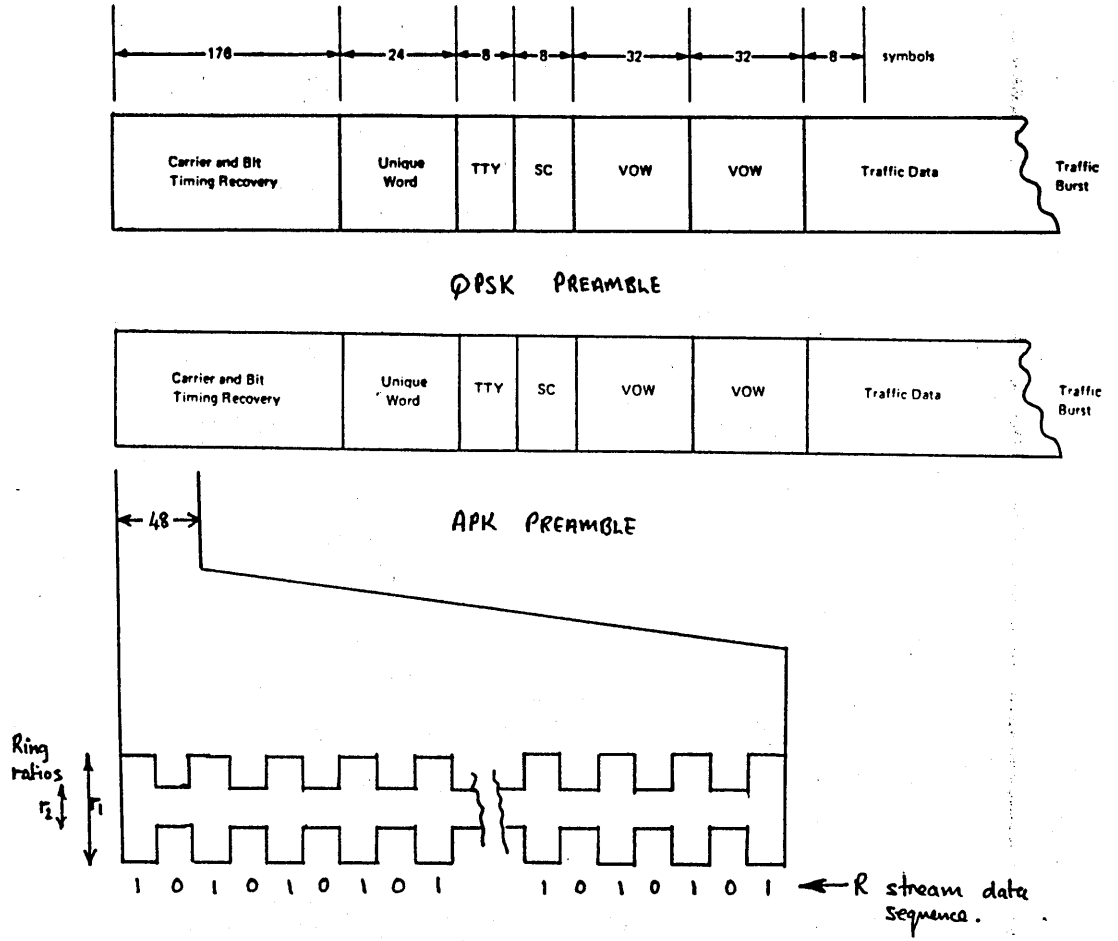

FIGURE 7.12 APK PREAMBLE

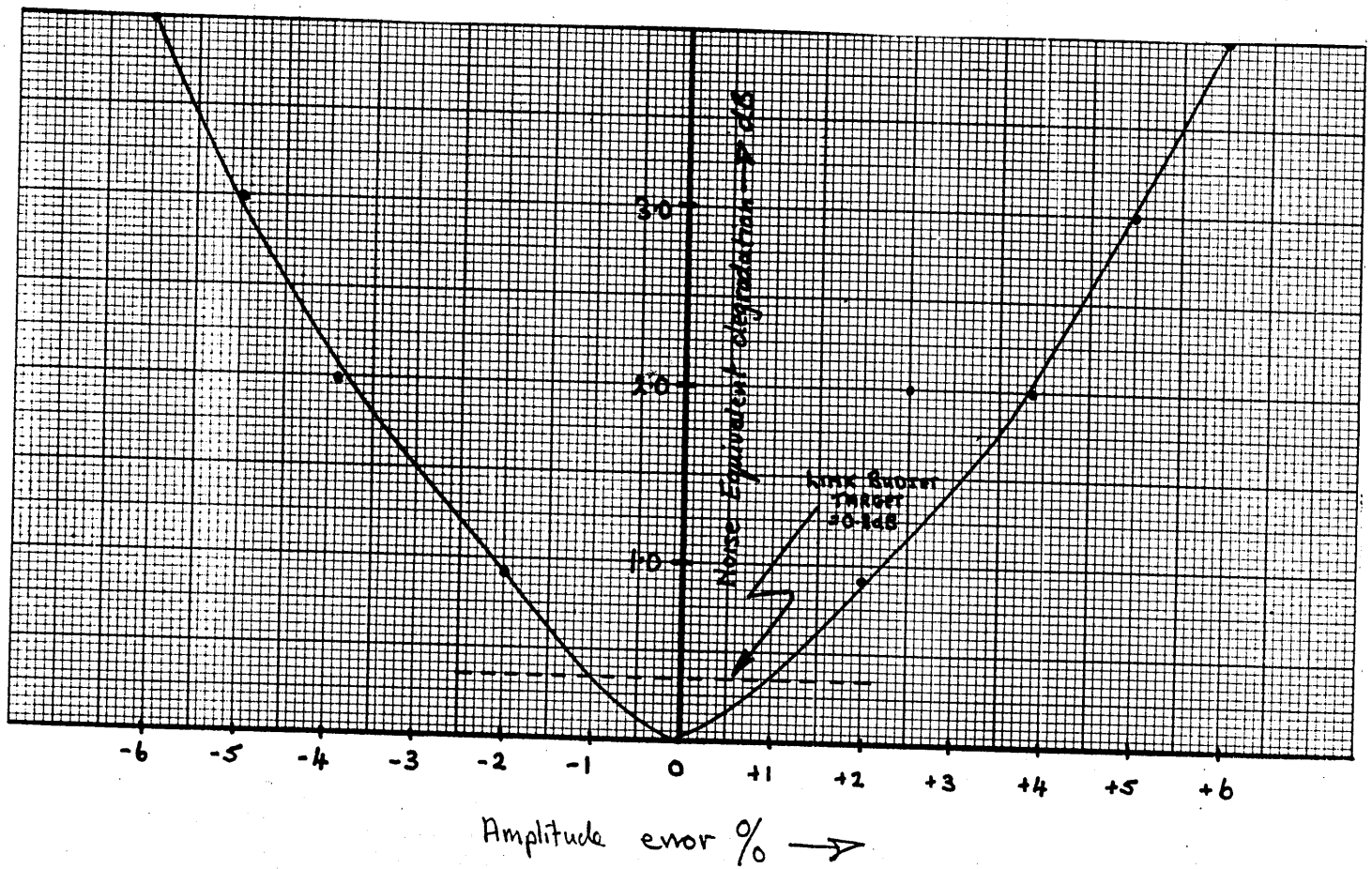

FIGURE 7.13 AMPLITUDE DECISION ERROR

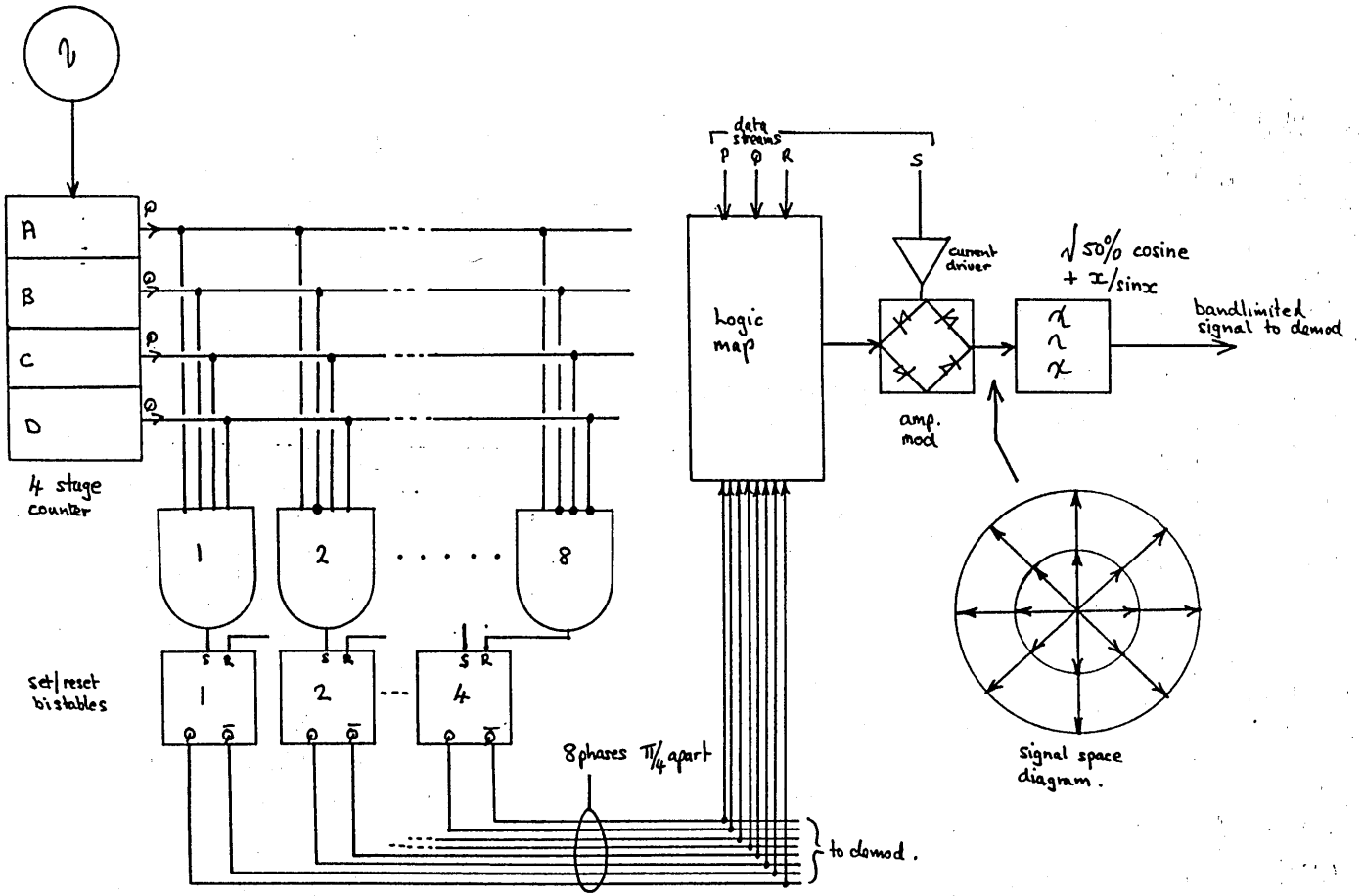

FIGURE 7.14 8-PHASE 2-AMPLITUDE MODULATOR

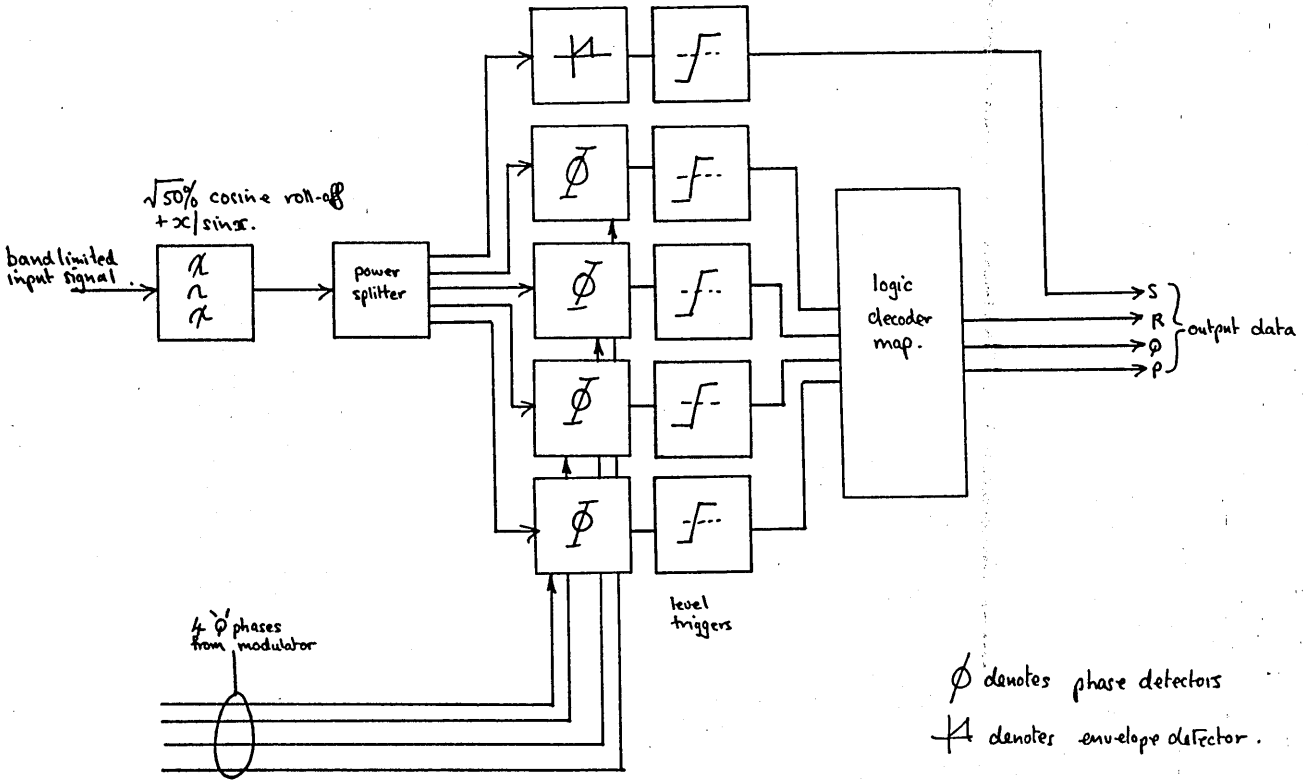

FIGURE 7.15 8-PHASE 2-AMPLITUDE DEMODULATOR

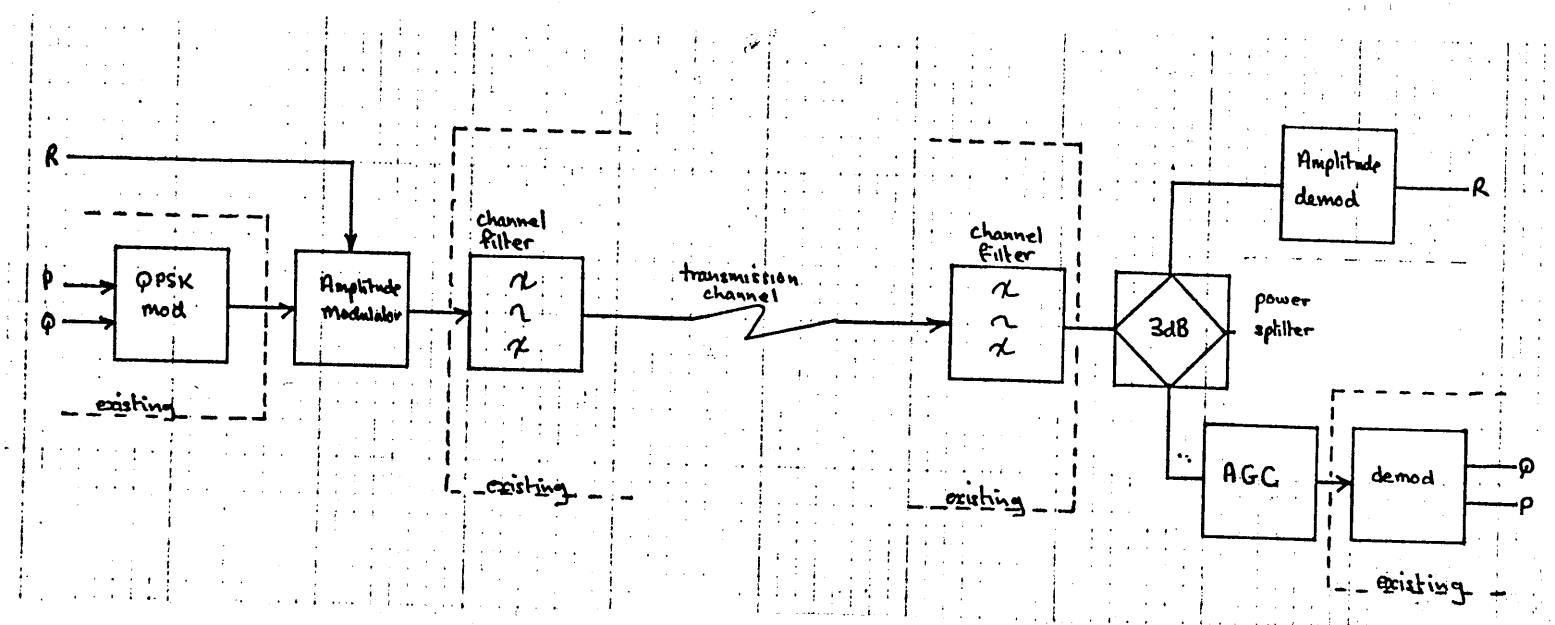

FIGURE 7.16 APK MODEM

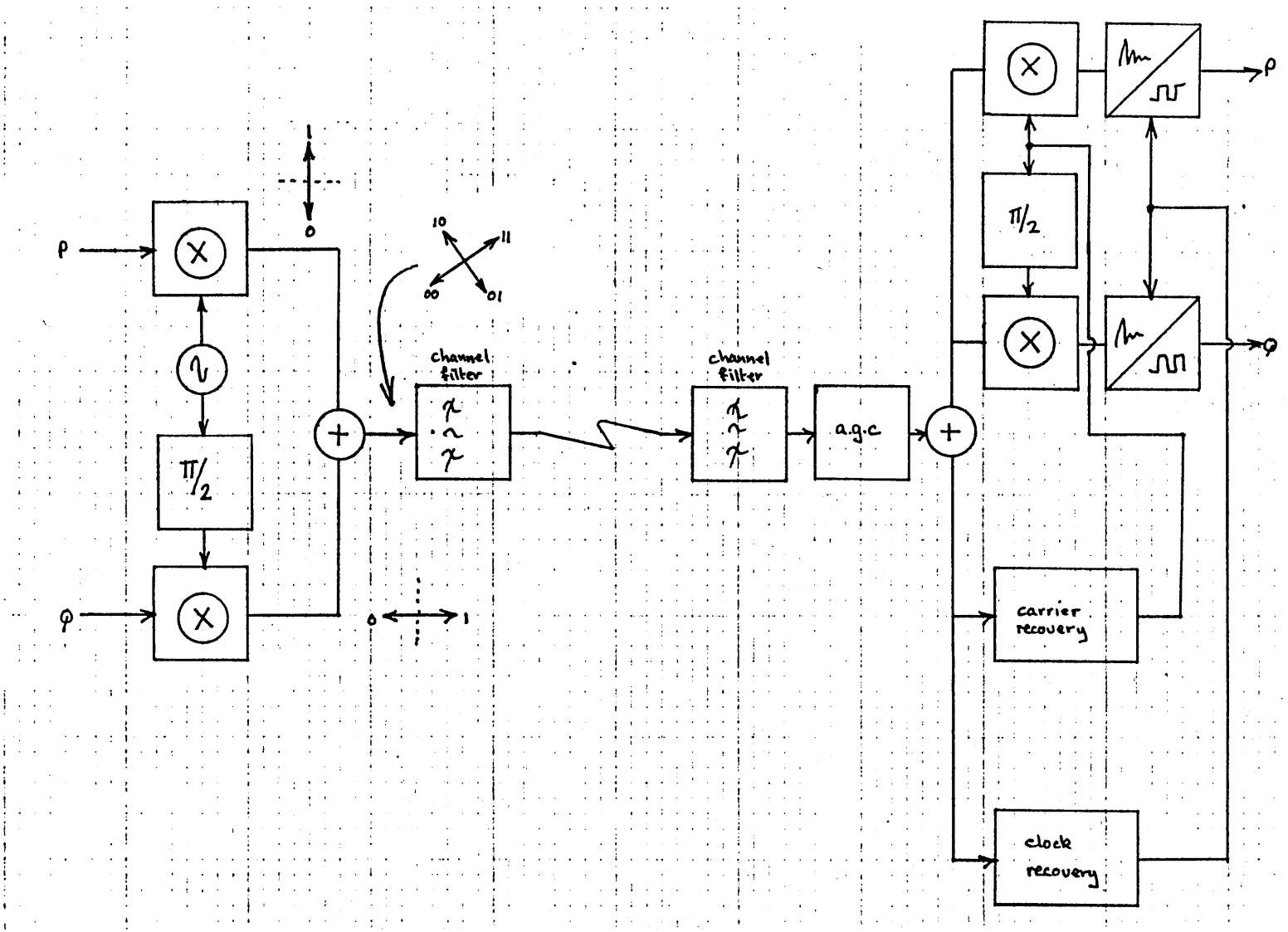

FIGURE 7.17 QPSK MODEM

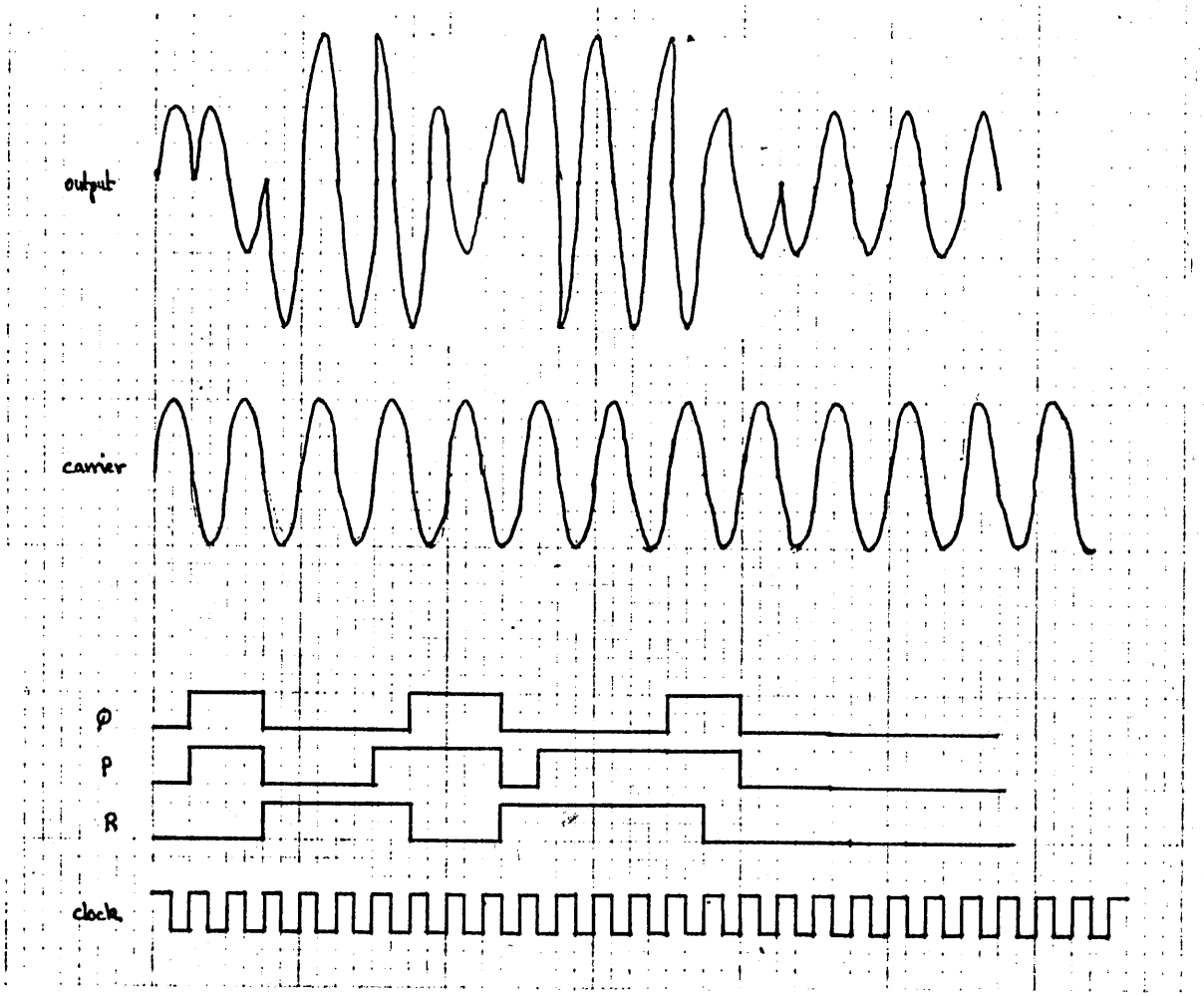

FIGURE 7.18 APK WAVEFORMS

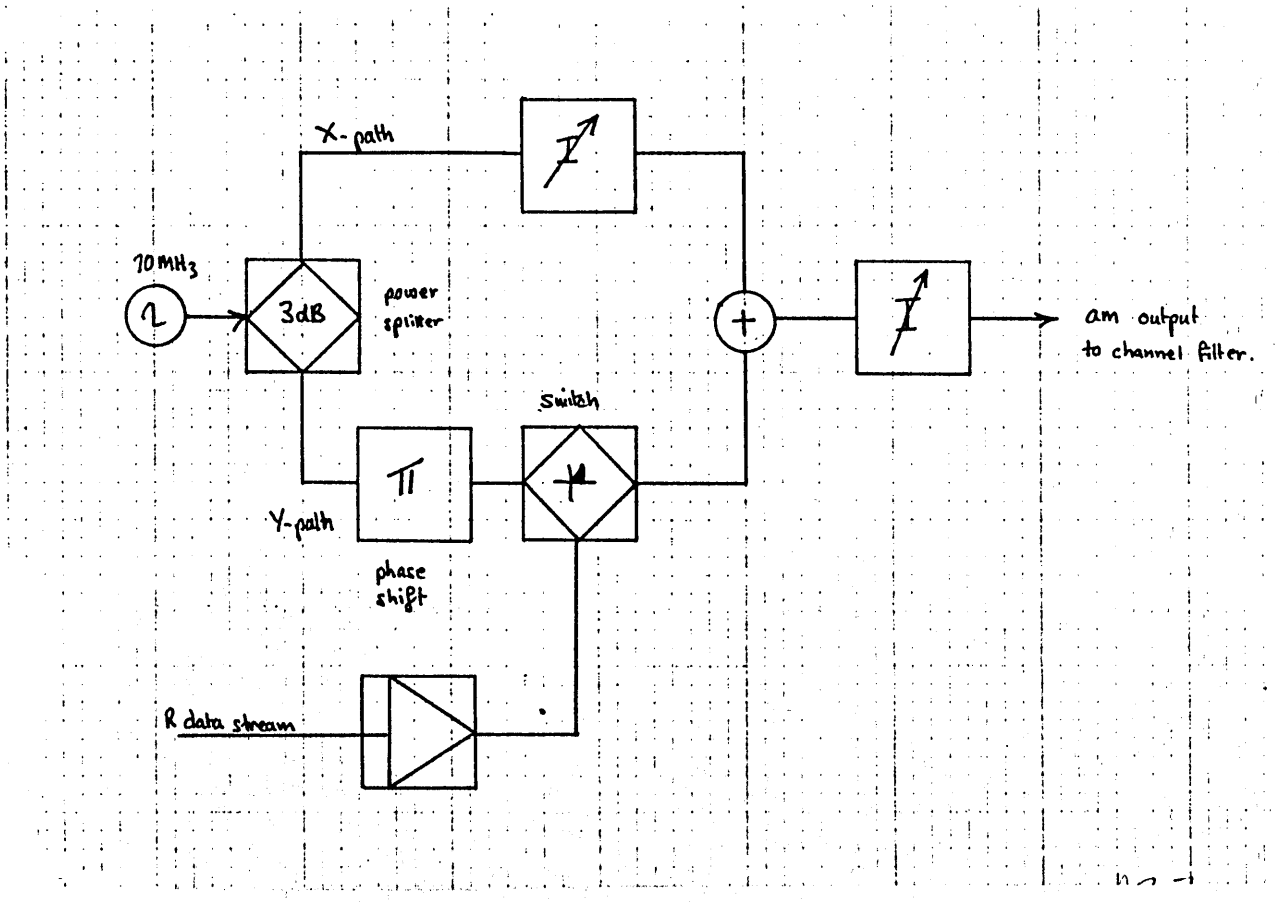

FIGURE 7.19 AMPLITUDE MODULATOR

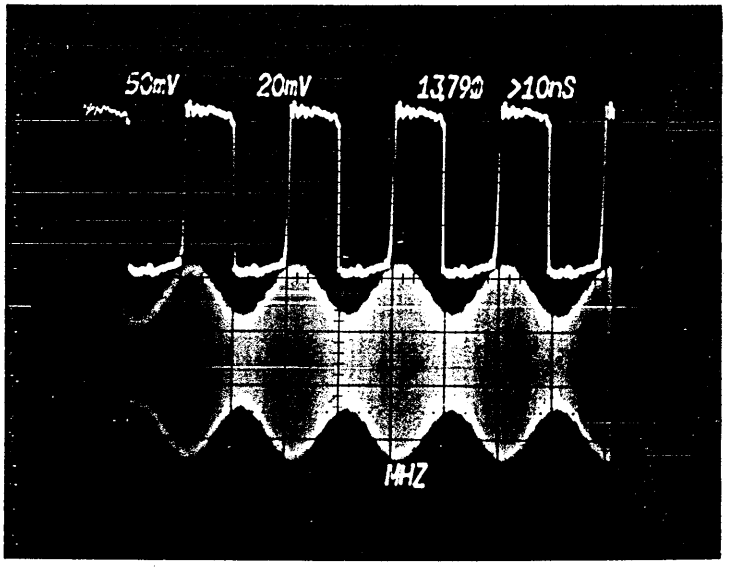

← Input data stream

← filtered am modulated output

FIGURE 7.20 AMPLITUDE MODULATOR PERFORMANCE WITH 1010 SEQUENCE FILTERED

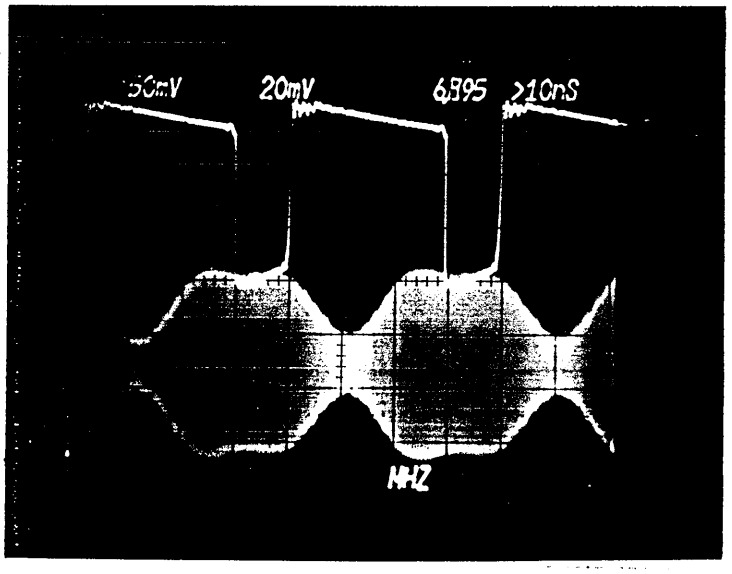

← Input data stream

← filtered am modulated output

FIGURE 7.21 AMPLITUDE MODULATOR PERFORMANCE WITH 1110 SEQUENCE FILTERED

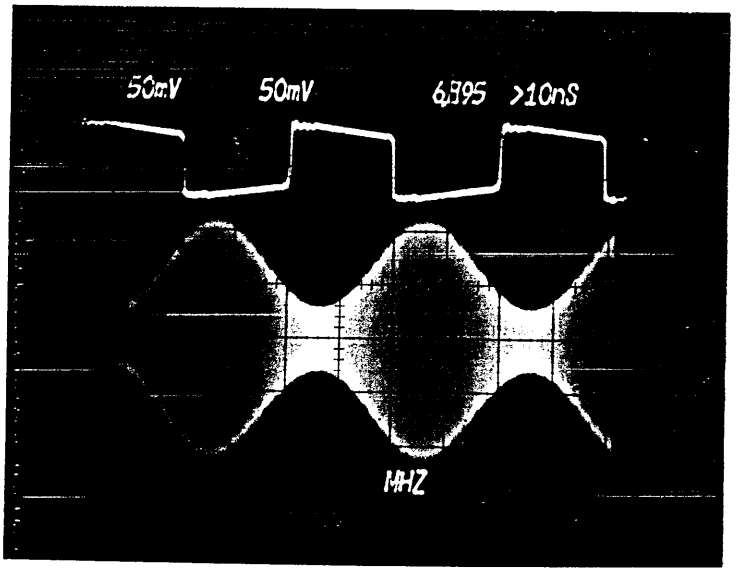

←Input data stream

←filtered output stream

FIGURE 7.22 AMPLITUDE MODULATOR PERFORMANCE WITH 1100 SEQUENCE FILTERED

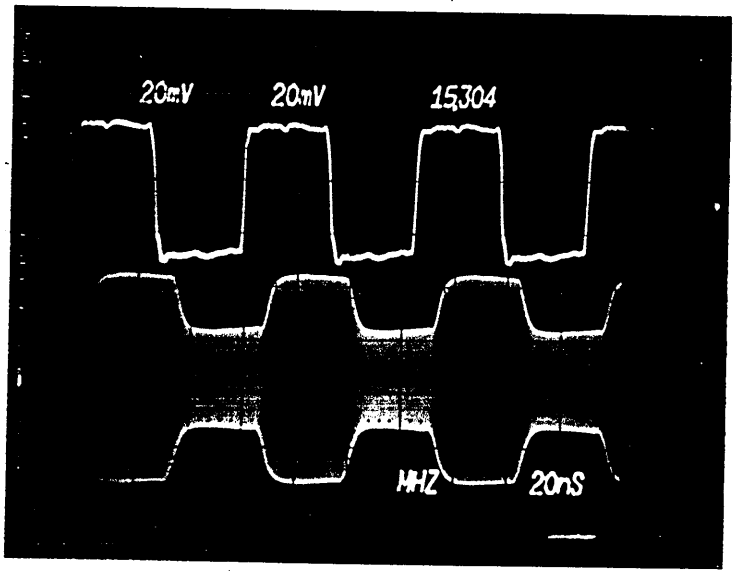

←Input data stream

←unfiltered output stream

FIGURE 7.23 AMPLITUDE MODULATOR PERFORMANCE WITH 1010 SEQUENCE UNFILTERED

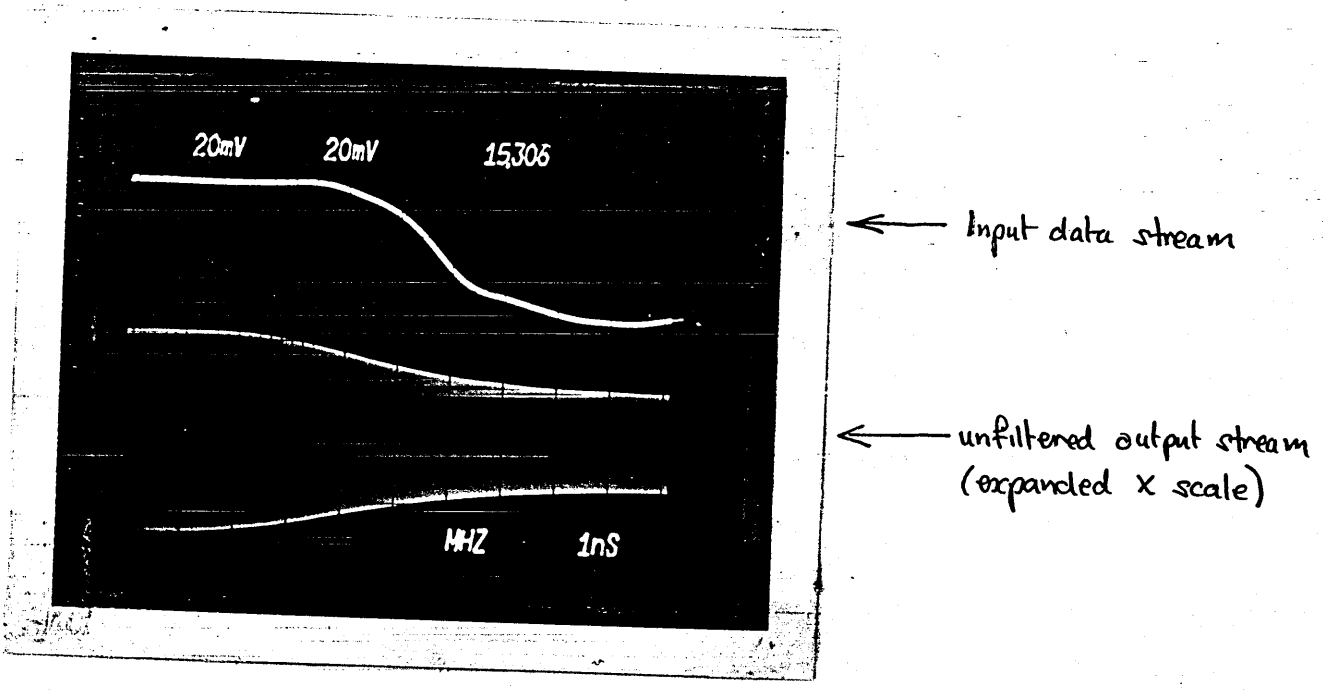

FIGURE 7.24 AMPLITUDE MODULATOR PERFORMANCE WITH SINGLE UNFILTERED EDGE

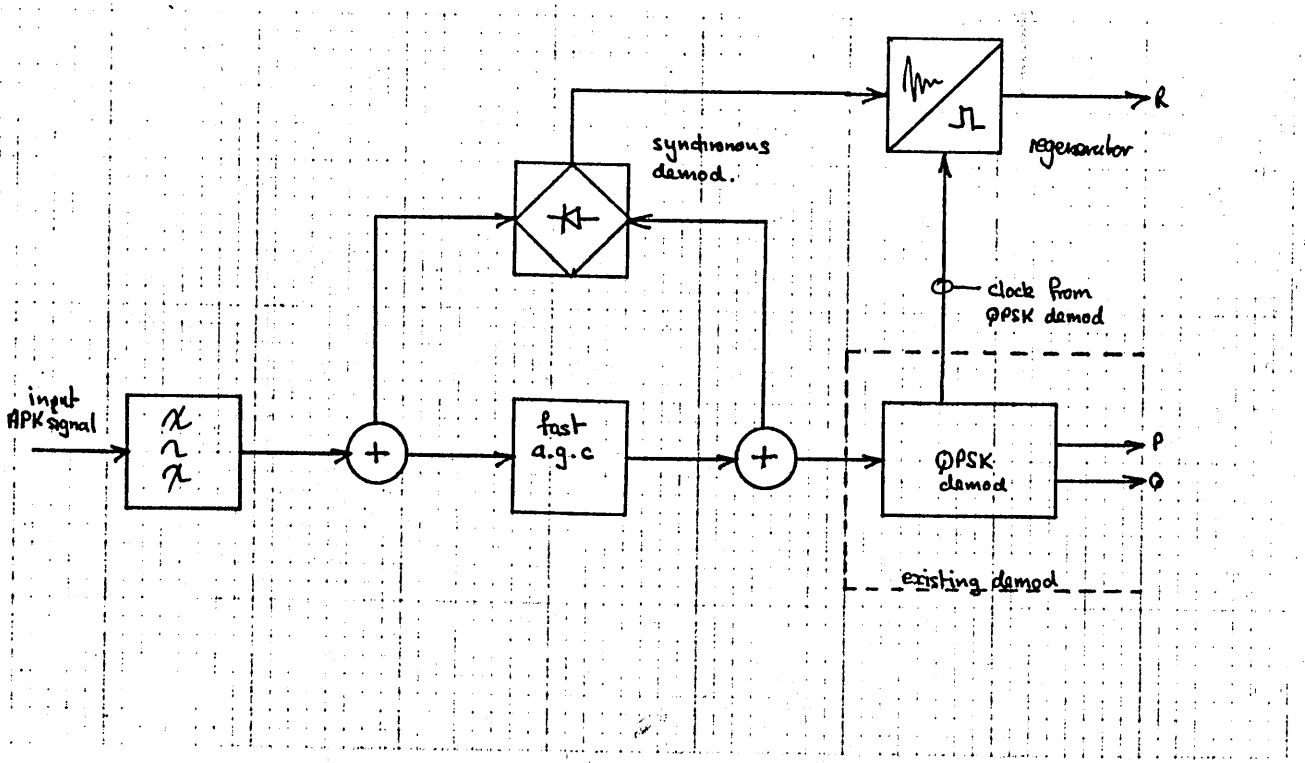

FIGURE 7.25 FIRST GENERATION APK DEMODULATOR

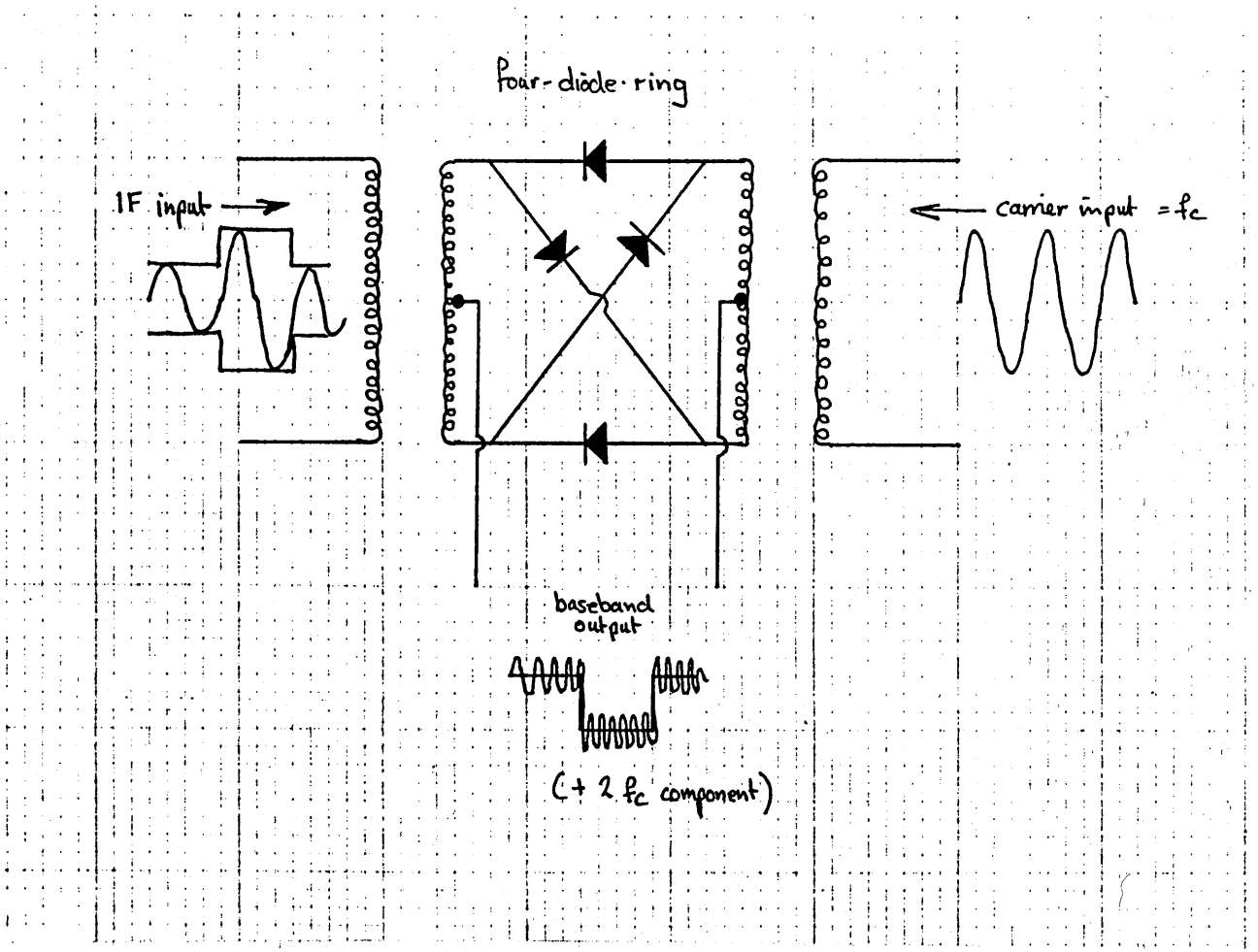

FIGURE 7.26 DOUBLE-BALANCED MIXER

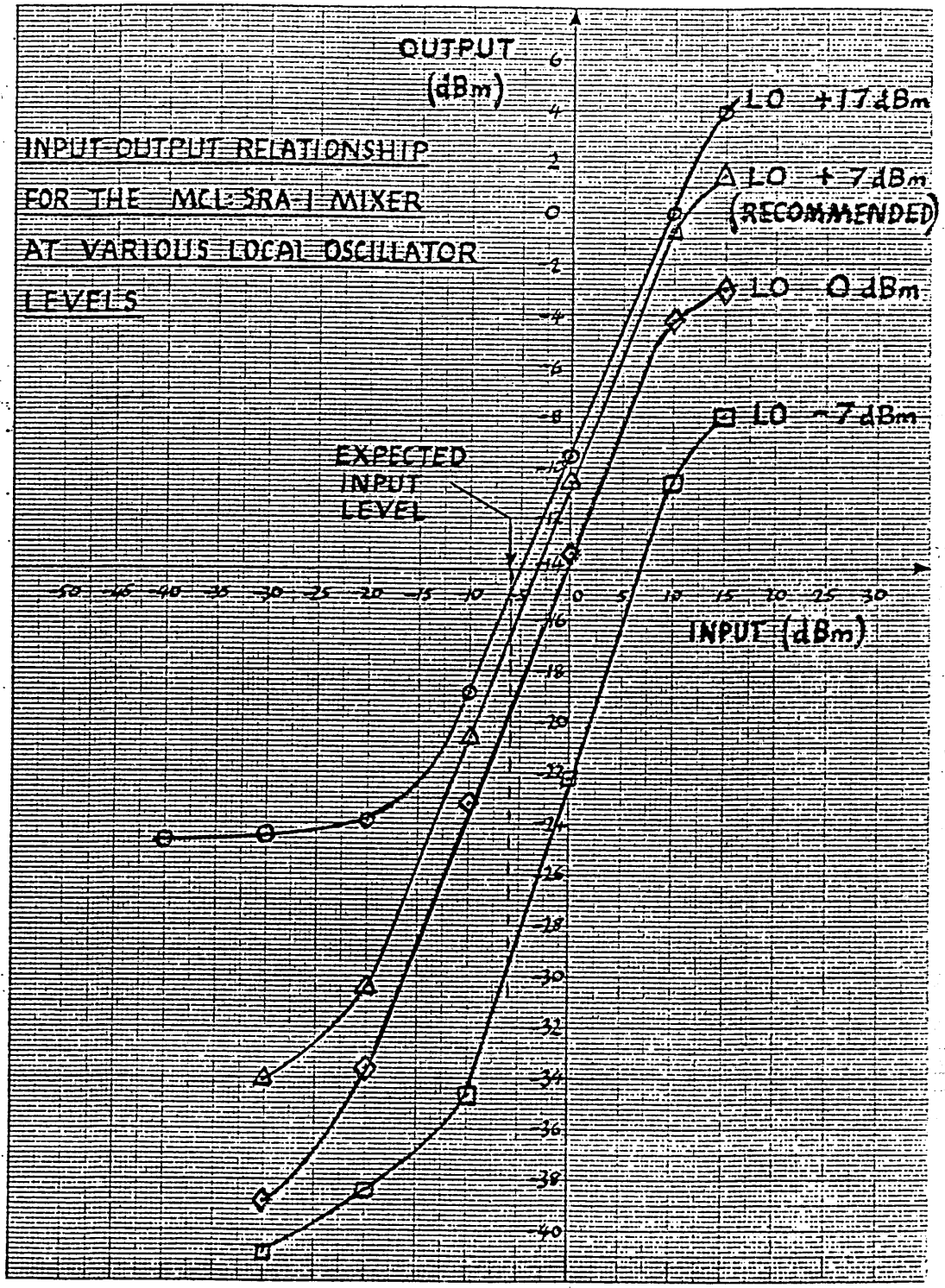

FIGURE 7.27 INPUT-OUTPUT POWER LEVEL RELATIONSHIP FOR SRA-1

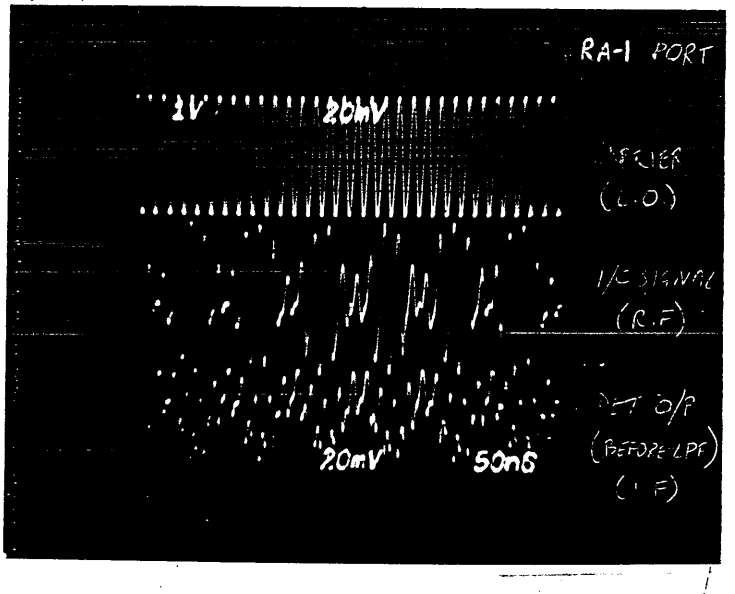

← carrier input

← amp. mod input

← unfiltered output signal

FIGURE 7.28 INPUT-OUTPUT WAVEFORMS OF DEMODULATOR WITHOUT LOW-PASS FILTER

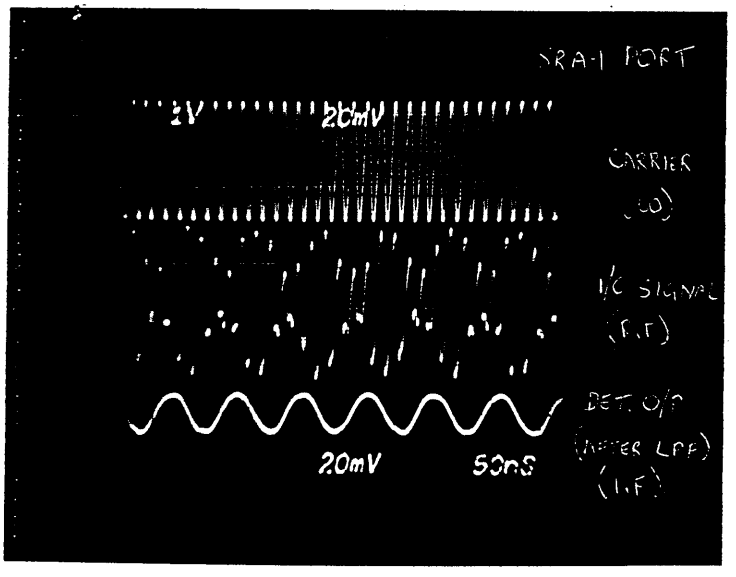

← carrier input

← amp mod input

← filtered output signal (to be regenerated.)

FIGURE 7.29 INPUT-OUTPUT WAVEFORMS OF DEMODULATOR WITH LOW-PASS FILTER

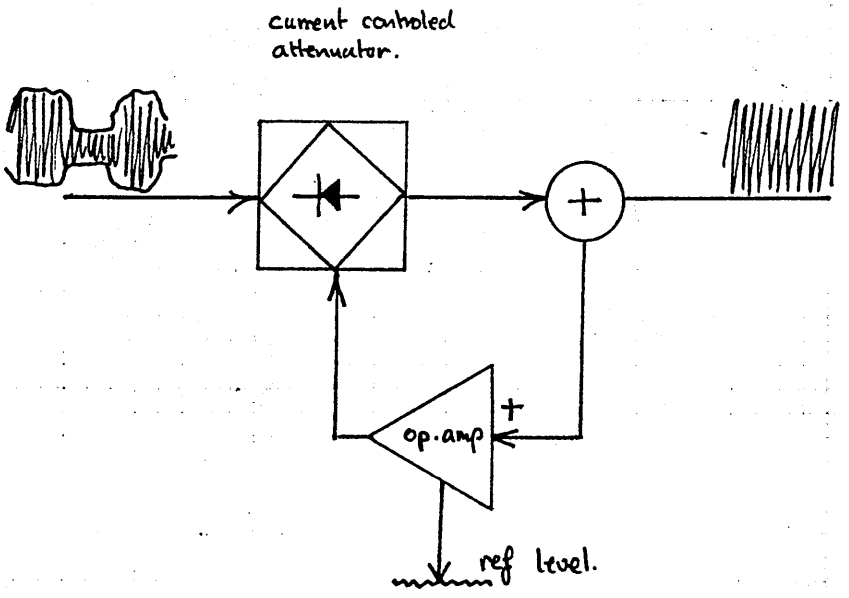

FIGURE 7.30 AGC DEVICE

FIGURE 7.31 PROTOTYPE EQUIPMENT PHOTOGRAPHS

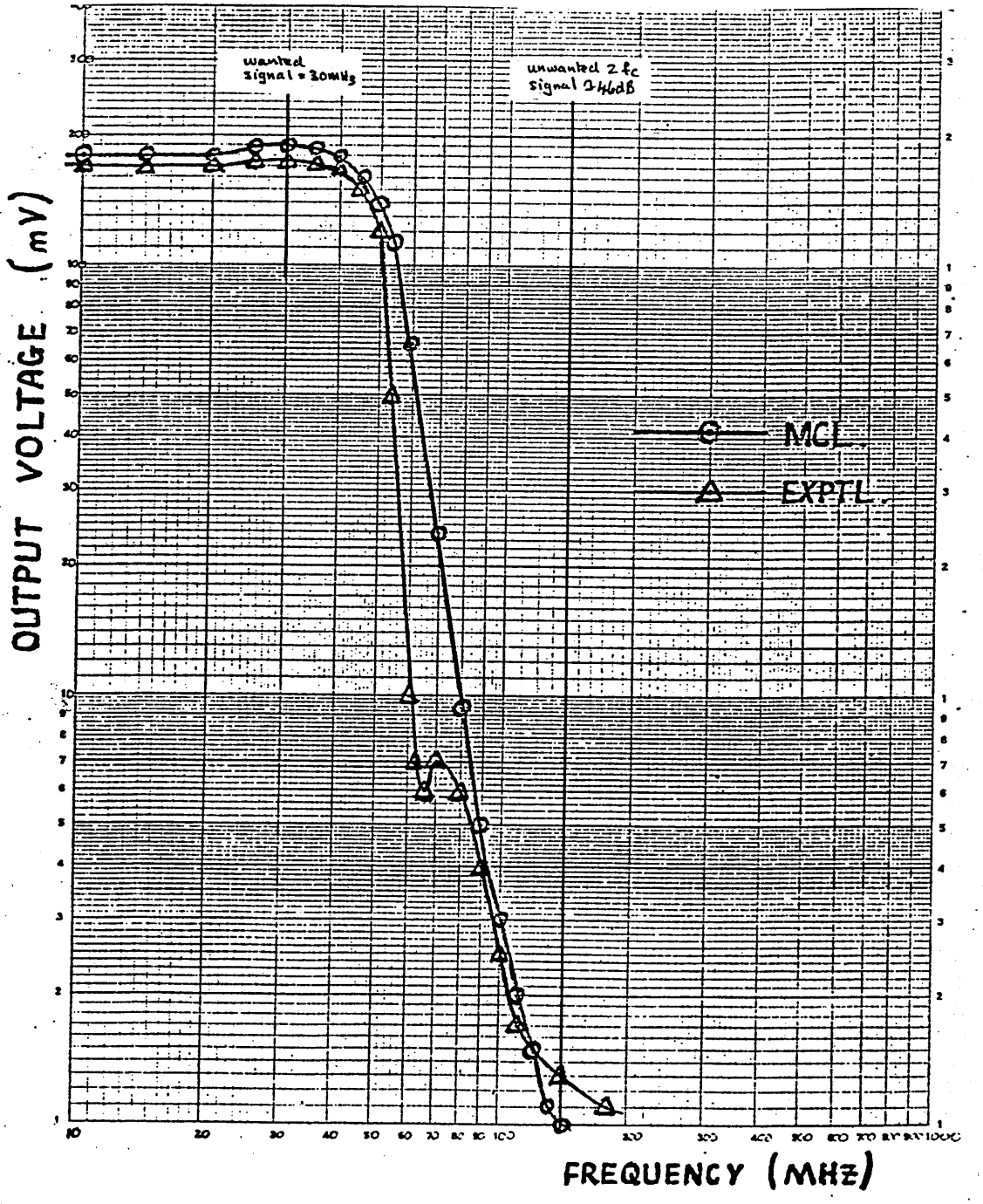

FIGURE 7.32 ATTENUATION/FREQUENCY RESPONSE OF LOW-PASS FILTER

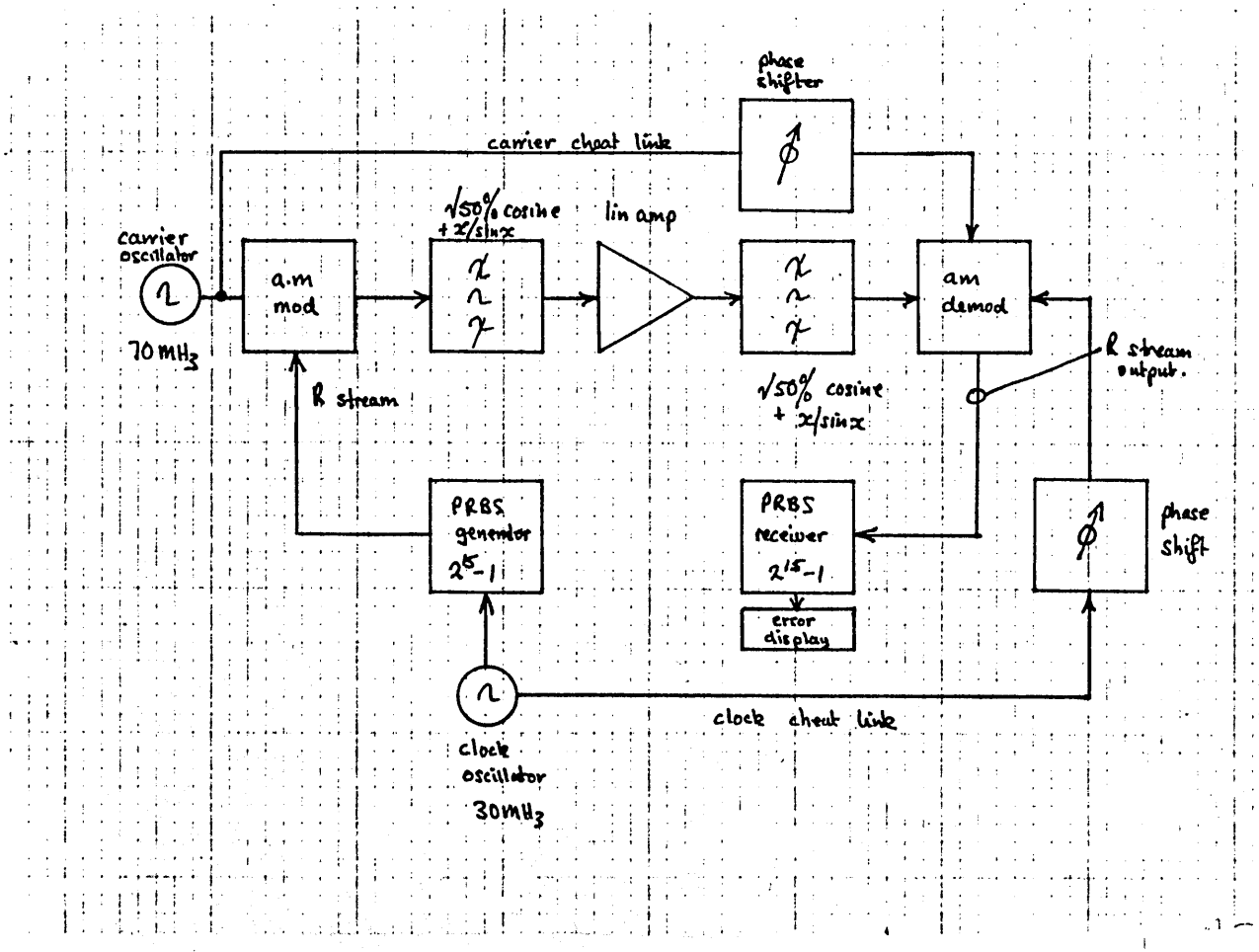

FIGURE 7.33 AMPLITUDE MODEM CIRCUIT CONFIGURATION

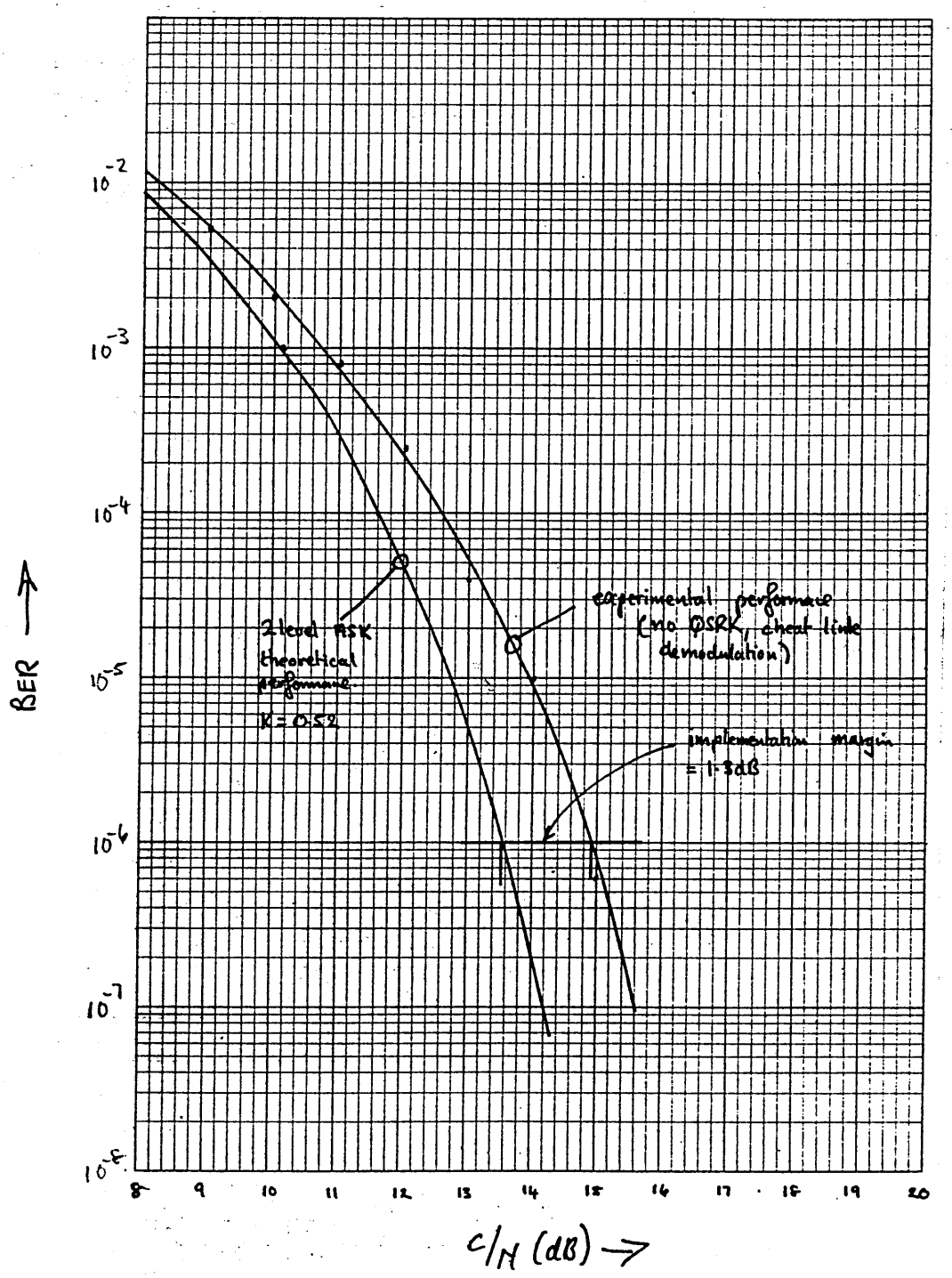

FIGURE 7.34 AMPLITUDE MODEM PERFORMANCE

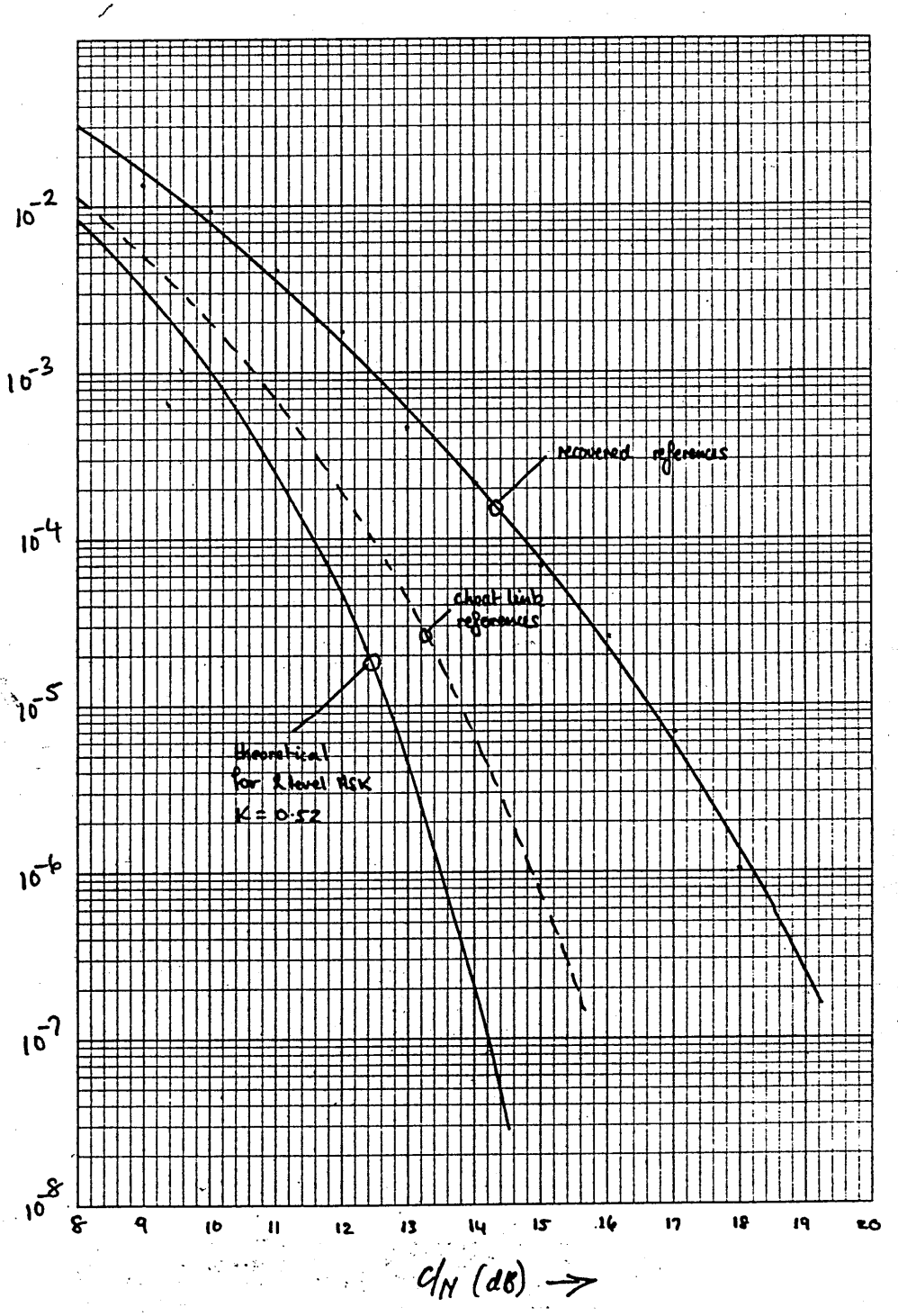

FIGURE 7.35 AMPLITUDE MODEM PERFORMANCE WITH RECOVERED REFERENCES

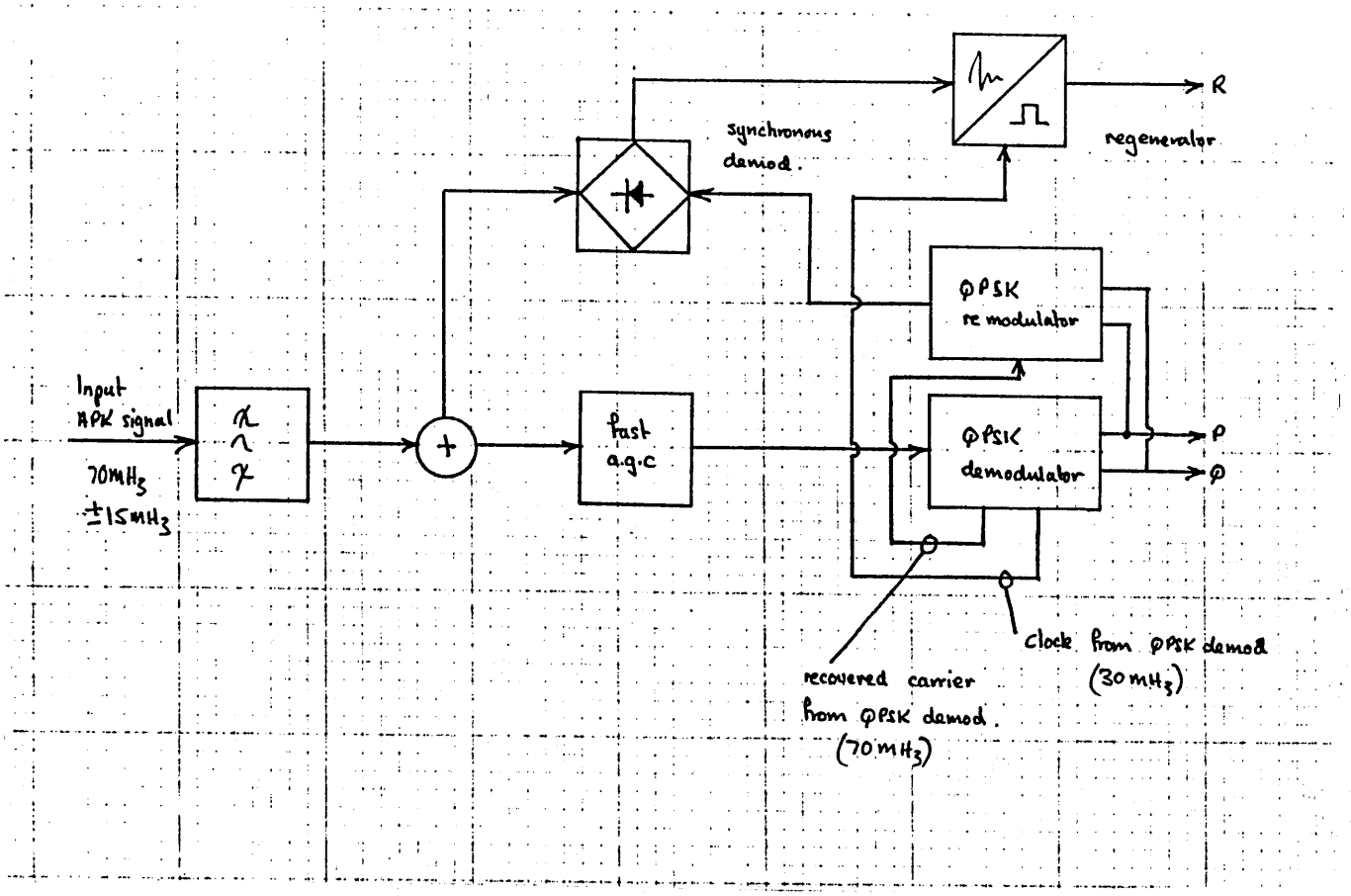

FIGURE 7.36 REMODULATION TECHNIQUE

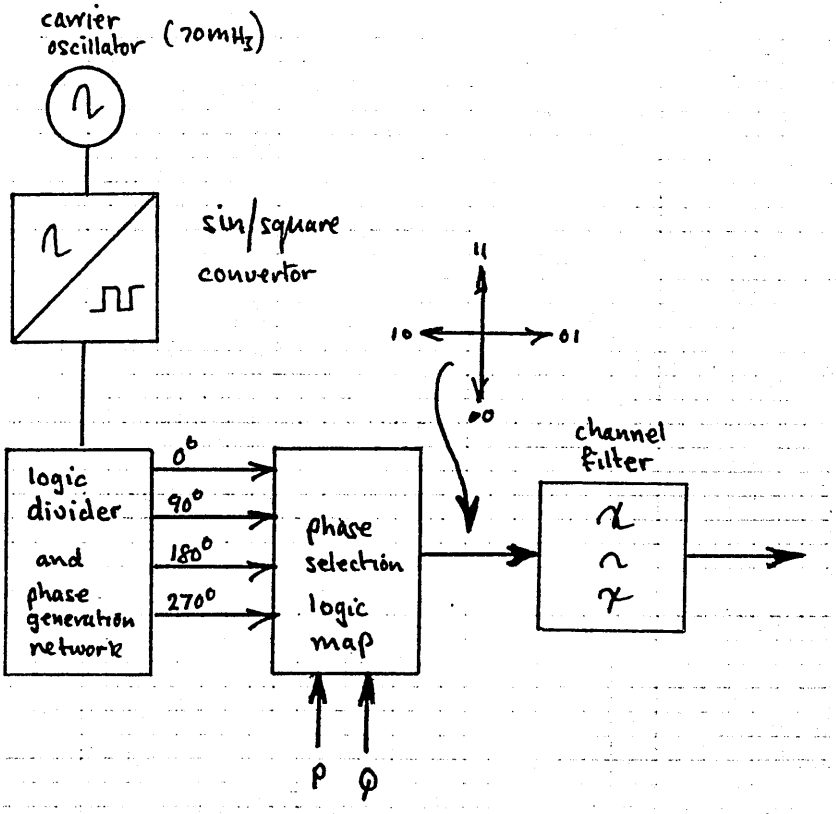

FIGURE 7.37 QPSK DIGITAL PHASE SELECTION MODULATOR

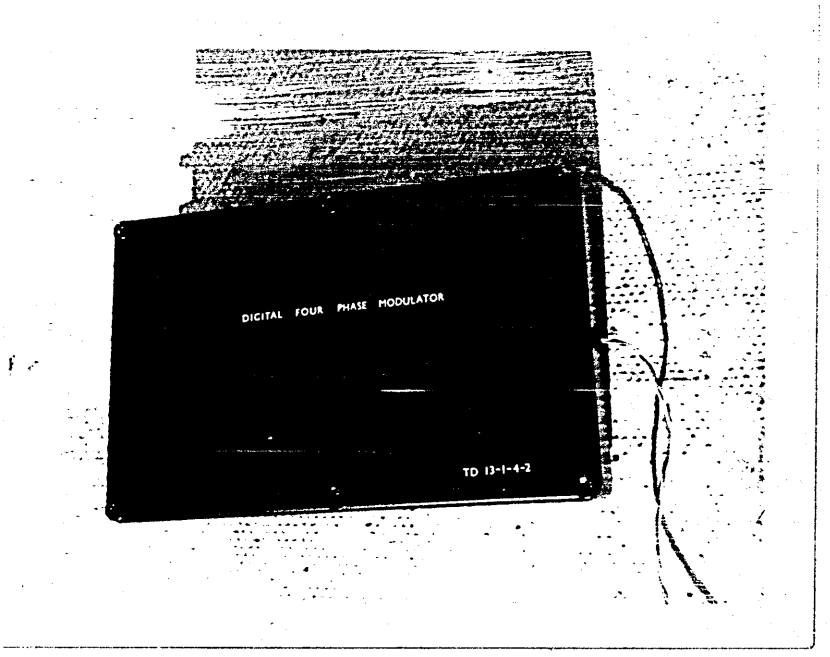

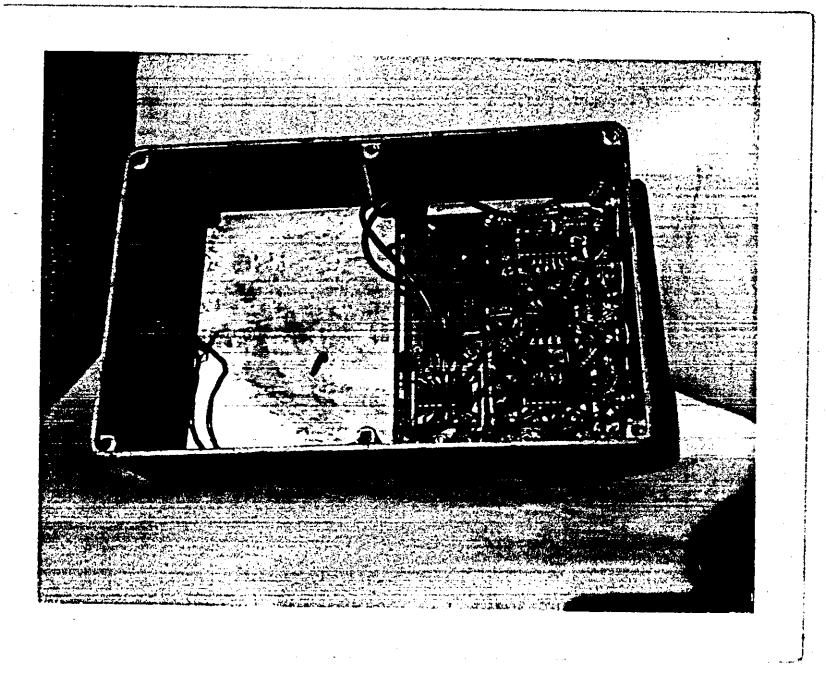

FIGURE 7.38 QPSK DIGITAL PHASE SELECTION MODULATOR EQUIPMENT

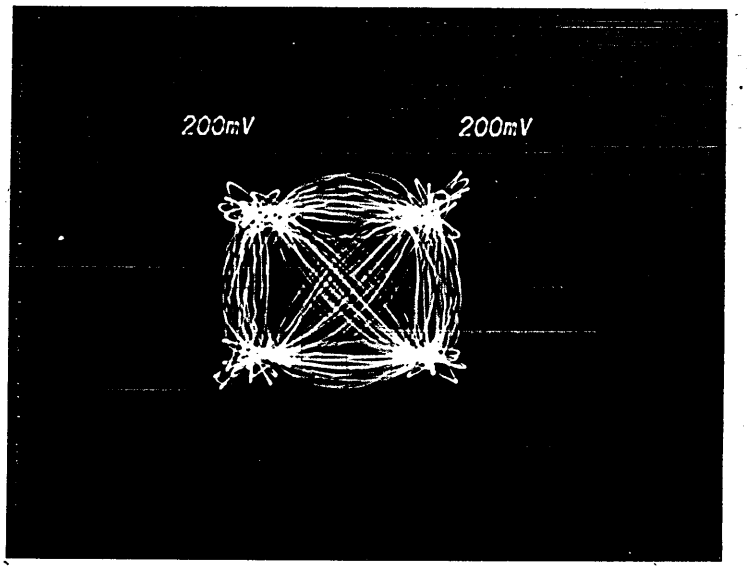

← Linear Channel
Signal Space Diagram

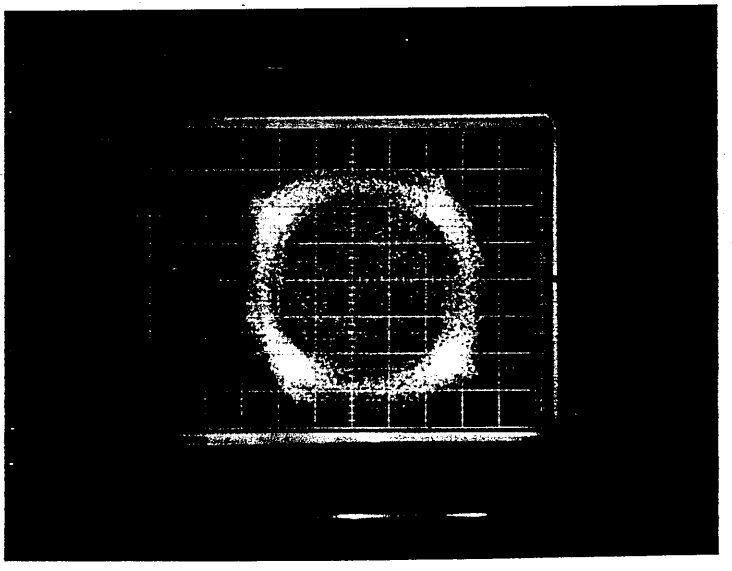

← Non-linear Channel
Signal Space Diagram

FIGURE 7.39 QPSK DIGITAL PHASE SELECTION MODULATOR SIGNAL SPACE DIAGRAM

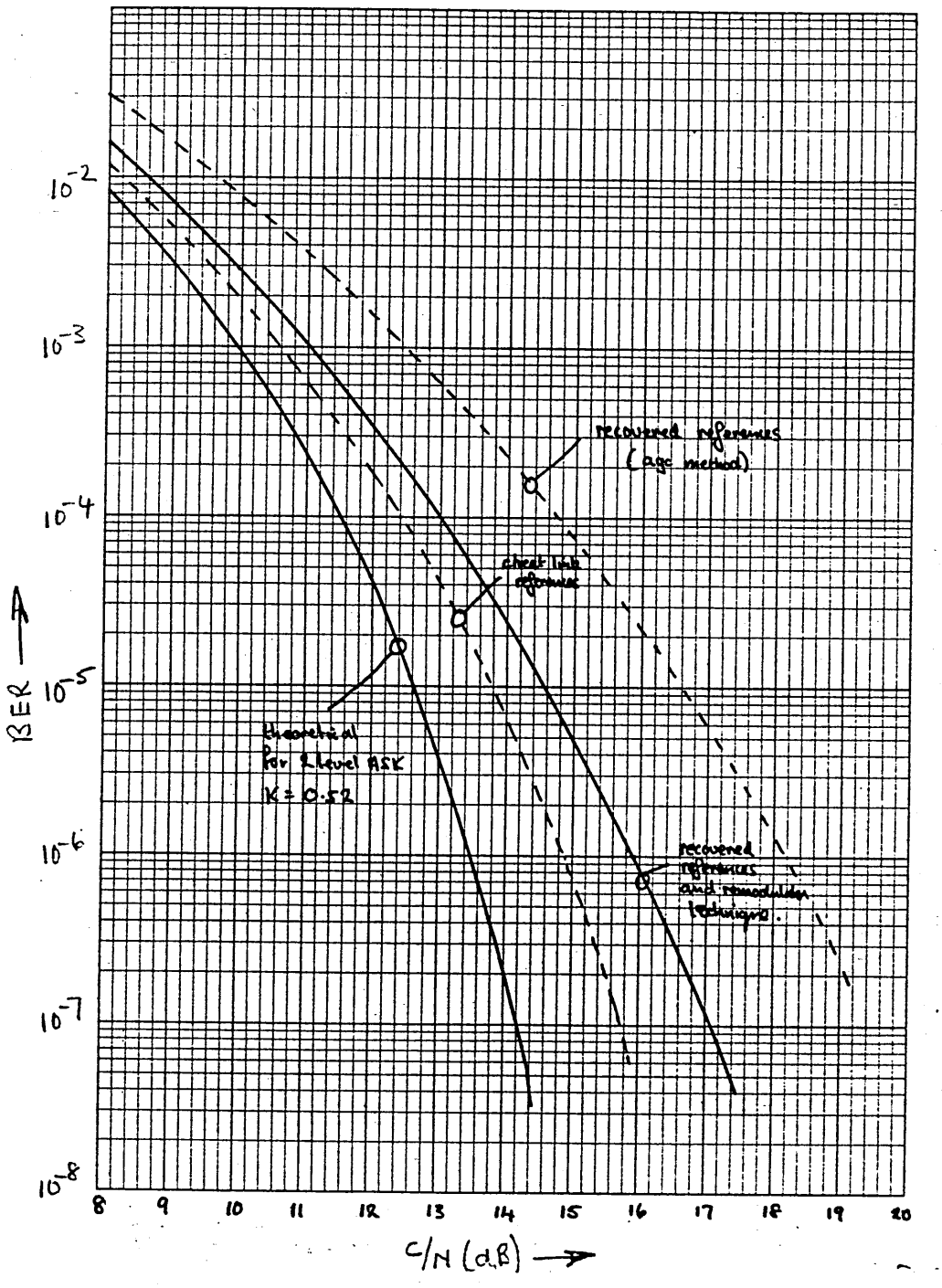

FIGURE 7.40 AMPLITUDE MODEM PERFORMANCE WITH REMODULATOR

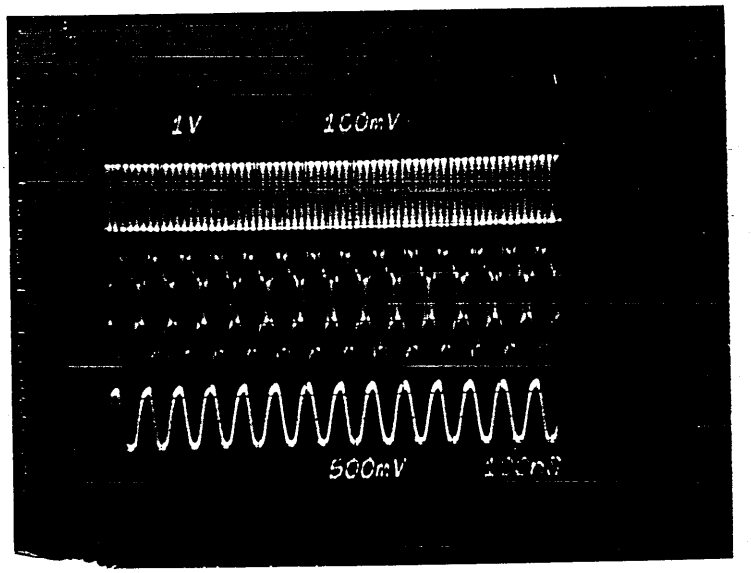

← recovered carrier

← APK input signal

← recovered 'R' stream (prior to regen) 1010 sequence

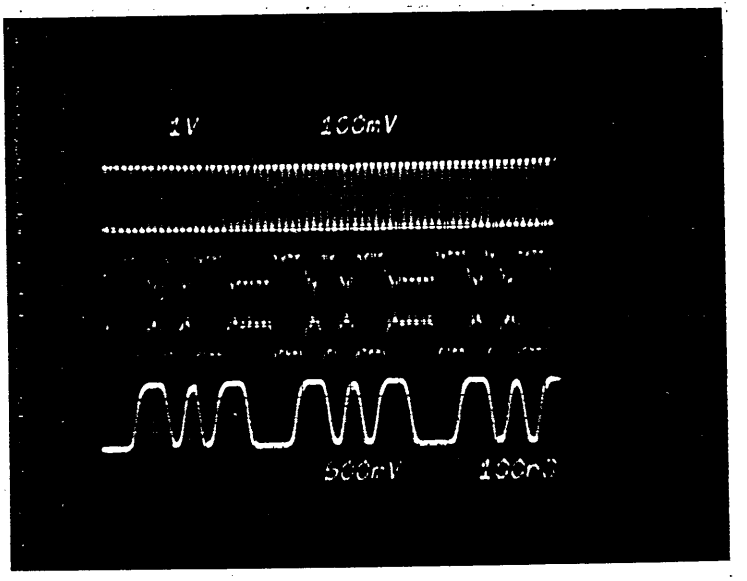

← recovered carrier

← APK input signal

← recovered 'R' stream (prior to regen) part of PRBS.

FIGURE 7.41 APK WAVEFORMS WITH 1010 AND PRBS SEQUENCE

SECTION 8

CONCLUSIONS

The need to expand the traffic carrying capacity of the INTELSAT system leads to the desire to improve the bandwidth efficiency by the use of higher order alphabets than the current 4-level QPSK system. A cursory examination showed that 16-ary systems could not be made to operate in the INTELSAT V environment because the required carrier-to-noise ratio cannot be supported by this satellite. Attention was thus directed to 8-ary signal sets. Several promising candidates were identified and evaluated. On the basis of the first examination, the number of candidates was narrowed to three: 8-phase PSK and two types of amplitude-phase shift keying called APK-A and APK-B. The objective of this study was to evaluate the performance of the three candidates in a realistic environment.

This study was limited by manpower and funding. To properly evaluate candidate modulation schemes, a combination of theoretical error rate analysis computer simulation and practical measurements would be required. At the outset, it was clear that practical measurements involving the construction of three different types of

high-performance modems was impractical. On the other hand, theoretical error rate analysis and a limited amount of computer simulations could be used. In addition, the author had conducted many hundred of hours of hardware simulations using the ECS satellite model and QPSK modulation . For these reasons, the study reported here has been extensively based on performance estimates obtained from converting the QPSK results into those expected from the candidate modulation schemes. Where possible, spot checks have been made using the theoretical error rate analysis and/or the computer simulations. These have been shown to be in good agreement, giving confidence in the technique. To complete the study, an APK modem was constructed with the intent of gaining further confidence in the results. However, the design and construction of a high-performance high-speed modem was quite clearly beyond the resources available to the author. Thus while broad agreement with the various assumptions was obtained from this exercise, it provided little in the way of solid supportive results. Nevertheless, nothing has been discovered that would indicate that the results obtained in this study are invalid, indeed, the results were predictable and mutually consistent. This the author considers to be an important test of any prediction/estimation exercise. On the basis of the work performed in this study, it is felt that the

modulation method known as APK-B shows great promise as a means of increasing by 50% the traffic capacity of a heavily interference limited satellite transponder.

The first step in this study was to identify candidate 8-ary signal sets. At the outset, compatibility with the existing QPSK system was a prime selection parameter. This was done to provide the possibility of producing hardware as an adjunct or overlay to the existing hardware. This would simplify the production and introduction of the new hardware in addition to reducing its cost. Unfortunately, this resulted in the elimination of some otherwise promising candidates (e.g., triangular designs). This is still considered as a correct course of action within the specific context of an INTELSAT V retrofit for increased capacity. Nevertheless, it is recommended that this step be re-examined with much broaded terms of reference with a view to identifying other promising modulation methods.

Once the acceptable candidates were identified, the theoretical error rate performance had to be obtained. To perform a detailed evaluation of the remaining candidates, a unified mathematical expression was developed which provides the error rate/carrier-to-noise performance of the three methods.

The unified expression was checked against 4-level (QPSK) and 8-level PSK and shown to provide good agreement with established results.

The unified approach was developed to evaluate the error rates of the candidates modulation methods while experimenting with the placement of their decision bounds. Considerable simplifications were made in the development of this unified method. This was done in order to provide rapid but reliable estimates of the error rates over a practical range of carrier to noise power ratios. The technique produces pessimistic results because it counts some error spaces more than once. Accordingly, it was considered necessary to further verify the results in addition to checking against the 4 and 8-phase PSK established results. These other checks involved graphical analysis and also a method of calculating the error contribution caused by the multiple error space counting. All the tests indicated that over the C/N ranges to be encountered in practice, good agreement could be expected between the methods. Indeed, the error contribution due to the multicounting of some errors has been shown to be more than three orders of magnitude smaller than the calculated error rate. Within the method's range of acceptable accuracy (say BER = 10^{-2} to 10^{-8}), it can be applied to any modulation method employing straight line decision bounds.

On the basis of this evaluation, the APK modulation methods showed inferior performance relative to 8-phase PSK when compared on a peak power basis (peak power comparisons are used because the satellite employs TWTA's which are peak power limited). However, it was noted that the average power requirements of APK signals was significantly less than of 8-phase PSK. This is a major advantage when operating in an INTELSAT V environment where co-channel interference is the dominant distortion mechanism.

The next steps entailed subjecting the three methods to a comprehensive linear and non-linear channel analysis. These analyses were based on methods established for the current QPSK system and were augmented by a purpose-designed computer-based channel simulator. In consequence the results are considered to be an accurate guide to the performance to be expected over the real system.

In the linear analysis, the mechanisms were examined which prevent the theoretically attainable performance being realized in a linear channel. As a first step, a practical satellite link was examined to identify those elements which influence channel performance. The elements were then combined into a simple channel model

and the various performance degradations grouped in perfect modulation and demodulation, channel filtering effects and co-channel, adjacent channel and multipath interference effects. A key feature of the analysis was the use of computer generated signal space diagrams which traced the vector space dynamic behaviour of the signals as they pass through the satellite channel. These diagrams provide a rapid insight into the transient behaviour of the modulation method and its interaction with the various channel elements. The author considers these diagrams important tools for future investigations and tutorial work in transmission analysis.

As indicated previously, QPSK results from the ESA/ESTEC OTS model were employed as the basis for assessing the behaviour of the candidate methods in the INTELSAT V environment. When one system's measurements are used as the basis of another system's estimated performance, considerable caution is required. Careful distinction must be drawn between results and effects which are completely general, those effect which are nominally identical and those effects which may be expected to be completely different. For example, in a linear channel, in-band distortion will be comparable if bandwidths and channel filters roll-offs are also comparable. On the other hand, multipath interference is

critically dependent on the various overlapping filter characteristics. In this case, although the characteristics may be nominally identical, very small differences (even between the various channels within a given simulator) will give markedly different results. Throughout this study great care was taken to identify those effects which are, or may be, unrepresentative of the INTELSAT V satellite system. In the linear analysis, all the various effects were considered sufficiently general to serve as the basis of the estimated performances using the C/I and C/N ratios obtained from the tentative link budgets shown in Table 2.2. Using these estimates the error rate was shown to be 6.2×10^{-5}, 1.2×10^{-3} and 2.1×10^{-5} for 8-phase PSK, APK-A and APK-B, respectively. Accordingly, on the basis of linear channel performance, the APK-B system now offers an advantage of almost 1 dB over the 8-phase PSK case which in turn is 3.4 dB better than the Type A system. These improvements reflect the lower average power of the APK signal sets and reveal for the first time why a modulation method with an apparently inferior performance under thermal noise condition should be of interest in a satellite system. A homogenous environment is assumed, where all the interferers use the same modulation method as the channel under investigation. While this is valid for a study of this nature, it not

universally true. A homogenous environment assumes that all adjacent and cross-polar channels together with all other potential sources of interference use the same modulation method. In the INTELSAT environment, other services may occasionally inhabit the adjacent and cross-polar channels (e.g., FM-TV and QPSK-FDMA-Single Channel Per Carrier (SCPC)). In addition, it is clear that INTELSAT would have little, if any, control over the sources of external interference. The assumption of a homogenous environment may therefore be viewed as limitation which was necessary to minimize the complexity of the study. However, when it is recall that the high level of interference arise from six separate sources it also becomes clear that the contribution of any one source is not significant. Accordingly, if two or three of the interference sources do not use the same modulation method as the wanted channel, it is considered that the overall result will be almost unaffected. Nevertheless, in the recommended detail follow-up study these possibilities should be considered carefully, although it is recognized that this will be very time consuming.

The linear channel is a poor approximation to the real case where the satellite TWTA will be operated close to saturation. Accordingly, the next step was to use the

techniques developed in the linear channel analysis, but this time to apply them to the QPSK results from the hardware simulator, operating with non-linear amplifiers.

At an early stage in the analysis, it became apparent that the basic linear channel Nyquist criteria cannot be applied directly to the non-linear case because the non-linearity is inserted between the two filters which together constitute the Nyquist shaping. Furthermore, the computer generated signal space diagrams revealed an interaction between the non-linearity and the subsequent filtering, the effect of which was to cause an increase in the inter-symbol interference (ISI) at the sampling instant. It was reasoned that this increased ISI is one of the main causes of degraded performance through a non-linear channel since it reduces the noise power required to cause an error. This ISI was expected to increase as the non-linearity was driven into saturation. However, since the output power (and hence the down-link C/N) was increasing under these conditions, a balance point was expected corresponding to an optimum operating point. Accordingly, the performance of the three methods was evaluated as a functional of TWT back-off (degree of non-linearity). This showed that the 8-phase system could operate close to saturation, but the APK signal sets required more than 4 dB greater back-off.

However, upon examination of the interaction of the APK signals sets and the non-linearity, it was found that the principal cause of the poor performance was the compression of the APK signal set ring ratios. In consequence, the calculations were repeated with the inclusion of a pre-compensation (expansion) technique designed to restore the post-TWTA ring-ratios to the optimum (linear) values. This resulted in a substantial improvement allowing all three candidates to operate at saturation and giving a four order of magnitude improvement in the attainable BER. At this stage, it was concluded that this amplitude compensation must be included in the link and attention was next directed to the amplitude-phase distortion characteristics of the TWTA. Using the same approach, a simple straight line phase equalizer was included in the link. A combination of amplitude and phase equalization was seen to restore the linear channel performance to the non-linear channel giving BER's of 10^{-6}, 10^{-8} and 10^{-9} for APK-A, APK-B and 8-phase PSK, respectively.

As in the case of the linear channel, considerable emphasis was placed on the effect of co-channel interference. The results showed, as in the linear channel, that the APK signal sets performed much better than PSK due to the lower average power of the APK

interferers in a homogenous interference environment. However, a very interesting effect was noticed. The amplitude compensation necessary to overcome the a.m.-a.m. compression of the TWTA by expansion of the ring ratios of the up-link further lowered the average power of the up-link APK interferers. This in turn further increased the APK performance advantage over 8-phase PSK. The same effect was noted for adjacent channel interference and multipath. The multipath results, however, showed very substantial levels of performance degradations and therefore these estimates are considered suspect as discussed earlier. At about the same time as this conclusion was reached, it was heard that the QPSK results obtained by the author were considered sufficiently troubling by ESA to force a redesign of the satellite I/OMUX filters and the transponders' center frequencies. It is understood that these modifications obviated the multipath effect and, accordingly, the multipath component is included separately in the link budgets for interest only. The overall results show that APK-B out performs 8-phase PSK and APK-A giving error rates of 10^{-5}, 3×10^{-3} and 10^{-2}, respectively. At this point, the 6/4 GHz study was complete and so it may be concluded that although the single channel thermal noise performance of 8-phase PSK is superior to APK, the heavily interference

limited environment of INTELSAT V leads to the APK-B system offering a potential improvement of more than two orders of magnitude in bit error rate.

It was recognized that the lower average power characteristics of the APK modulation method would provide an even greater improvement in link performance in the 14/11 GHz band. Operation in this band is usually characterized by a high clear weather C/(N+I) ratio, but also the occurrence of precipitation induced deep fades accompanied by a substantial increase in co-channel interference. The fades are time varying phenomena, which results in the satellite link being unusable for a certain amount of time per year (link outage). This occurs when the interference power exceeds a "spare" power margin built into the link budget. This margin and hence the duration of the link outage is dependent on the sensitivity of the modulation method to the link degradations. The main degradation under fading conditions was shown to be an increase in the co-channel interference and, as expected, the link budget shows the available clear weather C/N to be greatly in excess of that needed for a threshold error rate of 10^{-4}. These margins confirmed that the use of APK-B would result in the satellite system being available for 99.99% of the

year, which is 4 hours more per year than the 8-phase PSK case. Given the income potential of satellite circuits, these differences are considered very significant.

Finally, an attempt was made to assess the complexity and attainable performance of APK modems. From previous QPSK experience, the author was aware that the design of modems capable of yielding near-theoretical performance was a difficult task. To assess the performance of an APK modem, the same scaling or estimation methods were used to convert QPSK results into estimates of the candidates modulation methods' performance. The QPSK results used for the basis of these estimates were obtained from hardware measurements by the author and also from computer simulations produced by the European Space Agency. No major problem areas were discovered, although the acquisition and maintenance of a stable amplitude reference is an unproven area deserving further attention. By way of substantiation of these results, an APK modem was constructed. Due to manpower and financial limitations, a simple design had to be adopted. Accordingly, while again no major problems were encountered, the resulting hardware was not considered representative of that obtainable commercially and therefore the question of the stable amplitude reference remains.

Overall, a thorough study has been conducted on the application of 8-ary APK signal sets to an INTELSAT V environment. Although the basic single channel thermal noise performance of APK-B is inferior to 8-phase PSK, its lower average power requirements yield significant performance advantages in a heavily interference limited environment, especially 14/11 GHz. For this reason, it is strongly recommended that an 8 level APK-B system be further investigated for use as a retrofit of the INTELSAT V TDMA networks in order to increase the available traffic carrying capacity by 50%.

REFERENCES

1. C. R. CAHN
"Combined Digital Phase and Amplitude Modulation Communication Systems"
IRE Trans. on Comm. Tech., September 1960.

2. R. W. LUCKY and J. C. HANCOCK
"On the Optimum Performance of N-ary Systems Having Two Degrees of Freedom"
IRE Trans. on Comm. Sys., March 1962.

3. C. N. CAMPOPIANO and B. G. GLAZER
"A Coherent Digital Amplitude and Phase Modulation Scheme"
IRE Trans. on Comm. Sys., March 1962.

4. A. C. CLARKE
Extra-Terrestrial Relay, Can Rocket Stations Give World-wide Radio Coverage
Wireless World, October 1945.

5. W. C. JAKES
"Participation of Bell Telephone Laboratories in Project Echo and Experimental Results"
Bell Systems Tech Journal, 1961 4 Op 975.

6. NASA
"Final Report on Relay Programme"
Special Publication, 1968.

7. HMSO
"Satellite Communications"
Cmmd 2436, 1964.

8. R. E. BACK, D. WILKINSON, and D. J. WITHERS
"Commercial Satellite Communications"
IEE Electronics Record, 1972.

9. K. KAWAI, S. SHINTANI and H. YANAGIDAIRA
"Optimum Combination of Amplitude and Phase Modulation Scheme and its Applications to Data Transmission Modems"
Conference Record, IEEE Int'l Conference on Communications, Philadelphia, Pennsylvania, June 1972.

10. J. SALZ, J. R. SHEENAN and D. J. PARIS
"Data Transmission by Combined AM and PM"
B.S.T.J., Vol. 50, September 1971.

11. C. M. THOMAS and S. H. DURRANI
"Amplitude-Phase Keying: an Evaluation for Realistic Transponder Channels"
2nd Int'l Conf. on Digital Satellite Communications, Paris, November 1972.

12. S. BENEDETTO and E. BIGLIERI
"Performance of M-ary PSK Systems in the Presence of Intersymbol Interference and Additive Noise"
Alta Frequenza, Vol. 41, April 1972.

13. S. BENEDETTO, G. De VINCENTIIS and A. LUVISON
"Error Probability in the Presence of Intersymbol Interference and Additive Noise for Multilevel Digital Signals"
IEEE Trans. on Comm.

14. G. J. FOSCHINI, R. D. GITLIN and S. B. WEINSTEIN
"Optimization of Two-Dimensional Signal Constellations in the Presence of Gaussian Noise"
IEEE, Trans. on Comm., Vol. Com-22, No. 1, January 1974.

15. C. WEBER
"New Solutions to the Signal Design Problem for Coherent Channels"
IEEE Trans. on Info. Theory, April 1966.

16. B. DUNBRIDGE
"Optimal Signal Design for the Coherent Gaussian Channel"
Ph.D. Dissertation, Univ. of So. Calif., Los Angeles, December 1965.

17. B. DUNBRIDGE
"Asymmetric Signal Design for the Coherent Gaussian Channel"
IEEE Trans. on Info. Theory, July 1967.

18. A. V. BALAKRISHNAN
"A Contribution to the Sphere Packing Problem of Communication Theory"
J. Math. Anal. and Appl., December 1961.

19. C. M. THOMAS
"Final Report on Amplitude-Phase Keying Techniques"
INTELSAT Contract Final Report No. CSC-SS-292, August 1971.

20. G. ROBINSON, et al
"PSK Signal Power Spectrum Spread Produced by Memoryless TWTs"
COMSAT Technical Review, Vol. III, No. 2

21. W. Bennett and J. Davey
Data Transmission
McGraw-Hill

22. J. Spilker
Digital Communications via Satellite
Prentice Hall

23. CEPT/SET/test engineers group
"The Choice of an Optimum Filter for the OTS Field Trials"
CEPT/SET/TEG 1/77

24. R. A. HARRIS and R. A. GOUGH
"Factors Influencing the Choice of Pulse Shaping Filters for the ECS System"
Proc. ESA/SWISS PTT Colloq. on Frequency Reuse Transmission Experiment at 180 Mbps over the Jungfrau Link, ESA SP-120, June 1976.

25. C. DEVIEUX
"QPSK Bit Error Rate Performance as Affected by Cascaded Linear and Non-Linear Elements"
COMSAT Technical Review, Spring 1978.

26. R. J. COLBY
"A Preliminary Analysis of the Jungfrau QPSK Transmission Performance by Comparison with the OTS Breadboard Model Results"
Proceedings of the ESA - Swiss PTT Colloquium held at the Technical Centre in Berne, 24-25 June 1976.

27. R. HARRIS
"Performance Criteria for Satellite Digital Transmission Systems"
ISA Journal 1 (1), 1977.

28. S. E. DINWIDDY
"Atmospheric Attenuation and Noise in Satellite System at 11/14 GHz"
ESTEC Memorandum EC/9039/SED/sa.

29. C. ZUFFEREY
"Cross-Polarization Measurements at 13 GHz on a Slant Terrestrial Path"
Proc. ESA/SWISS PTT Colloq. on Frequency Reuse Transmission Experiment at 180 Mbps over the Jungfrau Link, ESA SP-120, June 1976.

30. R. J. COLBY
"Co-Channel Interference in QPSK Satellite Channels of the Proposed European Communications Satellite Breadboard Model"
British Post Office, THQ/TD13.1.4, April 1976

31. F. M. GARDNER
"Carrier and Clock Synchronization for TDMA Digital Communications"
ESA TM-169, December 1976.

32. F. M. GARDNER
"Phase Locked Loops"
ESA TM-134, March 1975.

33. D. W. BAKER and P. F. ROBINSON
"A Fast Acquisition Coherent PSK Demodulator Incorporating Passive Narrow Band Filters Operable in a Quenching Mode"
IEE Conference on Satellite Systems Technology.

34. CEPT/SET/TEST ENGINEERS GROUP
"60 Mbit/s Digital Measurements Using a Tuned Filter Type Demodulator Performed at ESTEC from November 1974 to March 1975"
CEPT/SET June, 1976.

35. R. J. COLBY
"Silent and Loaded Channel Multipath Interference in Adjacent QPSK Satellite Channels of the Proposed European Communication Satellite Breadboard Model"
British Post Office, THQ/TD13.1.4, May 1975.

36. R. J. COLBY
"Down-Link Adjacent Channel Interference in QPSK Satellite Channels of the Proposed European Communications Satellite Breadboard Model"
British Post Office, THQ/TD13.1.4, August 1976.

37. F. M. FITZGERALD
"A Synchronous AM Demodulator for Digital Satellite Transmission Systems"
Lanchester Polytechnic Project Thesis, January, 1976.

38. R. J. COLBY
"Tne Implications of Using High-Power Travelling-Wave-Tube Amplifiers with Uplink Power Control at OTS-Type Earth Stations"
ESA Journal, 1977, Volume I.

39. R. J. COLBY
A Preliminary Investigation into the Message Dependency Effect on the Bit Error Rate Performance of the PO/MCL 60 Mbit/s QPSK Demodulator"
BPO/TD13.1.4 Memorandum No. 69, December 1974.

40. R. J. COLBY
A Further Investigation into the Message Dependency Effect on the Bit Error Rate Performance of the PO/MCL 60 Mbit/s QPSK Demodulator"
BPO/TD13.1.4 Memorandum No. 76, April 1975.

41. B. A. PONTANO, J. L. DICKS, R. J. COLBY, G. FORCINA, AND J. PHIEL
"The INTELSAT TDMA/DSI SYSTEM"
IEEE Journal on Selected Areas in Communications, January 1983